Kristallisation, Polymorphiescreening und Kristallstrukturbestimmung aus Röntgenpulver- und Einkristallröntgenbeugungsdaten an industriellen organischen Pigmenten und pharmazeutischen Wirkstoffen sowie großtechnischen Zwischenprodukten

Dissertation

zur Erlangung des Doktorgrades

der Naturwissenschaften

vorgelegt beim Fachbereich für Biochemie, Chemie und Pharmazie

der Johann Wolfgang Goethe-Universität

in Frankfurt am Main

von

Lukas Tapmeyer

aus Hildesheim

Frankfurt 2021

(D30)

vom Fachbereich für Biochemie, Chemie und Pharmazie der
Johann Wolfgang Goethe-Universität als Dissertation angenommen.

Dekan:	Prof. Dr. Clemens Glaubitz
1. Gutachter:	Prof. Dr. Martin Ulrich Schmidt
2. Gutachter:	Priv.-Doz. Dr. Christoph Saal

Datum der Disputation: 15.10.2021

Inhalt

Danksagung

[Die Danksagung ist in der elektronisch publizierten Version nicht enthalten]

„Unendlich groß ist die Rolle des unendlich Kleinen in der Natur.“

[Louis Pasteur]

1 Einleitung

In dieser kumulativen Dissertation geht es um organische Festkörper. Da die Kristallstruktur viele Eigenschaften des Materials bestimmt, ist eine genaue Kenntnis über die Festkörperform in vielen Fällen unerlässlich. In dieser Arbeit sollen organische Verbindungen durch Kristallisation als Einkristalle oder mikrokristalline Pulver erhalten werden. Ihre Kristallstrukturen sollen bestimmt werden. Die Bedingungen, unter denen sich eine bestimmte kristalline Form bildet, sollten möglichst bekannt sein. Im Rahmen von Polymorphiescreenings soll daher nach weiteren möglichen Festkörperformen gesucht werden. Diese neuen Phasen sollen ebenfalls analysiert werden.

Kristallstrukturen werden üblicherweise aus Einkristallröntgenbeugungsdaten bestimmt, wann immer die Herstellung von Einkristallen möglich ist. Da dies bei weitem nicht immer gegeben ist, wird häufig auf die Pulverdiffraktometrie zurückgegriffen. Die Methoden zur Kristallstrukturbestimmung aus Pulverdiffraktogrammen haben vor allem in den letzten zwei Jahrzehnten bedeutende Fortschritte gemacht.[1–4]

Im Rahmen dieser Arbeit sollen diese Methoden um die Bestimmung der absoluten Konfiguration aus Pulverdaten erweitert werden. Ebenfalls sollen die Möglichkeiten der Kristallstrukturanalyse an Grenzfällen der Tauglichkeit der jeweiligen Methode demonstriert werden. Dabei sollen vor allem Verbindungen untersucht werden, die seit langem verwendet werden und von denen trotzdem bisher keine Kristallstruktur und teilweise noch nicht einmal die chemische Zusammensetzung bekannt ist. Hierbei sollen die Kristallstrukturen aufgeklärt, nach neuen Polymorphen und Solvaten gesucht und Struktur-Eigenschaftsbeziehungen erforscht werden. Bei den untersuchten Verbindungen handelt es sich um pharmazeutisch interessante Substanzen, Zwischenprodukte der Synthese in Industrie und Forschung sowie industrielle organische Pigmente.

Bei der Synthese einer neuen Verbindung ist die Stereochemie häufig unbekannt oder zumindest unsicher. Für die biologische Wirkung und die Zulassung als Medikament ist diese Information jedoch unerlässlich.[5] Bei pharmazeutisch interessanten Substanzen handelt es sich meist um chirale Verbindungen, insbesondere bei Wirkstoffmolekülen. Im Rahmen der hier dokumentierten Forschung soll eine Methode mitentwickelt werden, um die absolute Konfiguration einer Substanz zu bestimmen. Dies gelingt üblicherweise durch Einkristallröntgenstrukturanalyse.[6] Allerdings erfordert die Herstellung geeigneter Einkristalle einen verhältnismäßig großen Substanzeinsatz. Von in Entwicklung befindlichen Substanzen sind aber meist nur sehr geringe Mengen verfügbar. Daher soll ein Weg gefunden werden, um die Chiralität einer Verbindung aus minimalen Substanzmengen zu bestimmen. Dies soll durch Kristallstrukturanalyse aus Röntgenpulverbeugungsdaten erfolgen. Ziel ist es, die benötigte Substanzmenge von typischerweise 10 bis 100 mg Substanz pro Kristallisationsansatz auf unter ein Milligramm zu reduzieren.

Die absolute Konfiguration ist aus Pulverdaten allerdings nicht ohne Weiteres zugänglich, denn Enantiomere haben nicht nur die gleichen chemischen Eigenschaften, sie liefern auch identische Pulverdiagramme. Um dieses Problem zu umgehen, sollen die chiralen Substanzen in diastereomere Salze umgewandelt werden, deren Struktur bestimmt wird. Aus der Struktur der Salze mit Salzbildnern bekannter absoluter Konfiguration soll so auf die absolute Konfiguration der eingesetzten Substanz geschlossen werden. [Veröffentlichung LT1]

Neben der Strukturaufklärung aus Einkristallen und Pulvern, gewinnt die Strukturbestimmung durch Analyse der Paarverteilungsfunkion (Englisch: „*Pair Distribution Function*“, PDF) für organische Moleküle zunehmend an Bedeutung.[7–9] Bei dieser Methode können Beugungsdaten von nanokristallinen und sogar amorphen Proben ausgewertet werden. Auch für die Bestimmung der absoluten Konfiguration von Substanzen aus Pulverdaten kann die PDF zumindest als weiteres Kriterium für die Identifikation eines korrekten Modells verwendet werden.[10,11] Die Strukturbestimmung aus PDF-Daten von organischen Molekülen befindet sich in der Entwicklung. Als Testbeispiele werden einfache organische Moleküle verwendet. Die Methode wurde bereits erfolgreich an Substanzen mit zuvor bekannter Struktur demonstriert.[7] Jetzt besteht Bedarf an Testverbindungen, deren Struktur zwar vergleichsweise einfach ist (also wenige Parameter hat), aber noch nicht bestimmt wurde. An diesen Verbindungen soll die Strukturanalyse aus PDF-Daten weiterentwickelt werden. Die aus PDF-Daten bestimmten Strukturen sollen anschließend mit herkömmlichen Methoden bestätigt werden. Ein als Testfall geeignet erscheinendes kleines, organisches Molekül ist das Leukopterin (s. Abb. 1-1). Diese Verbindung kommt in der Natur als Weißpigment in Schmetterlingsflügeln vor.[12–14] Erstaunlicherweise ist die Kristallstruktur des Leukopterins bisher nicht bekannt. Daher soll diese Verbindung jetzt synthetisiert und kristallisiert werden. Als erstes muss festgestellt werden, ob nur eine oder mehrere stabile Phasen existieren und ob und wie Leukopterin reproduzierbar phasenrein und ggf. gut kristallin hergestellt werden kann. Ein Edukt in der Synthese des Leukopterins ist das 2,4,5-Triamino-6-hydroxypyrimidinsulfat (TAHP). Es ist kommerziell erhältlich als „$C_4H_7N_5O \cdot H_2SO_4 \cdot xH_2O$“ (Abb. 1-2).[12] Von dieser Verbindung ist bisher nur die Kristallstruktur des Anhydrats bekannt.[15] Da das kommerzielle Produkt vermutlich Wasser enthält, soll hier nach weiteren Hydratstufen und Polymorphen gesucht und deren Struktur aufgeklärt werden. [LT2]

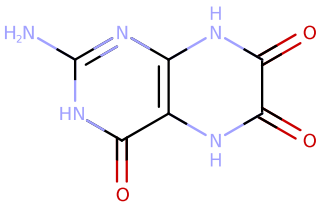

Abb. 1-1: Leukopterin.

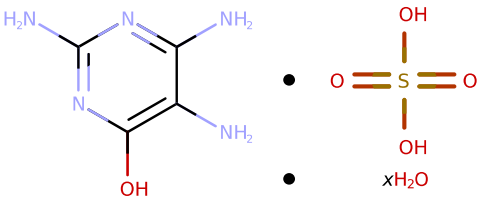

Abb. 1-2: TAHP als „$C_4H_7N_5O \cdot H_2SO_4 \cdot xH_2O$“.

Röntgenographische Methoden betrachten meist die komplette Kristallstruktur oder sogar die gesamte Probe. In der Elektronenspinresonanzspektroskopie (Englisch: „*Electron Paramagnetic Resonance*“, EPR) werden im Gegensatz dazu Marker verwendet. Diese Marker oder Label ermöglichen es, ausgewählte kleine Bereiche einer Probe zu analysieren. Ein solcher Marker für die EPR-Spektroskopie ist 1,1,3,3-Tetraethylisoindolin-5-isothiocyanate-2-oxyl. Dieses Label wird für die Markierung von RNS (Ribonukleinsäure) verwendet.[16] Die Synthese dieses Markers verläuft über mehrere Zwischenstufen.[17] Zwei dieser Zwischenstufen sind das 1,1,3,3-Tetraethyl-5-nitroisoindolin (TENI, s. Abb. 1-3) und seine Folgestufe, 1,1,3,3-Tetraethyl-5-nitroisoindolin-2-oxyl (TENO, s. Abb. 1-4). Das TENI konnte bisher nur als Öl erhalten werden.[17] Für eine bessere Handhabbarkeit soll diese Verbindung kristallisiert werden. Von TENI und TENO sollen die Kristallstrukturen aus Einkristallbeugungsdaten bestimmt werden. Besonderer Fokus liegt dabei auf Struktur-Eigenschafts-Beziehungen im Festkörper, da diese Aspekte bisher nicht untersucht worden zu sein scheinen. [LT3]

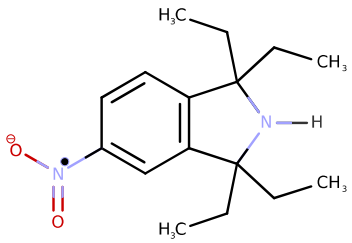

Abb. 1-3: TENI.

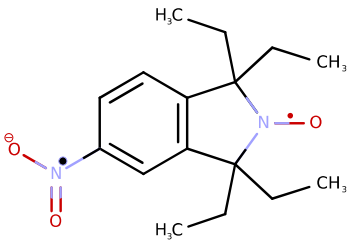

Abb. 1-4: TENO.

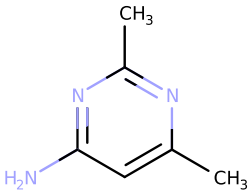

Abb. 1-5: ADMP.

Acetonitril, CH_3CN, ist ein gängiges Lösungsmittel. Unter stark alkalischen Bedingungen, beispielsweise in Gegenwart von Alkalialkoholaten, neigt es zur Trimerisierung, wobei 4-Amino-2,6-dimethylpyrimidin (ADMP, s. Abb. 1-5) entsteht.[18] Die Kristallstruktur von ADMP ist schon bekannt.[19–22] Sie soll mit Cu-K_α-Strahlung neu bestimmt werden. [LT4]

Metallalkoholate sind eine Gruppe von Chemikalien, die schon sehr lange bekannt sind. Sie werden häufig in Labor und Industrie verwendet.[23,24] Bereits Liebig beschrieb vor über 180 Jahren festes Natriumethanolat[25] (NaOEt). Die Kristallstruktur von NaOEt wurde allerdings erstaunlicherweise noch nicht publiziert. NaOEt soll synthetisiert und seine Kristallstruktur bestimmt werden. In der Literatur gibt es darüber hinaus Hinweise auf ein Solvat mit der Stöchiometrie NaOEt · 2 EtOH.[26,27] Auch dieses Solvat soll hergestellt, sowie nach weiteren Phasen und Solvaten gesucht werden. [LT5]

Andere Alkoholate, beispielsweise Natriumtertiäramylat, werden ebenfalls in industriellen Synthesen eingesetzt.[28] Dieses und weitere höhere Alkoholate sollen hergestellt und ihre Kristallstrukturen bestimmt werden. Auch hier soll nach Solvaten gesucht und deren Kristallstruktur bestimmt werden. Die Strukturen der Alkoholate und ihrer Solvate sollen untereinander verglichen werden. [LT6]

Verlackte Hydrazonpigmente sind seit mehr als 100 Jahren bekannt.[28] Heute gehören sie zu den wichtigsten Rotpigmenten. Sie werden weltweit unter anderem für den

Zeitungsdruck eingesetzt. Es ist bekannt, dass die Farbe unter anderem von der Hydratstufe abhängt.[29,30] Es ist entsprechend wichtig zu wissen, welche Hydratstufen existieren, unter welchen Bedingungen sie sich ineinander umwandeln und die Kristallstrukturen der einzelnen Phasen zu kennen. Umso erstaunlicher ist es, dass bisher die Kristallstrukturen der meisten verlackten Hydrazonpigmente nicht bekannt sind. Hierzu gehören Colour Index Pigment Red 52 (P.R.52, Abb. 1-9), dessen Isomer Pigment Red 48 (P.R.48, Abb. 1-7) und ihre Calcium- und Mangansalze. Diese Pigmente sollen synthetisiert und ihre stabilen Phasen und Hydratstufen gesucht werden. Die Kristallstrukturen sollen durch Einkristallröntgenstrukturanalyse oder Strukturbestimmung aus Pulverdaten bestimmt werden. Da viele dieser Pigmente mit Lösungsmitteln wie DMSO Solvate bilden, soll ebenfalls nach solchen gesucht und deren Kristallstruktur bestimmt werden. [LT7]

Außerdem soll das thermische Verhalten und die Phasenumwandlungen untersucht werden. Dies soll Ansatzpunkte für die weitere Forschung an anderen verlackten Hydrazonpigmenten liefern. [LT8]

Pigment Red 194 (P.R.194, Abb. 1-6) ist ein industrielles Perinon-Pigment.[28] Sein Isomer ist als Pigment Orange 43 (P.O.43, Abb. 1-8) registriert und kommerziell von größerem Interesse.[28] Die Kristallstrukturen beider Isomere sind bekannt.[31–33] In dieser Arbeit liegt der Fokus auf Zwischenprodukten, die seit mindestens 80 Jahren[34] hergestellt werden, von denen allerdings weder die Kristallstruktur noch die Molekülkonstitution bekannt sind. Diese Zwischenprodukte sind die „Trennsalze“. Die Synthese von Perinon liefert ein Isomerengemisch aus *cis*- und *trans*-Perinon (P.R.194 und P.O.43). Dieses Gemisch wird durch Reaktion (mit KOH/Ethanol) zu einem löslichen *cis*-Perinontrennsalz und einem schwerer löslichen *trans*-Perinontrennsalz getrennt. Von beiden Isomeren des Perinontrennsalzes sollen die Kristallstrukturen bestimmt werden. Das *cis*-Trennsalz soll dabei erstmalig als Festkörper hergestellt und untersucht werden. Die Kristallstrukturbestimmung soll mittels Pulverdiffraktometrie oder Einkristallröntgenbeugung erfolgen. [LT9]

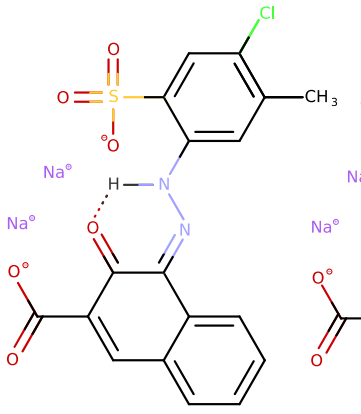

Abb. 1-9: P.R.52.

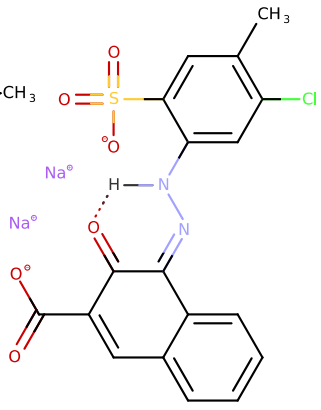

Abb. 1-7: P.R.48.

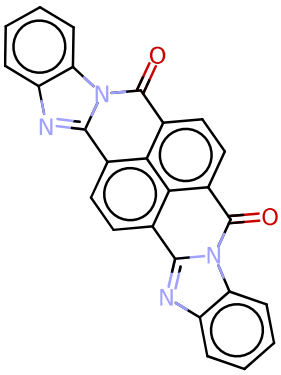

Abb. 1-6: P.R.194.

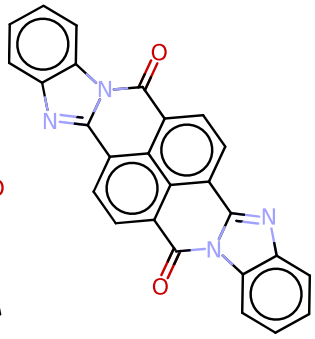

Abb. 1-8: P.O.43.

2 Projekte

2.1 Bestimmung der absoluten Konfiguration pharmazeutischer Wirkstoffe durch Röntgenpulverdiffraktometrie [Veröffentlichung LT1]

Bildung von diastereomeren Salzen und Strukturbestimmung aus Pulverdaten mit dem Ziel der Bestimmung der absoluten Konfiguration.

Die absolute Konfiguration einer Substanz wird heute meist aus Einkristallbeugungsdaten bestimmt. Sind keine ausreichend großen und guten Kristalle der Substanz verfügbar, muss eine Alternative gefunden werden.

Die Pulverdiffraktometrie ist eine solche Alternative. Die Strukturbestimmung aus Pulverdaten an einer chiralen Substanz liefert allerdings keine Informationen über deren absolute Konfiguration.[3,35]

Dieses Problem wurde durch Bildung von Salzen mit ebenfalls chiralen Salzbildnern gelöst. Saure (bzw. basische) chirale Wirkstoffe werden dazu mit ebenfalls chiralen Basen (oder Säuren) als Salz kristallisiert. Die relative Konfiguration der chiralen Substanz zur bekannten absoluten Konfiguration des Salzbildners lässt sich dann aus Pulverdaten bestimmen, wie an einigen Salzen von Beispielverbindungen gezeigt wurde.

Die Methode erwies sich als funktional. Die Ansatzgröße wurde minimiert. Bereits sehr kleine Substanzmengen waren ausreichend: Am Beispiel von (*R*)-Flurbiprofen und (*R*)-2-Phenylpropyl-1-amin wurde demonstriert, dass Ansätze mit je 50 µL einer 0,5 mM Lösung von Wirkstoff und Salzbildner ausreichend kristalline Pulver lieferten (Abb. 2-1). Die Kristallisation wurde dabei direkt in den Kapillaren für die Aufnahme der Pulverdiagramme durchgeführt.

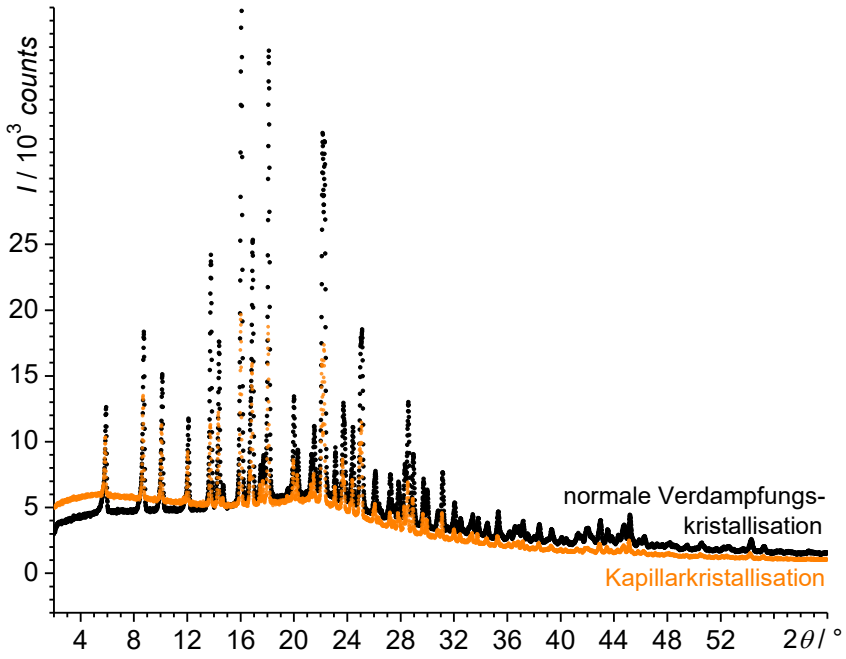

Abb. 2-1: Überlagerung der Pulverdiagramme (Langzeitaufnahmen in Kapillaren) einer Probe aus einer Verdampfungskristallisation üblicher Ansatzgröße (30 mg (*R*)-Flurbiprofen in 3 ml THF und 17 mg (*R*)-2-Phenylpropylamin in 1,7 ml THF, schwarz) und einer Kristallisation in einer Kapillare (orange).

Die direkte Kristallisation in der Kapillare wurde ursprünglich als Nachteil angesehen, da dabei Vorzugsorientierung auftreten kann, die sich nicht durch das sonst übliche Mörsern der Probe vor dem Abfüllen in Kapillaren zur Messung verringern lässt. Es zeigte sich, dass Vorzugsorientierung zumindest bei den untersuchten Proben nicht problematisch war. Berücksichtigung der Vorzugsorientierung rief keine signifikante Änderung der Anpassungsgüte hervor.

Eine Anwendung des Verfahrens zur Bestimmung der absoluten Konfiguration ist ebenfalls mit Cokristallen denkbar, was die Anwendbarkeit über Säuren und Basen hinaus erweitert.

[LT1]: C. Schlesinger, L. Tapmeyer, S. D. Gumbert, D. Prill, M. Bolte, M. U. Schmidt & C. Saal: *Absolute Configuration of Pharmaceutical Research Compounds Determined by X-ray Powder Diffraction*, Angew. Chem. Int. Ed. **2018**, 57, 9150-9153, DOI: 10.1002/anie.201713168.

Ebenfalls erschienen in einer deutschen Version:

C. Schlesinger, L. Tapmeyer, S. D. Gumbert, D. Prill, M. Bolte, M. U. Schmidt & C. Saal: *Bestimmung der absoluten Konfiguration pharmazeutischer Wirkstoffe durch Röntgenpulverdiffraktometrie*, Angew. Chem. **2018**, 130, 9289-9293, DOI: 10.1002/ange.201713168.

2.2 Kristallstruktur von 6-Amino-2-iminiumyl-4-oxo-1,2,3,4-tetrahydropyrimidin-5-aminiumsulfat Monohydrat (Vorprodukt von Leukopterin) [LT2]

Kristallisation und Einkristallstrukturbestimmung eines Edukts der Synthese von Leukopterin.

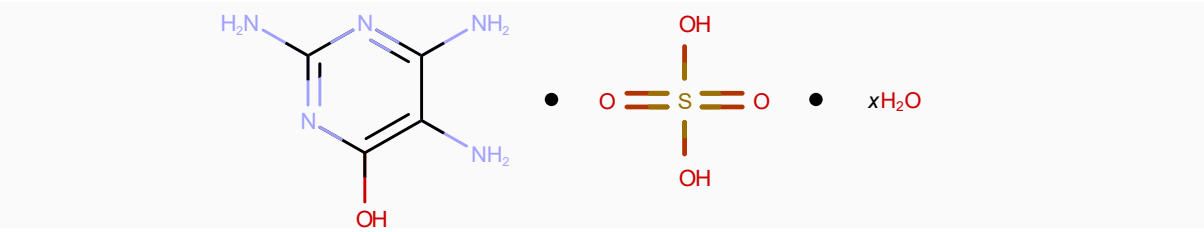

Abb. 2-2: Strukturformel von „2,4,5-Triamino-6-hydroxypyrimidinsulfat“ laut Produktbeschreibung.

Kristallstrukturen werden routinemäßig aus Röntgenbeugungsdaten von Einkristallen gelöst.[35] Sind keine Einkristalle einer Substanz verfügbar, werden Röntgenbeugungsdaten von Pulvern verwendet. Dafür müssen die Pulver gut kristallin sein.[3] Sind keine gut kristallinen Pulver einer Substanz verfügbar, kann auf die Analyse der Paarverteilungsfunktion (*Pair Distribution Function*, *PDF*) zurückgegriffen werden.[7,9]

Die Methode der Strukturaufklärung aus *PDF*-Daten befindet sich derzeit in Entwicklung. Der Arbeitskreis Schmidt hat maßgeblichen Anteil an dieser Entwicklung.

Für die *PDF*-Methodenentwicklung wurde ein kleines, starres Molekül mit bisher unbekannter Kristallstruktur gesucht. Ein solches Molekül ist das Leukopterin ($C_6H_5N_5O_3$, Abb. 2-3). Es konnte zwar nicht kommerziell bezogen werden, allerdings ist seine Synthese lange bekannt und relativ einfach.[12]

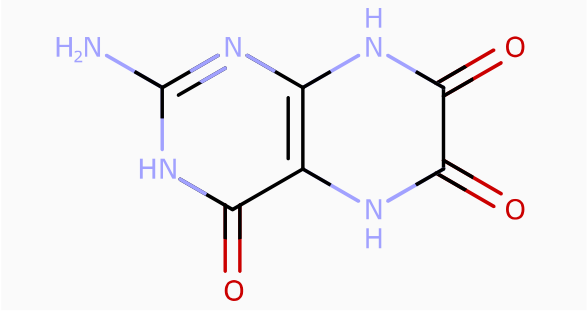

Abb. 2-3: Strukturformel von Leukopterin.

Zur Synthese wurde auf die Route nach Purrmann zurückgegriffen, die seit 1940 bekannt ist.[12] Leukopterin wird dabei durch gemeinsames Erhitzen von Oxalsäure und 2,4,5-Triamino-6-hydroxypyrimidin erhalten (Abb. 2-4). Die Struktur dieses Edukts ist bekannt und unter dem Namen „5-Amminium-6-amino-isocytosinium-sulfat“ mit dem Referenzcode HACDEU in der *CSD* zu finden.[15]

Das kommerziell bezogene „2,4,5-Triamino-6-hydroxypyrimidinsulfat“ (Abb. 2-2) wurde vor der Synthese röntgenografisch untersucht. Dabei wurde neben der

bekannten Phase des 2,4,5-Triamino-6-hydroxypyrimidinsulfates ein signifikanter Anteil Fremdphase gefunden.

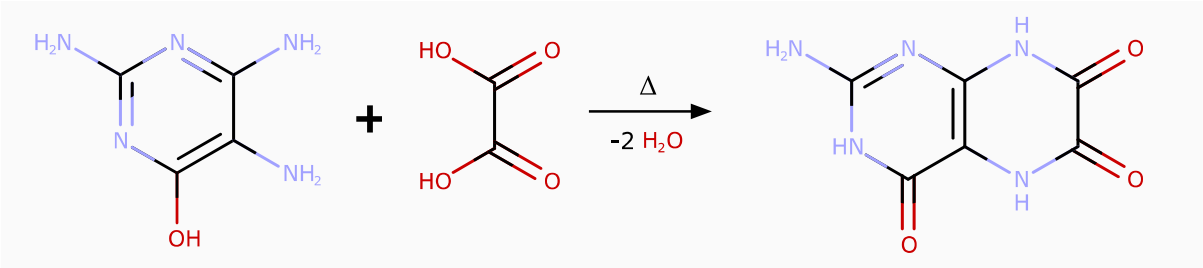

Abb. 2-4: Synthese von Leukopterin nach Purrmann.[12]

Durch Fällung mit verdünnter H_2SO_4 aus Lösung in 0,5 M NaOH konnte die unbekannte Phase rein und gut kristallin erhalten werden.

Die Röntgenstrukturanalyse identifizierte die neue Phase als 6-Amino-2-iminiumyl-4-oxo-1,2,3,4-tetrahydropyrimidin-5-aminiumsulfat Monohydrat (Abb. 2-5), also als ein Monohydrat des Sulfates des zweifach positiv geladenen 2,4,5-Triamino-6-hydroxypyrimidiniums. Diese Struktur war bisher nicht bekannt und wurde veröffentlicht (ORTEP des Moleküls in Abb. 2-5). [LT2]

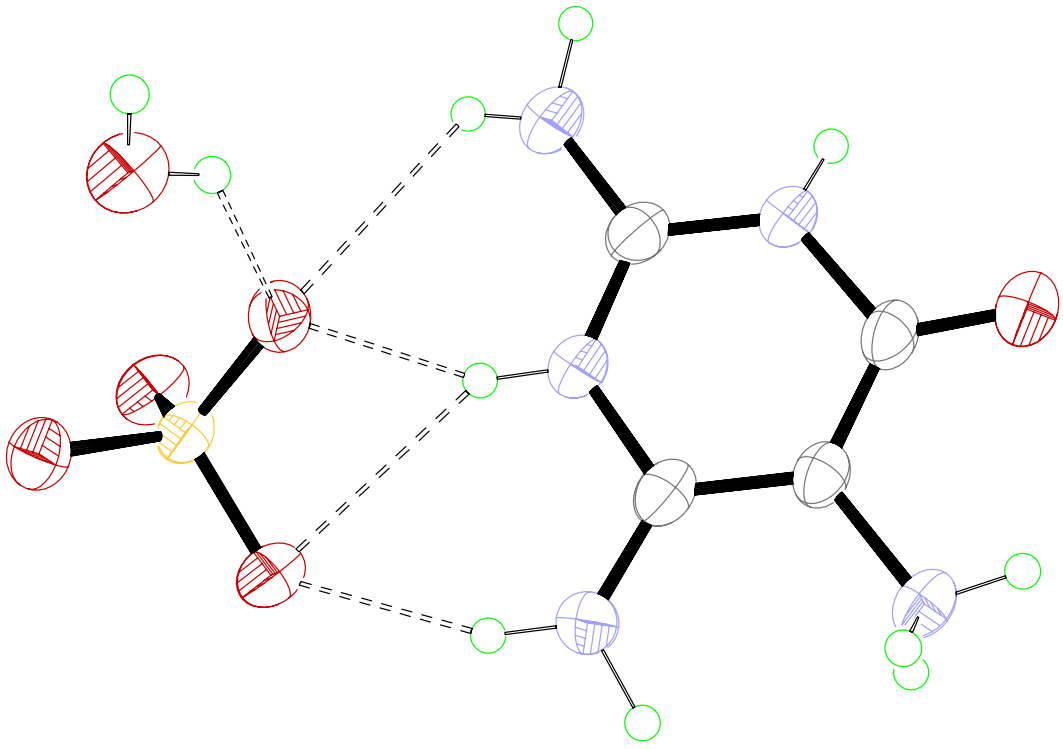

Abb. 2-5: ORTEP (50 % Aufenthaltswahrscheinlichkeit) der Struktur von 6-Amino-2-iminiumyl-4-oxo-1,2,3,4-tetrahydropyrimidin-5-aminiumsulfat Monohydrat mit Darstellung der Wasserstoffbrückenbindungen zwischen den Molekülen in der asymmetrischen Einheit.

[LT2]: L. Tapmeyer & D. Prill: *6-Amino-2-iminiumyl-4-oxo-1,2,3,4-tetrahydropyrimidin-5-aminium sulfate monohydrate*, IUCrData **2019**, 4, 1915747,
DOI: 10.1107/S2414314619006898.

2.3 Kristallstruktur von 1,1,3,3-Tetraethyl-5-nitroisoindolin (TENI) [LT3]

Zwei Einkristallstrukturanalysen und Identifikation eines Nebenprodukts.

Die Verbindung 1,1,3,3-Tetraethyl-5-nitroisoindolin (TENI, $C_{16}H_{24}N_2O_2$, Abb. 2-6) wurde in der Literatur bisher meist als gelbes Öl beschrieben und offenbar nie als Einkristall erhalten. Als Vorstufe eines Spinlabels wurde die Verbindung recht ausgiebig untersucht.[17,36] Die sorgfältige Synthese dieser Verbindung durch Jörn Plackmeyer[37] ergab ein Produkt, das bei Lagerung im Kühlschrank bei 4 °C gelbe Kristalle bildete. Diese Kristalle erwiesen sich als auch bei Raumtemperatur stabil. Es konnte ein Schmelzpunkt von 24 bis 25 °C bestimmt werden.

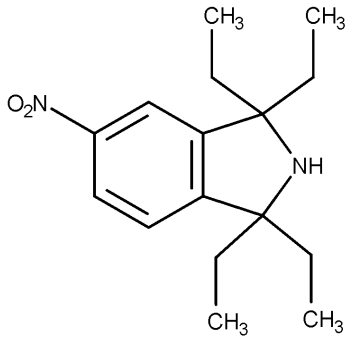

Abb. 2-6: 1,1,3,3-Tetraethyl-5-nitroisoindolin.

Die Einkristallstrukturbestimmung (bei -100 °C) an diesen Kristallen verlief problemlos und die Struktur konnte gelöst und verfeinert werden (*CSD*-Referenzcode: RUCJOR).[37]

Der Isoindolinring erwies sich als planar. Im Kristall sind die Isoindolinringe in Ebenen angeordnet. Die Ethylsubstituenten befinden sich als Abstandshalter zwischen diesen Ebenen. In Zusammenwirkung mit einer stark verlängerten N–H···O Wasserstoffbrückenbindung ($d_{H\cdots A}$ = 2,636(16) Å, vgl. Tabelle 2-1 und Abb. 2-7, links) erklärt dies den niedrigen Schmelzpunkt der Substanz von 24,5(10) °C. Die Wasserstoffbrücke ist lang – auch in Anbetracht der Tatsache, dass R-NO_2-Gruppen generell schlechte H-Brücken-Akzeptoren sind. Die einzigen weiteren intermolekularen Interaktionen, sind Dipol-Dipol-Interaktion und dispersive Wechselwirkungen wie die C–H···π-Kontakte zwischen dem aromatischen Ring und den Ethylgruppen der jeweils nächsten Schicht.

Tabelle 2-1: Geometrie der einzigen $D^1_1(8)$ Wasserstoffbrücke[38,39] in der Kristallstruktur von TENI im Vergleich mit *CSD*-Daten[40]. Abgesehen von dieser Interaktion gibt es in der Struktur nur schwache C–H···π- und Dispersionswechselwirkungen. D: Donor, A: Akzeptor und H: Wasserstoffatom.

D–H···A	d_{D-H} / Å	$d_{H\cdots A}$ / Å	$d_{D\cdots A}$ / Å	∢$_{D-H\cdots A}$ / °
N2–H2···O81	0,865(15)	2,634(16)	3,4860(18)	168,4(16)
CSD-Durchschnitt* [N–H···O]	-	2,1(2)	2,87(11)	-
CSD-Durchschnitt* [$(C-)_2$N–H···O(-NOR)]	-	2,28(19)	2,96(8)	-

*Suchfragment in eckigen Klammern. *CSD*-Version 5.40, Stand der Updates: August 2019.

Eine erneute, mutmaßlich gleich durchgeführte Synthese der Substanz lieferte ein gut kristallines und überraschenderweise nicht leicht schmelzendes Pulver (Röntgen-pulverdiagramm in Abb. 2-7, rechts). Nach *NMR*-Daten (in Lösung) handelte es sich um TENI, was allerdings durch den offenkundig höheren Schmelzpunkt und das stark abweichende Pulverdiagramm (Abb. 2-7, rechts) höchst zweifelhaft erschien. Da keine Einkristalle der Substanz hergestellt werden konnten, wurde das Pulverdiagramm näher untersucht.

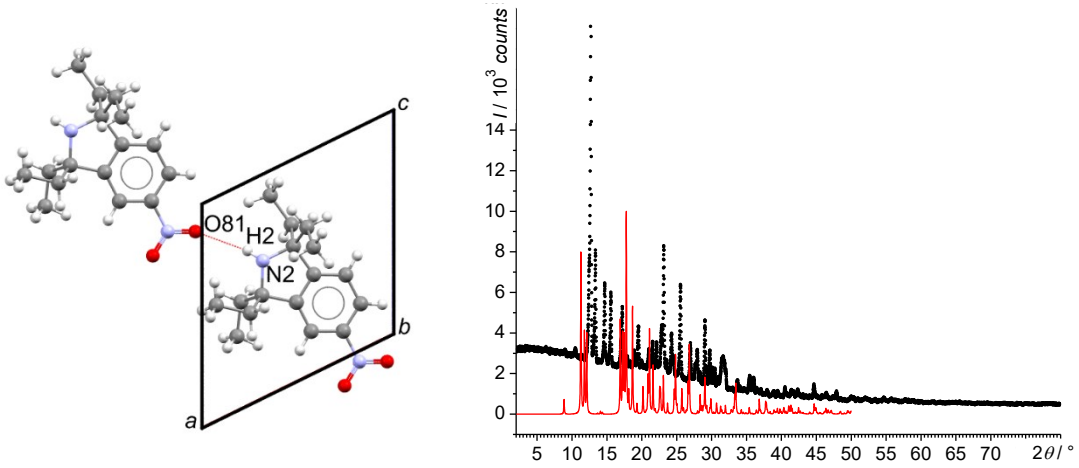

Abb. 2-7: Links: Elementarzelle mit asymmetrischer Einheit und einer Symmetriekopie aus der Kristallstruktur (RUCJOR) von TENI mit Blick entlang der *b*-Achse mit Benennung der an der Bildung der $D^1_1(8)$ Wasserstoffbrücke (rot gepunktete Linie) beteiligten Atome. Rechts: Pulverdiagramme von TENI (simuliert, unten, rote Linie) und seinem als Pulver angefallenen Salz (oben, schwarze Punkte).

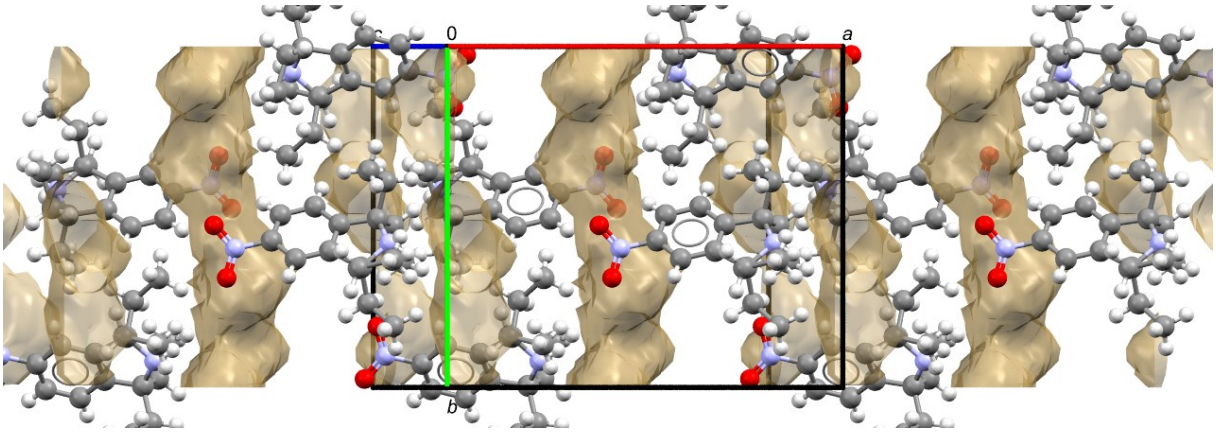

Abb. 2-8: Ausschnitt aus der Strukturlösung des Pulvers höheren Schmelzpunktes mit TENI als Strukturmodell. Lücken im Kristall sind gelbbraun hervorgehoben. Blick entgegen *c**.

Aus den neuen Pulverdaten konnte eine monokline Zelle (a = 13,26 Å, b = 8,691 Å, c = 14,95 Å, β = 103,9°; $P\,2_1/n$ mit Z = 4) bestimmt werden. Ein Strukturlösungsversuch mit TENI als Startmodell lieferte eine Struktur, die TENI als Gerüst enthält und deutliche Poren aufweist (vgl. Abb. 2-8). In den Poren befinden sich höchstwahrscheinlich Sulfat-Ionen. Die Existenz von Sulfationen in der Struktur ist plausibel, da die Synthese in Schwefelsäure durchgeführt wird und Sulfat gut zum erwarteten[41] und gefundenen Zellvolumen passt (vgl. Tabelle 2-2). Eine Verfeinerung mit einem halben SO_4^{2-} pro organischem Kation war signifikant besser als alle anderen Modelle.

NMR-Spektren konnten prinzipbedingt keine weiteren Erkenntnisse liefern. Ein Umsetzen der Substanz mit Natronlauge ergab erneut TENI als gelbes Öl. Somit war der Verbleib eines Großteiles der Ausbeute an TENI und die Identität der Substanz aufgeklärt und die Bemühungen wurden an dieser Stelle eingestellt. Auf Grund der schlechten Datenqualität wurde keine Struktur publiziert.

Tabelle 2-2: Volumina[41] möglicher Zusammensetzungen des hergestellten Pulvers.

Zusammensetzung (Z = 4)	Volumen / Å³	Unerklärtes Volumen / Å³
Experimentell	**1674,13**	**-**
TENI, $C_{16}H_{24}N_2O_2$*	1531,43	142,7
½ NO_3^- + TENI!	1623,37	50,76
½ NO_3^- + TENI + ½ H_2O!	1666,47	7,66
½ SO_4^{2-} + TENI	**1672,95**	**1,18**
½ NO_3^- + TENI + H_2O!	1709,57	-35,44
NO_3^- + TENI	1715,31	-41,18
½ SO_4^{2-} + TENI + ½ H_2O	1716,05	-41,92
NO_3^- + TENI + ½ H_2O	1758,41	-84,28
½ SO_4^{2-} + TENI + H_2O	1759,15	-85,02
NO_3^- + TENI + H_2O	1801,51	-127,38
SO_4^{2-} + TENI!	1814,47	-140,34

* Volumen aus Kristallstruktur RUCJOR ! unplausibel aus Gründen der Ionenladung

Darüber hinaus wurde ein Derivat der Verbindung, das 1,1,3,3-Tetraethyl-5-nitroisoindolin-2-oxyl (TENO, $C_{16}H_{23}N_2O_3$, Abb. 2-9) untersucht. Von dieser Substanz wurden Einkristalle erhalten. Die Röntgenstrukturanalyse verlief erfolgreich (s. Tabelle 2-3 und Abb. 2-10). Der Schmelzpunkt von TENO liegt höher, obwohl keine Wasserstoffbrücke ausgebildet wird. Dafür ist die Dichte dieser Substanz höher, was erneut auf interessante Struktur-Eigenschafts-Beziehungen hinweist. Eine Veröffentlichung dieser Ergebnisse steht aus.

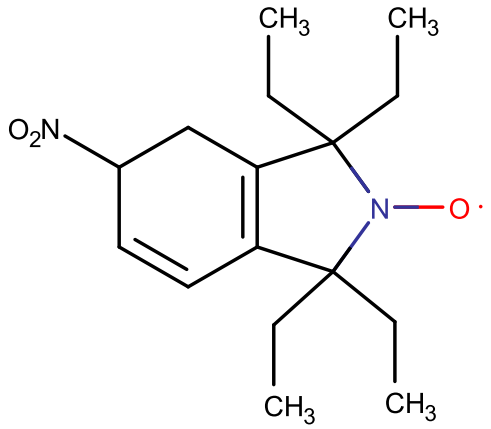

Abb. 2-9: 1,1,3,3-Tetraethyl-5-nitroisoindolin-2-oxyl.

Tabelle 2-3: Kristallographische Daten der Struktur von TENO.

a	11,224(2)
b	11,445(2)
c / Å	13,129(3)
β / °	106,44(3)
V / Å³	1617,7(6)
Raumgruppe	*P* $2_1/n$
Z, *Z'*	4, 1
T / K	173(2)
λ / Å	1,54178
GooF	1,22
R_{int}	0,076
R[F2 > 2σ(F2)]	0,136
wR(F2)	0,249

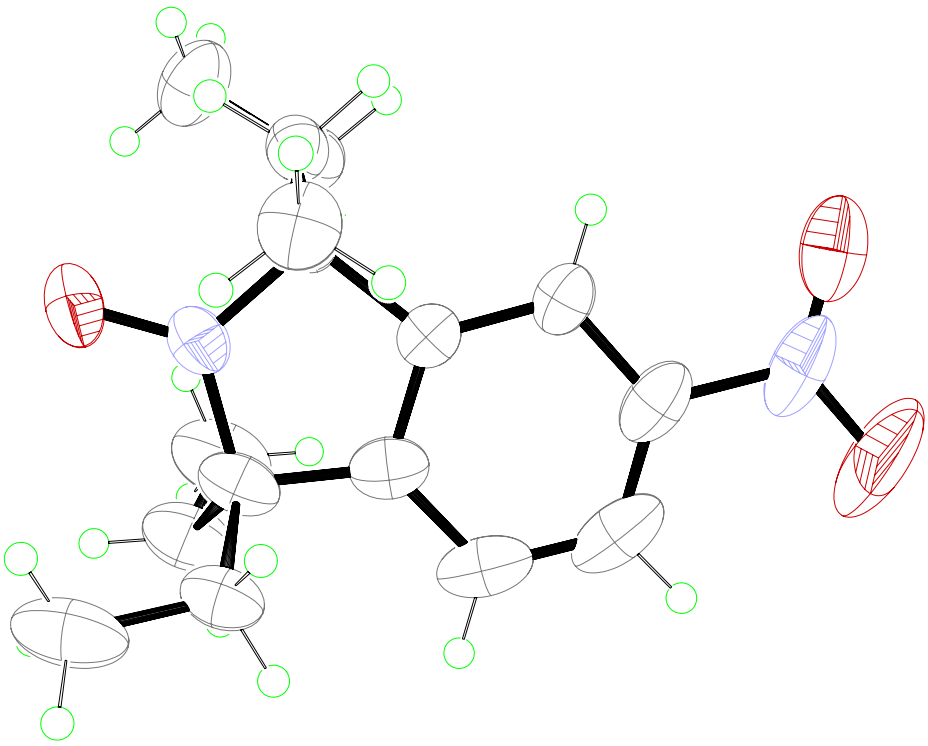

Abb. 2-10: ORTEP von TENO. Minderbesetzte Fehlordnung nicht dargestellt.

[LT3]: L. Tapmeyer, M. Beske & J. Plackmeyer: *1,1,3,3-Tetraethyl-5-nitroisoindoline*, IUCrData **2019**, 4, CCDC reference: 1969794, DOI: 10.1107/S2414314619016298.

2.4 Kristallstruktur von 4-Amino-2,6-dimethylpyrimidin (ADMP) [LT4]

Eine Synthese und Einkristallstrukturanalyse.

4-Amino-2,6-dimethylpyrimidin (ADMP) entsteht bei der Trimerisierung von Acetonitril in Gegenwart von starken Basen. Die Reaktion, die hier zu ADMP führte, war die Umkristallisation von Natriumisopropanolat (NaO^{i}Pr) in Acetonitril. Auf der Suche nach einem geeigneten Weg zur Herstellung von Einkristallen von NaO^{i}Pr wurden etliche Lösungsmittel ohne Ansehen eventueller Kompatibilitätsprobleme verwendet. Der Versuch der Umkristallisation in Acetonitril (vgl. Abb. 2-11) erwies sich als modifizierte Synthese von ADMP nach Schmidt (1902 publiziert).[18]

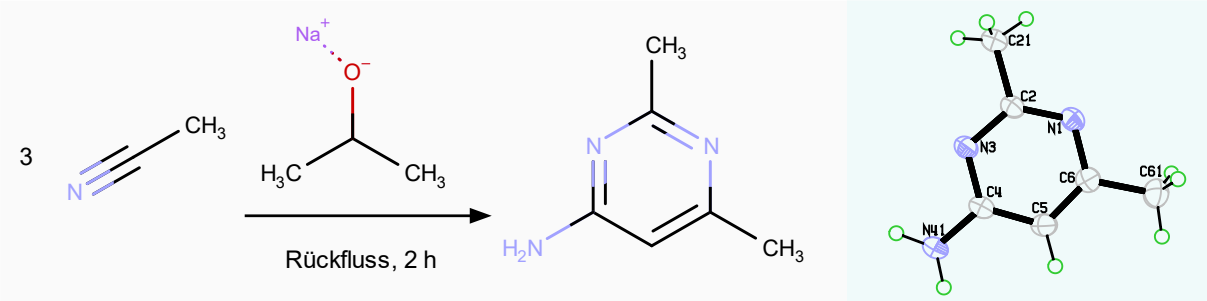

Abb. 2-11: Synthese von ADMP aus MeCN unter Katalyse durch NaO^{i}Pr (links) sowie *ORTEP* der bestimmten Struktur.

Da in der Veröffentlichung LT4 die Synthese nicht im Detail beschrieben wird, ist hier die Synthesevorschrift angegeben.

Acetonitril wurde unter Argon über Phosphorpentoxid getrocknet. 20 ml frisch destilliertes Acetonitril wurden unter Argonatmosphäre mit 0,2 g trockenem NaO^{i}Pr versetzt. Die Suspension wurde unter Auflösung des Feststoffes für zwei Stunden zum Rückfluss erhitzt. Die Lösung wurde im verschlossenen Schlenkkolben über 48 Stunden bei 4 °C im Kühlschrank gelagert. Große, farblose, block- bis nadelförmige Einkristalle konnten der Lösung entnommen werden, die sich als Kristalle von ADMP erwiesen.

Die Struktur von ADMP war bereits bekannt (*CSD*-Referenzcodes: FAGSUB*nn*[19–22]), ebenso wie ein vergleichbarer Syntheseweg,[18] weshalb die Neubestimmung der Struktur mit Cu-K_α-Strahlung bei 173 K mit dem Referenzcode FAGSUB05 in der *CSD* veröffentlicht wurde.[LT4]

[LT4]: CCDC 1975913: Experimental Crystal Structure Determination, *CSD Communication* **2020**, DOI: 10.5517/ccdc.csd.cc24b34r.

2.5 Natriumethanolat (NaOEt) [LT5]

Synthese, Kristallisation, Phasenanalyse und Kristallstrukturaufklärung aus Pulverdaten von NaOEt und Einkristallstrukturanalyse von NaOEt · 2 EtOH.

Natriumethanolat ist eine seit mindestens 1837 bekannte Standardchemikalie.[25] Verdampfungskristallisationen bei vermindertem Druck aus einer Lösung von $NaOC_2H_5$ in Ethanol lieferten zunächst einen zerfließlichen, weißen Feststoff. Weitere Trocknung lieferte ein unter Schutzgas stabiles Pulver, das röntgenografisch als Mischung von (mindestens) zwei Phasen identifiziert wurde.

Die beiden Phasen konnten isoliert und identifiziert werden. Es handelte sich um solvensfreies Natriumethanolat und Natriumethanolat-Diethanolsolvat.

Natriumethanolat-Diethanolsolvat konnte als Einkristall erhalten werden. Die Kristallstruktur des Disolvates wurde aus Einkristallbeugungsdaten bestimmt.[LT5]

Die Kristallstruktur des Ansolvats wurde aus Pulverdaten bestimmt. Dabei erwies sich die Bestimmung der Raumgruppe als Herausforderung. Sowohl in *P* 4/*n m m* als auch in *P* $\bar{4}$ 2_1 *m* ließen sich die Strukturmodelle gut verfeinern (Abb. 2-12).[LT5]

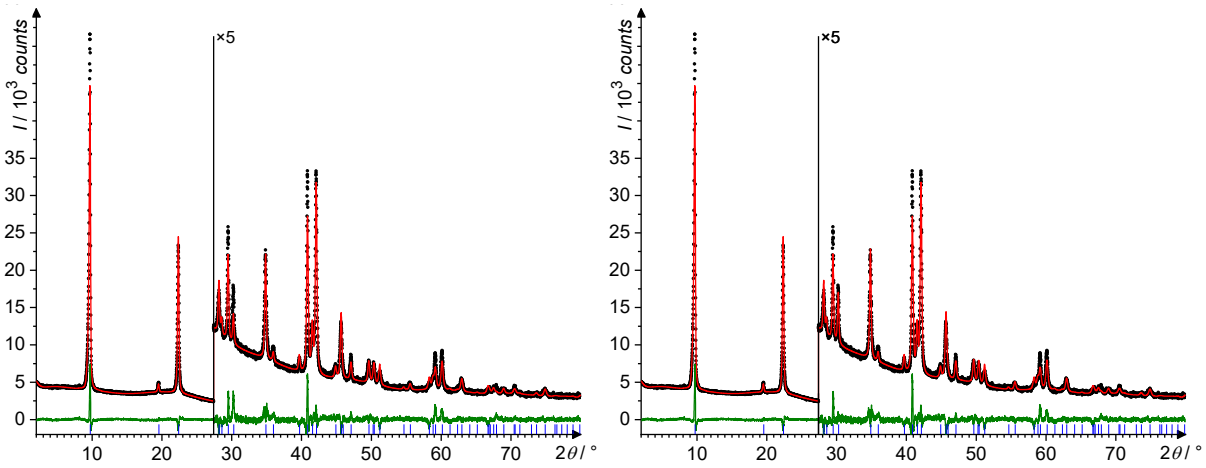

Abb. 2-12: Rietveldplots von NaOEt in den Raumgruppen *P* 4/*n m m* (links) und *P* $\bar{4}$ 2_1 *m* (rechts).

Die endgültige Raumgruppe wurde durch Aufstellen eines Bärnighausen-Baumes hergeleitet. Details dazu finden sich in der Veröffentlichung LT6. Es gab schwache Hinweise auf die Raumgruppe *P* $\bar{4}$ 2_1 *m*. NaOEt kristallisiert in einer Anti-PbO-Struktur und NaOEt · 2 EtOH in einer Kettenstruktur.

[LT5]: M. Beske, L. Tapmeyer & M. U. Schmidt: *Crystal structure of sodium ethoxide (C_2H_5ONa), unravelled after 180 years*, Chem. Comm. **2020**, 56, 3520-3523, DOI: 10.1039/C9CC08907A.

2.6 Höhere Natriumalkoholate (NaOR) [LT6]

Synthese, Kristallisation, Phasenanalyse und Kristallstrukturaufklärung aus Pulverdaten von Natrium-n-propanolat, Na-n-butanolat und Na-n-amylat und Einkristallstrukturbestimmung von Solvaten von NaO^{n}Pr, NaO^{i}Pr und NaO^{t}Am.

Nach der Aufklärung der Kristallstruktur von Natriumethanolat [LT5] wurden die Natriumalkoholate höherer Alkanole untersucht (NaO^{n}Pr, NaO^{n}Bu und NaO^{n}Am; Am = Amylat). Die Strukturen der Ansolvate ließen sich aus Pulverdaten bestimmen. Die höheren *n*-Alkoholat-Ansolvate kristallisieren in der Raumgruppe $P\,4/n\,m\,m$, während für Natriumethanolat die Raumgruppe $P\,\bar{4}\,2_1\,m$ bestimmt wurde. Das literaturbekannte[42] NaOMe kristallisiert ebenfalls in $P\,4/n\,m\,m$.

Die andere Raumgruppe beim NaOEt lässt sich durch den sterischen Anspruch der fehlgeordneten Alkylreste erklären, die auf einer 4-zähligen ($P\,4/n\,m\,m$) bzw. 2-zähligen Achse ($P\,\bar{4}\,2_1\,m$) liegen. Die Methylgruppen sind sphärisch, während NaOEt eher eine in einer Ebene verzerrte Anordnung der Ethylreste aufweist (Abb. 2-13). Die höheren Alkylreste sind durch Libration und Fehlordnung quasi-zylindrisch.

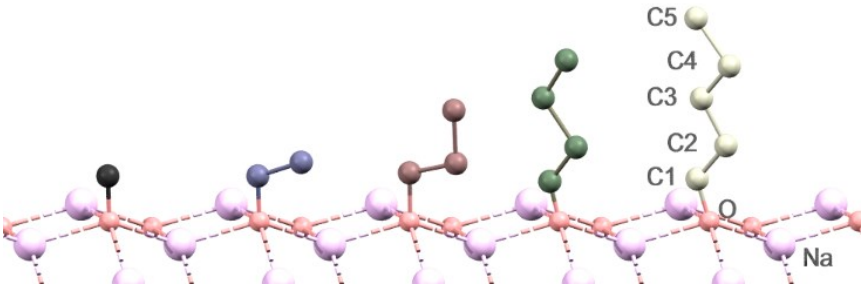

Abb. 2-13: Gemeinsame, vereinfachte Darstellung der Natriumalkoholate (von links nach rechts) NaOMe, NaOEt, NaO^{n}Pr, NaO^{n}Bu und NaO^{n}Am auf ihrem gemeinsamen Strukturmotiv: dem Na-O-Gitter. Die genaue Konformation der Kohlenstoffketten ist, basierend auf den vorliegenden Daten, nicht signifikant.

Die Platzierung der sphärischen oder zylindrischen Gruppen auf einer vierzähligen Achse ist günstig. Bei NaOEt ist dies nicht der Fall. Die geringere Fehlordnung von NaOEt in $P\,\bar{4}\,2_1\,m$ führt zu einer besseren Packung. Dies erklärt die um etwa 4 % höhere Dichte der Struktur (Abb. 2-14).[43]

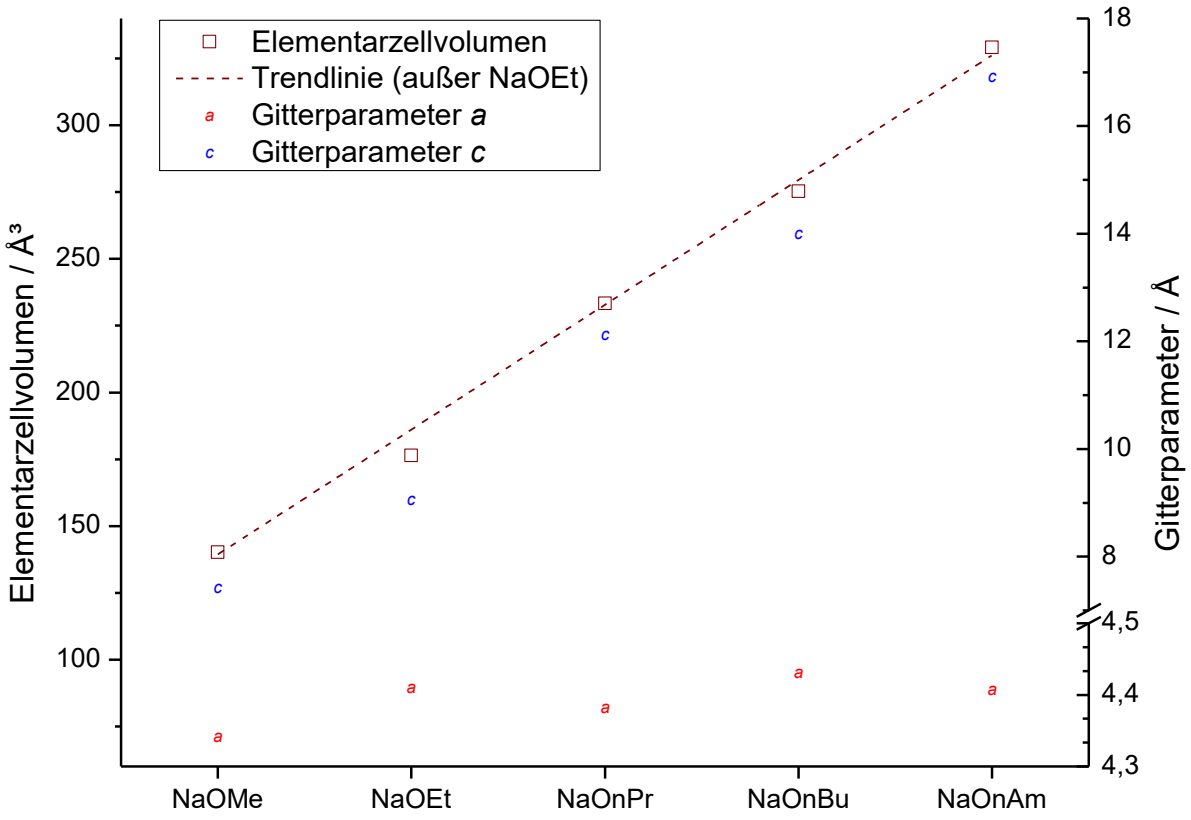

Abb. 2-14: Vergleich einiger Parameter der Strukturen von NaOMe, NaOEt, NaO^{n}Pr, NaO^{n}Bu und NaO^{n}Am. Linke Skala: Elementarzellvolumen (dunkelrot). Trend des Elementarzellvolumens unter Ausschluss von NaOEt (gestrichelte Linie). Rechte Skala: Gitterparameter *a* (rot) und *c* (blau).

Darüber hinaus konnten Einkristalle diverser Solvate hergestellt werden, aus denen die Strukturen von NaO^{n}Pr · 2 HO^{n}Pr, NaO^{i}Pr · 5 HO^{i}Pr und NaO^{t}Am · HO^{t}Am bestimmt werden konnten. Dabei zeigte sich eine mit zunehmender Kettenlänge abnehmende Stabilität der Kristalle. Außerdem zeigte das Wasserstoffbrückenbindungsmuster von NaO^{i}Pr · 5 HO^{i}Pr wenig Ähnlichkeit zu dem in festem Isopropanol. Die Wasserstoffbrückenbindungsmotive des NaO^{i}Pr · 5 HO^{i}Pr sind vielmehr ein plausibles Modell für die Situation in flüssigem Isopropanol.

[LT6]: M. Beske, S. Cronje, M. U. Schmidt & L. Tapmeyer: *Disordered sodium alkoxides from powder data: Crystal structures of sodium ethoxide, propoxide, butoxide, and pentoxide, and some of their solvates*, Acta Cryst. B **2020**, 77, 68-82, DOI: 10.1107/S205252062001584X.

2.7 Pigment Red 52 – Mononatriumsalz: Kristallstruktur des DMSO-Monosolvat-Monohydrates [LT7]

Synthese und Einkristallstrukturanalyse.

Colour Index Pigment Red 52 (P.R.52 $[C_{18}H_{11}ClN_2O_6S]Na_2$, Abb. 2-15, links) und seine Derivate sind kommerziell verwendete Rotpigmente aus der Gruppe der Monohydrazonpigmente. Besondere Bedeutung hat das Calciumsalz Pigment Red 52:1 (P.R.52:1, $[C_{18}H_{11}ClN_2O_6S]Ca$, Abb. 2-15, Mitte). Die Kristallstrukturen des P.R.52 und aller seiner Derivate sind bisher unbekannt.

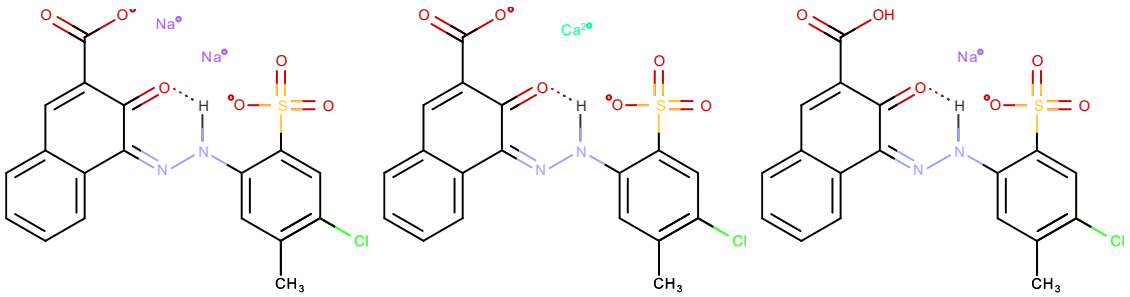

Abb. 2-15: Links: Pigment Red 52. Mitte: Pigment Red 52:1 Rechts: Pigment Red 52 Mononatriumsalz.

Um die Struktur von P.R.52 aufzuklären, wurde dieses synthetisiert. Die Kristallinität des erhaltenen Pulvers sollte durch diverse Umkristallisations- und Suspensionsversuche verbessert werden. Dabei wurde unter anderem DMSO als Lösungsmittel eingesetzt. Aus dieser Lösung des P.R.52 in DMSO konnten nach Verdampfungskristallisation Einkristalle gewonnen werden. Diese erweisen sich bei der Röntgenstrukturanalyse als DMSO-Monosolvat-Monohydrat des Mononatriumsalzes (Abb. 2-15, rechts) des Pigment Red 52 ($[C_{18}H_{12}ClN_2O_6S]Na \cdot H_2O \cdot DMSO$, Abb. 2-16).[LT7]

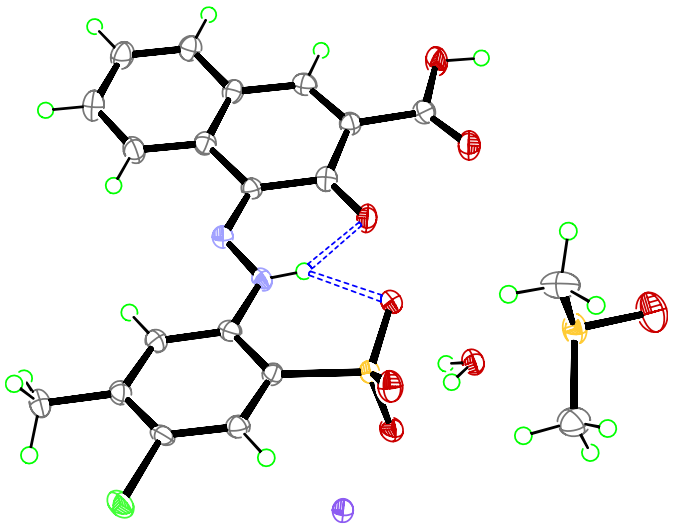

Die Kristallstruktur diente als Ausgangspunkt für die Strukturbestimmung von Pigment Red 52 und Pigment Red 52:1 aus Pulverdaten (Veröffentlichung in Vorbereitung).

Abb. 2-16: ORTEP der Struktur von P.R.52 Mononatriumsalz DMSO-Monosolvat-Monohydrat.

[LT7]: L. Tapmeyer, D. Eisenbeil, M. Bolte & M. U. Schmidt: *First crystal structure of a Pigment Red 52 compound: DMSO solvate hydrate of the monosodium salt*, Acta Cryst. E **2021**, 77, 402-405, DOI: 10.1107/S2056989021002577.

2.8 Pigment Red 48 – Mononatriumsalz: Kristallstrukturen von zwei Hydratstufen [LT8]

Synthese und Einkristallstrukturanalyse von zwei Hydratstufen und Analyse des thermischen Phasenverhaltens.

Colour Index Pigment Red 48 (P.R.48, $[C_{18}H_{11}ClN_2O_6S]Na_2$, Abb. 2-17, links) und seine Derivate sind kommerziell verwendete Rotpigmente aus der Gruppe der Monohydrazonpigmente. Pigment Red 48 ist ein Isomer von Pigment Red 52. Besondere Bedeutung hat das Calciumsalz Pigment Red 48:2 (P.R.48, $[C_{18}H_{11}ClN_2O_6S]Ca$, Abb. 2-17, Mitte).

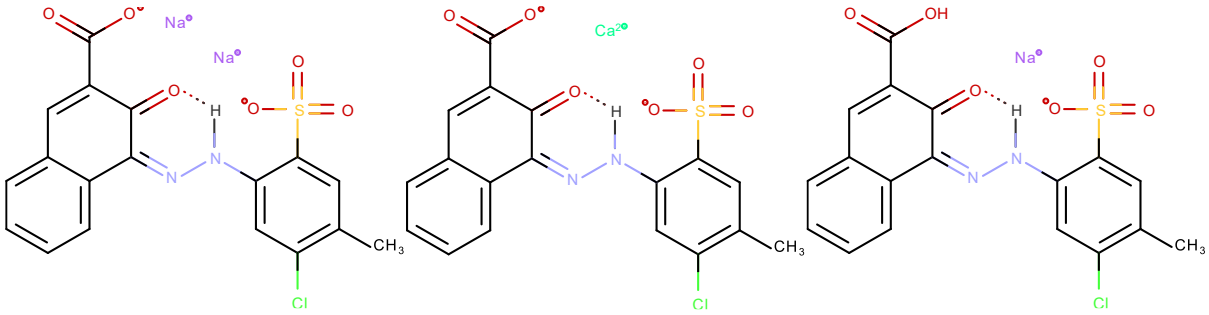

Abb. 2-17: Links: Pigment Red 48. Mitte: Pigment Red 48:2. Rechts: Pigment Red 48 Mononatriumsalz.

Diese Pigmente werden seit Anfang des 20. Jahrhunderts hergestellt.[28,44] Seither gibt es regelmäßig Beiträge zu verbesserten Synthesen, Derivaten und Struktur-Eigenschafts-Beziehungen.[29,30,45,46]

Die Kristallstrukturen des P.R.48 und all seiner Derivate sind bisher unbekannt. Generell sind bisher erst wenige Kristallstrukturen verlackter Hydrazonpigmente bekannt.[29,30,47]

Um die Struktur von P.R.48 aufzuklären, wurde dieses synthetisiert. Das erhaltene Pulver sollte durch diverse Umkristallisationsversuche und Suspensionsversuche in seiner Kristallinität verbessert werden.

Aus einer Suspension in Essigsäure wurde ein Pulver gewonnen, das im Pulverdiagramm Abweichungen zu dem Diagramm von P.R.48 zeigte. Bei Lagerung an Luft wurden erneut Abweichungen festgestellt, die auf eine weitere Phase hinwiesen.

Von zwei neuen Phasen konnten Einkristalle erhalten und die jeweilige Kristallstruktur aus Röntgenbeugungsdaten aufgeklärt werden.

Bei der ersten gefundenen Phase handelt es sich um das Monohydrat des Mononatriumsalzes von P.R.48 ($[C_{18}H_{12}ClN_2O_6S]Na \cdot H_2O$, Abb. 2-17, rechts).[LT8]

Diese Phase erwies sich bei Raumtemperatur als metastabil. Längere Lagerung an Luft liefert die zweite Phase, das Dihydrat des Mononatriumsalzes. Auch von dieser Phase konnte die Struktur aus Beugungsdaten bestimmt werden.[LT8]

Eine dritte Phase trat beim Erwärmen der Proben auf (Abb. 2-18), bei der es sich möglicherweise um das Anhydrat handelt. Die Kristallstruktur dieser Phase konnte nicht bestimmt werden. Es konnten keine Einkristalle hergestellt werden. Die Pulverdaten konnten bisher nicht sinnvoll indiziert werden. Es ist nicht auszuschließen, dass es sich um ein Phasengemisch handelt.

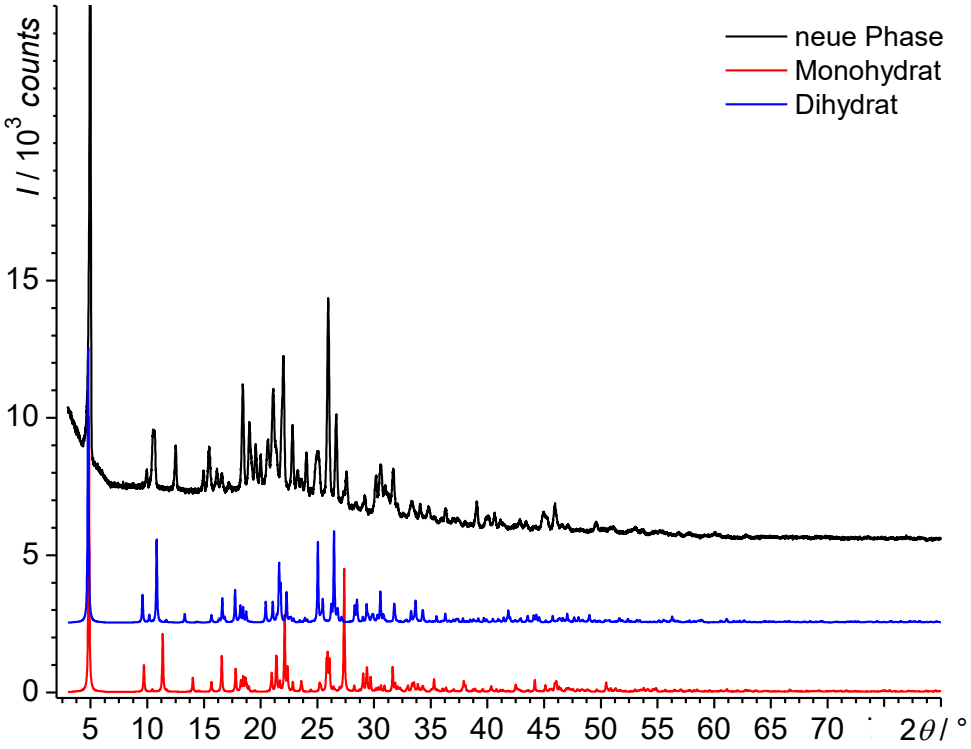

Abb. 2-18: Pulverdiagramm der dritten Phase (schwarz, oben) und simulierte Pulverdiagramme des Dihydrats (blau, Mitte) und des Monohydrats (rot, unten). Alle Proben bei Raumtemperatur.

[LT8]: L. Tapmeyer, S. Hill, M. Bolte & W. M. Hützler: *Two monosodium salt hydrates of Colour Index Pigment Red 48*, Acta Cryst. C **2020**, 76, 716-722,
DOI: 10.1107/S2053229620008530.

2.9 Perinontrennsalz [LT9]

Strukturaufklärung von drei industriellen Zwischenprodukten. Synthese, Kristallisation und Einkristallstrukturbestimmung, kombiniert mit weiteren Methoden.

In der chemischen Industrie werden viele Substanzen hergestellt. Einige davon werden im gleichen Werk wieder umgesetzt. Zwei Beispiele für meist direkt wieder umgesetzte Stoffe sind Phosgen und Diketen. Phosgen ist als potentieller Kampfstoff nicht unproblematisch.[48] Der Umgang damit unterliegt strengen Regularien.[49] Wegen seiner Vielseitigkeit in der Synthese[50] findet es aber trotzdem breite Anwendung.[51] Diketen wird ebenfalls wegen seiner erstaunlichen Reaktivität zur Herstellung von vielen weiteren Verbindungen verwendet. Die Bandbreite der Produkte aus Diketen reicht von Analgetika[52] über Pigmente[28] und weiter bis zu Süßstoffen[53]. Auch in der Papierherstellung findet Diketen Anwendung.[54]

Beide Substanzen, Phosgen und Diketen, werden normalerweise im selben Werk hergestellt und weiterverarbeitet.[55] Dabei werden Transporte auf öffentlichen Straßen vermieden.

Es gibt auch andere Substanzen, die das Werk nicht verlassen dürfen, weil sie nicht registriert sind. Für einen Transport auf öffentlichen Straßen wäre eine Registrierung notwendig. Für eine Registrierung ist eine genaue Kenntnis von Zusammensetzung und Struktur unabdingbar. Wenn Chemikalien im gleichen Werk weiterverarbeitet werden, ist eine genaue Kenntnis von Zusammensetzung oder Struktur also nicht notwendig.

So kann es vorkommen, dass Zwischenprodukte seit vielen Jahrzehnten hergestellt werden, ohne dass die genaue Zusammensetzung oder Struktur bekannt ist.

Ein solches Zwischenprodukt ist das *trans*-Perinon-„Trennsalz“[56]. Es tritt bei der Isomerentrennung von *trans*- und *cis*- Perinon auf.[28,57–59]

Die industrielle Synthese von Perinon und seiner beiden Isomere ist in Abb. 2-19 dargestellt. In der Synthese fallen beide Isomere in einem Verhältnis von etwa 1:1 an.

Das synthetisierte Gemisch ist rot. Es wurde als Küpenfarbstoff Vat Red 14 verwendet. Unter gleichem Namen wird es in geringem Maße auch als Pigment eingesetzt. Durch Trennung des Gemisches können die reinen Isomere erhalten werden.

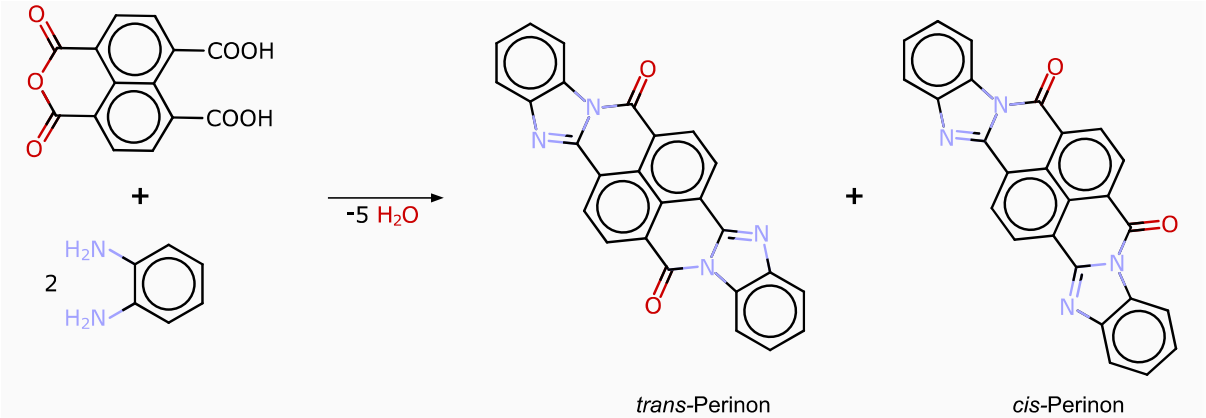

Abb. 2-19: Industrielle Synthese der Isomerenmischung von *trans*- und *cis*-Perinon.

Das reine *trans*-Perinon ist leuchtend orange. Es ist als Pigment Orange 43 im *Colour Index* gelistet. Dieses Pigment zeichnet sich durch seine leuchtende Farbe und exzellente Wetterechtheit aus. Daher wird es für die Färbung von Markisen und anderen Textilien und Polymeren eingesetzt.

Das reine *cis*-Perinon ist blaustichig rot. Es findet in geringem Maße Anwendung als Pigment Red 194 in Farben und Lacken. Dieses Pigment ist vergleichbar wetterecht wie Pigment Orange 43. Die verkaufte Menge von Pigment Red 194 ist wegen des trüben Farbtones gering.[28,32,60]

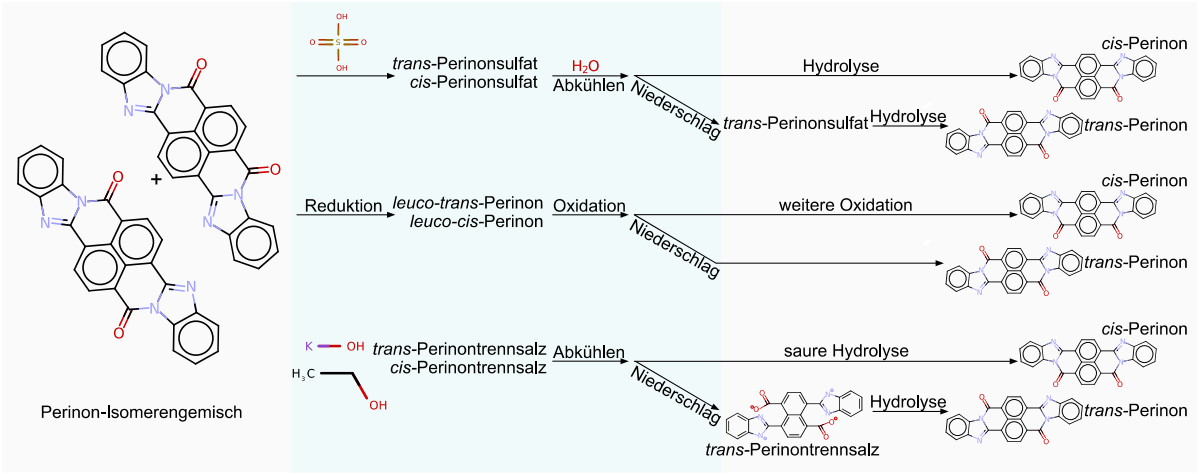

Abb. 2-20: Drei Wege zur Trennung der Isomerenmischung von *trans*- und *cis*-Perinon.

Zur Trennung der Isomere sind in der Literatur[28,61] drei Trennverfahren beschrieben, die in Abb. 2-20 skizziert sind.

Das erste Verfahren startet mit der Umsetzung des Gemisches der Isomere des Perinons mit Schwefelsäure zu löslichen Sulfaten. Beim Verdünnen der Lösung fallen dabei die beiden Isomere nacheinander aus. Das *trans*-Perinonsulfat fällt als erstes aus, das *cis*-Perinonsulfat bei weiterer Verdünnung. Die Sulfate werden getrennt und anschließend zu den einzelnen Perinon-Isomeren hydrolysiert.

Das zweite Verfahren beruht auf der Reduktion des Perinon-Isomerengemisches zu den entsprechenden *leuco*-Verbindungen. Vorsichtige Oxidation der resultierenden

Suspension führt zunächst zu einem Niederschlag von *trans*-Perinon. Dieses wird abfiltriert. Die Zugabe weiteren Oxidationsmittels führt zur Bildung von *cis*-Perinon.

Das dritte und technisch bedeutendste Verfahren führt über das „Trennsalz". Dabei wird das Gemisch der Isomeren von Perinon mit einer heißen Lösung von Ethanol, KOH und wenig Wasser behandelt, wobei lösliche Salze („Trennsalze") gebildet werden.

Aus der Lösung dieser „Trennsalze" fällt beim Abkühlen oder Verdünnen das *trans*-Perinontrennsalz aus. Das *cis*-Perinontrennsalz bleibt in Lösung. Das *trans*-Perinontrennsalz kann abfiltriert werden. Die Hydrolyse des *trans*-Perinontrennsalzes führt zu *trans*-Perinon. Die (leicht saure) Hydrolyse der verbliebenen Lösung führt zu *cis*-Perinon.

Dieses Verfahren wird seit 80 Jahren durchgeführt. Trotzdem waren weder die Zusammensetzungen noch die Strukturen dieser „Trennsalze" bekannt.

Wir konnten zwei Phasen des *trans*-Perinontrennsalzes isolieren. Von beiden Phasen konnten Einkristalle erhalten werden und die Kristallstrukturen aufgeklärt werden. In beiden Phasen wurde eine ring-geöffnete Struktur gefunden (Abb. 2-21, links). Das *trans*-Perinontrennsalz liegt in beiden Phasen als Tetraanion vor. Diese Struktur steht im Widerspruch zu bisherigen Strukturannahmen.

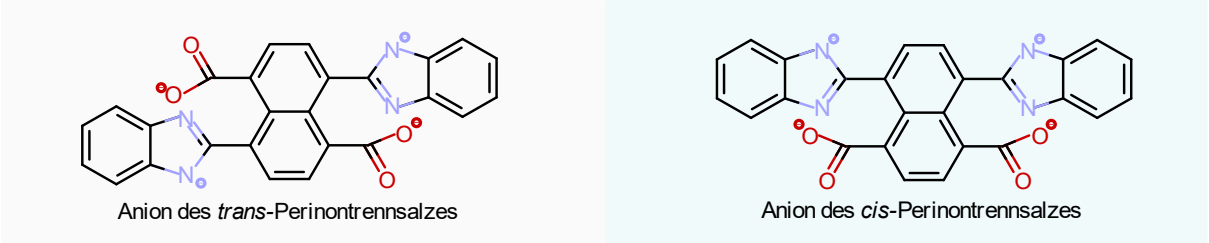

Abb. 2-21: Anionen im *trans*-Perinontrennsalz und im *cis*-Perinontrennsalz.

Beide Phasen des *trans*-Trennsalzes enthalten als Festkörper Ethanol und Wasser in unterschiedlichen Mengen (α-Phase: $K_4[C_{26}H_{12}N_4O_4] \cdot 3\ C_2H_5OH \cdot 6\ H_2O$ und β-Phase: $1{,}5\ (K_4[C_{26}H_{12}N_4O_4]) \cdot 5\ C_2H_5OH \cdot 4\ H_2O$).

Festkörper-*NMR*-Untersuchungen an der α-Phase zeigten, dass das Ethanol innerhalb der Struktur quasi flüssig und hoch mobil ist.

cis-Perinontrennsalz wird dadurch erhalten, dass das *cis*-Perinon mit wenig KOH/ Ethanol/Wasser erhitzt und anschließend abgekühlt wird. Die Kristallstruktur des *cis*-Perinontrennsalzes konnte ebenfalls aus Einkristallröntgenbeugungsdaten aufgeklärt werden.[56]

Auch das *cis*-Perinontrennsalz zeigt eine ring-geöffnete Struktur (Abb. 2-21, rechts).

Zu den anderen Trennverfahren:

Die beiden Perinonsulfate und *leuco*-Formen wurden mit vielfältigen Methoden analysiert. Es konnte keine Molekül- oder Kristallstruktur aufgeklärt werden. Es konnte lediglich festgestellt werden, dass es sich beim *trans*-Perinonsulfat tatsächlich um eine als Feststoff isolierbare Phase handelt. Es wurde erstmals ein Pulverdiagramm dieser Substanz veröffentlicht.

Als Fazit ergibt sich:

Obwohl Perinontrennsalze seit 80 Jahren produziert werden, konnten erstmals deren Zusammensetzungen, Molekül- und Kristallstrukturen aufgeklärt werden.

Details befinden sich in der angefügten Veröffentlichung [LT9].

[LT9]: L. Tapmeyer, M. Bolte, M. R. Chierotti & M. U. Schmidt: *Structure of the intermediates in the industrial separation of perinone isomers*, Dyes and Pigments **2020**, 181, 108422, DOI: 10.1016/j.dyepig.2020.108442.

3 Zusammenfassung

Im Rahmen des hier präsentierten Promotionsprojektes konnten neun Artikel veröffentlicht werden. Dabei wurden sechs Kristallstrukturen aus Pulverdaten[1] und elf Kristallstrukturen aus Einkristallen[2] bestimmt und publiziert. Fünf weitere Strukturen aus Pulverdaten konnten gelöst und abschließend verfeinert werden. Diese fünf Kristallstrukturen sind bereits bei der *Cambridge Structural Database* hinterlegt[3], die Veröffentlichung jedoch noch nicht eingereicht.

Im Rahmen dieser Arbeit konnte eine Methode mitentwickelt werden, die die Bestimmung der absoluten Konfiguration pharmazeutischer Verbindungen aus Röntgenpulverbeugungsdaten ermöglicht. Die Methode basiert auf der Bildung von Salzen. Die notwendige Herstellung dieser Salze mit Salzbildnern bekannter Konfiguration wurde hinsichtlich einer minimalen Ansatzgröße optimiert und erlaubt ein Arbeiten mit Mengen von unter zehn Mikrogramm. Die Kristallisation konnte sogar direkt in den Kapillaren für die Aufnahme der Pulverdiagramme durchgeführt werden. Die absolute Konfiguration einiger als Testfälle gewählter pharmazeutischer Wirkstoffe konnte auf diese Art erfolgreich bestimmt werden. Dies stellt eine erfolgreiche Erweiterung bisher verfügbarer Methoden dar.

Bei der Synthese von Leukopterin wurde in einem Edukt eine Fremdphase gefunden. Diese scheinbare Verunreinigung konnte als Hydrat des Edukts identifiziert werden. Die Kristallstruktur dieses 6-Amino-2-iminiumyl-4-oxo-1,2,3,4-tetrahydropyrimidin-5-aminiumsulfat-Monohydrats (TAHP) konnte problemlos bestimmt werden. Das Hydrat lässt sich durch Trocknung leicht in das Anhydrat überführen.

1,1,3,3-Tetraethyl-5-nitroisoindolin (TENI) und 1,1,3,3-Tetraethyl-5-nitroisoindolin-2-oxyl (TENO) sind Zwischenstufen in der Synthese von RNS-Spinlabeln für die EPR-Spektroskopie. Die Kristallstrukturen beider Verbindungen konnten aus Einkristallbeugungsdaten bestimmt werden. TENI hat einen Schmelzpunkt nahe der Raumtemperatur. TENO hat dagegen einen wesentlich höheren Schmelzpunkt, obwohl das Molekül nur ein Sauerstoffatom zusätzlich hat. Die Kristallstruktur liefert die Erklärung für dieses Phänomen: In der Kristallstruktur von TENI findet sich als stärkste intermolekulare Wechselwirkung eine einzelne schwache, sehr lange Wasserstoffbrückenbindung. Diese geringe Interaktion erklärt den niedrigen Schmelzpunkt der Verbindung. TENO dagegen weist in seiner Kristallstruktur keinerlei Interaktionen zwischen den Molekülen auf, die über Keesom- oder London-Kräfte hinausgehen. Allerdings sind diese stärker, was sich in einer dichteren Packung zeigt.

4-Amino-2,6-dimethylpyrimidin (ADMP) konnte bei der Reaktion von Acetonitril mit $NaO^{i}Pr$ als Katalysator als Einkristall erhalten werden. Die Kristallstruktur wurde mit

[1] *CSD*-Referenzcodes: **IGATUI**, **IGATIW**, IGAYEX, IGAVEU, IGAVAQ und IGATOC (Fettdruck bei Hauptbeitrag).

[2] *CSD*-Referenzcodes: **RUCJOR**, **NUGGII**, **EHAPOV**, **HUJWER**, **FAGSUB05**, **ELOCEQ**, ELOCAM, ELOBUF, HUJVIU, HUJVAM und NUGGEE (Fettdruck bei Hauptbeitrag).

[3] *CSD*-Einreichungsnummern: 1994654, 1994653, 1994652, 1994651, 1994650.

Cu-K_α-Strahlung neu bestimmt. ADMP zeigt eine typische organische Kristallstruktur in der Raumgruppe $P\,2_1/n$; alle Akzeptoren von Wasserstoffbrückenbindungen sind abgesättigt. [LT4]

Natriumethanolat wurde nach einer 180 Jahre alten Vorschrift von Liebig synthetisiert. Wie die Röntgenpulverdiagramme zeigen, bilden sich dabei jedoch Gemische von verschiedenen Phasen. Nach einigen experimentellen Schwierigkeiten konnte die Kristallstruktur von reinem NaOEt aus Pulverdaten bestimmt werden. Ebenfalls wurden ein Diethanolsolvat sowie zwei weitere Phasen identifiziert. Vom Diethanolsolvat NaOEt · 2 HOEt konnten Einkristalle hergestellt und die Kristallstruktur aus diesen bestimmt werden. Die Kristallstruktur von NaOEt zeigt erstaunliche Parallelen zur Struktur von Blei(II)oxid (Lithargit), wobei die Position der freien Elektronenpaare im PbO jener der Ethylgruppen im NaOEt entspricht. NaOEt kann also als Anti-PbO-Struktur bezeichnet werden. Während Lithargit in der Raumgruppe $P\,4/n\,m\,m$ kristallisiert, wurde für NaOEt die Untergruppe $P\,\bar{4}\,2_1\,m$ ermittelt. [LT5]

Die Kristallstrukturen von Natrium-*n*-propanolat (NaO^{n}Pr), Natrium-*n*-butanolat (NaO^{n}Bu) und Natrium-*n*-amylat (NaO^{n}Am) konnten ebenfalls aus Pulverdaten aufgeklärt werden. Sie weisen ein ähnliches Na-O-Gitter wie Natriumethanolat auf, allerdings kristallisieren sie in der Raumgruppe $P\,4/n\,m\,m$. Die abweichende Raumgruppe des NaOEt liegt am sterischen Anspruch der Ethylgruppe. Die längeren Alkylgruppen sind hochgradig fehlgeordnet und somit im Mittel zylinderförmig. Die Ethylgruppe dagegen hat einen weniger symmetrischen Raumbedarf. Aus diesem Grund ist die Ethylgruppe weniger fehlgeordnet, was die niedrigere Kristallsymmetrie erklärt. Die Solvate der Alkalialkoholate wurden mit zunehmender Länge der Alkylketten immer instabiler. Nichtsdestotrotz konnten drei verschiedene Solvate hergestellt werden: NaO^{n}Pr · 2 HO^{n}Pr, NaO^{i}Pr · 5 HO^{i}Pr und NaO^{t}Am · HO^{t}Am. Ihre Kristallstrukturen konnten aus Einkristallbeugungsdaten bestimmt werden. In diesen Strukturen zeigen sich sehr unterschiedliche Strukturmotive, die teilweise die mögliche Existenz weiterer Solvatstufen andeuten. Im Falle von NaO^{i}Pr · 5 HO^{i}Pr tragen fünf der sechs Isopropylgruppen eine Alkoholfunktion. Es handelt sich quasi zu 5/6 um festes Isopropanol. Das Wasserstoffbrückenbindungsnetzwerk unterscheidet sich deutlich von der Topologie in den beiden bekannten Kristallstrukturen von festem Isopropanol. Die Struktur ähnelt eher einer Anordnung, die in flüssigem Isopropanol zu erwarten ist. [LT6]

Die industriellen Rotpigmente Pigment Red 52 und Pigment Red 48 wurden im Labor unter verschiedenen Bedingungen synthetisiert. Dabei wurden neben den kommerziell verfügbaren Phasen einige neue Phasen identifiziert. Erstmals konnten Kristallstrukturen von P.R.52 und P.R.48 bestimmt werden. Von Pigment Red 52 konnte ein bisher unbekanntes Mononatriumsalz hergestellt werden. Von diesem Salz konnte ein DMSO-Solvat-Monohydrat kristallisiert werden. Aus erhaltenen Einkristallen konnte die Struktur bestimmt werden. [LT7]

Von Pigment Red 48 konnte ebenfalls ein bisher nicht literaturbekanntes Mononatriumsalz isoliert werden. Von zwei Hydratstufen dieser Verbindung konnten Einkristalle hergestellt und ihre Kristallstrukturen bestimmt werden. Eine weitere Phase wurde als Anhydrat identifiziert. [LT8] Eine Strukturbestimmung dieser Phase steht allerdings noch aus.

Vom Di-Natriumsalz des P.R.52 sowie von seinem Calciumsalz wurden insgesamt fünf verschiedene Hydratstufen gefunden. Die Kristallstrukturen dieser Hydrate konnten aus Röntgenpulverbeugungsdaten bestimmt werden. Von einer Hydratstufe konnte ebenfalls ein Einkristall erhalten und die Struktur bestätigt werden. Eine Veröffentlichung ist in Vorbereitung.

Das Orangepigment Perinon (Pigment Orange 43, *trans*-Perinon) fällt bei der industriellen Synthese als Gemisch mit einem roten *cis*-Isomer an. Die Isomere werden durch Überführung in „Trennsalze“ getrennt. Obwohl das Verfahren seit über 80 Jahren industriell genutzt wird, waren weder die Molekülkonstitution der Trennsalz-Ionen, noch die chemische Zusammensetzung der Feststoffe, noch deren Kristallstrukturen bekannt. Die industrielle Form des „*trans*-Trennsalzes“ konnte im Labor hergestellt und die Phasenidentität pulverdiffraktometrisch bestätigt werden. Eine weitere Phase des *trans*-Perinontrennsalzes konnte hergestellt und identifiziert werden. Der Versuch, die Kristallstrukturen der Trennsalze durch Röntgenpulverdiffraktometrie zu bestimmen, schlug fehl. Durch die nachfolgende Einkristallstrukturanalyse zeigte sich, dass die Trennsalze eine völlig andere Molekülkonstitution haben, als in der Literatur beschrieben war: Statt eines planaren Perinongerüsts enthält das Trennsalz ein verdrehtes Bis(benzimidazolat)naphthalindicarboxylat-tetraanion, dessen Ladung durch Kalium-Kationen kompensiert wird. Das bisher nie als Feststoff beschriebene *cis*-Perinontrennsalz wurde hergestellt und kristallisiert. Es konnten Einkristalle hergestellt und die Kristallstruktur aus diesen bestimmt werden. Die beim *trans*-Perinontrennsalz beobachtete Ringöffnung des Perinongerüsts liegt auch im *cis*-Perinontrennsalz vor. Alle Perinontrennsalze enthalten im Kristallgitter eine beträchtliche Anzahl Wasser- und Ethanolmoleküle. Durch Festkörper-NMR-Spektroskopie konnte gezeigt werden, dass das Wasser-Ethanol-Netzwerk stark dynamisch ist. Die Röntgenstrukturanalyse lieferte hier nur ein gemitteltes Bild, was sich beispielsweise in wesentlich zu kurzen intermolekularen Abständen zeigt. Bei der Hydrolyse der Trennsalze entstehen wieder die ursprünglichen, wasser- und lösungsmittelfreien Perinonpigmente. [LT9]

4 Ausblick

In dieser Dissertation wurde eine Methode entwickelt, um die absolute Konfiguration pharmazeutischer Wirkstoffe durch Röntgenpulverdiffraktometrie zu bestimmen, indem die Wirkstoffe mit chiralen Gegenionen zu Salzen umgesetzt werden. Statt Salzen könnten hier auch Cokristalle mit chiralen Co-Formern eingesetzt werden. Diese Experimente stehen noch aus. Ebenfalls sollte ein Standard-Satz von Salzbildnern ausgearbeitet werden, die bei der Mehrheit der zu untersuchenden Substanzen erfolgversprechend sind. Versuche mit Chinin als Base waren oft nicht erfolgreich. Die Chinin-Salze der untersuchten Wirkstoffe fielen meist gelartig an. Die Pulverdiagramme (s. Abb. 4-1) konnten daher nicht mit konventionellen Methoden ausgewertet werden. Allerdings sollte die PDF-Untersuchung an solchen nanokristallinen oder gelartigen Proben weiterverfolgt werden. Hier bieten sich eventuell neue Möglichkeiten für die Auswertung sehr schlecht kristalliner Proben.

TENO zeigt bei Raumtemperatur eine massive Fehlordnung der Ethylsubstituenten. Bei −100 °C ist diese deutlich verringert. Im Hinblick auf die geplante Anwendung als Marker sollten thermische Effekte an dieser Substanz im Detail erforscht werden.

Kaliumethanolat zeigt wie Natriumethanolat ein sehr kompliziertes Phasenverhalten. Bisher konnte keine Reinphase von lösungsmittelfreiem KOEt erhalten werden. Trotzdem konnte die Kristallstruktur von lösungsmittelfreiem KOEt aus Röntgenbeugungsdaten bestimmt werden. Eine Publikation ist in Vorbereitung. Weitere Untersuchungen der KOEt-Phasen sind geplant.

Die Strukturaufklärung von Leukopterin ist noch nicht abgeschlossen. Temperaturabhängige Röntgenpulverdiagramme deuten auf eine variable Hydratstufe hin. Dies ist eines der noch offenen Projekte für die Zeit nach dieser Arbeit.

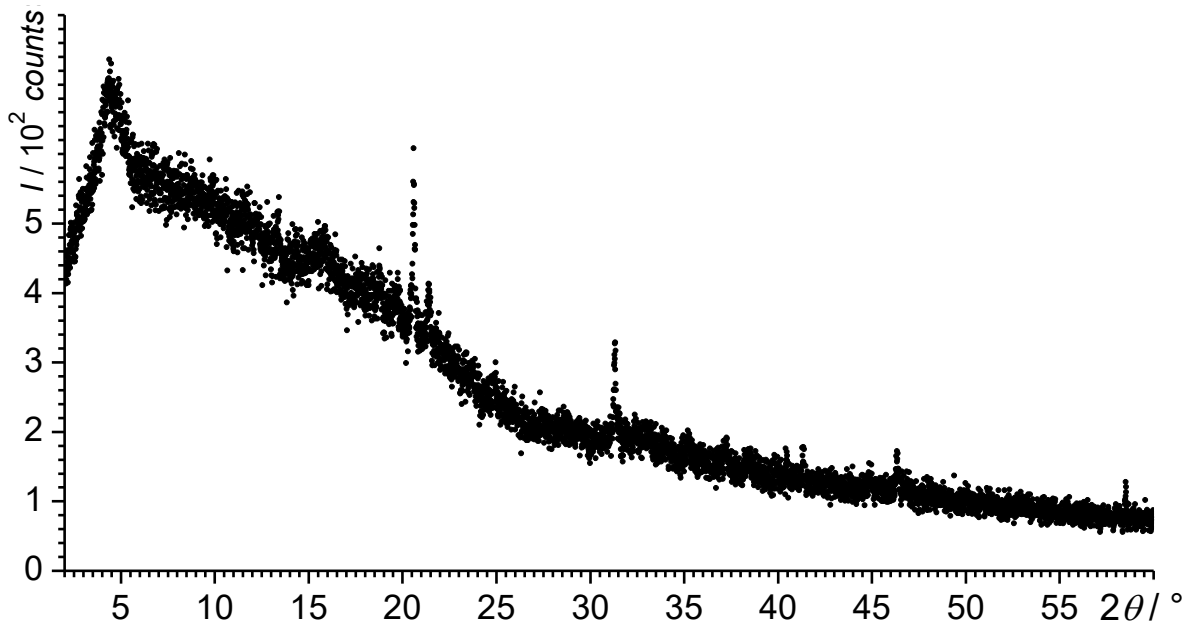

Abb. 4-1: Pulverdiagramm des Produkts der Verdampfungskristallisation von Lamivudin und Chinin in Ethanol.

In Kooperation mit Prof. Dr. Björn Winkler wird derzeit eine Syntheseroute entwickelt, um Amminboran (H_3NBH_3) möglichst effizient aus Borsäure zu synthetisieren. Ziel ist die Herstellung einer Probe im Grammmaßstab von isotopenreinem ^{10}B-Amminboran für kerntechnische Experimente.

Diese Schutzgassynthese stellt dabei quasi einen Rückblick auf mein Studium dar, da eines der ersten komplexeren Produkte, die ich in meinem Bachelorstudium im präparativen Praktikum herstellte, das Trimethylamminboran war (Abb. 4-2). Eine funktionierende Syntheseroute für Amminboran wurde inzwischen gefunden und bereits optimiert. Die Synthese der isotopenreinen Verbindung in größeren Mengen steht noch aus.

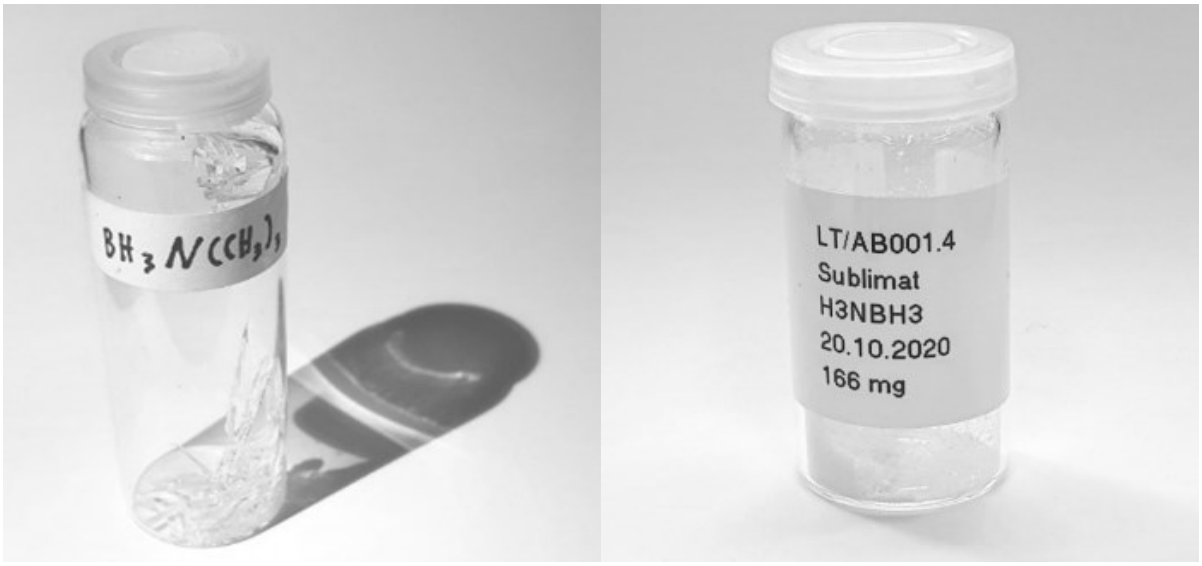

Abb. 4-2: Erste und letzte Studienphase: Trimethylamminboran aus dem Praktikum 2013 (links) und Amminboran von 2020 (rechts).

5 Literatur zu Kapitel 1 bis 3

Zusätzlich zu den in den jeweiligen Veröffentlichungen angegebenen Quellen:

[1] H. M. Rietveld, *Z. Kristallogr.* **2010**, *225*, 545–547.
[2] M. Etter, R. E. Dinnebier, *Z. anorg. allg. Chem.* **2014**, *640*, 3015–3028.
[3] R. Allmann, *Röntgenpulverdiffraktometrie: rechnergestützte Auswertung, Phasenanalyse und Strukturbestimmung*, Springer, Berlin, **2003**.
[4] M. Spiliopoulou, A. Valmas, D.-P. Triandafillidis, C. Kosinas, A. Fitch, F. Karavassili, I. Margiolaki, *Crystals* **2020**, *10*, 54-89.
[5] W. H. Brooks, W. C. Guida, K. G. Daniel, *Curr. Top. Med. Chem.* **2011**, *11*, 760–770.
[6] H. D. Flack, G. Bernardinelli, *Chirality* **2008**, *20*, 681–690.
[7] D. Prill, P. Juhás, S. J. L. Billinge, M. U. Schmidt, *Acta Cryst. A* **2016**, *72*, 62–72.
[8] S. J. L. Billinge, *Philos. Trans. Royal Soc. A* **2019**, *377*, 20180413.
[9] D. Prill, P. Juhás, M. U. Schmidt, S. J. L. Billinge, *J. Appl. Crystallogr.* **2015**, *48*, 171–178.
[10] C. Schlesinger, L. Tapmeyer, S. D. Gumbert, D. Prill, M. Bolte, M. U. Schmidt, C. Saal, *Angew. Chem.* **2018**, *130*, 9289–9293.
[11] C. Schlesinger, L. Tapmeyer, S. D. Gumbert, D. Prill, M. Bolte, M. U. Schmidt, C. Saal, *Angew. Chem. Int. Ed.* **2018**, *57*, 9150–9153.
[12] R. Purrmann, *Liebigs Ann. Chem.* **1940**, *544*, 182–190.
[13] C. Schöpf, H. Wieland, *Ber. Dtsch. Chem. Ges.* **1926**, *59*, 2067–2072.
[14] H. Wieland, H. Metzger, C. Schöpf, M. Bülow, *Liebigs Ann. Chem.* **1933**, *507*, 226–265.
[15] J. H. Bieri, R. Prewo, A. Linden, *CSD Commun.* **1993**.
[16] S. Saha, A. P. Jagtap, S. Th. Sigurdsson, *Chem. Commun.* **2015**, *51*, 13142–13145.
[17] M. M. Haugland, A. H. El-Sagheer, R. J. Porter, J. Peña, T. Brown, E. A. Anderson, J. E. Lovett, *J. Am. Chem. Soc.* **2016**, *138*, 9069–9072.
[18] K. F. M. J. Schmidt, *Ber. Dtsch. Chem. Ges.* **1902**, *35*, 1575–1579.
[19] L. Yingzhang, W. Jinguang, G. Hai, X. Guangxian, Y. Jiaxia, Q. Jinzi, H. Shenghua, F. Haifu, *Gaodeng Xuexiao Huaxue Xuebao ChemJChinUniv* **1986**, 600–604.
[20] Z. Deng, W. Qui, W. Li, Y. Li, *Chin. Sci. Bull.* **2004**, *49*, 127–130.
[21] J. Radtke, S. K. Mellerup, M. Bolte, H.-W. Lerner, S. Wang, M. Wagner, *Org. Lett.* **2018**, *20*, 3966–3970.
[22] A. Olejniczak, A. Katrusiak, *J. Phys. Chem. B* **2008**, *112*, 7183–7190.
[23] W. Dieckmann, *Ber. Dtsch. Chem. Ges.* **1900**, *33*, 2670–2684.
[24] M. Kumar, Raziullah, A. A. Khan, A. Ahmad, H. S. Dutta, R. Kant, D. Koley, *J. Org. Chem.* **2019**, *84*, 13624–13635.
[25] J. Liebig, *Ann. Pharm.* **1837**, *23*, 12–42.
[26] H. Lescoeur, *Compt. Rend. Acad. Sci.* **1895**, *121*, 691–692.
[27] J.-M. Blanchard, J. Bousquet, P. Claudy, J.-M. Letoffe, *J. Therm. Anal.* **1976**, *9*, 191–203.
[28] K. Hunger, M. U. Schmidt, *Industrial Organic Pigments: Production, Crystal Structures, Properties, Applications*, Wiley-VCH Verlag GmbH & Co. KGaA, Weinheim, **2018**.
[29] S. L. Bekö, S. M. Hammer, M. U. Schmidt, *Angew. Chem.* **2012**, *124*, 4814–4818.
[30] S. L. Bekö, S. M. Hammer, M. U. Schmidt, *Angew. Chem. Int. Ed.* **2012**, *51*, 4735–4738.
[31] J. Mizuguchi, *J. Phys. Chem. B* **2004**, *108*, 8926–8930.
[32] J. L. Teteruk, J. Glinnemann, J. van der Streek, K. E. Johansson, W. Heyse, M. U. Schmidt, *Acta Cryst. B* **2016**, *72*, 416-433.
[33] D. A. Zherebtsov, M. U. Schmidt, R. Niewa, C. P. Sakthidharan, F. V. Podgornov, Y. V. Matveichuk, S. A. Nayfert, M. A. Polozov, S. N. Ivashevskaya, A. I. Stash, Y.-S. Chen, D. E. Zhivulin, V. E. Zhivulin, S. V. Merzlov, E. V. Bartashevich, V. V. Avdin, H. S. Hsu, F. W. Guo, *Acta Cryst. B* **2019**, *75*, 384-392.

[34] W. Eckert, Heinrich Sieber, *Verfahren zum Trennen von Kuepenfarbstoffen*, **1932**, Deutsches Patent DE1930567210.
[35] W. Massa, *Kristallstrukturbestimmung*, Teubner, Wiesbaden, **2007**.
[36] H. Tönjes, K. Heidenbluth, R. Scheffler, *J. prakt. Chem.* **1964**, *26*, 218–224.
[37] L. Tapmeyer, M. Beske, J. Plackmeyer, *IUCrData* **2019**, *4*, x191629.
[38] J. Grell, J. Bernstein, G. Tinhofer, *Acta Cryst. B* **1999**, *55*, 1030–1043.
[39] M. C. Etter, J. C. MacDonald, J. Bernstein, *Acta Cryst. B* **1990**, *46*, 256–262.
[40] C. R. Groom, I. J. Bruno, M. P. Lightfoot, S. C. Ward, *Acta Cryst. B* **2016**, *72*, 171–179.
[41] D. W. M. Hofmann, *Acta Cryst. B* **2002**, *58*, 489–493.
[42] E. Weiss, *Z. Für Anorg. Allg. Chem.* **1964**, *332*, 197–203.
[43] A. Kitaigorodsky, *Molecular Crystals and Molecules*, Elsevier Science, Burlington, **2012**.
[44] R. Gley, O. Siebert, *Verfahren von besonders für die Herstellung von Farblacken geeigneten Monoazofarbstoffen aus 2,3-Oxynaphtoesäure*, **1903**, Deutsches Patent DE151205.
[45] W. Czajkowski, *Dyes Pigments* **1980**, *1*, 17–25.
[46] W. Czajkowski, *Dyes Pigments* **1987**, *8*, 141–150.
[47] A. R. Kennedy, C. McNair, W. E. Smith, G. Chisholm, S. J. Teat, *Angew. Chem. Int. Ed.* **2000**, *39*, 638–640.
[48] B. Friedrich, D. Hoffmann, J. Renn, F. Schmaltz, M. Wolf, Eds., *One Hundred Years of Chemical Warfare: Research, Deployment, Consequences*, Springer, New York, NY, **2017**.
[49] H. Falcke, S. Holbrook, I. Clenahan, A. Lopez Carretero, A. Sanalan, T. Brinkmann, J. Roth, B. Zerger, S. Roudier, L. Delgado Sancho, *Best Available Techniques (BAT) Reference Document for the Production of Large Volume Organic Chemicals. Industrial Emissions Directive 2010/75/EU (Integrated Pollution Prevention and Control)*, Publications Office Of The European Union, Luxembourg, **2017**.
[50] H. Babad, A. G. Zeiler, *Chem. Rev.* **1973**, *73*, 75–91.
[51] René Kleijn, Ester van der Voet, *Chlorine in Western Europe*, Centre For Environmental Science (CML), Leiden, **1998**.
[52] N. Uramaru, H. Shigematsu, A. Toda, R. Eyanagi, S. Kitamura, S. Ohta, *J. Med. Chem.* **2010**, *53*, 8727–8733.
[53] R. J. Clemens, *Chem. Rev.* **1986**, *86*, 241–318.
[54] A. Pingel Keuth, *Chem. Unserer Zeit* **2005**, *39*, 402–409.
[55] B. Elvers, F. Ullmann, Eds., *Ullmann's Fine Chemicals. Vol. 3*, Wiley-VCH, Weinheim, **2014**.
[56] L. Tapmeyer, M. Bolte, M. R. Chierotti, M. U. Schmidt, *Dyes Pigments* **2020**, *181*, 108442.
[57] E. Dietz, G. Kapaun, S. Schiessler, *Verfahren zur Herstellung von Küpenfarbstoffen und Pigmenten der Perinon-Reihe*, **1990**, DE3836674A1.
[58] W. Eckert, *Verfahren zur Darstellung von Küpenfarbstoffen*, **1926**, Deutsches Patent DE438197.
[59] W. Eckert, H. Greune, *Verfahren zur Darstellung von Küpenfarbstoffen*, **1924**, Deutsches Patent DE430632.
[60] L. Tapmeyer, Festkörperstrukturuntersuchungen an Perinon und an diastereomeren Salzen pharmazeutischer Wirkstoffe, Masterarbeit, Johann Wolfgang Goethe-Universität Frankfurt am Main, **2016**.
[61] W. Eckert, H. Sieber, *Verfahren zum Trennen von Küpenfarbstoffen*, **1932**, Deutsches Patent DE567210.

6 Angabe der eigenen Anteile an den Veröffentlichungen

In der Veröffentlichung [LT1] werden die Herstellung von diastereomeren Salzen und die Strukturbestimmung aus deren Pulverdaten mit dem Ziel der Bestimmung der absoluten Konfiguration beschrieben. Das Projekt wurde von Dr. Christoph Saal entwickelt und die Synthesen und Kristallisationen wurden durch Dr. Silke D. Gumbert begonnen. Als zweitgenannter Autor hatte ich (neben Carina Schlesinger) Anteil an der Fortsetzung der Synthese und Kristallisation diverser Salze. Die Strukturaufklärung aus Röntgenpulverbeugungsdaten an Salzen von (*R*)-Flurbiprofen und (*S*)-Flurbiprofen mit (*R*)-Phenylpropylamin ist mein Hauptbeitrag neben dem Schreiben des Entwurfs und der Korrekturen.

Die Veröffentlichung [LT2] beschäftigt sich mit der Kristallisation und Einkristallstrukturbestimmung eines Edukts der Synthese von Leukopterin. Die praktische Arbeit an diesem Projekt sowie das Schreiben des Entwurfs wurde von mir als erstgenanntem Autor der Veröffentlichung durchgeführt.

In der Veröffentlichung [LT3] wird die Röntgenstrukturanalyse von 1,1,3,3-Tetraethyl-5-nitroisoindolin beschrieben. Während die Substanz von Jörn Plackmeyer hergestellt wurde, oblagen mir als dem erstgenannten Autor der Veröffentlichung die Auswertung der Röntgenbeugungsdaten und das Schreiben des Entwurfs.

Die Veröffentlichung [LT4] umfasst eine Neubestimmung der Struktur von 2,6-Dimethylpyrimidin-4-amin. Die experimentelle Arbeit wurde größtenteils von Maurice Beske durchgeführt. Die Auswertung der Röntgenbeugungsdaten durch mich diente der Einweisung von Maurice Beske in diese Tätigkeit. Als erstgenannter Autor erstellte ich die zu publizierende Datei.

In der Veröffentlichung [LT5] wurden die Synthese und Strukturaufklärung aus Pulverdaten von NaOEt und Einkristallstrukturbestimmung von NaOEt · 2 EtOH beschrieben. Die meisten praktischen Arbeiten und die Strukturbestimmungen aus Pulverdaten erfolgten von Maurice Beske im Rahmen eines Masterpraktikums unter meiner Anleitung und Betreuung. Die entscheidenden Experimente wurden durch mich wiederholt und die Strukturen nachverfeinert. Die Einkristallstrukturanalyse des Solvats ist fast ausschließlich mein Beitrag.

Die Veröffentlichung [LT6] enthält Details zur Raumgruppenbestimmung der Struktur des NaOEt aus [LT5] und weitere Kristallstrukturen von Natriumalkoholaten. Die praktische Arbeit an diesem Projekt war Teil der von mir betreuten Masterarbeit von Maurice Beske. Meine Beiträge waren die Unterstützung bei Planung und Durchführung der Synthesen und Kristallisationen, Validation und teilweise Reproduktion der experimentellen Ergebnisse, Röntgenstrukturanalyse des Solvates $NaO^tAm \cdot HO^tAm$, das Schreiben des Entwurfs und Korrekturen an ebendiesem sowie Korrekturen und Nachverfeinerungen aller Strukturen. Daher habe ich in der Liste der Autoren der Publikation die letztgenannte Position.

In der Veröffentlichung [LT7] wird eine neue Solvat-Phase des bisher in seiner Kristallstruktur unbekannten Colour Index Pigment Red 52 beschrieben. Die Phase trat im Rahmen der von mir betreuten Bachelorarbeit von Daniel Eisenbeil auf. Als erstgenannter Autor waren das Schreiben des Entwurfs der Veröffentlichung sowie die Anleitung bei allen Versuchen mein Beitrag.

Die Veröffentlichung [LT8] behandelt zwei neue Phasen eines bisher unbekannten Salzes von Colour Index Pigment Red 48. Dieses neue Derivat trat im Rahmen eines von mir betreuten Vertiefungspraktikums von Steven Hill auf. Die Einkristallstruktur des Dihydrats wurde von Michael Bolte bestimmt. Das Monohydrat wurde von mir isoliert und seine Struktur aus Einkristallbeugungsdaten gemeinsam mit W. Maximilian Hützler bestimmt. Weitere Untersuchungen des Phasenverhaltens und das Erstellen des Publikationsentwurfs wurden von mir als erstgenanntem Autor durchgeführt.

In der Veröffentlichung [LT9] wurden die Kristallstrukturen von insgesamt drei Phasen zweier bisher strukturell und konstitutionell unbekannter Zwischenprodukte der Herstellung des Orangepigments Perinon beschrieben. Als Erstautor führte ich alle praktischen Arbeiten sowie die Röntgenstrukturanalyse des *cis*-Trennsalzes durch. Abgesehen vom historischen Abschnitt ist der Entwurf des Papers fast ausschließlich mein Beitrag.

Es folgen die Volltexte der Veröffentlichungen mit erneuter Auflistung der Beiträge der jeweiligen Autoren.

7 Eigene Veröffentlichungen (Volltext)

[LT1] C. Schlesinger, L. Tapmeyer, S. D. Gumbert, D. Prill, M. Bolte, M. U. Schmidt & C. Saal: *Absolute Configuration of Pharmaceutical Research Compounds Determined by X-ray Powder Diffraction*, Angew. Chem. Int. Ed. **2018**, 57, 9150-9153, DOI: 10.1002/anie.201713168. ..... S. 34

C. Schlesinger, L. Tapmeyer, S. D. Gumbert, D. Prill, M. Bolte, M. U. Schmidt & C. Saal: *Bestimmung der absoluten Konfiguration pharmazeutischer Wirkstoffe durch Röntgenpulverdiffraktometrie*, Angew. Chem. **2018**, 130, 9289–9293, DOI: 10.1002/ange.201713168. ..... S. 40

[LT2] L. Tapmeyer & D. Prill: *6-Amino-2-iminiumyl-4-oxo-1,2,3,4-tetrahydropyrimidin-5-aminium sulfate monohydrate*, IUCrData **2019**, 4, CCDC reference: 1915747, DOI: 10.1107/S2414314619006898. ..... S. 46

[LT3] L. Tapmeyer, M. Beske & J. Plackmeyer: *1,1,3,3-Tetraethyl-5-nitroisoindoline*, IUCrData **2019**, 4, CCDC reference: 1969794, DOI: 10.1107/S2414314619016298. ..... S. 51

[LT4] CCDC 1975913: Experimental Crystal Structure Determination, *2,6-dimethyl-pyrimidin-4-amine*, *CSD Communication* ***2020***, DOI: 10.5517/ccdc.csd.cc24b34r. ..... S. 55

[LT5] M. Beske, L. Tapmeyer & M. U. Schmidt: *Crystal structure of sodium ethoxide (C2H5ONa), unravelled after 180 years*, Chem. Comm. **2020**, 56, 3520-3523, DOI: 10.1039/C9CC08907A. ..... S. 60

[LT6] M. Beske, S. Cronje, M. U. Schmidt & L. Tapmeyer: *Disordered sodium alkoxides from powder data: Crystal structures of sodium ethoxide, propoxide, butoxide, and pentoxide, and some of their solvates*, Acta Cryst. B **2020**, 77, 68-82, DOI: 10.1107/S205252062001584X. ..... S. 65

[LT7] L. Tapmeyer, D. Eisenbeil, M. Bolte & M. U. Schmidt: *First crystal structure of a Pigment Red 52 compound: DMSO solvate hydrate of the monosodium salt*, Acta Cryst. E **2021**, 77, 402-405, DOI: 10.1107/S2056989021002577. ..... S. 81

[LT8] L. Tapmeyer, S. Hill, M. Bolte & W. M. Hützler: *Two monosodium salt hydrates of Colour Index Pigment Red 48*, Acta Cryst. C **2020**, 76, 716-722, DOI: 10.1107/S2053229620008530. ..... S. 86

[LT9] L. Tapmeyer, M. Bolte, M. R. Chierotti & M. U. Schmidt: *Structure of the intermediates in the industrial separation of perinone isomers*, Dyes and Pigments **2020**, 181, 108422, DOI: 10.1016/j.dyepig.2020.108442. ..... S. 94

7.1 [LT1] Absolute Configuration of Pharmaceutical Research Compounds Determined by X-ray Powder Diffraction

Bibliographische Daten:

Titel:	Absolute Configuration of Pharmaceutical Research Compounds Determined by X-ray Powder Diffraction
Journal:	Angewandte Chemie International Edition
Jahr / Ausgabe:	2018 / Volume 57, Issue 29
Seiten:	9150–9153
DOI:	10.1002/anie.201713168
URL:	https://onlinelibrary.wiley.com/doi/full/10.1002/anie.201713168
Autoren:	Carina Schlesinger, Lukas Tapmeyer, Silke Dorothea Gumbert, Dragica Prill, Michael Bolte, Martin Ulrich Schmidt, Christoph Saal
eSI:	https://onlinelibrary.wiley.com/action/downloadSupplement?doi=10.1002%2Fanie.201713168&file=anie201713168-sup-0001-misc_information.pdf
OpenAccess:	Nein.
	Abgedruckt mit freundlicher Genehmigung von *John Wiley & Sons, Inc.*

Beiträge:	Carina Schlesinger: Validation experimenteller Ergebnisse, Strukturaufklärung aus Röntgenpulverdaten, Schreiben des Entwurfs, Korrekturen. Lukas Tapmeyer: Synthese und Kristallisation, Strukturaufklärung aus Röntgenpulverdaten an Salzen von (*R*)-Flurbiprofen und (*S*)-Flurbiprofen mit (*R*)-Phenylpropylamin, Schreiben des Entwurfs, Korrekturen. Silke D. Gumbert: Anleitung, Synthese und Kristallisation, Anleitung zur Strukturaufklärung aus Röntgenpulverdaten, Korrekturen. Dragica Prill: Validation der Ergebnisse, Paarverteilungsanalyse, Korrekturen. Michael Bolte: Röntgenstrukturanalyse. Martin U. Schmidt: Anleitung, Schreiben des Manuskripts, Korrekturen. Christoph Saal: Projekt-Idee, Schreiben seines Teils des Entwurfs, Korrekturen.

Auch veröffentlicht auf Deutsch als:

Titel:	Bestimmung der absoluten Konfiguration pharmazeutischer Wirkstoffe durch Röntgenpulverdiffraktometrie
Journal:	Angewandte Chemie
Jahr / Ausgabe:	2018 / Band 130, Ausgabe 29
Seiten:	9289–9293
DOI:	10.1002/ange.201713168
URL:	https://onlinelibrary.wiley.com/doi/full/10.1002/ange.201713168
OpenAccess:	Nein.

Absolute Configuration

International Edition: DOI: 10.1002/anie.201713168
German Edition: DOI: 10.1002/ange.201713168

Absolute Configuration of Pharmaceutical Research Compounds Determined by X-ray Powder Diffraction

*Carina Schlesinger, Lukas Tapmeyer, Silke D. Gumbert, Dragica Prill, Michael Bolte, Martin U. Schmidt, and Christoph Saal**

Abstract: *The absolute configuration of active pharmaceutical ingredients (APIs) was determined by generating salts of the active pharmaceutical ingredient (API) with counterions of known chirality, and determining the crystal structures by X-ray powder diffraction. This approach avoids the (often tedious) growth of single crystals, and is successful with very limited quantities of material (less than 1 mg). The feasibility of the method is demonstrated on five examples, and its limitations are discussed as well.*

Today, most new active pharmaceutical ingredients (APIs) are chiral.[1] Whereas most new drugs were approved as racemates before 1980, the drug approval process has changed significantly over the last decades. The pharmacological activity, toxicological properties, and pharmacokinetics strongly depend on the enantiomeric form of a given API.[2] Consequently, it is imperative that the absolute configuration is known at a very early stage of research. However, the absolute stereochemistry of a new compound is not always obvious from the chemical synthesis or the separation of the enantiomers. This holds not only for pharmaceutical compounds, but also for natural products or organocatalysts, for example.

The absolute stereochemistry of a compound is usually determined by single-crystal X-ray diffraction.[3] This requires the growth of sufficiently large single crystals of high crystal quality, and a precise X-ray measurement.[4] Growing acceptable crystals is frequently a great challenge, especially for today's pharmaceutical research compounds, which typically have a high molecular mass, high molecular flexibility, and low solubility in water and many other solvents. Yet another challenge arises from the usually very limited amounts of available substance in early stages of research (typically a few milligrams or even less), which generally excludes a reliable series of crystal growth experiments.[5]

To overcome these impediments, we investigated an alternative approach to determine the absolute configuration of pharmaceutical research compounds by X-ray powder diffraction. X-ray powder diffraction by itself cannot differentiate between enantiomers. In contrast, diastereomers can be easily distinguished. Currently most new active pharmaceutical ingredients are either acidic or basic;[6] hence, they easily form salts with suitable counterions. If the counterions are chiral, different API enantiomers will give rise to diastereomeric salts. The crystal structures of these salts can be determined from X-ray powder data, revealing the relative configuration of the ions. From the known chirality of the counterion, the absolute configuration of the API can then be deduced.

Herein, the feasibility of this approach is shown on four enantiopure APIs, which were combined with one or two different salt formers each. The absolute configuration of the API was treated as unknown, and that of the salt formers as known. The APIs chosen are (*R*)-flurbiprofen (***R*1**), (*S*)-flurbiprofen (***S*1**), aminoglutethimide (**2**), and lamivudine (**3**; see Scheme 1). Flurbiprofen is a non-steroidal anti-inflammatory drug, which was originally approved as a racemate. Meanwhile the pure *R* enantiomer has also been approved as the antiphlogistic drug Tarenflurbil. Aminoglutethimide is an aromatase inhibitor, and lamivudine is a nucleoside analogue used in the treatment of HIV.

Flurbiprofen is acidic, and both enantiomers were crystallized with the chiral bases quinine (**a**) and (*R*)-2-phenylpropylamine (**b**). The other two APIs are basic and were crystallized with (*R*)-camphor-10-sulfonic acid (**c**; see Scheme 1).

For the preparation of crystalline salts, two methods were most successful:

1) On milligram scale, a solution of the API in a solvent, for example, acetone, was added to a solution of the salt former in a small test tube, and the resulting mixture was slowly evaporated.
2) On a microgram scale, about 2 μL of both solutions were soaked into an open capillary with a diameter of 0.7 mm and allowed to react within the capillary. Subsequently, the capillary was sealed on one end. After evaporation of the solvent, the capillary was directly mounted on the powder diffractometer. For this approach, about 100 μg of the API (or even less) are sufficient.

Both procedures gave crystalline powders of the five salts: ***R*1a**, ***R*1b**, ***S*1b**, **2c**, and **3c** (for experimental details see the Supporting Information). The sixth salt ***S*1a** always precipitated as a poorly crystalline powder, which resisted any attempt of structure determination. X-ray powder data of all samples were recorded in transmission mode on a STOE

[*] M. Sc. C. Schlesinger, M. Sc. L. Tapmeyer, Dr. S. D. Gumbert, Dr. D. Prill, Dr. M. Bolte, Prof. Dr. M. U. Schmidt
Goethe-Universität
Institut für Anorganische und Analytische Chemie
Max-von-Laue-Str. 7, 60438 Frankfurt am Main (Germany)
Dr. C. Saal
Merck KGaA, Site-Operations—Analytics Healthcare
Frankfurter Landstr. 250, 64293 Darmstadt (Germany)
E-mail: christoph.saal@merckgroup.com
Supporting information and the ORCID identification number(s) for the author(s) of this article can be found under: https://doi.org/10.1002/anie.201713168.

 © 2018 Wiley-VCH Verlag GmbH & Co. KGaA, Weinheim

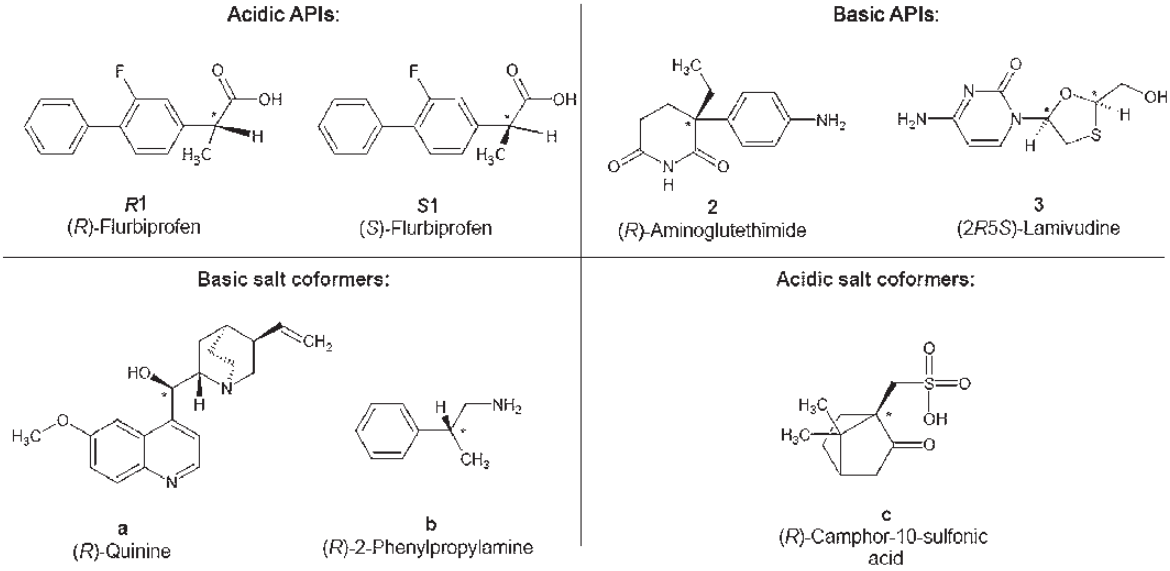

Scheme 1. Chemical structures of the investigated compounds (top) and the employed counterions (bottom). The relevant chiral atoms are highlighted with stars.

STADI-P diffractometer (for details see the Supporting Information).

The powder patterns were indexed with DICVOL04[7] as implemented in the DASH software.[8] Subsequently, possible space groups were determined from systematic extinctions. The number of molecules per unit cell was estimated using Hofmann's volume increments.[9] The indexing and space group assignments were confirmed by Pawley fit.[10]

The structures were solved by real-space methods[11] using simulated annealing within DASH. Lattice parameters, the space group, and the molecular geometry were given as input; the positions and spatial orientations of the molecules in the unit cell as well as intramolecular degrees of freedom (rotations around single bonds) were varied. The molecular geometries of the APIs and counterions were derived from crystal data of similar compounds from the Cambridge Structural Database (CSD).[12] The absolute configuration of the salt former was given as input and combined with both possible enantiomers of the API. The resulting diastereomeric salts were handled with two separate sets of DASH runs.

Structure solution from powder data by real-space methods becomes challenging when the total number of parameters (for the molecular position and orientation and the intramolecular degrees of freedom) exceeds 20.[13] This limit was exceeded by two compounds, **2c** and **3c**. Both salts crystallize in the space group $P2_1$ with $Z=4$, $Z'=2$. Each asymmetric unit contains two cations and two anions; both the cations and anions have two intramolecular degrees of freedom, resulting in a total number of 31 parameters.[14] The structure of **3c** could be reproducibly solved without difficulties. In contrast, all our attempts at solving the structure of **2c** were to no avail (see the Supporting Information for details). Serendipitously, we obtained a single crystal of **2c** and solved the structure by single-crystal X-ray analysis. This structure was used as input for the subsequent Rietveld refinements. For the wrong enantiomer of the API, we manually constructed three chemically sensible crystal structure models. All subsequent refinements of **2c** were performed in the same way as for the other salts.

The crystal structures of the other compounds (***R*1a**, ***R*1b**, and ***S*1b**) were solved from the powder data in routine manner. All (correct and wrong) structures were refined by the Rietveld method[15] with TOPAS.[16] To ensure sensible molecular geometries, restraints were used for all bond lengths, bond angles, and for planar groups.

In all cases, both diastereomeric salts (containing either one of the two API enantiomers) were treated identically, that is, with equivalent restraints as well as an identical refinement procedure. All refinements converged well. Crystallographic data and Rietveld plots of all investigated structural models are given in the Supporting Information.[17]

The synthesized salts ***R*1b** and ***S*1b** differ only in the configuration of the chiral C atom of the API. Nevertheless, the crystal structures deviate significantly, and show different counterion conformations and different molecular packing (Figure 1).

Close inspection of the refined structures revealed that all structures ("correct" as well as "wrong" ones) were chemically reasonable and exhibited plausible hydrogen bond patterns and intermolecular contacts, except in one of the three wrong enantiomeric models of **2c**, in which two NH groups were lacking a hydrogen bond. Hence, the refinement of only one diastereomeric structure is not sufficient to identify the correct enantiomer of the API.

To determine the configuration of the API, different refinement and analysis procedures were developed; furthermore, the pair distribution functions (PDFs) of the structural

 © 2018 Wiley-VCH Verlag GmbH & Co. KGaA, Weinheim

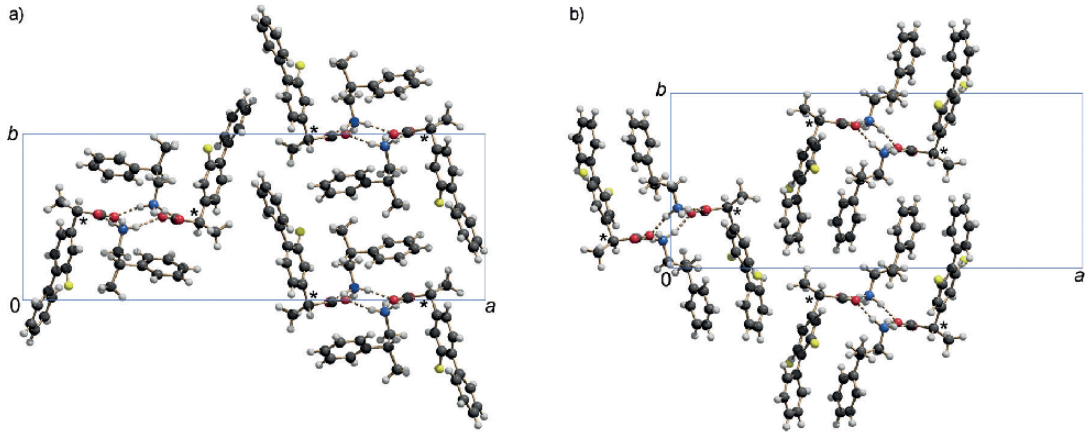

Figure 1. Comparison of the crystal structures of a) ***R*1 b** and b) ***S*1 b** (both with "correct" configurations). View along the hydrogen bond double chains; three chains are shown each. C black, H white, N blue, O red, F yellow.[18]

models were simulated and fitted to the experimental PDFs derived from powder data (see the Supporting Information). In four of the five salts, the *R* values of a standard Rietveld refinement already showed which enantiomer gives the better fit to the powder data (Table 1 and Figure 2). In the fifth salt (***R*1 a**), the *R* values were almost identical. However, two other criteria turned out to be even more decisive:

1) Which enantiomer is obtained when all geometrical restraints around the chiral carbon atoms are removed?
2) Which enantiomer gives the better fit to the powder data? To address this question, a disordered model was set up containing superpositions of both enantiomers of the API, and the occupancy of the corresponding atoms of the two enantiomers was refined.

For all five compounds, these criteria unambiguously yielded the correct enantiomers (Table 1). Hence, our method has been shown to work reliably, even with powder data of limited quality.

The method has three main limitations:

1) The method can only be applied to compounds that can form salts, meaning that the compounds need to be either acidic or basic. In today's pharmaceutical industry, most new compounds fulfil these conditions. However, co-crystallization with a chiral co-former may offer an extension of this method.[19]
2) For some APIs, all obtained powders were amorphous or poorly crystalline, so that the structure could not be determined (e.g., ***S*1 a**).
3) Sometimes, the structure solution from powder data fails, especially if the crystallinity of the powder is insufficient or if the structure has too many degrees of freedom (e.g., for **2 c**). In such instances, crystal structure prediction may offer an alternative way to solve the structure.[20]

This approach is certainly not the "holy grail" that solves all problems within this area, but it is a way forward to tackle some of the molecules for which the absolute configurations could not be solved by X-ray diffraction in the past. If the structure solution works well (which was the case in four of the five investigated cases), the presented approach provides an easy way to determine the absolute configuration of an API from minimal available amounts of substance. Of course, the procedure is not limited to pharmaceutical ingredients, but can also applied to natural products or chiral organometallic compounds, for example.

Table 1: Comparison of the Rietveld refinements of the diastereomeric salts with the correct and incorrect configuration of the API. In all cases, the better values have been italicized.

Compound	R_{wp} [%] (correct/wrong enantiomer)	Criterion 1 API enantiomer obtained by refinement[a]	Criterion 2 Occupancies of the correct/wrong enantiomers in the disordered model
***R*1 a**	*3.889*/*3.860*	***R*1** (correct)	*0.920(7)*/0.080(7)
***R*1 b**	*2.380*/2.727	***R*1** (correct)	*0.835(5)*/0.165(5)
***S*1 b**	*3.569*/3.805	***S*1** (correct)	*0.77(3)*/0.23(3)
2 c[b]	*2.513*/3.847	***R*2** (correct)	*0.976(3)*/0.024(3)
	3.492		*0.824(7)*/0.176(7)
	3.843		*0.901(3)*/0.099(3)
3 c	*5.132*/6.417	**(2*R*,5*S*)-3** (correct)	*0.842(6)*/0.158(6)

[a] Enantiomer of the API obtained in a refinement without restraints around the chiral C atoms. [b] One correct and three incorrect structural models.

Acknowledgements

We would like to thank Isolda M. Stais, René Meier, Haruko G. Gölz Carneo, and Kathrin Skorodumov (all students of Goethe University, Frankfurt) for their contributions in preparing the salts and preliminary evaluation of the powder data. We are grateful to Edith Alig (Goethe University, Frank-

 © 2018 Wiley-VCH Verlag GmbH & Co. KGaA, Weinheim

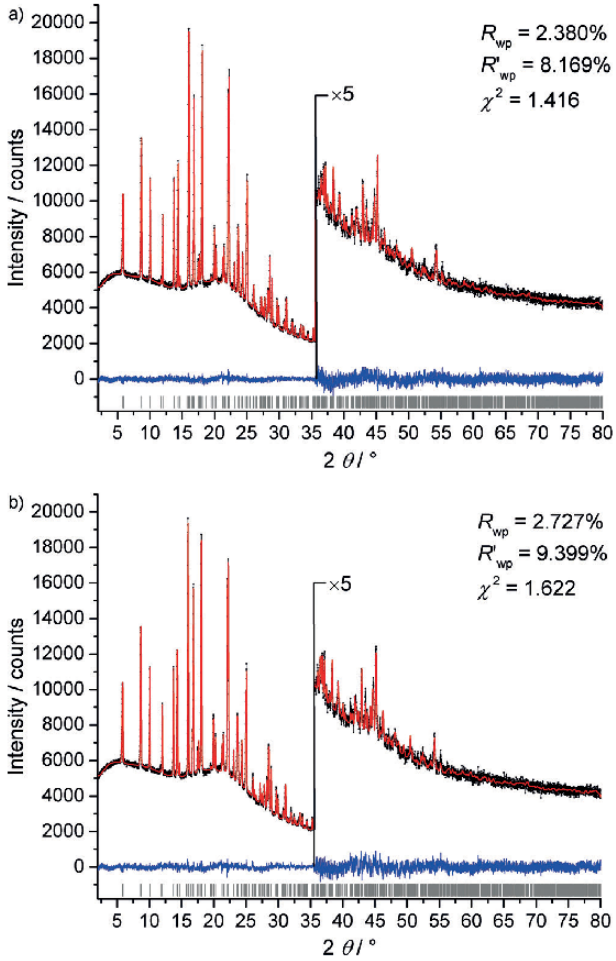

Figure 2. Rietveld plots of ***R*1b** obtained a) using the "correct" *R* enantiomer of **1**, and b) using the "wrong" *S* enantiomer of **1**. Observed intensities are denoted as black circles; calculated intensities are given as red lines. Difference curve below. The vertical ticks represent the reflection positions. It is clearly visible that the correct enantiomer of the API gives the better fit to the data.

furt) for the measurement of the X-ray powder patterns. C.Sch. thanks the Fonds der Chemischen Industrie for a generous scholarship.

Conflict of interest

The authors declare no conflict of interest.

Keywords: configuration determination · pharmaceutical compounds · Rietveld refinement · structure determination · X-ray powder diffraction

How to cite: *Angew. Chem. Int. Ed.* **2018**, *57*, 9150–9153
Angew. Chem. **2018**, *130*, 9289–9293

[1] a) W. H. Brooks, W. C. Guida, K. G. Daniel, *Curr. Top. Med. Chem.* **2011**, *11*, 760; b) S. S. Jayakrishnan, L. E. George, *Int. J. Res. Pharm. Biomed. Sci.* **2012**, *3*, 3; c) S. J. Mohan, E. C. Mohan, M. R. Yamsani, *Int. J. Pharm. Sci. Nanotechnol.* **2009**, *1*, 309; d) H. Murakami, *Top. Curr. Chem.* **2007**, *269*, 273.
[2] D. Pastoor, J. Gobburu, *Expert Opin. Drug Metab. Toxicol.* **2014**, *10*, 121: For example, citalopram, which is used to treat depression, was originally approved as the racemic mixture. Later on, the *S* enantiomer was approved as "escitalopram" with similar indications.
[3] H. D. Flack, G. Bernardinelli, *Chirality* **2008**, *20*, 681.
[4] a) R. W. W. Hooft, L. H. Straver, A. L. Spek, *J. Appl. Crystallogr.* **2008**, *41*, 96; b) S. Parsons, H. D. Flack, T. Wagner, *Acta Crystallogr. Sect. B* **2013**, *69*, 249.
[5] Very recently, a high-throughput screening method for the crystallization of organic salts from 0.2 μL of solution was developed; see: P. P. Nievergelt, M. Babor, J. Čejka, B. Spingler, *Chem. Sci.* **2018**, *9*, 3716.
[6] S. Paulekuhn, J. Dressman, C. Saal, *J. Med. Chem.* **2007**, *50*, 6665.
[7] A. Boultif, D. Louër, *J. Appl. Crystallogr.* **1991**, *24*, 987.
[8] W. I. F. David, K. Shankland, J. van de Streek, E. Pidcock, W. D. S. Motherwell, J. C. Cole, *J. Appl. Crystallogr.* **2006**, *39*, 910.
[9] D. W. M. Hofmann, *Acta Crystallogr. Sect. B* **2002**, *58*, 489.
[10] G. S. Pawley, *J. Appl. Crystallogr.* **1981**, *14*, 357.
[11] W. I. F. David, K. Shankland, *Acta Crystallogr. Sect. A* **2008**, *64*, 52.
[12] Cambridge Structural Database, Cambridge Crystallographic Data Centre, Cambridge, England, **2017**.
[13] P. Fernandes, K. Shankland, A. J. Florence, N. Shankland, A. Johnston, *J. Pharm. Sci.* **2007**, *96*, 1192.
[14] 4×3 parameters for rotation, 4×3−1 for translation (the *y* coordinate of the origin is floating in $P2_1$), and 4×2 parameters for intramolecular torsion.
[15] a) H. M. Rietveld, *Acta Crystallogr.* **1967**, *22*, 151; b) H. M. Rietveld, *J. Appl. Crystallogr.* **1969**, *2*, 65.
[16] TOPAS Academic V4.2; A. A.Coelho, Coelho Software, Brisbane, Australia, **2007**.
[17] CCDC 1812939, 1812887, 1812940, 1812941, 1812942, and 1832066 contain the supplementary crystallographic data of the Rietveld refinements of ***R*1a**, ***R*1b**, ***S*1b**, **2c**, **3c**, and the single crystal data of **2c**. These data can be obtained free of charge from The Cambridge Crystallographic Data Centre.
[18] SCHAKAL plot; E. Keller, SCHAKAL99, Kristallographisches Institut der Universität Freiburg, **1999**.
[19] a) D. A. Bock, C. W. Lehmann, *CrystEngComm* **2012**, *14*, 1534; b) G. Bolla, V. Chernyshev, A. Nangia, *IUCrJ* **2017**, *4*, 206.
[20] a) M. U. Schmidt, R. E. Dinnebier, *J. Appl. Crystallogr.* **1999**, *32*, 178; b) A. D. Bond, W. Jones, *Acta Crystallogr. Sect. B* **2002**, *58*, 233.

Manuscript received: December 21, 2017
Accepted manuscript online: February 6, 2018
Version of record online: June 19, 2018

 © 2018 Wiley-VCH Verlag GmbH & Co. KGaA, Weinheim

[LT1] Bestimmung der absoluten Konfiguration pharmazeutischer Wirkstoffe durch Röntgenpulverdiffraktometrie

Bibliographische Daten:

Titel:	Bestimmung der absoluten Konfiguration pharmazeutischer Wirkstoffe durch Röntgenpulverdiffraktometrie
Journal:	Angewandte Chemie
Jahr / Ausgabe:	2018 / Band 130, Ausgabe 29
Seiten:	9289–9293
DOI:	10.1002/ange.201713168
URL:	https://onlinelibrary.wiley.com/doi/full/10.1002/ange.201713168
Autoren:	Carina Schlesinger, Lukas Tapmeyer, Silke Dorothea Gumbert, Dragica Prill, Michael Bolte, Martin Ulrich Schmidt, Christoph Saal
eSI:	https://onlinelibrary.wiley.com/action/downloadSupplement?doi=10.1002%2Fanie.201713168&file=anie201713168-sup-0001-misc_information.pdf
OpenAccess:	Nein.
	Abgedruckt mit freundlicher Genehmigung von *John Wiley & Sons, Inc.*

GDCh Zuschriften Angewandte Chem

Absolute Konfiguration

Deutsche Ausgabe: DOI: 10.1002/ange.201713168
Internationale Ausgabe: DOI: 10.1002/anie.201713168

Bestimmung der absoluten Konfiguration pharmazeutischer Wirkstoffe durch Röntgenpulverdiffraktometrie

*Carina Schlesinger, Lukas Tapmeyer, Silke D. Gumbert, Dragica Prill, Michael Bolte, Martin U. Schmidt und Christoph Saal**

Abstract: *Die absolute Konfiguration pharmazeutischer Wirkstoffe lässt sich bestimmen, indem Salze der Wirkstoffe mit Gegenionen bekannter Chiralität hergestellt und ihre Kristallstrukturen durch Röntgenpulverdiffraktometrie bestimmt werden. Sehr kleine Substanzmengen (weniger als 1 mg) sind ausreichend. Die (oftmals schwierige) Züchtung von Einkristallen entfällt. Das Verfahren wird an fünf Beispielen gezeigt. Die Grenzen der Methode werden ebenfalls diskutiert.*

Heute sind die meisten neuen pharmazeutischen Wirkstoffmoleküle, die sich im Forschungsstadium befinden, chiral.[1] Vor 1980 wurden die meisten neuen Wirkstoffe als Racemate zugelassen. Dies ist heute nicht mehr der Fall, da sich die Anforderungen in den Zulassungsverfahren deutlich geändert haben. Die pharmakologische Aktivität, das toxikologische Profil und die Pharmakokinetik hängen stark davon ab, welches Enantiomer des Wirkstoffes eingesetzt wird.[2] Daher muss die Stereochemie eines neuen Wirkstoffes bereits in einem sehr frühen Forschungsstadium bekannt sein. Bei der Synthese einer neuen Verbindung oder bei einer Enantiomerentrennung ist jedoch die Zuordnung der absoluten Konfiguration häufig unklar. Dies betrifft nicht nur pharmazeutische Verbindungen, sondern unter anderem auch Naturstoffe und Organokatalysatoren.

Die absolute Stereochemie einer Verbindung wird normalerweise durch Einkristall-Röntgenstrukturanalyse bestimmt.[3,4] Die Züchtung des dafür notwendigen, genügend großen Einkristalls mit guter Kristallqualität ist oftmals schwierig, insbesondere, weil die meisten heutzutage in der Pharmaforschung untersuchten Moleküle eine hohe Molmasse und eine flexible Molekülgeometrie aufweisen und schlecht in Wasser und organischen Lösungsmitteln löslich sind. Ein zweites Problem ist die begrenzte Substanzmenge, die in einer frühen Forschungsphase zur Verfügung steht (typischerweise nur wenige Milligramm), was die Durchführung von Kristallzüchtungsexperimenten weiter erschwert.[5]

[*] M. Sc. C. Schlesinger, M. Sc. L. Tapmeyer, Dr. S. D. Gumbert, Dr. D. Prill, Dr. M. Bolte, Prof. Dr. M. U. Schmidt
Goethe-Universität
Institut für Anorganische und Analytische Chemie
Max-von-Laue-Straße 7, 60438 Frankfurt am Main (Deutschland)
Dr. C. Saal
Merck KGaA, Site-Operations – Analytics Healthcare
Frankfurter Landstraße 250, 64293 Darmstadt (Deutschland)
E-Mail: christoph.saal@merckgroup.com
Hintergrundinformationen und die Identifikationsnummer (ORCID) eines Autors sind unter: https://doi.org/10.1002/ange.201713168 zu finden.

Wir verfolgen daher einen anderen Ansatz und bestimmen die absolute Konfiguration pharmazeutischer Wirkstoffe durch Röntgenpulverdiffraktometrie. Im Röntgenpulverdiagramm kann zwar nicht zwischen Enantiomeren unterschieden werden, jedoch problemlos zwischen Diastereomeren. Da heute die meisten Pharma-Wirkstoffe saure oder basische Gruppen enthalten,[6] können sie leicht mit Gegenionen zu Salzen umgesetzt werden. Wenn die Gegenionen chiral sind, bildet sich aus den beiden Enantiomeren des Wirkstoffes ein Paar diastereomerer Salze. Die Kristallstrukturen dieser Salze lassen sich durch Röntgenpulverdiffraktometrie bestimmen. Hierdurch erhält man die relative Konfiguration der Stereozentren, womit sich bei bekannter Stereochemie des Gegenions die absolute Konfiguration des Wirkstoffmoleküles ergibt.

Dieses Verfahren wird im Folgenden an vier enantiomerenreinen Wirkstoffen demonstriert. Die Wirkstoffe wurden mit jeweils einem oder zwei Salzbildnern kombiniert. Die absolute Konfiguration des Wirkstoffs wurde als unbekannt angenommen, die des Salzbildners als bekannt. Als Wirkstoffe wurden gewählt: (*R*)-Flurbiprofen (***R*1**), (*S*)-Flurbiprofen (***S*1**), Aminoglutethimid (**2**) und Lamivudin (**3**; siehe Schema 1). Flurbiprofen ist ein nichtstereoidaler Entzündungshemmer, der ursprünglich als racemische Mischung zugelassen wurde. Inzwischen wird das reine *R*-Enantiomer unter dem Namen Tarenbufil ebenfalls als Antiphlogistikum vermarktet. Aminoglutethimid ist ein Aromatase-Hemmer. Lamivudin ist ein Nukleosid-Analogon und wird in der HIV-Therapie eingesetzt.

Die beiden Enantiomere von Flurbiprofen (***R*1** und ***S*1**) wurden mit den chiralen Basen Chinin (**a**) und (*R*)-2-Phenylpropylamin (**b**) umgesetzt. Die anderen beiden Wirkstoffe (**2** und **3**) sind Basen; sie wurden mit (*R*)-Camphersulfonsäure (**c**) umgesetzt (Schema 1).

Zur Herstellung der Salze haben sich zwei Methoden bewährt:

(1) Im Milligramm-Maßstab: Eine Lösung des Wirkstoffes in einem Lösungsmittel (z.B. Aceton) wird in einem Rollrandgläschen mit einer Lösung des Salzbildners in demselben Lösungsmittel vereinigt; anschließend lässt man das Lösungsmittel langsam verdampfen.

(2) Im Mikrogramm-Maßstab: Mit einer auf beiden Seiten offenen 0.7-mm-Kapillare werden ca. 2 μL beider Lösungen nacheinander aufgesaugt, wobei die Salzbildung in der Kapillare erfolgt. Die Kapillare wird anschließend auf einer Seite verschlossen. Nach dem Verdampfen des Lösungsmittels wird die Kapillare ohne weitere Behandlung auf das Pulverdiffraktometer aufgesetzt. Für

 © 2018 Wiley-VCH Verlag GmbH & Co. KGaA, Weinheim

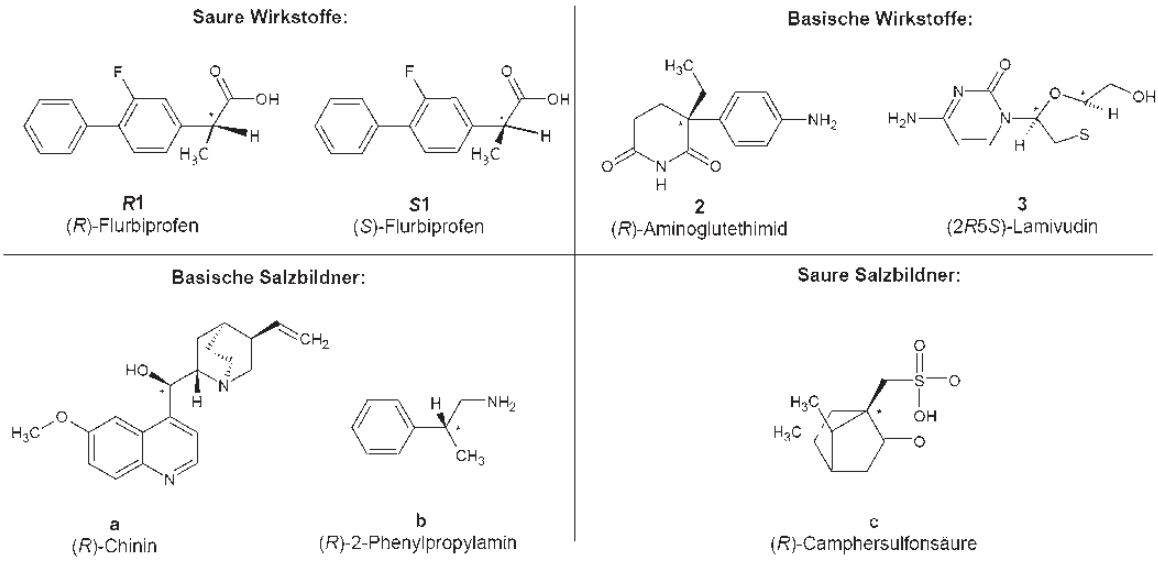

Schema 1. Strukturen der untersuchten Wirkstoffe und der dazugehörigen Gegenionen. Die relevanten chiralen Atome sind mit einem Stern markiert.

dieses Verfahren genügen ca. 100 μg des Wirkstoffs oder sogar noch weniger.

Mit beiden Verfahren erhielten wir mikrokristalline Pulver von fünf Salzen: ***R*1a**, ***R*1b**, ***S*1b**, **2c** und **3c** (für experimentelle Details, siehe die Hintergrundinformationen). Das sechste Salz ***S*1a**, fiel stets als schlecht kristallines Pulver an und widerstand jedem Versuch der Strukturbestimmung.

Die Röntgenpulverdiffraktogramme aller Proben wurden in Transmission auf einem STOE STADI-P Diffraktometer gemessen (Details siehe die Hintergrundinformationen).

Die Pulverdiagramme wurden mit DICVOL04[7] innerhalb des Programmpakets DASH[8] indiziert. Aus den systematischen Auslöschungen wurden die möglichen Raumgruppen bestimmt. Die Anzahl der Moleküle pro Elementarzelle wurde aus den Volumeninkrementen nach Hofmann[9] berechnet. Eine anschließende Pawley-Anpassung[10] bestätigte in allen Fällen die Indizierung und die Raumgruppe.

Die Strukturen wurden in DASH durch Realraummethoden[11] mit „Simulated Annealing“ gelöst. Dabei wurden die Gitterkonstanten, die Raumgruppe und die Molekülgeometrie vorgegeben. Die Position und die Orientierung der Moleküle in der Elementarzelle sowie die intramolekularen Freiheitsgrade (Rotationen um Einfachbindungen) wurden variiert. Die Molekülgeometrie des Wirkstoffes und des Gegenions wurde aus Kristallstrukturdaten ähnlicher Verbindungen aus der Cambridge Structural Database (CSD)[12] konstruiert. Die absolute Konfiguration des Gegenions wurde vorgegeben, während für den Wirkstoff beide möglichen Enantiomere in zwei getrennten DASH-Läufen verwendet wurden.

Erfahrungsgemäß ist die Lösung von Kristallstrukturen aus Röntgenpulverdaten mit Realraummethoden problematisch, sobald die Gesamtzahl der zu bestimmenden Parameter (für die Position und Orientierung der Moleküle und die intramolekularen Freiheitsgrade) eine Grenze von etwa 20 übersteigt.[13] Diese Grenze wurde bei den Verbindungen **2c** und **3c** überschritten: Beide Salze kristallisieren in $P2_1$ mit $Z=4$ und $Z'=2$. Die asymmetrische Einheit enthält zwei Anionen und zwei Kationen. Beide haben jeweils zwei intramolekulare Torsionsfreiheitsgrade, sodass insgesamt 31 Parameter zu bestimmen waren.[14] Während sich die Kristallstruktur von **3c** problemlos und reproduzierbar lösen ließ, widersetzte sich die Verbindung **2c** jeglichen Strukturlösungsversuchen (siehe die Hintergrundinformationen). Glücklicherweise fanden wir in einem der Kristallisationsansätze von **2c** einen Einkristall, und konnten so die Struktur durch Einkristallröntgenstrukturanalyse bestimmen. Die so erhaltene Struktur wurde als Startmodell für die folgenden Rietveld-Verfeinerungen verwendet. Für das falsche Enantiomer wurden drei chemisch sinnvolle Kristallstrukturen konstruiert. Alle folgenden Verfeinerungen von **2c** wurden in gleicher Weise wie für die anderen Salze durchgeführt.

Die Kristallstrukturen der übrigen drei Verbindungen (***R*1a**, ***R*1b** und ***S*1b**) wurden ohne Schwierigkeiten aus Röntgenpulverdaten gelöst.

Alle richtigen und falschen Strukturen wurden einer Rietveld-Verfeinerung[15] mit TOPAS[16] unterzogen. Um eine chemisch sinnvolle Molekülgeometrie zu gewährleisten, wurden Restraints (Sollwertvorgaben) für Bindungslängen, Bindungswinkel und planare Gruppen verwendet.

Für die richtigen und die falschen Enantiomere erfolgten die Verfeinerungen unter exakt den gleichen Bedingungen (gleiche Verfeinerungsstrategie, gleiche Restraints usw.). Alle Rietveld-Verfeinerungen konvergierten problemlos. Kristallographische Daten und Rietveld-Diagramme aller richtigen und falschen Strukturen sind in den Hintergrundinformationen zu finden.[17]

 © 2018 Wiley-VCH Verlag GmbH & Co. KGaA, Weinheim

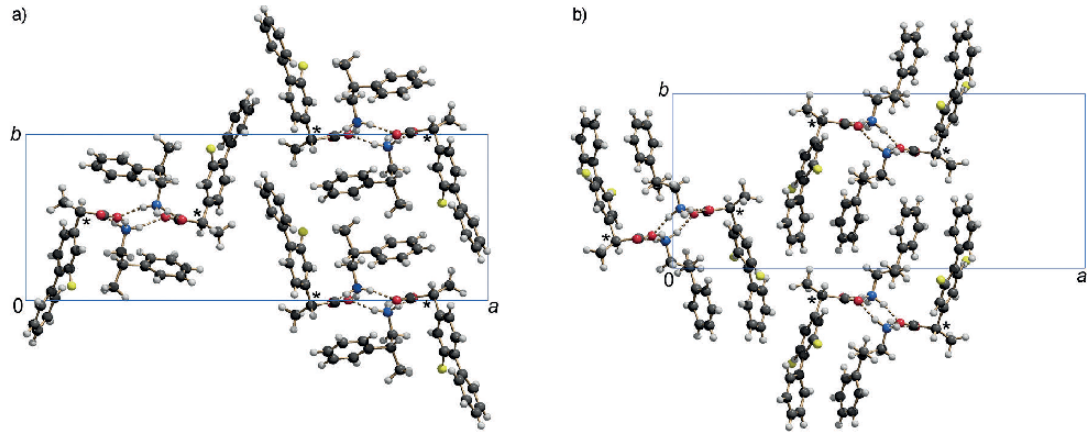

Abbildung 1. Vergleich der experimentell ermittelten Kristallstrukturen von a) ***R*1 b** und b) ***S*1 b**, beide mit der „richtigen" Konfiguration. Die Ionen sind durch Wasserstoffbrücken zu Doppelketten verbunden. Blick entlang der Doppelketten. C schwarz, H weiß, N blau, O rot, F gelb.[18]

Formal unterscheiden sich die Salze ***R*1 b** und ***S*1 b** nur in der Konfiguration des chiralen Kohlenstoffatoms des Flurbiprofens. Nichtsdestotrotz haben sie verschiedene Kristallstrukturen. Sowohl die Konformation des Gegenions, als auch die Anordnung der Moleküle im Festkörper ist deutlich unterschiedlich, siehe Abbildung 1.

Alle Kristallstrukturen – sowohl die mit den richtigen, als auch diejenigen mit den falschen Enantiomeren der Wirkstoffe – erschienen chemisch sinnvoll. Auch die intermolekularen Abstände und die Wasserstoffbrückenmuster entsprachen in allen Fällen den Erwartungen. Lediglich in einem der drei falschen Modelle für **2 c** fehlten die Wasserstoffbrücken an zwei NH-Gruppen. Wenn also nur eines der Diastereomere verfeinert wird, ist aus den Ergebnissen nicht ersichtlich, ob es sich um das richtige oder das falsche Enantiomer des Wirkstoffes handelt.

Zur Bestimmung der absoluten Konfiguration der Wirkstoffe wurden verschiedene Verfeinerungs- und Auswertungsverfahren entwickelt; zusätzlich wurden die Paarverteilungsfunktionen (PDFs) der Strukturmodelle simuliert und an die aus den Pulverdaten berechneten PDFs angepasst (siehe die Hintergrundinformationen). Bei vier der fünf Salze war bereits aus den *R*-Werten der routinemäßigen Rietveld-Verfeinerungen ersichtlich, welches das richtige Diastereomer war (Tabelle 1, Abbildung 2). Beim fünften Salz (***R*1 a**) waren die *R*-Werte praktisch gleich.

Zwei weitere Kriterien erwiesen sich als noch aussagekräftiger:

(1) Welches Enantiomer ergibt sich, wenn alle Restraints am chiralen C-Atom entfernt werden?

(2) Welches Enantiomer führt zu einer besseren Anpassung an das Röntgenpulverdiagramm? Hierzu wurde ein fehlgeordnetes Modell verwendet, das beide möglichen Enantiomere enthält, und die Besetzung der entsprechenden Atomgruppen wurde verfeinert.

Diese beiden Kriterien lieferten für alle fünf Salze eindeutig das richtige Enantiomer (Tabelle 1). Die absolute Konfiguration eines Wirkstoffes lässt sich also durch Röntgenpulverdiffraktometrie an diastereomeren Salzen zweifelsfrei bestimmen, auch wenn die Röntgenpulverdaten nur von mäßiger Qualität sind.

Das Verfahren stößt in folgenden Fällen an seine Grenzen:

(1) Die Methode kann nur bei Wirkstoffen eingesetzt werden, die saure oder basische Gruppen enthalten. Dies ist jedoch bei den heutigen Wirkstoffmolekülen meist der Fall. Anderenfalls kann man versuchen, durch gemeinsame Kristallisation mit einer zweiten chiralen Verbindung einen diastereomeren Co-Kristall zu erhalten.[19]

(2) Bei manchen Wirkstoffen führen die Kristallisationsversuche nur zu amorphen oder sehr schlecht kristallinen Proben, sodass die Kristallstrukturen nicht bestimmt

Tabelle 1: Ergebnisse der Rietveld-Verfeinerungen der Diastereomerenpaare mit richtiger und falscher Konfiguration des Wirkstoffes. Der bessere Wert ist jeweils kursiv hervorgehoben.

Verbindung	R_{wp}/% (richtiges/falsches Enantiomer)	Kriterium 1 Enantiomer aus der Rietveld-Verfeinerung[a]	Kriterium 2 Besetzungsfaktoren für das richtige/falsche Enantiomer in einem Fehlordnungsmodell
***R*1 a**	*3.889*/3.860	***R*1** (richtig)	*0.920(7)*/0.080(7)
***R*1 b**	*2.380*/2.727	***R*1** (richtig)	*0.835(5)*/0.165(5)
***S*1 b**	*3.569*/3.805	***S*1** (richtig)	*0.77(3)*/0.23(3)
2 c[b]	*2.513*/3.847	***R*2** (richtig)	*0.976(3)*/0.024(3)
	3.492		*0.824(7)*/0.176(7)
	3.843		*0.901(3)*/0.099(3)
3 c	*5.132*/6.417	**(2*R*5*S*)-3** (richtig)	*0.842(6)*/0.158(6)

[a] Enantiomer des Wirkstoffes, das bei einer Verfeinerung ohne Restraints am chiralen C-Atom des Wirkstoffes erhalten wird. [b] Ein Strukturmodell für das richtige Enantiomer von **2 c**, drei Strukturmodelle für das falsche Enantiomer.

 © 2018 Wiley-VCH Verlag GmbH & Co. KGaA, Weinheim

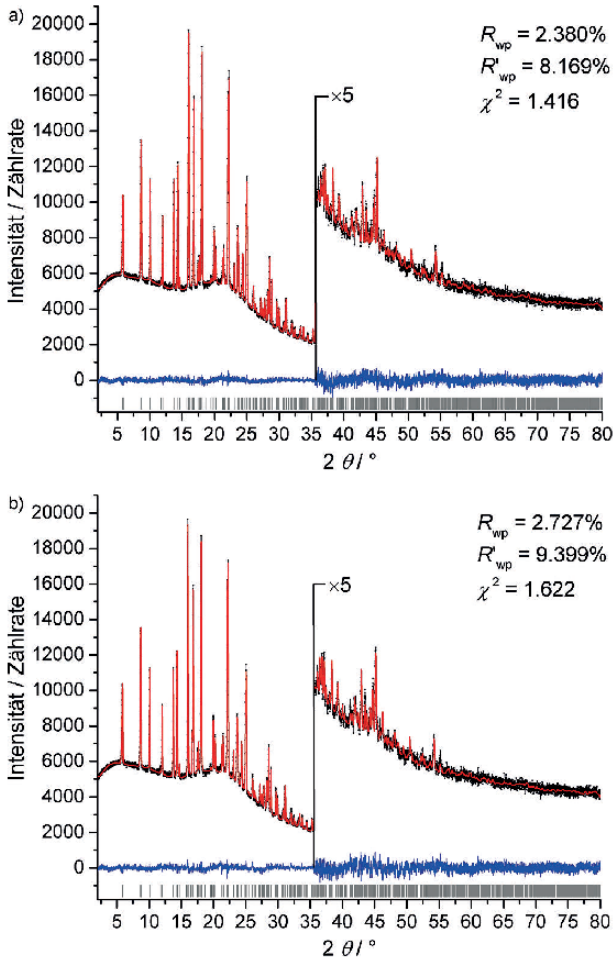

Abbildung 2. Rietveld-Diagramme von ***R*1b**: a) mit dem richtigen Enantiomer von **1**; b) mit dem falschen Enantiomer (*S* statt *R*) von **1**. Gemessene Intensitäten sind als schwarze Kreise dargestellt, berechnete Intensitäten als rote Linie, darunter die Differenzkurve in blau. Die senkrechten Striche geben die Reflexpositionen an. Das richtige Enantiomer führt zu einer besseren Anpassung.

werden können (Beispiel: ***S*1a**).

(3) In einigen Fällen scheitert die Kristallstrukturbestimmung aus Röntgenpulverdaten, insbesondere dann, wenn die Kristallinität des Pulvers nicht ausreicht, oder wenn die Moleküle zu viele Freiheitsgrade enthalten (wie bei **2c**). In solchen Fällen kann man versuchen, die Kristallstruktur durch eine Kristallstrukturvorhersage zu lösen.[20]

Das hier vorgestellte Verfahren ist sicherlich nicht die „eierlegende Wollmilchsau“, mit der alle Probleme in diesem Bereich gelöst werden können. Wenn jedoch die Strukturlösung aus Pulverdaten gelingt, was hier bei vier von fünf Salzen der Fall war, ist das vorgestellte Verfahren eine einfache und schnelle Methode, um die absolute Konfiguration von Wirkstoffen mit sehr kleinen Mengen in einem frühen Forschungsstadium zu bestimmen. Dasselbe gilt für die Fälle, in denen selbst mit größeren Substanzmengen kein geeigneter Einkristall des Wirkstoffs gezüchtet werden kann. Das Verfahren ist natürlich nicht auf pharmazeutische Wirkstoffe beschränkt, sondern eignet sich ebenso für Naturstoffe, chirale metallorganische Verbindungen und ähnliches.

Danksagung

Wir danken den Studierenden Isolda M. Stais, René Meier, Haruko G. Gölz Carneo und Kathrin Skorodumov (Goethe-Universität, Frankfurt) für ihre Beiträge zur Herstellung der Salze und der Vorauswertung der Röntgenpulverdaten. Wir danken Edith Alig (Goethe-Universität, Frankfurt) für die Messung der Röntgenpulverdiffraktogramme. C.Sch. dankt dem Fonds der Chemischen Industrie für ein Doktorandenstipendium.

Interessenkonflikt

Die Autoren erklären, dass keine Interessenkonflikte vorliegen.

Stichwörter: Konfigurationsbestimmung · Pharmazeutische Verbindungen · Rietveld-Verfeinerung · Röntgenpulverdiffraktometrie · Strukturaufklärung

Zitierweise: *Angew. Chem. Int. Ed.* **2018**, *57*, 9150–9153
Angew. Chem. **2018**, *130*, 9289–9293

[1] a) W. H. Brooks, W. C. Guida, K. G. Daniel, *Curr. Top. Med. Chem.* **2011**, *11*, 760; b) S. S. Jayakrishnan, L. E. George, *Int. J. Res. Pharm. Biomed. Sci.* **2012**, *3*, 3; c) S. J. Mohan, E. C. Mohan, M. R. Yamsani, *Int. J. Pharm. Sci. Nanotechnol.* **2009**, *1*, 309; d) H. Murakami, *Top. Curr. Chem.* **2007**, *269*, 273.
[2] D. Pastoor, J. Gobburu, *Expert Opin. Drug Metab. Toxicol.* **2014**, *10*, 121: Beispielsweise wurde das Antidepressivum Citalopram ursprünglich als Racemat eingesetzt; später wurde das *S*-Enantiomer unter dem Namen „Escitalopram“ mit ähnlichen Indikationen zugelassen.
[3] H. D. Flack, G. Bernardinelli, *Chirality* **2008**, *20*, 681.
[4] a) R. W. W. Hooft, L. H. Straver, A. L. Spek, *J. Appl. Crystallogr.* **2008**, *41*, 96; b) S. Parsons, H. D. Flack, T. Wagner, *Acta Crystallogr. Sect. B* **2013**, *69*, 249.
[5] Kürzlich wurde eine Hochdurchsatzscreening-Methode zur Kristallisation organischer Salze im 0.2-μL-Maßstab entwickelt: P. P. Nievergelt, M. Babor, J. Čejka, B. Spingler, *Chem. Sci.* **2018**, *9*, 3716.
[6] S. Paulekuhn, J. Dressman, C. Saal, *J. Med. Chem.* **2007**, *50*, 6665.
[7] A. Boultif, D. Louër, *J. Appl. Crystallogr.* **1991**, *24*, 987.
[8] W. I. F. David, K. Shankland, J. van de Streek, E. Pidcock, W. D. S. Motherwell, J. C. Cole, *J. Appl. Crystallogr.* **2006**, *39*, 910.
[9] D. W. M. Hofmann, *Acta Crystallogr. Sect. B* **2002**, *58*, 489.
[10] G. S. Pawley, *J. Appl. Crystallogr.* **1981**, *14*, 357.
[11] W. I. F. David, K. Shankland, *Acta Crystallogr. Sect. A* **2008**, *64*, 52.
[12] Cambridge Structural Database, Cambridge Crystallographic Data Centre, Cambridge, England, **2005**.
[13] P. Fernandes, K. Shankland, A. J. Florence, N. Shankland, A. Johnston, *J. Pharm. Sci.* **2007**, *96*, 1192.
[14] 4×3 Parameter für die Molekülorientierung, 4×3−1 für die Molekülposition (die *y*-Koordinate des Ursprungs ist frei in $P2_1$),

 © 2018 Wiley-VCH Verlag GmbH & Co. KGaA, Weinheim

und 4 × 2 Parameter für die intramolekularen Torsionsfreiheitsgrade.
[15] a) H. M. Rietveld, *Acta Crystallogr.* **1967**, *22*, 151; b) H. M. Rietveld, *J. Appl. Crystallogr.* **1969**, *2*, 65.
[16] TOPAS Academic V4.2; A. A.Coelho, Coelho Software, Brisbane, Australia, **2007**.
[17] CCDC-1812939, -1812887, -1812940, -1812941, -1812942 und -1832066 enthalten die kristallographischen Daten der Rietveld-Verfeinerungen von ***R*1a**, ***R*1b**, ***S*1b**, **2c**,**3c** und der Einkristallstrukturanalyse von **2c**. Die Daten sind kostenlos beim Cambridge Crystallographic Data Centre erhältlich.
[18] SCHAKAL-Darstellung: E. Keller, SCHAKAL99, Kristallographisches Institut der Universität Freiburg, **1999**.
[19] a) D. A. Bock, C. W. Lehmann, *CrystEngComm* **2012**, *14*, 1534; b) G. Bolla, V. Chernyshev, A. Nangia, *IUCrJ* **2017**, *4*, 206.
[20] a) M. U. Schmidt, R. E. Dinnebier, *J. Appl. Crystallogr.* **1999**, *32*, 178; b) A. D. Bond, W. Jones, *Acta Crystallogr. Sect. B* **2002**, *58*, 233.

Manuskript erhalten: 21. Dezember 2017
Akzeptierte Fassung online: 6. Februar 2018
Endgültige Fassung online: 19. Juni 2018

 © 2018 Wiley-VCH Verlag GmbH & Co. KGaA, Weinheim

7.2 [LT2] 6-Amino-2-iminiumyl-4-oxo-1,2,3,4-tetrahydropyrimidin-5-aminium sulfate monohydrate

Bibliographische Daten:

Titel:	6-Amino-2-iminiumyl-4-oxo-1,2,3,4-tetrahydropyrimidin-5-aminium sulfate monohydrate
Journal:	IUCrData
Jahr / Ausgabe:	2019 / 4
Artikel:	x190689
DOI:	10.1107/S2414314619006898
URL:	http://scripts.iucr.org/cgi-bin/paper?rz4030
Autoren:	Lukas Tapmeyer, Dragica Prill
eSI:	http://scripts.iucr.org/cgi-bin/paper?rz4030 https://doi.org/10.1107/S2414314619006898/rz4030sup1.cif
OpenAccess:	Ja.

Beiträge:	Lukas Tapmeyer: Synthese und Kristallisation, Röntgenstrukturanalyse, Schreiben des Entwurfs, Korrekturen. Dragica Prill: Schreiben des Entwurfs, Korrekturen.

electronic reprint

IUCrData

ISSN: 2414-3146
iucrdata.iucr.org/x

6-Amino-2-iminiumyl-4-oxo-1,2,3,4-tetrahydropyrimidin-5-aminium sulfate monohydrate

Lukas Tapmeyer and Dragica Prill

IUCrData (2019). **4**, x190689

IUCr Journals
CRYSTALLOGRAPHY JOURNALS ONLINE

This open-access article is distributed under the terms of the Creative Commons Attribution Licence http://creativecommons.org/licenses/by/4.0/legalcode, which permits unrestricted use, distribution, and reproduction in any medium, provided the original authors and source are cited.

data reports

IUCrData

ISSN 2414-3146

6-Amino-2-iminiumyl-4-oxo-1,2,3,4-tetrahydropyrimidin-5-aminium sulfate monohydrate

Lukas Tapmeyer* and Dragica Prill

Institute of Inorganic and Analytical Chemistry, Goethe University Frankfurt am Main, Max-von-Laue-Str. 7, Frankfurt am Main, Hessen, 60438, Germany. *Correspondence e-mail: tapmeyer@chemie.uni-frankfurt.de

Received 24 April 2019
Accepted 13 May 2019

Edited by C. Rizzoli, Universita degli Studi di Parma, Italy

Keywords: crystal structure; triaminodihydropyrimidinone; hydrogen bonds.

CCDC reference: 1915747

Structural data: full structural data are available from iucrdata.iucr.org

The title compound, $C_4H_9N_5O^{2+}\cdot SO_4^{2-}\cdot H_2O$, is the monohydrate of the commercially available compound '$C_4H_7N_5O\cdot H_2SO_4\cdot xH_2O$'. It is obtained by reprecipitation of $C_4H_7N_5O\cdot H_2SO_4\cdot xH_2O$ from dilute sodium hydroxide solution with dilute sulfuric acid. The crystal structure of anhydrous 2,4,5-triamino-1,6-dihydropyrimidin-6-one sulfate is known, although called by the authors 5-amminium-6-amino-isocytosinium sulfate [Bieri *et al.* (1993). Private communication (refcode HACDEU). CCDC, Cambridge, England]. In the structure, the sulfate group is deprotonated, whereas one of the amino groups is protonated ($R_2C-NH_3^+$) and one is rearranged to a protonated imine group ($R_2C{=}NH_2^+$). This arrangement is very similar to the known crystal structure of the anhydrate. Several tautomeric forms of the investigated molecule are possible, which leads to questionable proton attributions. The measured data allowed the location of all hydrogen atoms from the residual electron density. In the crystal, ions and water molecules are linked into a three-dimensional network by N—H···O and O—H···O hydrogen bonds.

3D view

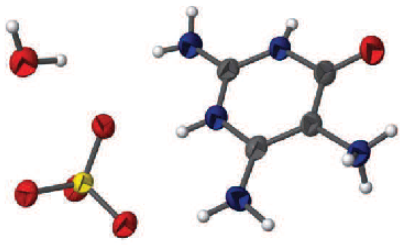

Chemical scheme

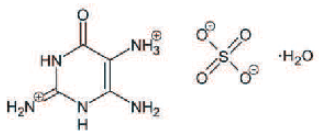

Structure description

2,4,5-Triamino-1,6-dihydropyrimidin-6-one (also called 2,4,5-triamino-6-hydroxypyrimidine sulfate) and/or its tautomer 2,4,5-triamino-6-hydroxypyrimidine are relevant starting materials for either very basic (Traube, 1900) or more advanced organic syntheses, including natural materials such as butterfly-wing pigments (Purrmann, 1940) and potential novel antiviral lead structures (Abbas *et al.*, 2017). The structure of the monohydrate form is herewith elucidated and confirms the protonation of the known structure (CSD refcode: HACDEU; Bieri *et al.*, 1993).

The title compound crystallizes in the triclinic space group $P\overline{1}$. The asymmetric unit is composed of one organic dication ($[C_4H_9N_5O]^{2+}$), one sulfate anion and one water

OPEN ACCESS

electronic reprint

Table 1
Hydrogen-bond geometry (Å, °).

D—H···A	D—H	H···A	D···A	D—H···A
N8—H8A···O4^{i}	0.89	2.46	3.113 (4)	131
N8—H8A···O5^{i}	0.89	1.99	2.827 (4)	157
N8—H8B···O3^{ii}	0.89	1.94	2.788 (4)	159
N8—H8C···O5^{iii}	0.89	2.13	2.942 (4)	152
N9—H9···O4^{iv}	0.82 (4)	1.93 (4)	2.739 (5)	168 (4)
N10—H10···O2	0.88 (4)	1.87 (4)	2.677 (4)	152 (3)
N10—H10···O4	0.88 (4)	2.58 (5)	3.329 (4)	143 (4)
N11—H11A···O2	0.80 (5)	2.56 (7)	3.106 (6)	126 (5)
N11—H11A···OW1^{v}	0.80 (5)	2.29 (5)	2.956 (4)	142 (5)
N11—H11B···O3^{iv}	0.89 (6)	2.00 (6)	2.845 (6)	158 (5)
N13—H13A···OW1^{ii}	0.98 (6)	1.98 (7)	2.924 (5)	161 (5)
N13—H13B···O4	0.91 (5)	2.10 (5)	2.961 (4)	156 (5)
OW1—HW12···O2	0.96 (6)	2.10 (6)	2.798 (4)	128 (5)
OW1—HW11···OW1^{vi}	0.96 (3)	2.59 (5)	3.390 (5)	141 (3)

Symmetry codes: (i) $-x, -y+1, -z+1$; (ii) $-x+1, -y+1, -z+1$; (iii) $x, y-1, z+1$; (iv) $x, y-1, z$; (v) $-x+1, -y+1, -z$; (vi) $-x+2, -y+1, -z$.

molecule (Fig. 1). The present tautomer is the 2,4,5-triamino-1,6-dihydropyrimidin-6-one. The molecule is almost planar [r.m.s. deviation = 0.026 Å, maximum deviation 0.046 (4) Å for N13], except for the amino group H atoms.

The title compound shows a layered structure with the most polar compartments oriented in the (100) plane (Fig. 2). Within the layers, the dicationic molecules form hydrogen bonds to the water molecules and to the sulfate dianions. The layers are interlinked by hydrogen bonds between the sulfate dianion and the organic dication (Table 1).

Powder data confirmed the phase identity of the single crystals with experimentally obtained bulk material. Furthermore, a commercial sample of $C_4H_7N_5O{\cdot}H_2SO_4{\cdot}xH_2O$ could be quantitatively analyzed by Rietveld refinement with *TOPAS* (Coelho, 2018; Rietveld, 2010), resulting in a composition of 76.4 (3)% of the known anhydrate phase and 23.6 (3)% of the monohydrate described in this paper (Fig. 3). Since the monohydrate is a yellow solid and the anhydrous form rather colorless, the brown color of the commercial sample could be attributed to minor (and probably amorphous) impurities.

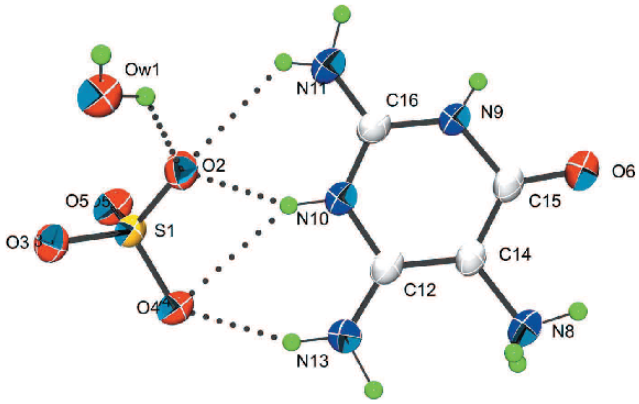

Figure 1
The asymmetric unit of the title compound with displacement ellipsoids drawn at the 50% probability level. Hydrogen bonds are shown as dashed lines.

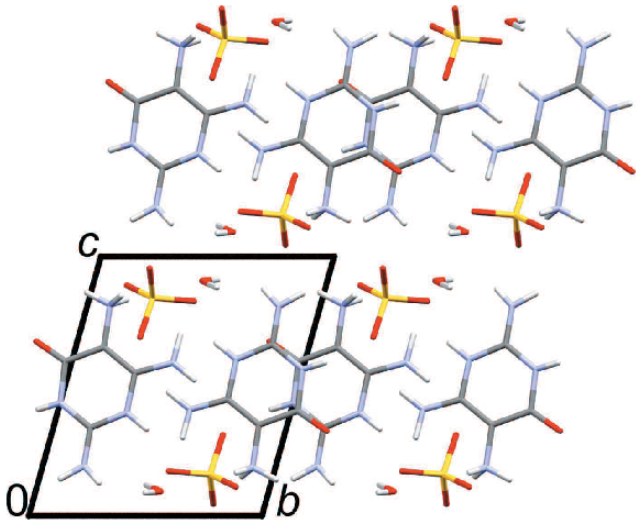

Figure 2
Partial packing diagram of the title compound viewed along the *a* axis.

Synthesis and crystallization

5 g (~20 mmol) of brown 2,4,5-triamino-6-hydroxypyrimidine sulfate ($C_4H_7N_5OH_2{\cdot}SO_4{\cdot}xH_2O$) as purchased from TCI (purity > 90.0%) were dissolved under stirring at 70°C in 100 ml of water with 2 g of sodium hydroxide (~50 mmol). The resulting reddish orange solution (with a pH of about 9–10) was filtered into a solution of 2.6 g of H_2SO_4 (96%, 25 mmol) in 900 ml water. The instantaneously formed red-to-brown aggregates were left to settle down for two h and the suspension was then filtered. The yellow filtrate was left at room temperature overnight. The formed pale-yellow crystals of the title compound were filtered off on a nutsch flask. The obtained yield for one purification cycle was about 15%. For efficiency, the filtrate can be boiled down and the brown solid precipitate can be reused in the next batch.

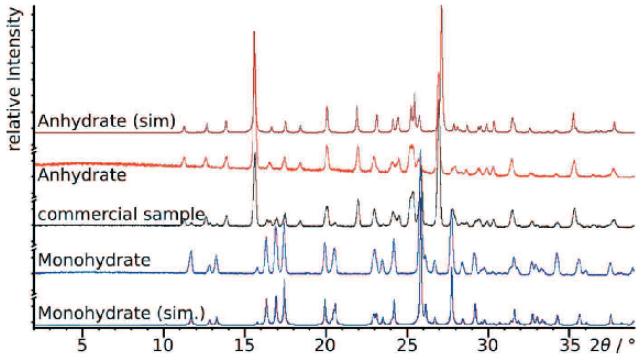

Figure 3
X-ray powder diagrams of (from top to bottom) the known anhydrous title compound (simulated, dark red), the vacuum-dried title compound (red), the commercial sample (black), the title compound (blue) and the pattern simulated from the title compound's single-crystal structure (dark blue).

electronic reprint

Table 2
Experimental details.

Crystal data	
Chemical formula	$C_4H_9N_5O^{2+}\cdot SO_4^{2-}\cdot H_2O$
M_r	257.24
Crystal system, space group	Triclinic, $P\overline{1}$
Temperature (K)	296
a, b, c (Å)	7.0128 (7), 7.9882 (8), 9.0732 (9)
α, β, γ (°)	74.121 (4), 86.734 (4), 79.290 (4)
V (Å^3)	480.36 (8)
Z	2
Radiation type	Cu $K\alpha$
μ (mm^{-1})	3.34
Crystal size (mm)	0.2 × 0.15 × 0.1
Data collection	
Diffractometer	Siemens Bruker CCD
Absorption correction	Multi-scan (*SADABS*; Bruker, 2015)
T_{min}, T_{max}	0.526, 0.753
No. of measured, independent and observed [$I > 2\sigma(I)$] reflections	20827, 1720, 1599
R_{int}	0.051
Refinement	
$R[F^2 > 2\sigma(F^2)]$, $wR(F^2)$, S	0.080, 0.281, 1.40
No. of reflections	1720
No. of parameters	179
No. of restraints	20
H-atom treatment	H atoms treated by a mixture of independent and constrained refinement
$\Delta\rho_{max}$, $\Delta\rho_{min}$ (e Å^{-3})	0.63, −1.04

Computer programs: *APEX3* (Bruker, 2012), *SAINT* (Bruker, 2015), *SHELXT* (Sheldrick, 2015*a*), *SHELXL2018* (Sheldrick, 2015*b*), *Mercury* (Macrae *et al.*, 2008), *ORTEPIII* (Burnett & Johnson, 1996) and *publCIF* (Westrip, 2010).

Refinement

Crystal data, data collection, and structure refinement details are summarized in Table 2.

X-ray powder diffraction data were recorded at room temperature in transmission geometry on a Stoe Stadi-P diffractometer equipped with a curved Ge(111) primary monochromator and a linear position-sensitive detector, using Cu $K\ \alpha_1$ radiation (λ =1.5406 Å). Samples were rotated in 0.7 mm glass capillaries during measurement.

Acknowledgements

The authors wish to express their gratitude to Edith Alig (Goethe-University), who provided us with the X-ray powder measurements, and to Wilhelm Maximilian Hützler, who helped with the interpretation of the single-crystal data.

References

Abbas, Z. A. A., Abu-Mejdad, N. M. J., Atwan, Z. W. & Al-Masoudi, N. A. (2017). *J. Heterocycl. Chem.* **54**, 895–903.
Bieri, J. H., Prewo, R. & Linden, A. (1993). Private communication (refcode HACDEU). CCDC, Cambridge, England
Bruker (2012). *APEX3*. Bruker AXS Inc., Madison, Wisconsin, USA.
Bruker (2015). *SAINT* and *SADABS*. Bruker AXS Inc., Madison, Wisconsin, USA.
Burnett, M. N. & Johnson, C. K. (1996). *ORTEPIII*. Report ORNL-6895. Oak Ridge National Laboratory, Tennessee, USA.
Coelho, A. A. (2018). *J. Appl. Cryst.* **51**, 210–218.
Macrae, C. F., Bruno, I. J., Chisholm, J. A., Edgington, P. R., McCabe, P., Pidcock, E., Rodriguez-Monge, L., Taylor, R., van de Streek, J. & Wood, P. A. (2008). *J. Appl. Cryst.* **41**, 466–470.
Purrmann, R. (1940). *Justus Liebigs Ann. Chem.* **544**, 182–190.
Rietveld, H. M. (2010). *Z. Kristallogr.* **225**, 545–547.
Sheldrick, G. M. (2015*a*). *Acta Cryst.* A**71**, 3–8.
Sheldrick, G. M. (2015*b*). *Acta Cryst.* C**71**, 3–8.
Traube, W. (1900). *Ber. Dtsch. Chem. Ges.* **33**, 1371–1383.
Westrip, S. P. (2010). *J. Appl. Cryst.* **43**, 920–925.

electronic reprint

7.3 [LT3] 1,1,3,3-Tetraethyl-5-nitroisoindoline

Bibliographische Daten:

Titel:	1,1,3,3-Tetraethyl-5-nitroisoindoline
Journal:	IUCrData
Jahr / Ausgabe:	2019 / 4
Artikel:	x191629
DOI:	10.1107/S2414314619016298
URL:	http://scripts.iucr.org/cgi-bin/paper?rz4034
Autoren:	Lukas Tapmeyer, Maurice Beske, Jörn Plackmeyer
eSI:	http://scripts.iucr.org/cgi-bin/paper?rz4034 https://doi.org/10.1107/S2414314619016298/rz4034sup1.cif
OpenAccess:	Ja.

Beiträge:

Lukas Tapmeyer:
Röntgenstrukturanalyse, Schreiben des Entwurfs, Korrekturen.

Maurice Beske:
Röntgenstrukturanalyse, Korrekturen.

Jörn Plackmeyer:
Synthese und Kristallisation, Schreiben des Entwurfs, Korrekturen.

data reports

IUCrData

ISSN 2414-3146

1,1,3,3-Tetraethyl-5-nitroisoindoline

Lukas Tapmeyer,[a] Maurice Beske[a] and Jörn Plackmeyer[b]*

[a]Institut für Anorganische und Analytische Chemie, Goethe-Universität, Max-von-Laue-Str. 7, D-60438 Frankfurt am Main, Germany, and [b]Institut für Physikalische und Theoretische Chemie, Goethe-Universität, Max-von-Laue-Str. 7, D-60438 Frankfurt am Main, Germany. *Correspondence e-mail: jp@prisner.de

Received 19 November 2019
Accepted 3 December 2019

Edited by C. Rizzoli, Universita degli Studi di Parma, Italy

Keywords: crystal structure; structure–property relationship; organic synthesis.

CCDC reference: 1969794

Structural data: full structural data are available from iucrdata.iucr.org

The title compound, $C_{16}H_{24}N_2O_2$, previously obtained as a yellow oil, exhibits a rather low melting point close to room temperature 297–298 K). In the molecule, the isoindoline ring system is approximately planar and coplanar to the nitro group, forming a dihedral angle of 5.63 (15)°. In the crystal, only weak N—H···O and C—H···π interactions are observed, linking molecules into chains parallel to the [101] direction.

3D view

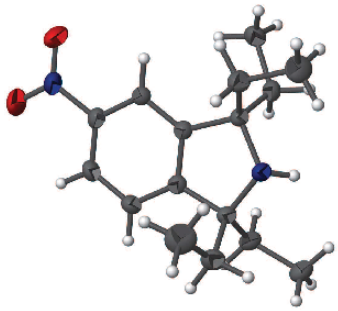

Chemical scheme

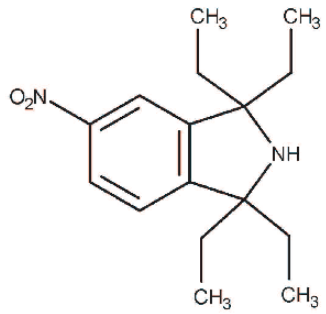

Structure description

1,1,3,3-Tetraethyl-5-nitroisoindoline is a precursor in the synthesis of 1,1,3,3-tetraethyl-isoindolin-5-isothiocyanate-2-oxyl, which in turn is a versatile reduction-resistant spin label for RNA (Saha *et al.*, 2015). The atomic connectivity of the title compound has been established by NMR spectroscopy and confirmed by several analytical methods (Haugland *et al.*, 2016) but its crystal structure remained unknown, mainly due to its low melting point of 297–298 K (Tönjes *et al.*, 1964).

The title compound (Fig. 1) crystallizes in the monoclinic space group $P2_1/n$ with one molecule in the asymmetric unit. The isoindoline ring system is approximately planar [r.m.s deviation of the nine fitted atoms = 0.0542 Å; maximum deviation 0.1005 (14) Å for atom N2] and forms a dihedral angle of 5.63 (15)° with the plane through the nitro group. In the crystal structure, each N—H group links *via* a weak hydrogen bond (Table 1) to the O—N group of an adjacent molecule. Centrosymmetrically related chains are further connected by weak C—H···π interactions (Table 1), forming chains parallel to [101]. Other interactions such as π–π stacking are not observed, which could be explained by the sterically demanding ethyl groups. This lack of strong intermolecular interactions may account for the low melting point of the substance.

A search of the Cambridge Structural Database (CSD, version 5.40, update August 2019; Groom *et al.*, 2016) for lengths of hydrogen bonds has been performed with a search

OPEN ACCESS

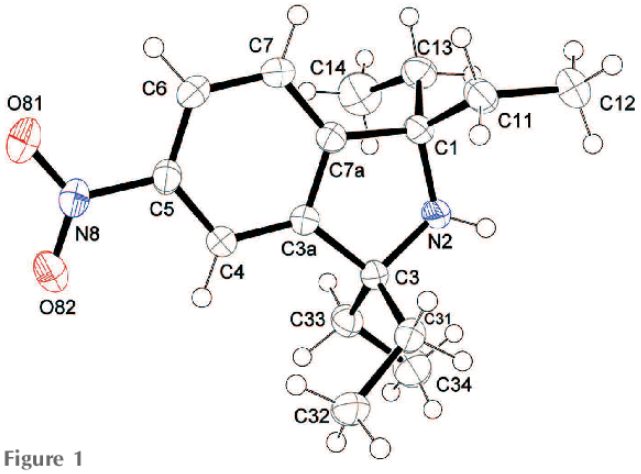

Figure 1
The molecular structure of the title compound with displacement ellipsoids drawn at the 50% probability level.

fragment of a twofold carbon-bound N—H donor to a carbon-bound NO_2 acceptor (Fig. 2). The mean length of (C–)$_2$N—H···O(–NO*R*) hydrogen bonds in deposited structures was found to be 2.28 (19) Å. This renders the H2···O81 length of 2.634 (16) Å found in the title compound a rather long but plausible peculiarity. Since the position of the H atom was freely refined against X-ray data, the H···O distance as well as the (still plausible) N—H distance is not fully trustworthy. The mean donor–acceptor distance for hydrogen bonds was found to be 2.96 (8) Å with a maximum of 3.07 Å. This confirms the value of 3.4860 (18) Å found for N2···O81 to be rather long.

Synthesis and crystallization

The title compound was synthesized in-house, using a modified literature procedure (Haugland *et al.*, 2016) as follows: to a solution of 1,1,3,3-tetraethylisoindoline (2.192 g, 9.47 mmol) in 21.9 ml sulfuric acid (95%), 21.9 ml of fuming nitric acid (100%) was added dropwise. During the addition, the reaction flask was cooled with ice/sodium chloride in order to hold the reaction temperature between −5 and 0°C (internal temperature control). The onset of the reaction was accompanied by a strong rise of temperature. After complete addition of nitric acid, the yellow solution was stirred at 0°C for 60 min. The cold reaction mixture was poured carefully into a cooled beaker containing 30 g of sodium hydroxide and 300 ml of ice/water. The pH of the resulting pale-yellow suspension was adjusted to 10 by the addition of more sodium hydroxide and the solution was stirred for 15 min. The aqueous solution was extracted four times with 100–150 ml of dichloromethane. The combined organic phases were washed with brine and dried over Na_2SO_4. After removing the solvent, the yellow residue was purified by means of column chromatography (alumina, 4% H_2O, 3×28 cm) with hexanes/ethyl acetate (95:5 *v*/*v*). The product was obtained as a yellow oil. Yield: 2.583 g (9.34 mmol, 98.7%). Crystals were obtained after storing the product at 277 K for 48 h. Several good-looking, yellow crystals could then be picked from the yellow oil. NMR analysis of the measured crystal confirmed its chemical identity with the yellow oil.

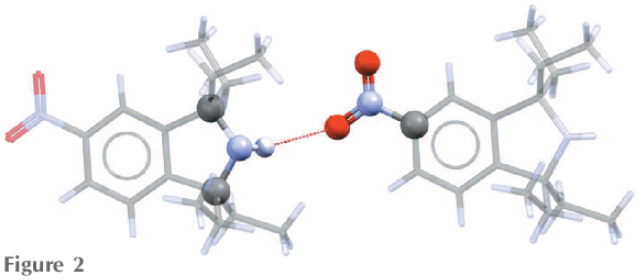

Figure 2
Search fragment for relevant hydrogen bonds in the CSD.

Table 1
Hydrogen-bond geometry (Å, °).

*Cg*1 is the centroid of the C3*A*/C4/C5/C6/C7/C7*A* benzene ring.

D—H···*A*	*D*—H	H···*A*	*D*···*A*	*D*—H···*A*
N2—H2···O81^{i}	0.865 (15)	2.634 (16)	3.4860 (18)	168.4 (16)
C11—H11*B*···*Cg*1^{ii}	0.99	2.91	3.7552 (18)	144

Symmetry codes: (i) $x+1, y, z+1$; (ii) $-x+1, -y+1, -z+1$.

Table 2
Experimental details.

Crystal data	
Chemical formula	$C_{16}H_{24}N_2O_2$
M_r	276.37
Crystal system, space group	Monoclinic, $P2_1/n$
Temperature (K)	173
a, *b*, *c* (Å)	9.0277 (6), 19.9356 (13), 9.4811 (7)
β (°)	116.169 (2)
V (Å^3)	1531.43 (18)
Z	4
Radiation type	Cu *K*α
μ (mm^{-1})	0.63
Crystal size (mm)	1.20 × 0.60 × 0.60
Data collection	
Diffractometer	Siemens Bruker three circle
Absorption correction	Multi-scan (*SADABS*; Bruker, 2015)
T_{min}, T_{max}	0.568, 0.753
No. of measured, independent and observed [$I > 2\sigma(I)$] reflections	32894, 2769, 2699
R_{int}	0.053
(sin $\theta/\lambda)_{max}$ (Å^{-1})	0.608
Refinement	
$R[F^2 > 2\sigma(F^2)]$, $wR(F^2)$, *S*	0.051, 0.134, 1.09
No. of reflections	2769
No. of parameters	185
H-atom treatment	H atoms treated by a mixture of independent and constrained refinement
$\Delta\rho_{max}$, $\Delta\rho_{min}$ (e Å^{-3})	0.38, −0.25

Computer programs: *APEX3* and *SAINT* (Bruker, 2015), *SHELXT* (Sheldrick, 2015*a*), *SHELXL2018/3* (Sheldrick, 2015*b*), *Mercury* (Macrae *et al.*, 2006), *ORTEP-3 for Windows* (Farrugia, 2012) and *publCIF* (Westrip, 2010).

Refinement

Crystal data, data collection and structure refinement details are summarized in Table 2.

Acknowledgements

We are grateful to Professor Dr Thomas Prisner and Professor Dr Martin U. Schmidt (both of Goethe-Universität) for giving us the opportunity to obtain and publish these results. We thank Professor M. U. Schmidt for fruitful discussions.

Funding information

JP is thankful for financial support by the DFG (Deutsche Forschungsgemeinschaft) (CRC902: Molecular Principles of RNA-Based Regulations).

References

Bruker (2015). *APEX3*, *SAINT* and *SADABS*. Madison, Wisconsin: Bruker AXS Inc.

Farrugia, L. J. (2012). *J. Appl. Cryst.* **45**, 849–854.

Groom, C. R., Bruno, I. J., Lightfoot, M. P. & Ward, S. C. (2016). *Acta Cryst.* B**72**, 171–179.

Haugland, M. M., El-Sagheer, A. H., Porter, R. J., Peña, J., Brown, T., Anderson, E. A. & Lovett, J. E. (2016). *J. Am. Chem. Soc.* **138**, 9069–9072.

Macrae, C. F., Edgington, P. R., McCabe, P., Pidcock, E., Shields, G. P., Taylor, R., Towler, M. & van de Streek, J. (2006). *J. Appl. Cryst.* **39**, 453–457.

Saha, S., Jagtap, A. P. & Sigurdsson, S. Th. (2015). *Chem. Commun.* **51**, 13142–13145.

Sheldrick, G. M. (2015*a*). *Acta Cryst.* A**71**, 3–8.

Sheldrick, G. M. (2015*b*). *Acta Cryst.* C**71**, 3–8.

Tönjes, H., Heidenbluth, K. & Scheffler, R. (1964). *J. Prakt. Chem.* **26**, 218–224.

Westrip, S. P. (2010). *J. Appl. Cryst.* **43**, 920–925.

7.4 [LT4] 2,6-dimethylpyrimidin-4-amine

Bibliographische Daten:

Titel:	2,6-dimethylpyrimidin-4-amine
Journal:	CSD Communications
Jahr:	2020
Refcode:	FAGSUB05 (zuvor JUDQUX)
DOI:	10.5517/ccdc.csd.cc24b34r
CCDC-Nr.:	1975913
Autoren:	Lukas Tapmeyer, Maurice Beske, Martin Ulrich Schmidt
OpenAccess:	Nein.
	Abgedruckt ist eine „preprint"-Version der eingereichten Struktur.

Beiträge:

Lukas Tapmeyer:
Röntgenstrukturanalyse.

Maurice Beske:
Synthese und Kristallisation.

Martin U. Schmidt:
Korrekturen.

data reports

Redetermination: 4-Amino-2,6-dimethylpyrimidine at 173 K with copper radiation

Lukas Tapmeyer, Maurice Beske and Martin U. Schmidt*

Institut für Anorganische u. Analytische Chemie, Johann Wolfgang Goethe-Universität, Max-von-Laue-Str. 7, D-60438 Frankfurt am Main
Correspondence email: m.schmidt@chemie.uni-frankfurt.de

Abstract

The crystal structure of 4-amino-2,6-dimethylpyrimidine was determined from data obtained with copper radiation at 173 K. This redetermiantion is new in terms of radiation-type and temperature.The readily growing crystals of 4-amino-2,6-dimethylpyrimidine were obtained by reacting sodium isopropoxide with acetonitrile at reflux and freezing out the product at 277 K.

Introduction

Experimental

Synthesis and crystallization

Refinement

Crystal data, data collection and structure refinement details are summarized in Table 1.

Results and discussion

Structure description

The structure of 4-amino-2,6-dimethylpyrimidine is of fishbone-type and dominated by hydrogen bonds and π-stacking. The title compound crystallizes in the monoclinic space group $P\ 2_1/n$ with unit cell dimensions of a = 7.466 (5) Å, b = 7.783 (2) Å, c = 11.766 (2) Å and a monoclinic angle of β = 99.10 (3)°. The structure is in accordance with the previously determined structures (Yingzhang *et al.*, 1986; Deng *et al.*, 2004; Olejniczak & Katrusiak, 2008; Radtke *et al.*, 2018) of which the 2018 structure by Radtke *et al.* (using MoKα radiation at 173 K) is of comparable quality.

Computing details

Data collection: *APEX3* (Bruker, 2012); cell refinement: *APEX3* (Bruker, 2012); data reduction: *APEX3* (Bruker, 2012); program(s) used to solve structure: *SHELXS* (Sheldrick, 2008); program(s) used to refine structure: *SHELXL2014*/7 (Sheldrick, 2015); molecular graphics: *ORTEP-3 for Windows* (Farrugia, 1997); software used to prepare material for publication: *publCIF* (Westrip, 2010).

References

Bruker (2012). *APEX3 and SAINT.* Bruker AXS Inc., Madison, Wisconsin, USA.

Deng, Z., Qiu, W., Li, W. & Li, Y. (2004). *Chin. Sci. Bull.* **49**, 127.

Farrugia, L. J. (1997). *J. Appl. Cryst.* **30**, 565.

Olejniczak, A. & Katrusiak, A. (2008). *J. Phys. Chem. B*, **112**, 24, 7183–7190.

Radtke, J., Mellerup, S. K., Bolte, M., Lerner, H.-W., Wang, S. & Wagner, M. (2018). *Org. Lett.* **20**, 13, 3966–3970.

Schmidt, J. K. F. M. (1902). *Chem. Ber.* **35**, 1577.

Sheldrick, G. M. (2008). *Acta Cryst.* A**64**, 112–122.

Sheldrick, G. M. (2015). *Acta Cryst.* C**71**, 3–8.

Westrip, S. P. (2010). *J. Appl. Cryst.* **43**, 920–925.

Yingzhang, L., Jinguang, W., Hai, G., Guangxian, X., Jiaxia, Y., Jinzi, Q., Shenghua, H. & Haifu, F. (1986). *Chem. J. Chin. Univ.* **7**, 600.

4-Amino-2,6-Dimethylpyrimidine

Crystal data

$C_6H_9N_3$
M_r = 123.16
Monoclinic, $P2_1/n$
a = 7.466 (5) Å
b = 7.783 (2) Å
c = 11.766 (2) Å
β = 99.10 (3)°
V = 675.1 (5) Å^3
Z = 4
$F(000)$ = 264
D_x = 1.212 Mg m^{-3}
Cu $K\alpha$ radiation, λ = 1.54178 Å
Cell parameters from 83 reflections
θ = 9–69.3°
μ = 0.63 mm^{-1}
T = 173 K
Block, colorless
1.0 × 0.8 × 0.6 mm

Data collection

Siemens-Bruker three circle diffractometer with microfocus tube and APEX2 decector
Radiation source: microfocus tube, Incoatec microfocus tube
ω scans
Absorption correction: multi-scan *SADABS2014*/5 - Bruker AXS area detector scaling and absorption correction
T_{min} = 0.510, T_{max} = 0.753
18850 measured reflections
1236 independent reflections
1232 reflections with $I > 2\sigma(I)$
R_{int} = 0.030
θ_{max} = 69.3°, θ_{min} = 9.5°
h = −9→9
k = −9→9
l = −14→13

Refinement

Refinement on F^2
Least-squares matrix: full
$R[F^2 > 2\sigma(F^2)]$ = 0.042
$wR(F^2)$ = 0.120
S = 1.10
1236 reflections
94 parameters
0 restraints
Primary atom site location: structure-invariant direct methods
Secondary atom site location: difference Fourier map
Hydrogen site location: mixed
H atoms treated by a mixture of independent and constrained refinement
$w = 1/[\sigma^2(F_o^2) + (0.0703P)^2 + 0.1687P]$ where $P = (F_o^2 + 2F_c^2)/3$
$(\Delta/\sigma)_{max} < 0.001$
$\Delta\rho_{max}$ = 0.19 e Å^{-3}
$\Delta\rho_{min}$ = −0.19 e Å^{-3}
Extinction correction: *SHELXL2014*/7 (Sheldrick, 2015), $Fc^*=kFc[1+0.001xFc^2\lambda^3/\sin(2\theta)]^{-1/4}$
Extinction coefficient: 0.081 (10)

Special details

Geometry. All esds (except the esd in the dihedral angle between two l.s. planes) are estimated using the full covariance matrix. The cell esds are taken into account individually in the estimation of esds in distances, angles and torsion angles; correlations between esds in cell parameters are only used when they are defined by crystal symmetry. An approximate (isotropic) treatment of cell esds is used for estimating esds involving l.s. planes.

Fractional atomic coordinates and isotropic or equivalent isotropic displacement parameters (Å²) for (ADMP)

	x	*y*	*z*	U_{iso}*/U_{eq}
N1	0.52141 (13)	0.64362 (13)	0.67993 (8)	0.0278 (3)
C2	0.36124 (16)	0.56474 (14)	0.67476 (10)	0.0263 (3)
C21	0.32696 (19)	0.4688 (2)	0.78012 (11)	0.0404 (4)
H21A	0.201012	0.477841	0.787338	0.061*
H21B	0.399679	0.517219	0.847034	0.061*
H21C	0.358310	0.350038	0.773248	0.061*
N3	0.22551 (13)	0.56243 (12)	0.58503 (8)	0.0268 (3)
C4	0.25197 (16)	0.65208 (15)	0.49046 (10)	0.0270 (3)
N41	0.11339 (15)	0.65526 (16)	0.40224 (10)	0.0370 (4)
H41A	0.014 (3)	0.592 (2)	0.4088 (14)	0.044*
H41B	0.122 (2)	0.720 (2)	0.3402 (15)	0.044*
C5	0.41823 (17)	0.73678 (15)	0.48714 (10)	0.0298 (3)
H51	0.438424	0.796493	0.421888	0.036*
C6	0.54946 (16)	0.72849 (15)	0.58313 (10)	0.0283 (4)
C61	0.73220 (18)	0.81250 (19)	0.58892 (12)	0.0392 (4)
H61A	0.753028	0.888014	0.654187	0.059*
H61B	0.735350	0.877268	0.519831	0.059*
H61C	0.824802	0.725825	0.596440	0.059*

Atomic displacement parameters (Å²) for (ADMP)

	U^{11}	U^{22}	U^{33}	U^{12}	U^{13}	U^{23}
N1	0.0286 (6)	0.0294 (6)	0.0239 (5)	−0.0011 (4)	−0.0002 (4)	−0.0031 (4)
C2	0.0285 (6)	0.0260 (6)	0.0229 (6)	0.0010 (4)	0.0001 (4)	−0.0012 (4)
C21	0.0375 (7)	0.0537 (9)	0.0275 (7)	−0.0084 (6)	−0.0025 (5)	0.0101 (6)
N3	0.0279 (6)	0.0281 (6)	0.0230 (5)	0.0001 (4)	−0.0004 (4)	0.0003 (4)
C4	0.0311 (7)	0.0268 (6)	0.0221 (6)	0.0035 (4)	0.0005 (4)	−0.0007 (4)
N41	0.0331 (6)	0.0482 (7)	0.0266 (6)	−0.0041 (5)	−0.0048 (4)	0.0107 (5)
C5	0.0355 (7)	0.0288 (6)	0.0252 (6)	−0.0006 (5)	0.0047 (5)	0.0025 (4)
C6	0.0316 (7)	0.0253 (6)	0.0281 (6)	−0.0004 (5)	0.0050 (5)	−0.0043 (4)
C61	0.0355 (7)	0.0414 (8)	0.0403 (8)	−0.0088 (6)	0.0047 (5)	−0.0015 (6)

Geometric parameters (Å, º) for (ADMP)

N1—C2	1.3369 (17)	C4—C5	1.4114 (19)
N1—C6	1.3612 (16)	N41—H41A	0.90 (2)
C2—N3	1.3430 (16)	N41—H41B	0.897 (18)
C2—C21	1.5035 (17)	C5—C6	1.3746 (18)
C21—H21A	0.9600	C5—H51	0.9300
C21—H21B	0.9600	C6—C61	1.5047 (19)
C21—H21C	0.9600	C61—H61A	0.9600
N3—C4	1.3541 (16)	C61—H61B	0.9600
C4—N41	1.3450 (17)	C61—H61C	0.9600
C2—N1—C6	116.07 (10)	C4—N41—H41B	119.7 (10)
N1—C2—N3	126.89 (11)	H41A—N41—H41B	122.6 (15)
N1—C2—C21	117.27 (10)	C6—C5—C4	118.10 (11)
N3—C2—C21	115.84 (11)	C6—C5—H51	121.0

C2—C21—H21A	109.5	C4—C5—H51	121.0
C2—C21—H21B	109.5	N1—C6—C5	121.76 (11)
H21A—C21—H21B	109.5	N1—C6—C61	115.55 (11)
C2—C21—H21C	109.5	C5—C6—C61	122.69 (12)
H21A—C21—H21C	109.5	C6—C61—H61A	109.5
H21B—C21—H21C	109.5	C6—C61—H61B	109.5
C2—N3—C4	116.69 (11)	H61A—C61—H61B	109.5
N41—C4—N3	116.70 (12)	C6—C61—H61C	109.5
N41—C4—C5	122.86 (12)	H61A—C61—H61C	109.5
N3—C4—C5	120.44 (11)	H61B—C61—H61C	109.5
C4—N41—H41A	117.7 (11)		

C6—N1—C2—N3	−0.85 (17)	N41—C4—C5—C6	178.54 (11)
C6—N1—C2—C21	179.54 (11)	N3—C4—C5—C6	−1.43 (17)
N1—C2—N3—C4	−1.36 (17)	C2—N1—C6—C5	1.97 (16)
C21—C2—N3—C4	178.25 (10)	C2—N1—C6—C61	−178.34 (10)
C2—N3—C4—N41	−177.51 (10)	C4—C5—C6—N1	−0.89 (17)
C2—N3—C4—C5	2.46 (16)	C4—C5—C6—C61	179.45 (11)

7.5 [LT5] Crystal structure of sodium ethoxide (C_2H_5ONa), unravelled after 180 years

Bibliographische Daten:

Titel:	Crystal structure of sodium ethoxide (C_2H_5ONa), unravelled after 180 years
Journal:	Chemical Communications
Jahr / Ausgabe:	2020 / 24
Seiten:	3520–3523
DOI:	10.1039/C9CC08907A
URL:	https://pubs.rsc.org/en/Content/ArticleLanding/CC/2020/C9CC08907A
Autoren:	Maurice Beske, Lukas Tapmeyer, Martin Ulrich Schmidt
eSI:	http://www.rsc.org/suppdata/c9/cc/c9cc08907a/c9cc08907a1.pdf http://www.rsc.org/suppdata/c9/cc/c9cc08907a/c9cc08907a2.cif
OpenAccess:	Nein.
	Reproduced by permission of The Royal Society of Chemistry.

Beiträge:

Maurice Beske:
Synthese und Kristallisation, Röntgenstrukturaufklärung aus Pulverdaten der Ansolvatphase, Schreiben des Entwurfs, Korrekturen.

Lukas Tapmeyer:
Beratung bei Synthese und Kristallisation; Validierung der experimentellen Ergebnisse, Röntgenstrukturanalyse der Disolvatphase, Korrekturen.

Martin U. Schmidt:
Schreiben des Manuskripts, erstellen der meisten Abb.en, Korrekturen.

ChemComm

COMMUNICATION

Check for updates

Cite this: *Chem. Commun.*, 2020, **56**, 3520

Received 15th November 2019,
Accepted 5th February 2020

DOI: 10.1039/c9cc08907a

rsc.li/chemcomm

Crystal structure of sodium ethoxide (C_2H_5ONa), unravelled after 180 years†

Maurice Beske, Lukas Tapmeyer and Martin U. Schmidt*

As early as 1837, Liebig synthesised solid C_2H_5ONa. Today, C_2H_5ONa is one of the standard bases in organic synthesis. Here, we report the identification of different solid phases and the crystal structures and phase transformations of C_2H_5ONa and $C_2H_5ONa{\cdot}2C_2H_5OH$.

Sodium ethoxide (sodium ethanolate, C_2H_5ONa, **1**) is a very common base in organic synthesis.[1] In the laboratory, it is generally synthesised *in situ* from sodium and excess ethanol and used as a solution or a suspension. Solid C_2H_5ONa was synthesised by Liebig as early as 1837, see Fig. 1.[2] Surprisingly, the structure of solid sodium ethoxide has not been determined hitherto.

When a solution of C_2H_5ONa in ethanol is evaporated to dryness *in vacuo* at room temperature, a metastable, white residue remains, which turns into a liquid after a few minutes of storage under argon. Further evaporation results in a residue, which again liquidifies under argon after a few minutes. Finally, the evaporation leads to a white, hygroscopic solid which is stable under argon. We investigated this solid by X-ray powder diffraction. A mixture of two phases was found, which turned out to be sodium ethoxide (C_2H_5ONa, **1**) and sodium ethoxide ethanol disolvate ($C_2H_5ONa{\cdot}2C_2H_5OH$, **2**). This mixture is formed, when the excess ethanol is distilled off at ambient pressure, or the ethanol is removed at room temperature *in vacuo*. Pure C_2H_5ONa is obtained upon further evaporation *in vacuo* at 50 °C. We determined the solid-state structures and phase transitions of both phases, C_2H_5ONa and $C_2H_5ONa{\cdot}2C_2H_5OH$.

We could not obtain single crystals of C_2H_5ONa. Therefore, its crystal structure was determined by X-ray powder diffraction. The powder pattern could be indexed with DICVOL[3] resulting in a tetragonal unit cell, which contains two formula units of C_2H_5ONa. The structure was solved with the real-space method with the program DASH[4] and Rietveld-refined[5] with TOPAS.[6] The Rietveld plot is shown in Fig. 2. Crystallographic data are given in Table 1.

C_2H_5ONa crystallises in the tetragonal space group $P\bar{4}2_1m$.‡ The structure does not contain discrete complexes, but consists of layers. The Na^+ ions form a square planar lattice. The oxygen atoms are situated at the centres of all meshes, alternatingly shifted above and below the Na^+ layer by 0.734(3) Å (Fig. 3a). Correspondingly, every Na^+ ion is coordinated to four oxygen atoms in a squeezed tetrahedron. The oxygen atoms have five neighbours, which arrange in a square pyramid: the four Na^+ ions on the corners and the ethyl group on top of the pyramid, see Fig. 3b and c. The ethyl groups are disordered on two orientations.

The Na and O atoms exhibit the same arrangement as the O^{2-} and Pb^{2+} ions in red PbO (litharge, see Fig. 3d). The ethyl groups in C_2H_5ONa are in the same positions as the lone pairs of the Pb^{2+} ions in PbO.[7] Hence, the structure of C_2H_5ONa could be described as an "anti-PbO type".

The methyl derivatives, sodium methoxide[8] and lithium methoxide,[9] exhibit a layer structure similar to **1**. In contrast, sodium *tert*-butoxide does not crystallise in layers, but forms hexamers and nonamers in the solid state.[10]

As mentioned by Liebig, the addition of an excess of sodium to ethanol at 50 °C leads to a termination of the H_2 evolution with left-over sodium. Upon cooling to room temperature, the mixture solidifies. In contrast to Liebig's observation, we did not obtain "grossblättrige Krystalle" (large plate-shaped crystals), but obtained a gel. From this gel, we isolated needle-shaped colourless single crystals of $C_2H_5ONa{\cdot}2C_2H_5OH$ after three months. A phase composed of $C_2H_5ONa{\cdot}2C_2H_5OH$ was already observed in 1895 in composition-dependent vapour-pressure measurements.[12]

The crystal structure of $C_2H_5ONa{\cdot}2C_2H_5OH$ (**2**) was determined by single-crystal X-ray diffraction.‡ In the structure of **2**, the Na^+ ions are tetrahedrally coordinated to two ethoxide ions and two ethanol molecules. The ethoxide ions bridge two Na^+ ions resulting in a helical chain. The chain is additionally stabilised by hydrogen bonds, see Fig. 4a. The chains are arranged in a distorted hexagonal pattern (Fig. 4b). Neighbouring chains are connected

Goethe University, Institute of Inorganic and Analytical Chemistry, Max-von-Laue-Str. 7, 60438 Frankfurt am Main, Germany. E-mail: m.schmidt@chemie.uni-frankfurt.de

† Electronic supplementary information (ESI) available: Syntheses, IR-spectra, X-ray powder data, phase analysis, and crystal structures of **1** and **2**. CCDC 1943793 and 1943794. For ESI and crystallographic data in CIF or other electronic format see DOI: 10.1039/c9cc08907a

This journal is © The Royal Society of Chemistry 2020

Liebig (1837)

Wenn man Kalium oder Natrium in absoluten Alkohol bringt, so wird das Hydratwasser des Alkohols zerlegt, denn es entwickelt sich reines Wasserstoffgas; durch eine schwache Erwärmung, nicht über 50°, geht diese Zerlegung rasch vor sich, die neue Verbindung löst sich bei dieser Temperatur auf, und wenn man soviel Kalium oder Natrium eingetragen hat, dass der noch nicht zerlegte Alkohol damit gesättigt ist, so scheiden sich, wenn man noch mehr von diesen Metallen hineinbringt, weisse durchsichtige, bei dem Natrium grossblättrige Krystalle ab, zu denen die ganze Flüssigkeit erstarrt, wenn man sie bei diesem Zeitpunkte erkalten lässt. Diese Krystalle sind eine Verbindung von Aether (Aethyloxyd) mit wasserfreiem Kalium- oder Natriumoxyd; sie lassen sich unter einer Glocke mit concentrirter Schwefelsäure völlig trocken erhalten und nachher bis zu 80° erhitzen, ohne dass sie etwas Flüchtiges abgeben oder ihre Beschaffenheit verändern.

Translation

If one adds potassium or sodium into absolute alcohol, the hydrate water of the alcohol is decomposed, because pure hydrogen gas evolves; by gentle heating, not more than 50°C, this decomposition occurs rapidly, the new compound is dissolved at this temperature, and if one has added so much potassium or sodium, that the non-decomposed alcohol is saturated with them, and if one adds even more of these metals, then white, transparent, in the case of sodium large plate-shaped crystals precipitate, into which the entire liquid solidifies, if it is allowed to cool at this moment. These crystals are a composition of ether (ethyl oxide) with anhydrous potassium or sodium oxide; they can be obtained entirely dry under a bell jar with concentrated sulfuric acid, and heated afterwards to 80°C without causing them to release any volatiles or to change their nature.

Fig. 1 Original description of the synthesis of C_2H_5ONa by Liebig (1837),[2] from page 32 of the paper "Über die Äthertheorie" ("On the theory of ether"). Liebig assumed that ethanol is the hydrate of ether – which is not completely far fetched: $(C_2H_5)_2O{\cdot}H_2O$ corresponds to $2C_2H_5OH$. Consequently, Liebig postulated that the reaction product of ethanol and sodium is an adduct of diethyl ether and sodium oxide – which actually matches the correct stoichiometry: $(C_2H_5)_2O{\cdot}Na_2O$ corresponds to $2C_2H_5ONa$. Reproduced from ref. 2 with permission (Copyright 1837 Universitäts-Buchhandlung von C. F. Winter, Heidelberg, now Wiley VCh Verlag GmbH & Co. KGaA).

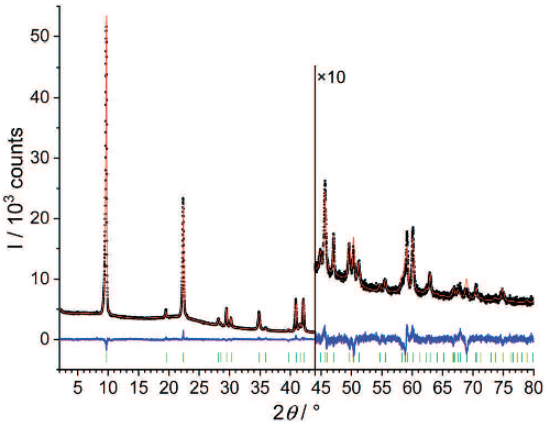

Fig. 2 Rietveld refinement of C_2H_5ONa. Experimental powder pattern (black dots), calculated pattern (red line through the dots), difference curve (blue line below) and reflection positions (vertical green dashes).

Table 1 Crystallographic data of C_2H_5ONa and $C_2H_5ONa{\cdot}2C_2H_5OH$

	C_2H_5ONa (**1**)	$C_2H_5ONa{\cdot}2C_2H_5OH$ (**2**)
Crystal structure determined from	Powder data	Single crystals
CCDC	1943793	1943794
M_W/g mol^{-1}	68.05	160.18
Crystal system	Tetragonal	Monoclinic
Space group (no.)	$P\bar{4}2_1m$ (113)	$P2_1/n$ (14)
a/Å	4.41084 (4)	11.622 (6)
b/Å	4.41084 (4)	5.1926 (9)
c/Å	9.06779 (17)	17.682 (6)
α/°	90	90
β/°	90	104.03 (3)
γ/°	90	90
V/Å^3	176.418 (5)	1035.0 (7)
Z, Z'	2, 1/4	4, 1
D_{calc}/Mg m^{-3}	1.281	1.028
Crystal size (mm)	Powder	0.8 × 0.08 × 0.02
T/K	298 (3)	238 (2)
Radiation type	Cu-Kα_1	Cu-Kα
λ/Å	1.5406	1.5418
2θ range/°	2–80	4.14–59.9
R_p/%	2.33	—
R_{wp}/%	3.39	—
R_1/%	—	16.88
wR_2/%	—	27.10
GOF	1.58	0.979
Site symmetry of Na, O and C atoms	$\bar{4}$.., 2.mm, ..m	1, 1, 1

by van der Waals interactions between the ethyl groups only (Fig. 4b). This structure explains the observed needle-like morphology of the crystals.

The crystal structures of **1** and **2** agree with the X-ray powder data published in 1976 by Blanchard,[13] and with the unit cell parameters of C_2H_5ONa published by Chandran *et al.*[14] The lithium methoxide analogue of **2**, $CH_3OLi{\cdot}2CH_3OH$, does not form chains, but tetramers.[15]

In C_2H_5ONa, the ionic Na–O layers are surrounded by non-polar ethyl groups on both sides. Neighbouring layers are connected by van der Waals contacts only (Fig. 3c). Thus, a

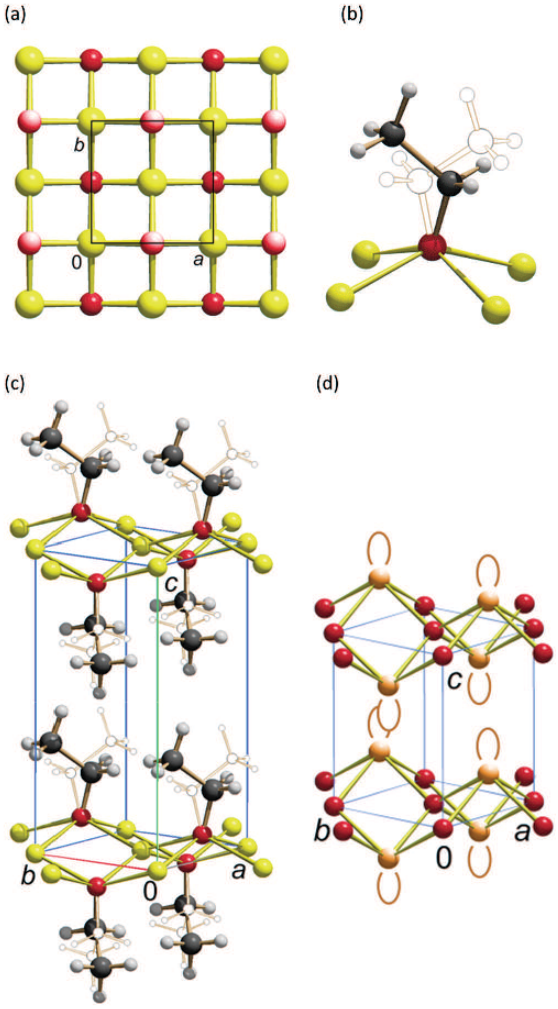

Fig. 3 Crystal structure of C_2H_5ONa. (a) Layer of Na cations and O atoms. The Na^+ ions (yellow) are situated in the paper plane, the light red O atoms above and the dark red O atoms below it. (b) Coordination of the ethoxide group by four Na^+ ions. The ethyl moiety is disordered on two orientations with 50% occupancy each. (c) Crystal structure of C_2H_5ONa. (d) Crystal structure of red PbO. Na yellow, O red, C black, H white, Pb light brown. Empty circles in (b) and (c) denote the second orientation of the disordered ethyl groups. Brown arcs in (d) indicate the position of the lone pairs of the Pb^{2+} ions. Drawings were made with SCHAKAL.[11]

non-polar solvent, such as toluene, could penetrate between the layers, and eventually exfoliate the layers, but cannot break the ionic layers themselves. The large layers will remain intact, which explains the observed low solubility of C_2H_5ONa in non-polar solvents.

In polar solvents, especially with solvent molecules containing oxygen atoms, the layers are easily destroyed by the solvent. The crystal structure of $C_2H_5ONa{\cdot}2C_2H_5OH$ resembles the first step in the dissolution of C_2H_5ONa by ethanol: the Na–O layers of C_2H_5ONa are reduced to Na–O chains, which are surrounded by

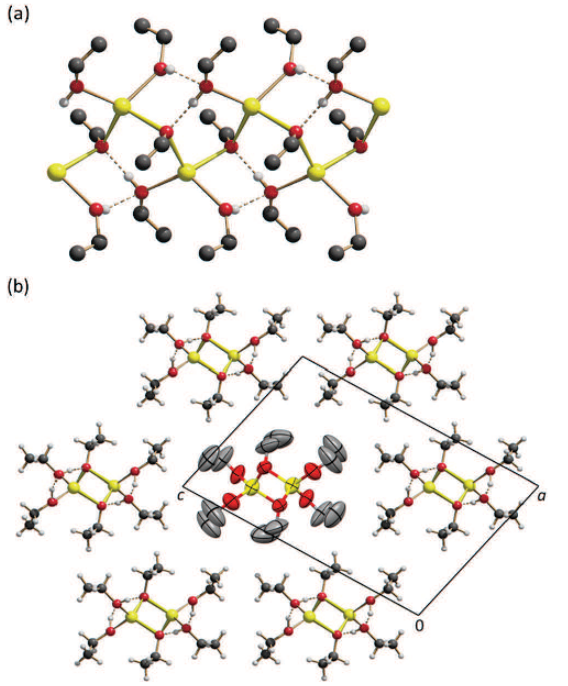

Fig. 4 Crystal structure of $C_2H_5ONa{\cdot}2C_2H_5OH$ (**2**). (a) Helical chain (yellow) composed of Na^+ and ethoxide ions with terminal ethanol molecules. View direction [3 0 2]. (b) Arrangement of the chains. View along the chains, view direction [0 −1 0]. The central chain is shown with anisotropic displacement parameters with a 50% probability level.

ethanol molecules. Further solvation leads to a molecular complex in solution.

Apart from the phases **1** and **2**, we observed two additional phases, **3** and **4**. They occured together with **1** and **2** in varying amounts in several experiments upon the evaporation of an ethanolic solution of C_2H_5ONa, depending on the applied conditions (for details, see ESI†). However, we could neither isolate the phases **3** or **4**, nor grow single crystals. Hitherto, all our attempts to determine the crystal structures of **3** and **4** from X-ray powder data of the phase mixtures were to no avail. Correspondingly, the chemical composition and the crystal structures of **3** and **4** remain obscure.

At room temperature, the disolvate **2** is stable only in the presence of ethanol vapours. The crystals decompose upon contact with dry air or dry nitrogen. Under vacuum at 50 °C, **2** converts to the solvent-free **1**, too. In reverse, **1** reacts with moisture from the air to a mixture which contains all four phases **1**–**4** in varying amounts. This complex phase behavior, and the absence of single crystals of C_2H_5ONa might be the reason why the crystal structure of sodium ethoxide was not determined earlier.

In conclusion, this work reveals that the standard base sodium ethoxide exhibits a layer structure of the "anti-PbO type" in the solid state, which explains the limited solubility of C_2H_5ONa in non-polar solvents. The disolvate $C_2H_5ONa{\cdot}2C_2H_5OH$, which apparently precipitates first on synthesis, forms a chain

 This journal is © The Royal Society of Chemistry 2020

structure, which resembles the first step of the dissolution of C_2H_5ONa with ethanol. Thus, the crystal structures of these simple compounds were finally unravelled – a 180 years after their first synthesis.

The authors thank Edith Alig for recording numerous X-ray powder diagrams, and Lothar Fink (both Goethe University, Frankfurt am Main) for the support in the single-crystal structure determination of the disolvate.

Conflicts of interest

There are no conflicts of interest to declare.

Notes and references

‡ CCDC 1943793 and 1943794 contain the crystallographic data of **1** and **2**.

1 W. Dieckmann, *Ber. Dtsch. Chem. Ges.*, 1900, **33**, 2670–2684; L. F. Fieser, M. Fieser and T.-L. Ho, *Fieser & Fieser's Reagents for Organic Synthesis*, Wiley, 2006; K. S. Whitaker and D. T. Whitaker, *e-EROS Encyclopedia of Reagents for Organic Synthesis*, 2001, pp. 1–4; For recent applications see, *e.g.*: M. Kumar, *et al.*, *J. Org. Chem.*, 2019, **84**, 13624–13635; H. J. Trubenstein, *et al.*, *New J. Chem.*, 2019, **43**, 14305–14312.

2 J. Liebig, *Ann. Pharm.*, 1837, **23**, 12–42.

3 A. Boultif and D. Louër, *J. Appl. Crystallogr.*, 1991, **24**, 987–993.

4 K. Shankland, E. Pidcock, J. van de Streek, W. I. F. David and W. D. S. Motherwell, *J. Appl. Crystallogr.*, 2006, **39**, 910–915.

5 B. O. Loopstra and H. M. Rietveld, *Acta Crystallogr., Sect. B: Struct. Crystallogr. Cryst. Chem.*, 1969, **25**, 787–791; H. M. Rietveld, *J. Appl. Crystallogr.*, 1969, **2**, 65–71; *The Rietveld Method. IUCr Monographs on Crystallography 5*, ed. R. A. Young, International Union of Crystallography and Oxford Science Publications, 1995; B. van Laar and H. Schenk, *Acta Crystallogr., Sect. A: Found. Adv.*, 2018, **74**, 88–92.

6 A. A. Coelho, *J. Appl. Crystallogr.*, 2018, **51**, 210–218.

7 A. F. Wells, *Structural Inorganic Chemistry*, Oxford University Press, Oxford, 1984, p. 119.

8 E. Weiss, *Z. Anorg. Allg. Chem.*, 1964, **332**, 197–203.

9 P. J. Wheatley, *J. Chem. Soc.*, 1961, 4270–4274.

10 J. E. Davies, J. Kopf and E. Weiss, *Acta Crystallogr., Sect. B: Struct. Crystallogr. Cryst. Chem.*, 1982, **38**, 2251–2253; H. Nekola, F. Olbrich and U. Behrens, *Z. Anorg. Allg. Chem.*, 2002, **628**, 2067–2070; E. Østreng, H. H. Sønsteby, S. Øien, O. Nielsen and H. Fjellvåg, *J. Chem. Soc., Dalton Trans.*, 2014, **43**, 16666–16672.

11 E. Keller, *SCHAKAL99*, Kristallographisches Institut der Universität Freiburg, Deutschland, 1999.

12 H. Lescoeur, *Compt. Rend. Acad. Sci.*, 1895, **121**, 691–692.

13 J.-M. Blanchard, J. Bousquet, P. Claudy and J.-M. Letoffe, *J. Therm. Anal.*, 1976, **9**, 191–203.

14 K. Chandran, R. Nithya, K. Sankaran, A. Gopalan and V. Ganesan, *Bull. Mater. Sci.*, 2006, **29**, 173–179.

15 Z. A. Starikova, E. P. Turevskaya, N. Y. Turova and A. I. Yanovsky, *J. Chem. Soc., Dalton Trans.*, 2000, 3237–3238.

This journal is © The Royal Society of Chemistry 2020

7.6 [LT6] Disordered sodium alkoxides from powder data: crystal structures of sodium ethoxide, propoxide, butoxide and pentoxide, and some of their solvates

Bibliographische Daten:

Titel:	Disordered sodium alkoxides from powder data: crystal structures of sodium ethoxide, propoxide, butoxide and pentoxide, and some of their solvates
Journal:	Acta Crystallographica Section B
Jahr / Ausgabe:	2021 / B77
Seiten:	68–82
DOI:	10.1107/S205252062001584X
URL:	https://scripts.iucr.org/cgi-bin/paper?S205252062001584X
Autoren:	Maurice Beske, Stephanie Cronje, Martin Ulrich Schmidt und Lukas Tapmeyer
eSI:	http://scripts.iucr.org/cgi-bin/paper?ne5003
OpenAccess:	Nein.
	Reproduced by permission of International Union of Crystallography
Beiträge:	Maurice Beske: Synthese und Kristallisation, Röntgenstrukturaufklärung aus Pulverdaten der Ansolvatphasen, Röntgenstrukturanalyse $NaO^nPr \cdot 2\ HO^nPr$ und $NaO^iPr \cdot 5\ HO^iPr$, Korrekturen.
	Stephanie Cronje. Korrekturen.
	Martin U. Schmidt: Symmetrieanalyse von NaOEt, Anleitungen für Rietveldverfeinerungen, Schreiben des Entwurfs, Überarbeiten des Manuskriptes, Korrekturen.
	Lukas Tapmeyer: Planung und Unterstützung bei der Synthese und Kristallisation, Validation der experimentellen Ergebnisse, Röntgenstrukturanalyse $NaO^tAm \cdot HO^tAm$, Schreiben des Entwurfs, Korrekturen sowie Korrekturen und Nachverfeinerungen aller Strukturen.

research papers

STRUCTURAL SCIENCE CRYSTAL ENGINEERING MATERIALS

ISSN 2052-5206

Disordered sodium alkoxides from powder data: crystal structures of sodium ethoxide, propoxide, butoxide and pentoxide, and some of their solvates

Maurice Beske,[a,b] Stephanie Cronje,[a] Martin U. Schmidt[a]* and Lukas Tapmeyer[a]

[a]Institut für Anorganische und Analytische Chemie, Goethe-Universität, Max-von-Laue-Strasse 7, 60438 Frankfurt am Main, Germany, and [b]Department Chemie, Johannes Gutenberg-Universität Mainz, Duesbergweg 10-14, 55128 Mainz, Germany. *Correspondence e-mail: m.schmidt@chemie.uni-frankfurt.de

Received 28 April 2020
Accepted 3 December 2020

Edited by R. B. Neder, University of Erlangen-Nürnberg, Germany

Dedicated to Ulrich Müller on the occasion of his 80th birthday.

Keywords: sodium alkoxide; powder data; solvate; isopropanol; Bärnighausen tree; PXRD.

CCDC references: 1943793; 1943794; 1998221; 1998220; 1998219; 1998224; 1998225; 1998227

Supporting information: this article has supporting information at journals.iucr.org/b

The crystal structures of sodium ethoxide (sodium ethanolate, NaOEt), sodium *n*-propoxide (sodium *n*-propanolate, NaO^{n}Pr), sodium *n*-butoxide (sodium *n*-butanolate, NaO^{n}Bu) and sodium *n*-pentoxide (sodium *n*-amylate, NaO^{n}Am) were determined from powder X-ray diffraction data. NaOEt crystallizes in space group $P\bar{4}2_1m$, with $Z = 2$, and the other alkoxides crystallize in $P4/nmm$, with $Z = 2$. To resolve space-group ambiguities, a Bärnighausen tree was set up, and Rietveld refinements were performed with different models. In all structures, the Na and O atoms form a quadratic net, with the alkyl groups pointing outwards on both sides (anti-PbO type). The alkyl groups are disordered. The disorder becomes even more pronounced with increasing chain length. Recrystallization from the corresponding alcohols yielded four sodium alkoxide solvates: sodium ethoxide ethanol disolvate (NaOEt·2EtOH), sodium *n*-propoxide *n*-propanol disolvate (NaO^{n}Pr·2^{n}PrOH), sodium isopropoxide isopropanol pentasolvate (NaO^{i}Pr·5^{i}PrOH) and sodium *tert*-amylate *tert*-amyl alcohol monosolvate (NaO^{t}Am·^{t}AmOH, ^{t}Am = 2-methyl-2-butyl). Their crystal structures were determined by single-crystal X-ray diffraction. All these solvates form chain structures consisting of Na^+, $-O^-$ and –OH groups, encased by alkyl groups. The hydrogen-bond networks diverge widely among the solvate structures. The hydrogen-bond topology of the ^{i}PrOH network in NaO^{i}Pr·5^{i}PrOH shows branched hydrogen bonds and differs considerably from the networks in pure crystalline ^{i}PrOH.

1. Introduction

1.1. General

Even today, there are simple chemical compounds for which the crystal structures are not known. The reasons for this deficiency in knowledge include synthetic difficulties, complex phase behaviour, instability in a vacuum and under an inert atmosphere, lack of single crystals, unusual or ambiguous space groups, and disorder. All these difficulties can be found in sodium alkoxides (sodium alcoholates) NaO*R* and their solvates NaO*R*·*x*ROH, with *R* being a lower alkyl group. In principle, these compounds can be easily prepared by the reaction of sodium with the corresponding alcohol. However, in practice, the synthesis of the pure phases presents some obstacles. For example, when sodium is reacted with ethanol and the ethanol excess is removed *in vacuo*, a white powder remains. This powder turns into a liquid within a few minutes under argon. Further evaporation under vacuum results in a powder, which again liquefies under argon. Finally, a white residue is obtained, which consists of a mixture of two to four different phases, including sodium ethoxide (NaOEt) and its ethanol disolvate NaOEt·2EtOH (Beske *et al.*, 2020). Phase-

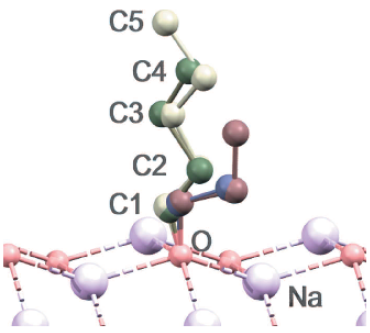

OPEN ACCESS

pure NaOEt is only obtained after a few hours of evaporation under vacuum at 50 °C. The initially formed solvate NaOEt·2EtOH decomposes under vacuum, and even under dry argon, and is stable only in the presence of ethanol vapour. Similar difficulties are observed for other sodium alkoxides (see below). Additionally, all the compounds are very sensitive to moisture.

In industry, as well as in the laboratory, sodium alkoxides are widely used as bases and as reagents in organic synthesis. This is not only true for NaOEt, but also for other alkoxides. For example, sodium *tert*-amylate (sodium 2-methyl-2-butoxide, NaO^{t}Am) is used industrially on a multi-ton scale in the synthesis of diketopyrrolopyrrole pigments, which today are the most commonly used pigments for red car coatings (Hunger & Schmidt, 2018).

1.2. Historical notes on NaOEt

Sodium ethoxide was synthesized as early as 1837 by Liebig (Liebig, 1837; Beske *et al.*, 2020). Since ethanol was considered the hydrate of ethyl ether (2EtOH $\hat{=}$ $Et_2O{\cdot}H_2O$), sodium ethoxide was regarded as an adduct of diethyl ether and sodium oxide, which actually corresponds to the correct stoichiometry: $Et_2O{\cdot}Na_2O \hat{=} 2NaOEt$. Correspondingly, the name 'Aethernatron' (Geuther, 1868*a*,*b*) was used besides the names 'Natriumalkoholat' (Geuther, 1859) and 'Natriumäthylat' (Wanklyn, 1869).

Many years later, the crystal structure of sodium methoxide (NaOMe) was determined from powder X-ray diffraction (PXRD) data (Weiss, 1964). Surprisingly, the crystal structure of NaOEt was not determined, although it is isostructural with NaOMe. It would have been an easy task to index the powder pattern of NaOEt manually, because NaOEt crystallizes in the tetragonal crystal system, and the lattice parameters *a* and *b* of NaOEt are almost identical to those in NaOMe.

In 1976, the PXRD patterns of NaOEt and NaOEt·2EtOH were published in an article devoted to the thermal stability of alkali ethoxides (Blanchard *et al.*, 1976). Again, no attempt was made to index the powder data.

As much as 30 years later, the powder data of NaOEt and sodium *n*-propoxide (NaO^{n}Pr) were indexed, but the crystal structures remained indeterminate (Chandran *et al.*, 2006). Finally, we determined the crystal structure of NaOEt from powder data, and of NaOEt·2EtOH from single-crystal data a few months ago. The crystal structures were recently briefly described in a chemical journal (Beske *et al.*, 2020), without any discussion on the ambiguity of the space group or of the crystal symmetry. Here, we report a full discussion of the ambiguities of the space group of NaOEt, including a Bärnighausen tree of the possible space groups and their subgroups.

1.3. Previous work on other alkoxides

The first determined crystal structure of a sodium alkoxide was that of NaOMe (Weiss, 1964). NaOMe is isotypical to LiOMe (Wheatley, 1961) and crystallizes in a layer structure in the space group $P4/nmm$, with $Z = 2$.

Potassium methoxide, KOMe, crystallizes in the same space group type as NaOMe, but the structure is different: whereas the Na^+ ions in NaOEt are coordinated to four O atoms, the K^+ ions in KOMe are coordinated to five O atoms in a square-pyramidal geometry (Weiss, 1963; Weiss & Alsdorf, 1970). The O atom is surrounded by five K^+ ions and the methyl group has a distorted octahedral geometry. A similar structure was found for partially hydrolysed NaOMe with the composition $Na(OMe)_{1-x}(OH)_x$, with $x \approx 1/3$ (Weiss, 1964).

Sodium *tert*-butoxide, NaO^{t}Bu, exists in two polymorphic forms. Both structures were determined by single-crystal X-ray diffraction. One of the phases consists of hexamers and crystallizes in the space group $P2_12_12_1$, with $Z = 20$, with five hexamers per asymmetric unit (Østreng *et al.*, 2014). The other phase contains a 1:1 mixture of hexamers and nonamers in the space group $R\bar{3}$, with $Z = 6$, with 90 formula units per unit cell (Greiser & Weiss, 1977; Davies *et al.*, 1982; Nekola *et al.*, 2002). Accordingly, both phases have quite large unit cells.

1.4. Solvates

Sodium alkoxides can form solvates with their corresponding alcohols. Already in 1837 Liebig had prepared an ethanol solvate of NaOEt by the reaction of sodium with ethanol at 50 °C and subsequent cooling of the solution to room temperature, whereupon the mixture turned into a solid (Liebig, 1837). However, Liebig apparently did not recognize this precipitate as a solvate. In 1868, Scheitz determined the composition of this solvate as NaOEt·2EtOH (Geuther, 1868*a*). This result was confirmed by Marsh (Geuther, 1868*b*), whereas Wanklyn (1869) determined the composition to be NaOEt·3EtOH. In 1880, Frölich again found a composition of NaOEt·2EtOH using a different method (Geuther & Frölich, 1880). Lescoeur (1895) measured the vapour pressure during slow evaporation of a suspension of NaOEt in EtOH and observed that the vapour pressure did not change between compositions of NaOEt·1.7EtOH and nearly pure NaOEt, and thus concluded that the solvate had the composition NaOEt·2EtOH.

The crystal morphology of NaOEt·2EtOH was described as 'völlig durchsichtige farblose nadelförmige Krystalle' (fully transparent, colourless, needle-like crystals) (Geuther, 1868*a*).

Geuther & Frölich (1880) also described a solvate with a composition of NaO^{n}Pr·2^{n}PrOH. A ^{t}AmOH solvate of NaO^{t}Am was mentioned by Friedrich *et al.* (1999), but no composition as given.

The solvates are thermally remarkably stable. NaOEt·2EtOH must be heated at ambient pressure to 200 °C and NaO^{n}Pr·2^{n}PrOH even to 220 °C before the pure solvent-free alkoxides are obtained (Geuther & Frölich, 1880). Solvent-free NaOEt is also quite stable. According to differential thermal analysis, the decomposition starts at 50 °C, but this decomposition is very slow and occurs over a large temperature range. Finally, at 310 °C the decomposition 'adopts an explosive character' ('prendre un charactère explosif'; Blanchard *et al.*, 1976).

Crystals of the solvates of NaO^{n}Pr, NaO^{i}Pr and NaO^{t}Am do form easily when sodium is reacted with the corresponding alcohols and the solution is subsequently carefully evaporated. However, no structure of any sodium alkoxide solvate was determined between 1837 and 2019 (Beske *et al.*, 2020). The reason might be the pronounced sensitivity of the crystals to moisture, air, vacuum and dry inert gas.

1.5. Work in this article

In this article, we describe the synthesis, structure determination, crystal structure and disorder of NaOEt, NaO^{n}Pr, NaO^{n}Bu and NaO^{n}Am, and of the solvates NaOEt·2EtOH, NaO^{n}Pr·2^{n}PrOH, NaO^{i}Pr·5^{i}PrOH and NaO^{t}Am·^{t}AmOH. The structures of the solvent-free compounds were determined by PXRD and the structures of the solvates by single-crystal X-ray analyses. In the cases of NaOEt and NaO^{n}Pr, the space-group symmetry was ambiguous, and the corresponding symmetry relationships were elaborated using a Bärnighausen tree.

2. Experimental details

2.1. Syntheses

All synthetic procedures were performed under an argon atmosphere using Schlenk techniques. All alcohols, as well as toluene, were dried over sodium and freshly distilled.

2.1.1. NaOEt. 0.34 g (15 mmol) of sodium were added to 10 ml (170 mmol) of ethanol. The mixture was allowed to react for 30 min at room temperature. The obtained solution was heated to 50 °C and the excess ethanol was removed under vacuum. The resulting solid product was evaporated at 50 °C under vacuum for 3 h, gently crushed with a glass rod and again evaporated for one additional hour under the same conditions. A phase-pure white powder of NaOEt was obtained.

2.1.2. NaO^{n}Pr, NaO^{n}Bu and NaO^{n}Am. NaO^{n}Pr, NaO^{n}Bu and NaO^{n}Am were synthesized in a similar manner to NaOEt. Details are given in the supporting information.

2.1.3. NaOEt·2EtOH. 0.34 g of sodium (15 mmol) were added to 5.0 ml (85 mmol) of ethanol. After reacting for 30 min, a gel was obtained. This gel was stored for three months at room temperature, resulting in a pale-brown solution and colourless needles of NaOEt·2EtOH with a size of up to 1 mm.

2.1.4. NaO^{n}Pr·2^{n}PrOH, NaO^{i}Pr·5^{i}PrOH and NaO^{t}Am·^{t}AmOH. Syntheses and crystal growth of these compounds resembled the procedure used for NaOEt·2EtOH. Details are given in the supporting information.

2.2. Pre-characterization

The stoichiometry of the solvent-free alkoxides was confirmed by decomposition experiments with HCl, which verified their stoichiometry. Details are reported in the supporting information. For the solvates, this analysis could not be performed, because the solvates decomposed rapidly when removed from their alcoholic mother liquor.

2.3. Powder X-ray diffraction (PXRD)

For the PXRD studies, the samples were sealed in glass capillaries with a 1.0 mm diameter. The PXRD patterns were measured in transmission mode on a Stoe Stadi-P diffractometer equipped with a Ge(111) monochromator and a linear position-sensitive detector. The capillaries were spun during the measurements. All measurements were performed at room temperature, using Cu $K\alpha_1$ radiation (λ = 1.5406 Å), with a 2θ range of 2–100° (2–80° for NaOEt).

2.4. Structure determination from powder data

The crystal structures of the solvent-free alkoxides NaOEt, NaO^{n}Pr, NaO^{n}Bu and NaO^{n}Am were determined from PXRD data. The powder data were indexed with the program *DICVOL* (Boultif & Louër, 1991) within the program package *DASH* (David *et al.*, 2006). The structures were solved by the real-space method with simulated annealing using *DASH*. Subsequently, Rietveld refinements were performed using *TOPAS* (Coelho, 2018).

For all four compounds indexing led to a tetragonal unit cell with Z = 2. The systematic extinction indicated *P*4/*n*, *P*4/*nmm* and $P\bar{4}2_1m$ as possible space groups. The structures were successfully solved in *P*4/*nmm* and $P\bar{4}2_1m$, using two fragments, an Na atom and a rigid alkoxide moiety. The Na atom was placed on the special position, which allowed a distorted tetrahedral coordination [Wyckoff position 2*a* ($\frac{3}{4}$, $\frac{1}{4}$, 0) in *P*4/*nmm* origin choice 2; 2*a* (0, 0, 0) in $P\bar{4}2_1m$], as explained in §3.1. The alkoxide fragment was placed on a general position, with an occupancy of 0.125 (in *P*4/*nmm*) or 0.25 (in $P\bar{4}2_1m$). In the resulting structures, the C atoms moved close to a site with *..m* symmetry, and were subsequently placed on this site, resulting in an occupancy of 0.25 (in *P*4/*nmm*) or 0.5 (in $P\bar{4}2_1m$). In the Rietveld refinements of NaOEt, restraints were only necessary for the H atoms. For NaO^{n}Pr, NaO^{n}Bu and NaO^{n}Am, additional restraints were applied to the O—C and C—C bond lengths, and to the O—C—C and C—C—C bond angles. All H atoms were refined using restraints on the bond lengths and angles with quite high weights. Further details of the Rietveld refinements are given in the supporting information.

Note that there are two different origin choices for *P*4/*nmm*. Origin choice 2 (origin on $\bar{1}$) was used for the structure solution, due to the requirements of *DASH*. In contrast, the origin choice 1 (origin on $\bar{4}$, as in $P\bar{4}2_1m$) was used for the Bärnighausen tree.

2.5. Single-crystal X-ray diffraction

A single crystal of NaOEt·2EtOH was placed in a sealed glass capillary and data were collected at −38 (2) °C. Single crystals of NaO^{n}Pr·2^{n}PrOH and NaO^{i}Pr·5^{i}PrOH were mounted by freezing them in a drop of oil and their data collected under a cold nitrogen stream at −100 (2) °C using an Oxford Cryosystems cryostream device. Crystals of NaO^{t}Am·^{t}AmOH were sealed in a glass capillary under paraffin oil (dried with Na) and their data collected at room temperature.

Single-crystal data were collected on a Bruker SMART APEX three-circle diffractometer equipped with an Incoatec IμS Cu microfocus source with mirror optics and an APEX II CCD detector. The software package *APEX3* (Bruker, 2015) was used for data collection and data reduction. The structures were solved by direct methods with *SHELXT* (Sheldrick, 2015*a*) and refined with *SHELXL* (Sheldrick, 2015*b*). All non-H atoms, except for disordered C atoms, were refined anisotropically. Disordered C atoms were refined isotropically. H atoms bonded to C atoms were treated with the riding model. In the case of NaOEt·2EtOH and NaO^{n}Pr·2^{n}PrOH, all OH protons could be located by Fourier synthesis. In NaO^{i}Pr·5^{i}PrOH, it was not possible to detect which of the four ligands coordinating to the Na^+ ion is the ^{i}PrO$^-$ anion, and which are the three ^{i}PrOH molecules. (The H atom could not be located, all Na—O bonds were of a similar length, all C—O bonds were of similar length, and in addition no decision could be made based on the size of the angles; furthermore, there is a twofold axis through the Na^+ ion, hence there are always pairs of symmetrically equivalent ligands.) All O atoms of NaO^{i}Pr·5^{i}PrOH are part of a complex hydrogen-bond network, and obviously the H atoms are disordered within this network. Therefore, for each Na^+ cation, H atoms with occupancies of 0.75 were placed at all four O atoms connected to the Na^+ cation. For NaO^{t}Am·^{t}AmOH, the electron density indicates that the H atoms of the OH groups are located along hydrogen bonds. However, the limited data quality did not allow an unrestrained refinement of the positions of these H atoms. According to the charge compensation, the H atoms should be disordered, too.

The single crystals of NaO^{i}Pr·5^{i}PrOH are highly sensitive; they decompose within seconds except when they are kept in their mother liquor under an inert atmosphere. Therefore, only rather poor diffraction data could be obtained. Correspondingly, a large number of restraints had to be used in the refinement. The disordered C atoms were refined isotropically, with restraints on the C—C and C—O bond lengths. The ordered C atoms were refined anisotropically, but their anisotropic displacement parameters were restrained to be similar to those of neighbouring atoms.

3. Results and discussion

3.1. Space group and disorder of sodium ethoxide (NaOEt)

Sodium ethoxide is difficult to obtain as a pure phase. The reaction of sodium with ethanol, with subsequent evaporation at room temperature under vacuum or evaporation at the boiling point at ambient pressure, results in a mixture of two to four phases, including NaOEt and NaOEt·2EtOH. Evaporation under vacuum at 50 °C for several hours leads to phase-pure NaOEt. Nevertheless, most of our recorded powder patterns were contaminated by traces of other phases.

The powder pattern of NaOEt could be indexed with a tetragonal unit cell, with $a = b = 6.2$, $c = 9.1$ Å and $V = 352$ Å^3. According to Hofmann's volume increments (Hofmann, 2002), the unit-cell volume corresponds to $Z = 4$. The systematic extinctions pointed to the space group *P*4/*nbm*. Further experiments revealed that some of the weak peaks in the powder pattern were actually caused by foreign phases. The pattern of the phase-pure NaOEt could be indexed with a unit cell of half of the initial volume, with $a = b = 4.41$, $c = 9.07$ Å, $\alpha = \beta = \gamma = 90°$, $V = 176.4$ Å^3 and $Z = 2$.

The systematic extinctions lead to the extinction symbol *Pn*−−, which corresponds to the space group *P*4/*n* or *P*4/*nmm* (Hahn, 2005). In *P*4/*nmm*, the structure could be solved without difficulty by the real-space method with simulated annealing using the program *DASH* (David *et al.*, 2006). The unit cell contains two formula units. In *P*4/*nmm* there are three different Wyckoff positions with a multiplicity of two: positions 2*a* and 2*b* with site symmetry $\bar{4}m2$, and 2*c* with site symmetry 4*mm*. A tetrahedral coordination of the Na^+ ion agrees with a $\bar{4}m2$ site symmetry. Correspondingly, the Na^+ ion

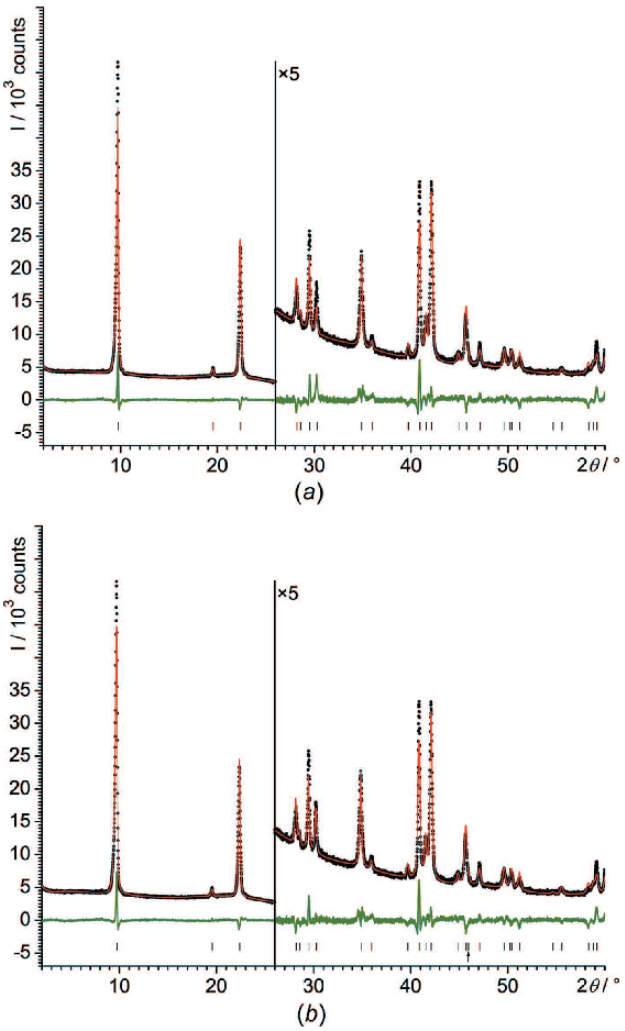

Figure 1
Rietveld plots of NaOEt performed in different space groups under identical conditions, *i.e.* (*a*) *P*4/*nmm* and (*b*) $P\bar{4}2_1m$. Experimental data are shown as black dots and simulated data as a red line, with the difference curve in green below. The vertical tick marks denote the reflection positions. The small arrow in (*b*) denotes the 210 reflection, which is extinct in *P*4/*nmm*, but present in $P\bar{4}2_1m$.

Table 1
Rietveld refinement of NaOEt in *P*4/*nmm* and $P\bar{4}2_1m$ under identical conditions, with restrained H-atom positions and a 2θ range of 2–60°.

The values marked by a ′ are background-subtracted values. *N*(param) is the number of structural parameters, including the occupancy parameter.

	*P*4/*nmm*	$P\bar{4}2_1m$	$P\bar{4}2_1m$ with both orientations of Et
R_{wp} (%)	4.320	4.146	4.149
R_{wp}' (%)	16.98	16.30	16.30
R_p (%)	3.205	3.122	3.126
R_p' (%)	18.21	17.74	17.75
Goodness-of-fit	2.016	1.935	1.936
N(param)	13	13	13 + 1 (occupancy)
Occupancy of the ethyl group	0.25 (fixed)	0.5 (fixed)	0.476 (6):0.024 (6)

was set at position 2*a*. A rigid C_2H_5O fragment was placed on the general position (16*k*) with an occupancy of 0.125. The best solution was found in about 10 out of 25 runs and had a good profile-χ^2 value of 7.26. The O atom was found very close to the 4*mm* site (Wyckoff position 2*c*), hence it could be set at this site. The ethyl group is disordered around the 4*mm* site. The two C atoms could be situated on the general position (16*k*), resulting in eightfold disorder, or on mirror planes parallel to (100) and (010) (Wyckoff position 8*i*, site symmetry *.m*.), or on diagonal mirror planes (Wyckoff position 8*j*, site symmetry *..m*), each with fourfold disorder.

The structure was refined by the Rietveld[1] method (Loopstra & Rietveld, 1969) with *TOPAS*, with the C atoms on the general position (16*k*). During the refinement, the C atoms moved close to the diagonal mirror planes. Correspondingly, they were set to the sites 8*j* (*..m*). The refinements converged with good *R* values (Table 1) and smooth difference curves (Fig. 1*a*). The ethyl groups are fourfold disordered around the fourfold axes, see Fig. 2(*a*). A corresponding structure was also found for lithium methoxide (LiOMe) (Wheatley, 1961) and sodium methoxide (NaOMe) (Weiss, 1964).

A symmetry analysis revealed that in the subgroup $P\bar{4}2_1m$ the ethyl groups would have a twofold disorder only. $P\bar{4}2_1m$ is a *translationengleiche* subgroup of *P*4/*nmm* (Wondratschek & Müller, 2004; Aroyo, 2016) [see Fig. 2(*b*)]. These two space groups are difficult to distinguish from each other using the systematic extinctions in PXRD. *P*4/*nmm* requires the reflection condition *hk*0: $h+k = 2n$, whereas $P\bar{4}2_1m$ requires only *h*00: $h = 2n$ and 0*k*0: $k = 2n$ (Hahn, 2005). However, in the 2θ range up to 60°, the powder pattern contains only one reflection, which is systematically absent in *P*4/*nmm* but can be present in $P\bar{4}2_1m$. This is the 210 reflection, which has an intensity of close to zero (see Fig. 1*b*). Hence, an examination of the systematic extinctions left the space group ambiguous.

As a test for the space group, Rietveld refinements were performed in *P*4/*nmm* and $P\bar{4}2_1m$ under identical conditions (identical treatment of background, profile parameters, anisotropic peak broadening, *etc*.). It is an interesting peculiarity that the number of structural parameters is identical in both space groups, which is a very rare case for an organic crystal structure in a group–subgroup relationship. Hence, the resulting confidence values of both space groups can be compared directly. The difference in the *R* values is slightly in favour of $P\bar{4}2_1m$ (see Table 1). The Rietveld plots are very similar, just the 111 reflection at $2\theta = 30.28°$ is significantly better fitted in $P\bar{4}2_1m$ (see Fig. 1).

In both space groups, the structure is very similar, except for the disorder of the ethyl groups. In *P*4/*nmm* the ethyl group is disordered around a fourfold axis, which changes to a twofold axis in $P\bar{4}2_1m$ [see Figs. 2(*a*) and 2(*b*)].

As a further test for the space group, a Rietveld refinement was performed in the space group $P\bar{4}2_1m$ with two sets of ethyl groups, one in the position $x, x+\frac{1}{2}, z$ (Wyckoff position 8*j*) according to the $P\bar{4}2_1m$ structure, and the other on the posi-

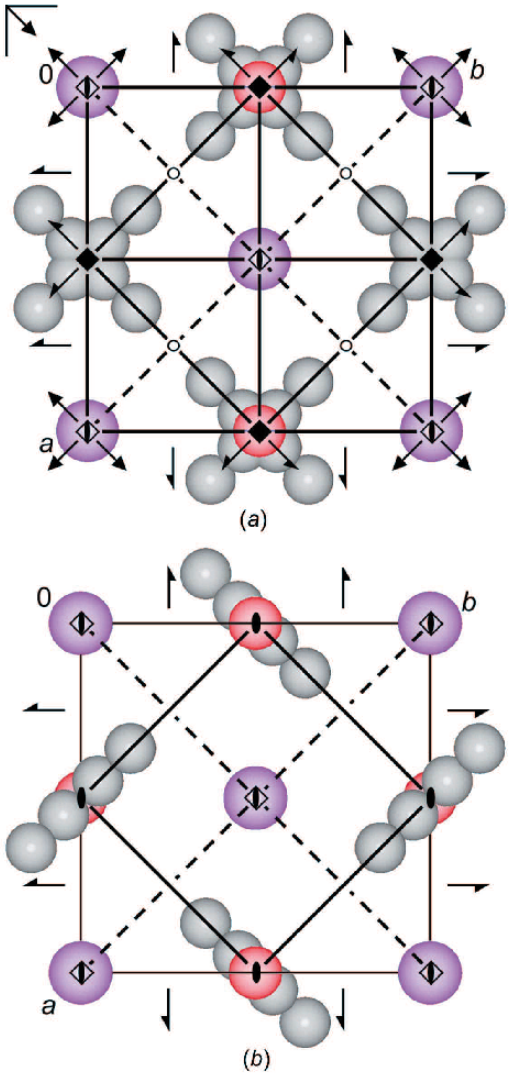

Figure 2
Structural models of NaOEt in (*a*) *P*4/*nmm* (origin choice 1) and (*b*) $P\bar{4}2_1m$. Colour key: Na violet, O red and C grey (disordered). H atoms have been omitted for clarity. The view direction is [001]. The crystallographic symmetry elements are included.

[1] For a discussion on the name 'Rietveld method' *versus* the name 'Loopstra method', see van Laar & Schenk (2018).

tion $-x$, $x + \frac{1}{2}$, z, which is occupied in $P4/nmm$, but not in $P\bar{4}2_1m$ (see Fig. 2). The occupancies of both sets were set at p and $\frac{1}{2} - p$. For $P\bar{4}2_1m$, p would be $\frac{1}{2}$ and for $P4/nmm$, p is $\frac{1}{4}$. The parameter p refined to 0.476 (6). This value and the similarity of the R values between this refinement and the refinement in $P\bar{4}2_1m$ clearly indicate that, within the limitations of the powder data, the correct space group is $P\bar{4}2_1m$ instead of $P4/nmm$.

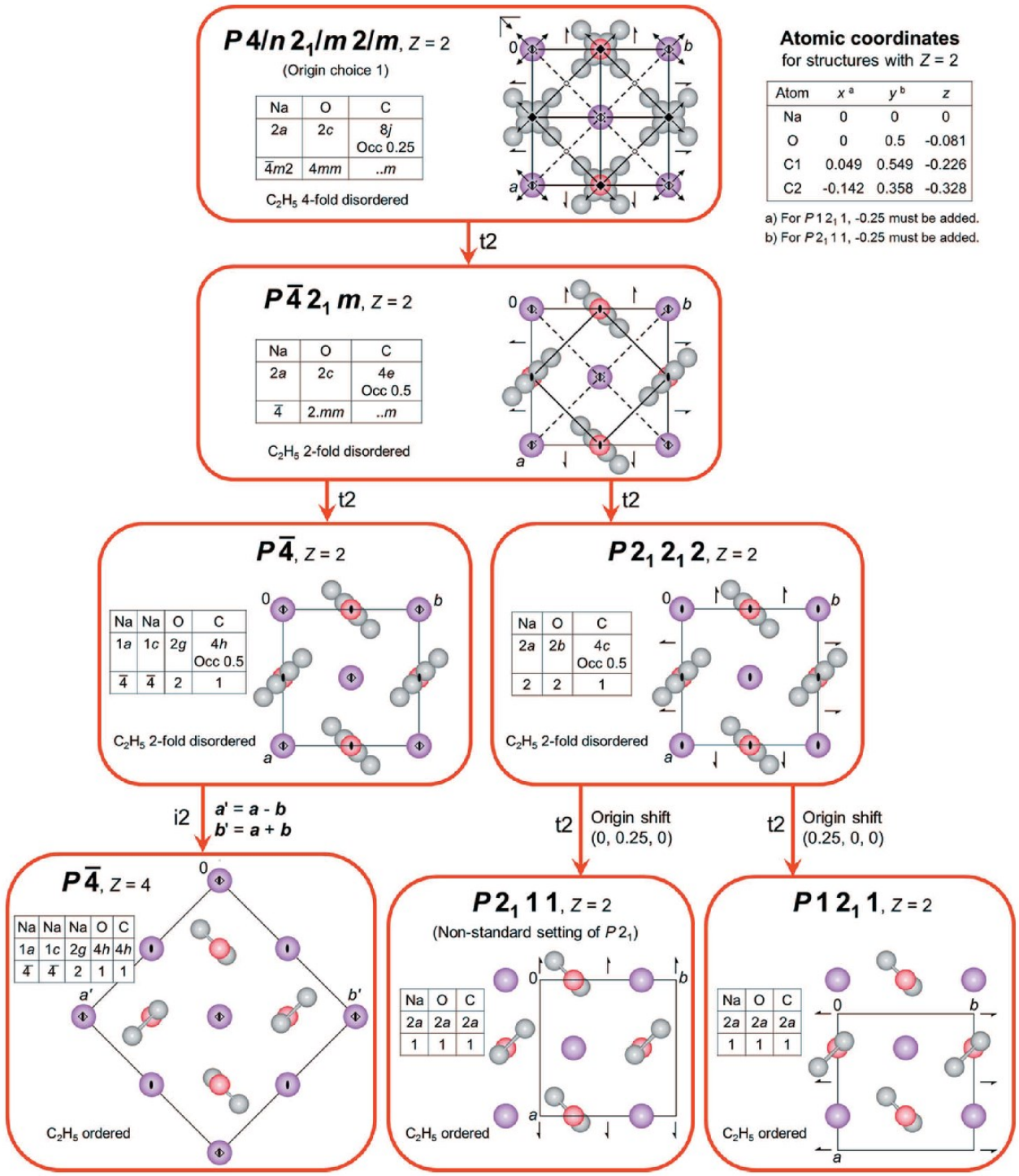

Figure 3
The Bärnighausen tree of NaOEt. Colour key: Na violet, O red and C grey. H atoms have been omitted for clarity. The view direction is [001]. t2 denotes a *translationengleiche* subgroup of index two and i2 an isomorphous subgroup of index two. The small tables give the atom types, Wyckoff positions and site symmetries. Occ denotes the occupancy, if different from one. The experimental crystal symmetry is $P\bar{4}2_1m$, with $Z = 2$.

Table 2
Experimental details for NaOMe, NaOEt, NaO^{n}Pr, NaO^{n}Bu and NaO^{n}Am.

	NaOMe (Weiss, 1964)	**NaOEt**	**NaO^{n}Pr**	**NaO^{n}Bu**	**NaO^{n}Am**
Crystal data					
Chemical formula	CH_3ONa	C_2H_5ONa	C_3H_7ONa	C_4H_9ONa	$C_5H_{11}ONa$
CCDC number	–	1943793	1998221	1998220	1998219
M_r	54.02	68.05	82.08	96.10	109.12
Crystal system	Tetragonal	Tetragonal	Tetragonal	Tetragonal	Tetragonal
Space group (No.)	*P*4/*nmm* (129)	$P\bar{4}2_1m$ (113)	*P*4/*nmm* (129)	*P*4/*nmm* (129)	*P*4/*nmm* (129)
Z, Z'	2, $\frac{1}{8}$	2, $\frac{1}{4}$	2, $\frac{1}{8}$	2, $\frac{1}{8}$	2, $\frac{1}{8}$
Temperature (K)	298	298	298	298	298
a (Å)	4.343 (5)	4.41084 (4)	4. 38439 (5)	4.43232 (9)	4.4084 (2)
c (Å)	7.432 (10)	9.06779 (17)	12.1431 (3)	14.0143 (9)	16.9376 (12)
V (Å^3)	140.2 (2)	176.418 (5)	233.426 (8)	275.318 (19)	329.16 (4)
ρ_{calc} (10^3 kg m^{-3})	1.28	1.28	1.17	1.16	1.11
Radiation type	Cu $K\alpha$	Cu $K\alpha_1$	Cu $K\alpha_1$	Cu $K\alpha_1$	Cu $K\alpha_1$
Wavelength (Å)	1.5418	1.5406	1.5406	1.5406	1.5406
μ (mm^{-1})	–	1.845	1.473	1.314	1.154
Data collection					
Diffractometer	Goniometer with counting tube	Stoe Stadi-P	Stoe Stadi-P	Stoe Stadi-P	Stoe Stadi-P
Specimen mounting	Powder in N_2 stream between polymer films	1.0 mm glass capillary	1.0 mm glass capillary	1.0 mm glass capillary	1.0 mm glass capillary
Data collection mode	Transmission	Transmission	Transmission	Transmission	Transmission
Detector	Counting tube	Linear position-sensitive	Linear position-sensitive	Linear position-sensitive	Linear position-sensitive
$2\theta_{min}$ (°)	11	2.0	2.0	2.0	2.0
$2\theta_{max}$ (°)	103	80.0	100	100	100
$2\theta_{step}$ (°)	–	0.01	0.01	0.01	0.01
Refinement					
R_p	0.159	0.0233	0.0373	0.0347	0.0376
R_{wp}	–	0.0339	0.0479	0.0471	0.0535
R_{exp}	–	0.0214	0.0295	0.0240	0.0273
$R_p'^{(a)}$	–	0.133	0.161	0.175	0.120
$R_{wp}'^{(a)}$	–	0.134	0.159	0.187	0.158
$R_{exp}'^{(a)}$	–	0.085	0.0981	0.0951	0.0806
Goodness-of-fit	–	1.42	1.62	1.96	1.96
No. of data points	64 observed intensities	7800	9800	9800	9800
No. of parameters	4	40	56	61	72
No. of restraints	0	8	11	21	26
H-atom treatment	f_H included in C atom	Refined with restraints	Refined with restraints	Refined with restraints	Refined with restraints

Note: (*a*) R_p', R_{wp}' and R_{exp}' values are background-corrected data according to Coelho (2018).

A complete ordering of the ethyl groups would require further reduction of symmetry, *e.g.* to $P\bar{4}$ or $P2_1$. The corresponding Bärnighausen tree (Bärnighausen, 1980; Chapuis, 1992; Müller, 2004, 2006, 2012) is shown in Fig. 3. Such a symmetry reduction would result in a deviation from tetragonal symmetry and/or in a larger unit cell (supercell). Both effects should be clearly visible in the powder pattern. However, the powder pattern of NaOEt gave no indication of either effect. Hence, the space group is likely to be $P\bar{4}2_1m$.

A transition into a *translationengleiche* subgoup of index 2 is frequently associated with twinning. Correspondingly, the NaOEt crystals may be twinned, *i.e.* in one domain the orientation of the ethyl groups is that shown in Fig. 2*b* and in the other domain the groups are rotated by 90°. However, such a twinning cannot be observed by powder diffraction; hence, it remains unclear if the crystals are actually twinned.

The final Rietveld refinements were carried out in $P\bar{4}2_1m$. No restraints were applied to the Na, C and O atoms. Restraints were only necessary for the H-atom positions. The final Rietveld plot is shown in Fig. 4. Crystallographic data are included in Table 2.

The crystal structure of NaOEt (Fig. 5*b*) is similar to the structures of NaOMe and LiOMe (LiOMe type; Fig. 5*a*). The Na^+ ions form a quadratic net in the (001) plane. The O atoms are situated in the centre of each mesh 0.734 (3) Å above or below the plane. The ethyl groups point away from the nets on both sides; hence, they form covering nonpolar layers on both sides of the ionic Na–O nets. Subsequent layers are stacked in the [001] direction. This structure can be regarded as an anti-PbO structure. In red PbO (litharge; Boher *et al.*, 1985), the Pb^{2+} and O^{2-} ions form the same net as the O and Na atoms in NaOEt, and the lone pairs of the Pb^{2+} ion in PbO resemble the positions of the ethyl groups in NaOEt (see Figs. 5*b* and 5*c*).

LiOMe and NaOMe crystallize in the space group *P*4/*nmm* (Z = 2), with the methyl group on the fourfold axis, which causes no problems, because the shape of the methyl group is close to spherical. In contrast, in NaOEt, the crystal symmetry is reduced to $P\bar{4}2_1m$. Astonishingly, NaO^{n}Pr and the higher sodium alkoxides again adopt the higher symmetry *P*4/*nmm* (Z = 2), with a fourfold disorder of the alkyl groups (see below). This raises the question, why does NaOEt not adopt *P*4/*nmm* symmetry? An 'intuitive' explanation for the lower

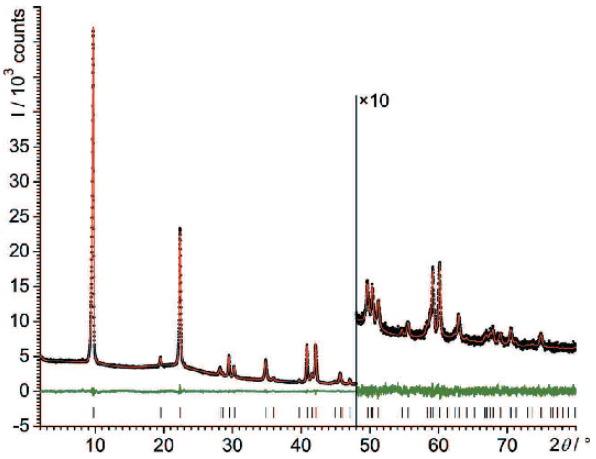

Figure 4
Final Rietveld plot of NaOEt. Experimental data are shown as black dots and simulated data as a red line, with the difference curve in green below. The vertical tick marks denote the reflection positions.

symmetry of NaOEt would be that an ethyl group has a 'less cylindrical' shape than a methyl or propyl group and, hence, avoids being situated on a fourfold axis. The reduced disorder of the ethyl groups of NaOEt in $P\bar{4}2_1m$ leads to a more efficient packing and a higher density. Actually, the density of NaOEt is 4% higher than the average density of NaOMe and NaO^{n}Pr, both of which crystallize in *P*4/*nmm*.

3.2. Crystal structures, space group and disorder of NaO^{n}Pr, NaO^{n}Bu and NaO^{n}Am

Sodium *n*-propoxide (NaO^{n}Pr), sodium *n*-butoxide (NaO^{n}Bu) and sodium *n*-amylate (sodium *n*-pentoxide, NaO^{n}Am) were synthesized from sodium and the corresponding alcohols. Upon evaporation of the alcoholic solutions, the solvates precipitated initially (as a mixture with the solvent-free phases). Further evaporation led to the solvent-free forms. The compounds are very sensitive to water; hence, any trace of moisture, also from air, had to be avoided during synthesis, evaporation and PXRD measurements.

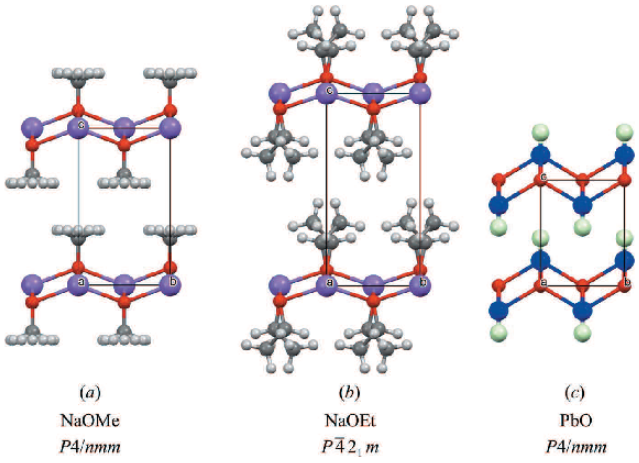

Figure 5
The crystal structures of (*a*) NaOMe, (*b*) NaOEt and (*c*) PbO (litharge). Colour key: Na violet, O red, C grey, H white and Pb blue. In part (*c*), the large light-green balls represent the lone pairs of the Pb^{2+} ions. The view direction is [100]. For a better comparison, the unit cell of NaOMe was shifted by $(0, 0, \frac{1}{2})$ with respect to the original data of Weiss (1964) and the H atoms of NaOMe were added in calculated positions (with a fourfold disorder). Drawings were made with *Mercury* (Macrae *et al.*, 2020).

Table 3
Rietveld refinement of NaO^{n}Pr in *P*4/*nmm* and $P\bar{4}2_1m$ under identical conditions, with restraints on the C and H atoms.

The values marked by a ′ are background-subtracted values. The last column denotes a refinement in $P\bar{4}2_1m$ with two sets of propyl groups, one corresponding to the orientation in $P\bar{4}2_1m$ and the other rotated by 90°, which is occupied in *P*4/*nmm*, but empty in $P\bar{4}2_1m$. *N*(param) is the number of structural parameters, including the occupancy parameter.

	*P*4/*nmm*	$P\bar{4}2_1m$	$P\bar{4}2_1m$ with both orientations of ^{n}Pr
R_{wp} (%)	5.424	5.654	5.386
R_{wp}' (%)	17.953	18.714	17.832
R_p (%)	4.198	4.376	4.238
R_p' (%)	18.139	18.908	18.324
Goodness-of-fit	1.837	1.915	1.824
N(param)	18	18	18 + 1 (occupancy)
Occupancy *p*	0.25 (fix)	0.5 (fix)	0.38 (3):0.12 (3)

The powder diagrams could be easily indexed with tetragonal unit cells, with $Z = 2$. The structures were solved by the real-space method and refined by the Rietveld method.

The crystal structures are similar to that of NaOEt (anti-PbO type). In the case of NaO^{n}Pr, the space group is ambiguous. A refinement in $P\bar{4}2_1m$ with two sets of alkyl groups, as performed for NaOEt, did not yield clear results. The occupancies refined to values of 0.38 (3) and 0.12 (3), which is exactly midway between 0.25 (for *P*4/*nmm*) and 0.5 (for $P\bar{4}2_1m$) (see Table 3). However, the refinement with one set of alkyl groups gave significantly lower confidence values in *P*4/*nmm* than in $P\bar{4}2_1m$. For NaO^{n}Bu and NaO^{n}Am, refinements in *P*4/*nmm* also provided a better fit than in $P\bar{4}2_1m$ (Table 4). Correspondingly, the final refinements of all three compounds were performed in *P*4/*nmm*. The final Rietveld plots are shown in Fig. 6. Crystallographic data are included in Table 2. The crystal structures are shown in Fig. 7.

The lattice parameters and the space group of NaO^{n}Pr agree with the data determined by Chandran *et al.* (2006).

The *n*-butyl and *n*-amyl groups are highly disordered, and the electron density is smeared out, especially for the terminal and the next-to-terminal C atoms. The description of these structures in *P*4/*nmm* with fourfold disordered alkyl groups on Wyckoff position 8*j* is only an approximation of the actual electron density.

We tried to prepare phase-pure powders of solvent-free NaO^{i}Pr and NaO^{t}Am, but the crystal structures could not be solved by PXRD yet. The samples probably contained mixtures of different phases.

3.3. Solvates

By crystallization from the corresponding alcohols, we obtained single crystals of four alcohol solvates of sodium alkoxides: NaOEt·2EtOH, NaO^{n}Pr·2^{n}PrOH, NaO^{i}Pr·5^{i}PrOH

and NaO^{t}Am·^{t}AmOH. All of these solvates are sensitive to moisture and air. In a vacuum and under argon (or nitrogen), they decompose into their solvate-free forms. The decomposition is comparably slow for NaOEt·2EtOH, but fast for NaO^{i}Pr·5^{i}PrOH. Correspondingly, the solvates must be stored in their mother liquor or in the presence of vapours of the corresponding alcohols or kept at low temperature.

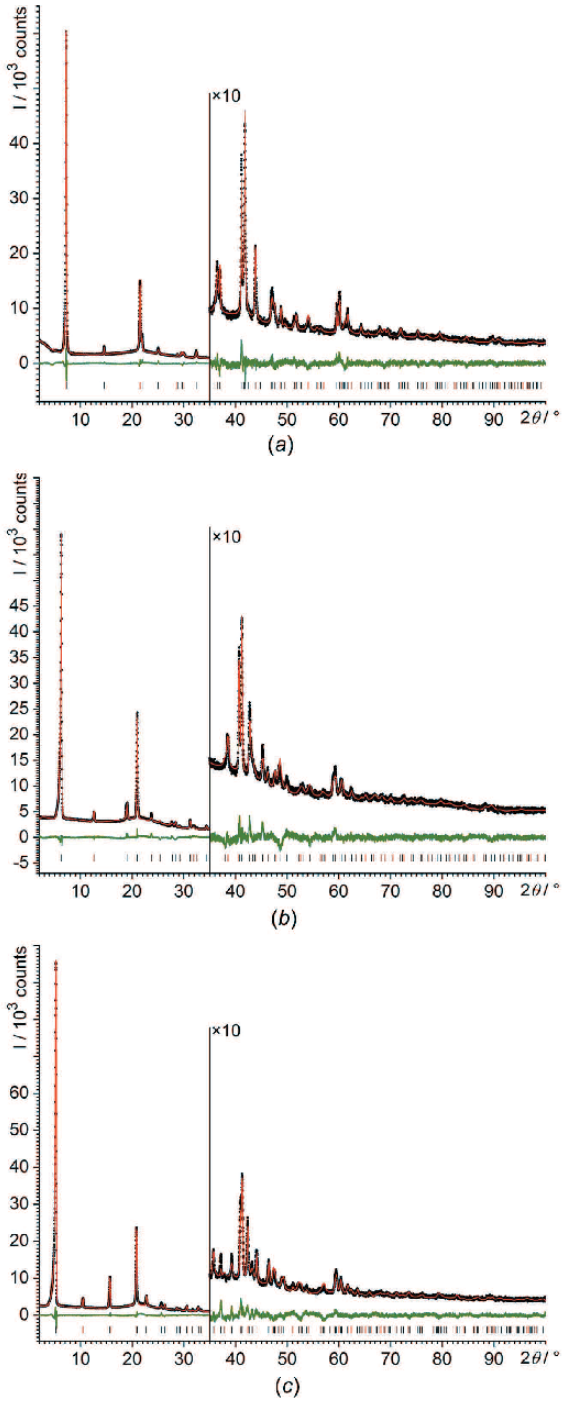

Figure 6
Final Rietveld plots of (*a*) NaO^{n}Pr, (*b*) NaO^{n}Bu and (*c*) NaO^{n}Am. Experimental data are shown as black dots and simulated data as a red line, with the difference curve in green below. The vertical tick marks denote the reflection positions.

Table 4
Rietveld refinement of NaO^{n}Bu and NaO^{n}Am in *P*4/*nmm* and $P\bar{4}2_1m$ under identical conditions, with restraints on the C and H atoms.

N(param) is the number of structural parameters, including the occupancy parameter.

	NaO^{n}Bu		NaO^{n}Am	
	*P*4/*nmm*	$P\bar{4}2_1m$	*P*4/*nmm*	$P\bar{4}2_1m$
R_{wp} (%)	4.620	4.884	5.403	5.762
R_{wp}' (%)	18.52	19.30	15.87	17.03
R_p (%)	3.578	3.766	3.875	4.071
R_p' (%)	18.73	19.11	12.44	13.13
Goodness-of-fit [*S*]	1.924	2.032	1.974	2.106
N(param)	23	23	28	28

The chemical compositions and crystal structures of these four solvates were determined by single-crystal X-ray diffraction. However, there were three obstacles: (i) the mounting of the crystals on the diffractometer was challenging due to their sensitivity to air, moisture, vacuum and dry inert gas; (ii) the crystal quality was limited, especially for NaO^{i}Pr·5^{i}PrOH; (iii) the crystal structures of NaO^{n}Pr·2^{n}PrOH and NaO^{i}Pr·5^{i}PrOH are highly disordered. In NaO^{n}Pr·2^{n}PrOH, the disorder affects all of the propyl groups. In NaO^{i}Pr·5^{i}PrOH, four of the ten ^{i}PrOH units are disordered over two widely separated positions each.

The stability of the solvates of the sodium *n*-alkoxides decreases with increasing chain length. Correspondingly, crystal structures could be determined only for the solvates of NaOEt and NaO^{n}Pr, whereas the solvates of NaO^{n}Bu and NaO^{n}Am are highly instable, poorly crystalline and decompose rapidly, even under cold dry nitrogen.

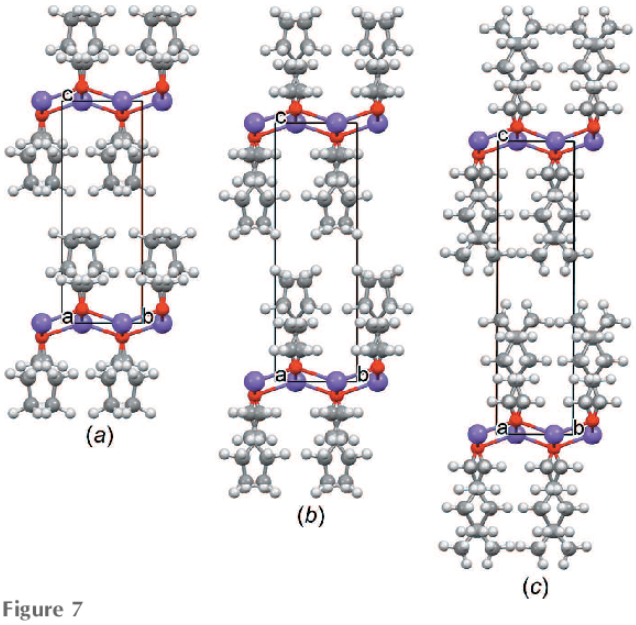

Figure 7
The crystal structures of (*a*) NaO^{n}Pr, (*b*) NaO^{n}Bu and (*c*) NaO^{n}Am. Colour key: Na violet, O red, C grey and H white. The view direction is [100].

Table 5
Experimental details for the sodium alkoxide solvates.

All determinations were carried out with Cu $K\alpha$ radiation using a Siemens Bruker three-circle diffractometer with an APEXII detector, an Incoatec Iμs microfocus source and mirror optics.

	NaOEt·2EtOH	NaO^{n}Pr·2^{n}PrOH	NaO^{i}Pr·5^{i}PrOH	NaO^{t}Am·^{t}AmOH
Crystal data				
Chemical formula	$C_2H_5ONa·2C_2H_5OH$	$C_3H_7ONa·2C_3H_7OH$	$C_3H_7ONa·5C_3H_7OH$	$C_5H_{11}ONa·C_5H_{11}OH$
CCDC number	1943794	1998225	1998224	1998227
M_r	160.18	202.26	382.55	198.27
Crystal system	Monoclinic	Monoclinic	Monoclinic	Monoclinic
Space group (No.)	$P2_1/n$ (14)	$C2/c$ (15)	$C2/c$ (15)	$P2_1/c$ (14)
Z, Z'	4, 1	8, 1	8, 1	4, 1
Temperature (K)	238 (2)	173 (2)	173 (2)	296 (2)
a (Å)	11.622 (6)	23.745 (5)	21.2073 (18)	10.1260 (8)
b (Å)	5.1926 (9)	5.0750 (11)	17.1307 (13)	6.0299 (5)
c (Å)	17.682 (6)	24.174 (5)	17.825 (2)	20.6944 (18)
β (°)	104.08 (3)	111.589 (10)	123.871 (5)	104.16
V (Å^3)	1035.0 (7)	2708.7 (10)	5376.9 (10)	1225.18 (18)
ρ_{calc} (10^3 kg m^{-3})	1.03	0.992	0.945	1.08
Wavelength (Å)	1.54178	1.54178	1.54178	1.54178
μ (mm^{-1})	1.006	0.849	0.686	0.869
Crystal habit	Needle	Needle	Needle	Needle
Crystal size (mm)	0.8 × 0.08 × 0.02	0.5 × 0.05 × 0.05	0.4 × 0.02 × 0.02	1 × 0.02 × 0.01
Data collection				
θ range (°)	4.14–59.9	3.93–50.9	3.60–40.2	4.41–50.7
Absorption correction	Multi-scan (*SADABS*; Bruker, 2015)			
T_{min}, T_{max}	0.2700, 0.7486	0.5182, 0.7500	0.771, 0.875	0.477, 0.991
No. of measured reflections	5735	10 777	9647	13194
No. of unique reflections	1124	1616	1652	1300
R_{int}	0.317	0.0887	0.0724	0.112
Refinement				
No. of parameters	95	114	239	118
No. of restraints	0	0	84	15
$wR(F^2)$	0.2709	0.2984	0.3669	0.1613
$R[F^2 > 2\sigma(F^2)]$	0.2178	0.0954	0.1215	0.0574
S	0.980	1.064	1.196	1.002
$\Delta\rho_{max}$, $\Delta\rho_{min}$ (e$^-$ Å^{-3})	0.16, −0.20	0.24, −0.20	0.22, −0.17	0.30, −0.26

3.3.1. NaOEt·2EtOH and NaO^{n}Pr·2^{n}PrOH. Sodium ethoxide and sodium *n*-propoxide crystallize as needles (see Fig. 8). The single-crystal X-ray analysis (Table 5) revealed the compounds to be disolvates with the composition NaO*R*·2*R*OH, as determined by Geuther (1868*a*,*b*) and Frölich (Geuther & Frölich, 1880). Both solvates are isostructural. The O atom of the alkoxide anion (RO^-) bridges two Na^+ ions, leading to helical Na—O—Na—O chains. The chains follow a crystallographic 2_1 screw axis. The Na^+ ions are additionally coordinated to two alcohol molecules (*R*OH), resulting in a distorted tetrahedral coordination geometry for the Na^+ ions. In NaO^{n}Pr·2^{n}PrOH, all the propyl groups are disordered and

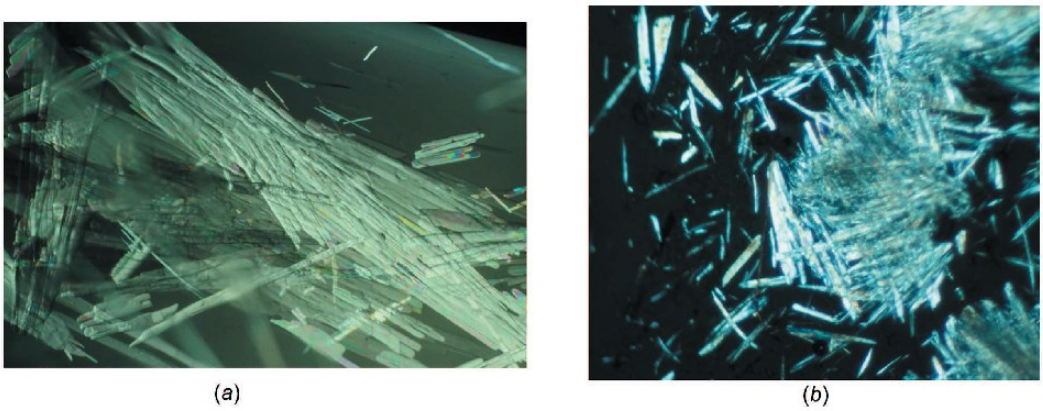

(*a*) (*b*)

Figure 8
The crystals of (*a*) NaO^{n}Pr·2^{n}PrOH (image width about 15 mm) and (*b*) NaO^{t}Am·^{t}AmOH (image width about 2 mm), both in polarized light.

most of the C atoms were refined with split positions, with occupancies between 0.40 and 0.60. The OH groups of the alcohol molecules form hydrogen bonds to neighbouring *R*OH molecules and RO^- anions, which additionally stabilize the chains (see Fig. 9). The alkyl groups point outwards. Hence the chains are like tubes, with a polar/ionic inner region and a nonpolar outer region. In the crystal, all the tubes are arranged parallel and form a distorted hexagonal packing (see Fig. 10). However, the space group is different, *i.e.* $P2_1/c$ for NaOEt·2EtOH and $C2/c$ for NaO^{n}Pr·2^{n}PrOH.

Between the 'tubes' there are only van der Waals contacts between the alkyl groups. This structure explains the observed needle-like morphology of both compounds, with the needle axes parallel to the chain direction [010]. The weak interactions between the 'tubes' allow them to librate around their long axis, which is manifested in the anisotropic displacement parameters of NaOEt·2EtOH (see Fig. 10*a*). In the case of NaO^{n}Pr·2^{n}PrOH, the limited crystal quality and the disorder of the propyl groups prevent an interpretation of the displacement ellipsoids.

The corresponding lithium methoxide solvate, LiOMe·2MeOH, is a disolvate, like NaOEt·2EtOH and NaO^{n}Pr·2^{n}PrOH, but its structure is different. LiOMe·2MeOH consists of $Li_4(OMe)_4(MeOH)_6$ tetramers, which are connected through hydrogen bonds *via* MeOH molecules to form a two-dimensional network. As in NaOEt, the interior layer of this network consists of metal ions and O atoms, whereas the alkyl groups point outwards. These layers are stacked through van der Waals contacts between the methyl groups only.

3.3.2. NaO^{i}Pr·5^{i}PrOH. Sodium isopropoxide forms a solvate which contains as many as five molecules of isopropanol per NaO^{i}Pr unit. Hence, this structure can be regarded as an isopropanol in which one sixth of the protons of the OH groups are replaced by sodium ions. Correspondingly, the structure of NaO^{i}Pr·5^{i}PrOH provides an insight into the structure of liquid isopropanol itself.

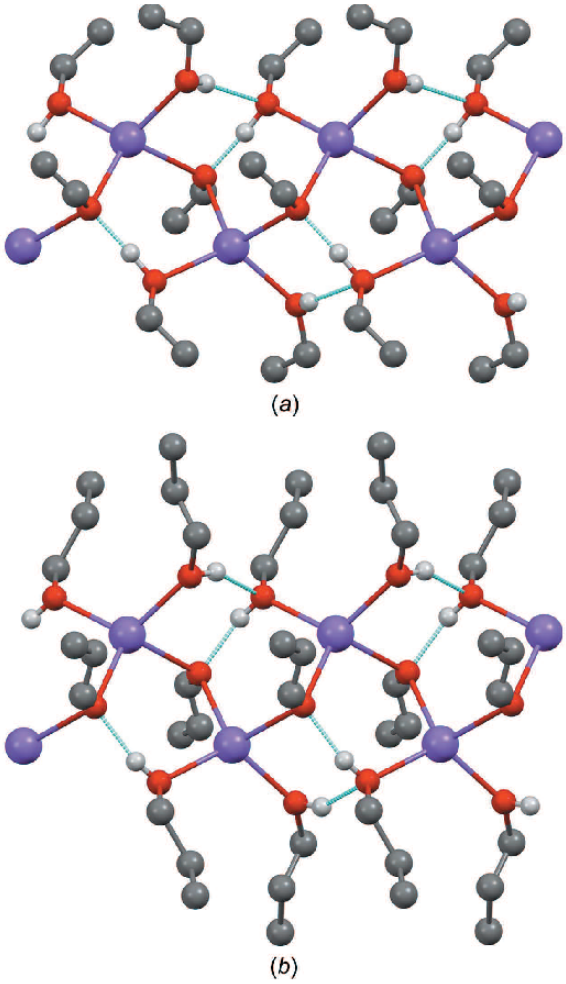

Figure 9
Helical chains in (*a*) NaOEt·2EtOH and (*b*) NaO^{n}Pr·2^{n}PrOH. Colour key: Na violet, O red, C grey and H white. Hydrogen bonds are drawn as dotted light-blue lines. The H atoms of the alkyl groups have been omitted for clarity. In part (*b*), the disordered propyl groups are represented by their major-occupied atomic positions only.

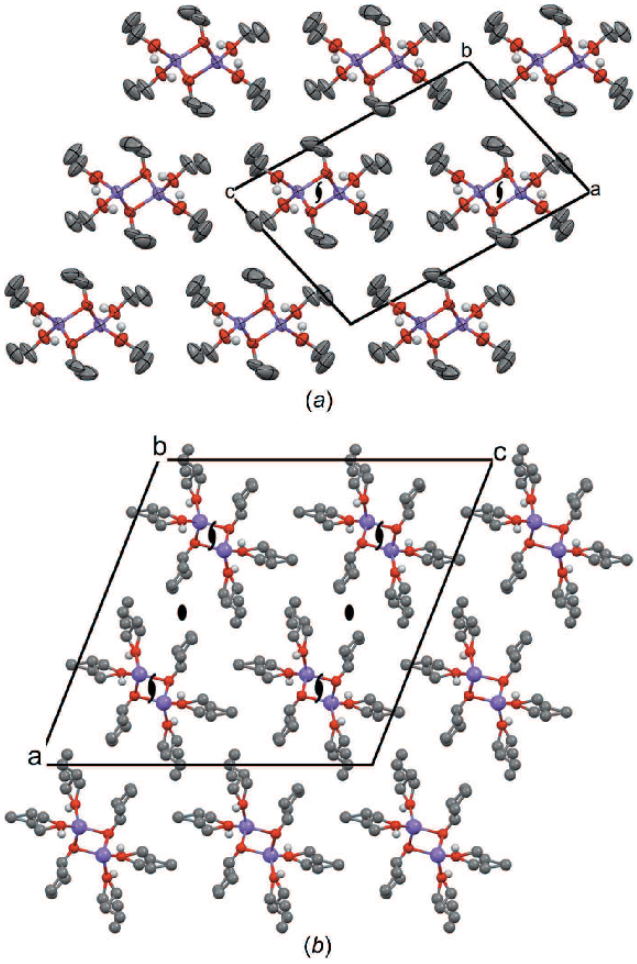

Figure 10
The crystal structures of (*a*) NaOEt·2EtOH (space group $P2_1/c$, view direction [010] and displacement ellipsoids at the 50% probability level) and (*b*) NaO^{n}Pr·2^{n}PrOH (space group $C2/c$, view direction [$0\bar{1}0$]). Selected symmetry elements are shown. In both structures, there is a 2_1 screw axis in the middle of each chain.

The solvate crystallizes in the space group $C2/c$, with $Z = 8$. There are two symmetrically independent Na^+ ions, both on the twofold axis. Each Na^+ ion coordinates to four O atoms of ^{i}PrO$^-$ and ^{i}PrOH moieties (Fig. 11*a*). The H atoms of the OH groups could not be located reliably, as they are probably dynamically disordered. Because of the charge compensation, it is expected that in any instance each Na^+ cation is surrounded by one ^{i}PrO$^-$ ligand and three ^{i}PrOH molecules. These Na(^{i}PrO)(^{i}PrOH)$_3$ units are connected by further ^{i}PrOH molecules to form a chain along the twofold axis parallel to [010] (see Figs. 11*a* and 11*b*). All isopropanol molecules which are not directly coordinated to sodium have an occupancy of 0.5. All isopropyl groups show disorder.

The geometry of the chain is close to $\not{1}12/m$ symmetry (rod group No. 11; Kopský & Litvin, 2010).

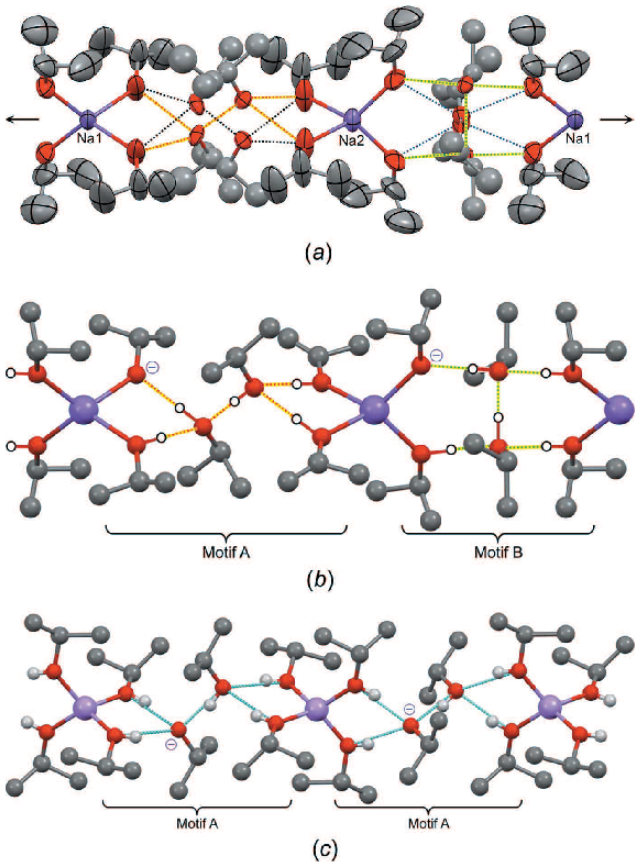

Figure 11
(*a*) The crystal structure of NaO^{i}Pr·5^{i}PrOH, showing one chain. The view direction is [001], with the *b* axis horizontal. Displacement ellipsoids are drawn at the 20% probability level. All ^{i}PrOH molecules not directly coordinated to Na have an occupancy of 0.5 only. Dotted lines represent the four independent hydrogen-bond networks. The arrows indicate the crystallographic twofold axis. (*b*) Selected hydrogen-bond networks in NaO^{i}Pr·5^{i}PrOH. (*c*) The crystal structure of LiO^{i}Pr·5^{i}PrOH. The disorder of the ^{i}Pr groups is not shown. In parts (*b*) and (*c*), the H atoms are shown as white spheres in calculated positions. The H-atom positions shown here represent only one possibility; actually, the H atoms are disordered and could not be located experimentally. Minus (−) signs denote the anions.

There are four independent hydrogen-bond networks in each chain, each with an occupancy of 0.5 (see Fig. 11*a*). Two of these networks are shown in Fig. 11*b*.

The hydrogen-bond networks are considerably different from those in pure solid isopropanol. Pure isopropanol forms different hydrogen-bond networks, depending on the experimental conditions: the high-pressure polymorph exhibits eight-membered rings, whereas the low-temperature polymorph forms helical chains with local 3_1 or 3_2 symmetry (see Fig. 12) (Ridout & Probert, 2014). In contrast, the hydrogen-bond network of NaO^{i}Pr·5^{i}PrOH contains branching between the alcohol molecules, *i.e.* alcohol molecules are connected by hydrogen bonds to three other alcohol molecules. There are two different topologies, marked as 'Motif A' and 'Motif B' in Fig. 11(*b*). Motif A is also present in LiO^{i}Pr·5^{i}PrOH (Mehring *et al.*, 2002). Motifs A and B can neither be found in other sodium alkoxide solvates nor in the crystal structures of pure isopropanol. In liquid isopropanol, one could expect to find a mixture of all three motifs, namely, rings, chains and branchings.

In NaO^{i}Pr·5^{i}PrOH, the hydrogen-bonded chains are surrounded by the nonpolar isopropyl groups. Between the chains, there are only van der Waals contacts between the isopropyl groups (see Fig. 13). Similarly, in both polymorphs of

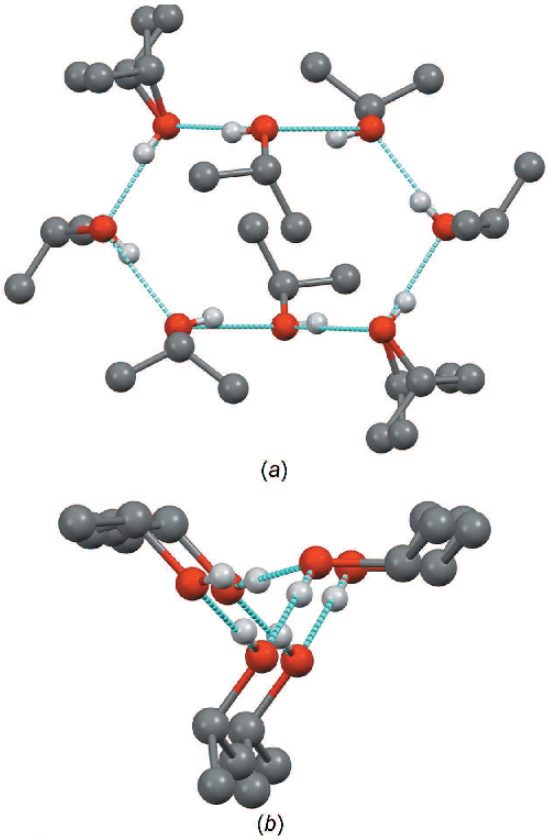

Figure 12
The hydrogen-bond networks of solid pure isopropanol. (*a*) Eight-membered ring in the high-pressure phase. (*b*) Threefold screw axis in the low-temperature phase. In both structures, some of the isopropyl groups are disordered.

pure ^{i}PrOH, the rings and chains have polar surfaces, and are connected to neighbouring rings or chains by van der Waals interactions (see Figs. S1 and S2 in the supporting information).

The chains of NaO^{i}Pr·5^{i}PrOH are arranged in a distorted hexagonal packing. The packing seems to be similar to the chain packing in NaO^{n}Pr·2^{n}PrOH. The space group is also the same (*i.e.* *C*2/*c*). However, the chains in NaO^{i}Pr·5^{i}PrOH are situated on a twofold rotation axis, whereas the chains of NaO^{n}Pr·2^{n}PrOH are placed on a 2_1 screw axis (see Figs. 10*b* and 13).

3.3.3. NaO^{t}Am·^{t}AmOH. The X-ray structure analysis revealed that sodium *tert*-amylate (sodium 2-methyl-2-butanolate, NaO^{t}Am) forms a monosolvate with *tert*-amyl alcohol (2-methyl-2-butanol). In this structure, neighbouring Na^+ ions are bridged by two ligands in the form of a square. The square shares corners with two other squares, leading to chains (see Fig. 14). Each square is centred by a crystallographic inversion centre. The squares are additionally connected by hydrogen bonds. The H atom engaged in this bond is probably disordered, so that in any instance each square contains one ^{t}AmO$^-$ anion and one ^{t}AmOH ligand, due to electrostatic considerations. The squares form an interplanar angle of 49.8° only, which is apparently caused by the hydrogen bonds. The *tert*-amyl groups point outwards, as in the other solvates.

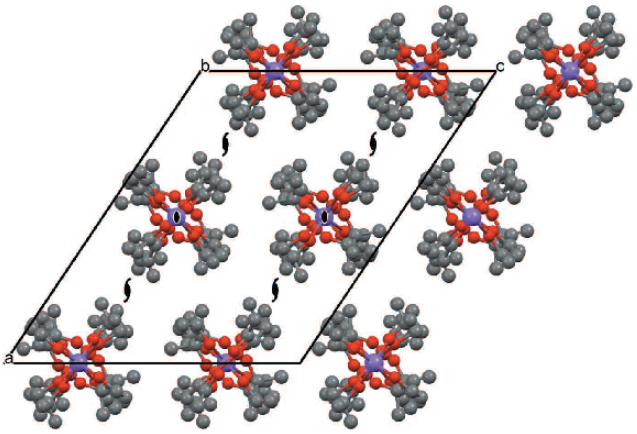

Figure 13
The crystal structure of NaO^{i}Pr·5^{i}PrOH (space group *C*2/*c*, view along the chains and view direction [0$\bar{1}$0]). The chains are located on twofold rotation axes, in contrast to the 2_1 screw axes for NaO^{n}Pr·2^{n}PrOH (see Fig. 10*b*).

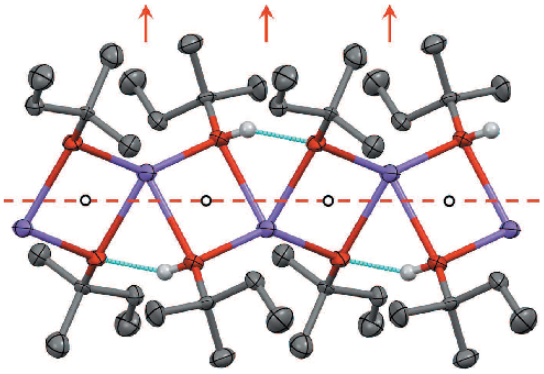

Figure 14
A view of the structure of NaO^{t}Am·^{t}AmOH, with displacement ellipsoids drawn at the 50% probability level. The H atoms of the *tert*-amyl groups have been omitted for clarity. The light-blue lines denote the hydrogen bonds. The H atom is disordered along the hydrogen bond. The black circles represent crystallographic inversion centres. The red symmetry elements represent the approximated local symmetry of the chain (p2/*b*11).

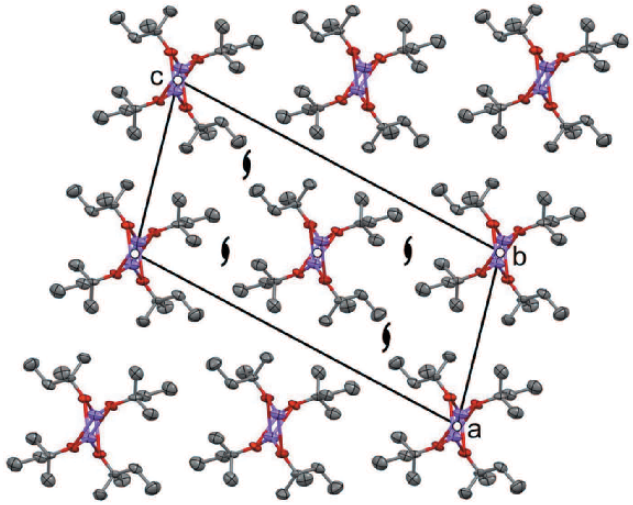

Figure 15
The crystal structure of NaO^{t}Am·^{t}AmOH, viewed along the chains (space group $P2_1/n$, view direction [010]), with displacement ellipsoids drawn at the 50% probability level. Selected symmetry elements are shown.

The chain has approximately p2/*b*11 symmetry, which is a nonstandard setting of p2/*c*11 (rod group No. 7; Kopský & Litvin, 2010). In the crystal, only the inversion symmetry is maintained in the space-group symmetry $P12_1/n1$.

The arrangement of the chains (Fig. 15) is similar to that in NaOEt·2EtOH (Fig. 10*a*). The space group is also the same ($P2_1/c$, here in the $P2_1/n$ setting). However, in NaOEt·2EtOH, the chains are aligned along the 2_1 axis, whereas in NaO^{t}Am·^{t}AmOH, the chains contain inversion centres.

4. Conclusion

In this study, we determined the crystal structures of a series of sodium alkoxides NaO*R* (*R* = Et, ^{n}Pr, ^{n}Bu and ^{n}Am) and of a series of solvates of the composition NaO*R*·*x*ROH (*R* = Et, ^{n}Pr, ^{i}Pr and ^{t}Am; *x* = 1, 2 and 5). Surprisingly, the crystal structures were unknown. Only the structures of NaOMe, NaO^{t}Bu and NaOMe·2MeOH had been determined previously.

The solvates show a variety of compositions, from the monosolvate NaO^{t}Am·^{t}AmOH *via* the disolvates NaO*R*·2*R*OH (*R* = Et and ^{n}Pr) to the pentasolvate NaO^{i}Pr·5^{i}PrOH. The solvates were obtained from saturated solutions of the alkoxides in the corresponding alcohols. We did not systematically investigate a variation of compositions, temperature and vapour pressure. Presumably, other solvate phases with different compositions may also exist.

In all the solvated and solvate-free structures, the Na^+ ion is coordinated in a distorted tetrahedral geometry to four O atoms. In the solvent-free compounds NaO*R*, the O atom has five neighbouring atoms: four Na^+ ions and the alkyl group. Such a fivefold coordination is quite unusual for organic O atoms. The O atoms in organic compounds generally have a maximum of three or four neighbours, when counting counter-ions, alkyl groups, H atoms and accepted hydrogen bonds. In most crystal structures of alcohols *R*OH, the O atoms have only three neighbours: one alkyl group, one H atom and one hydrogen bond as acceptor. The overcrowded coordination of the O atoms in sodium alkoxides is the reason why they so readily form solvates. Already with one additional alcohol molecule, the coordination number of oxygen drops from 5 to 4, as can be seen in NaO^{t}Am·^{t}AmOH. Any additional alcohol molecule increases the number of threefold-coordinated O atoms. This stabilization is reflected in the thermal stability of the solvates: to obtain the solvent-free alkoxides, NaOEt·2EtOH must be heated at ambient pressure to about 200 °C and NaO^{n}Pr·^{n}PrOH even to about 220 °C (Geuther & Frölich, 1880). In contrast to sodium alkoxides, the sodium alkanoates $RCOO^-\cdot Na^+$ and sulfonates $RSO_3^-\cdot Na^+$ rarely form solvates with alcohol or *R*COOH molecules. There, the higher number of O atoms provides a sufficient number of donor atoms for the coordination of the Na^+ ion, even with higher coordination numbers of Na^+, *e.g.* 6 in $CH_3COO^-\cdot Na^+$ (Dittrich *et al.*, 2018) or 6–7 in $CH_3SO_3^-\cdot Na^+$ (Wei & Hingerty, 1981).

Four different topologies are present in sodium alkoxides: the alkoxides with linear alkyl chains (*R* = Me, Et, ^{n}Pr, ^{n}Bu and ^{n}Am) form layers of Na^+ and O^- atoms, NaO^{t}Bu forms clusters (hexamers and nonamers), NaOMe·2MeOH forms tetramers, which are connected by hydrogen bonds into layers, and the other solvates form chains of differing composition. In all cases, polar and nonpolar regions are clearly separated: the interior of the layers, clusters and chains consist of Na^+ and $-O^-$ ions and is held together by electrostatic forces, whereas the outer regions are composed of the nonpolar alkyl groups. Neighbouring layers, clusters or chains are connected by van der Waals contacts only. As a result, the chain structures of all the solvates form needles. NaO^{t}Bu forms prisms or cubes. For the layer structures of NaO*R*, a plate-like morphology could be expected.

The compound NaO^{i}Pr·5^{i}PrOH differs from pure isobutanol only by the substitution of every sixth proton of an OH group with a sodium cation. The crystal structure exhibits a complicated chain structure with branched hydrogen bonds between the isopropanol molecules. Such branchings are not present in the crystal structures of pure isopropanol, but give an interesting insight into the structural diversity of liquid isopropanol.

Acknowledgements

The authors thank Daniel Kratzert (Albert Ludwigs University, Freiburg) for his kind assistance with the refinement of the disordered alkyl groups of NaO^{i}Pr·5^{i}PrOH, Ulrich Müller (Philipps University, Marburg) for helpful suggestions for improvement of the Bärnighausen tree, Edith Alig (Goethe University, Frankfurt) for the measurement of numerous powder diagrams, Lothar Fink (Goethe University, Frankfurt) for support with the single-crystal structure determination and excellent maintenance of all of our diffractometers, Tanja Reipen (Clariant, Frankfurt) for providing information on industrial sodium *tert*-amylate, and Trixi Cronje for assistance with the correction of the English. Open access funding enabled and organized by Projekt DEAL.

References

Aroyo, M. I. (2016). *International Tables for Crystallography*, Vol. A, *Space-group Symmetry*, 6th ed. Chester: International Union of Crystallography.
Bärnighausen, H. (1980). *MATCH Commun. Math. Comput. Chem.* **9**, 139–175.
Beske, M., Tapmeyer, L. & Schmidt, M. U. (2020). *Chem. Commun.* **56**, 3520–3523.
Blanchard, J.-M., Bousquet, J., Claudy, P. & Letoffe, J.-M. (1976). *J. Therm. Anal.* **9**, 191–203.
Boher, P., Garnier, P., Gavarri, J. R. & Hewat, A. W. (1985). *J. Solid State Chem.* **57**, 343–350.
Boultif, A. & Louër, D. (1991). *J. Appl. Cryst.* **24**, 987–993.
Bruker (2015). *APEX3*. Bruker AXS GmbH, Karlsruhe, Germany.
Chandran, K., Nithya, R., Sankaran, K., Gopalan, A. & Ganesan, V. (2006). *Bull. Mater. Sci.* **29**, 173–179.
Chapuis, G. C. (1992). *Symmetry relationships between crystal structures and their practical application*, in *Modern Perspectives in Inorganic Chemistry*, edited by E. Parté, pp. 1–16. Dordrecht: Kluwer Academic Publishers.
Coelho, A. A. (2018). *J. Appl. Cryst.* **51**, 210–218.
David, W. I. F., Shankland, K., van de Streek, J., Pidcock, E., Motherwell, W. D. S. & Cole, J. C. (2006). *J. Appl. Cryst.* **39**, 910–915.
Davies, J. E., Kopf, J. & Weiss, E. (1982). *Acta Cryst.* B**38**, 2251–2253.
Dittrich, B., Bergmann, J., Roloff, P. & Reiss, G. J. (2018). *Crystals*, **8**, 213–224.
Friedrich, H., Guth, J., Schweinzer, J., Letzelter, T. & Bender, H.-J. (1999). European Patent EP 1086067 B1.
Geuther, A. (1859). *Justus Liebigs Ann. Chem.* **109**, 71–79.
Geuther, A. (1868*a*). *Jena. Z. Med. Naturwiss.* **4**, 16–18.
Geuther, A. (1868*b*). *Jena. Z. Med. Naturwiss.* **4**, 241–263.
Geuther, A. & Frölich, O. (1880). *Justus Liebigs Ann. Chem.* **202**, 288–331.
Greiser, T. & Weiss, E. (1977). *Chem. Ber.* **110**, 3388–3396.
Hahn, T. (2005). Editor. *International Tables for Crystallography*, Vol. A, *Space-group symmetry*, 5th ed., with corrections. Chester: International Union of Crystallography.
Hofmann, D. W. M. (2002). *Acta Cryst.* B**58**, 489–493.
Hunger, K. & Schmidt, M. U. (2018). In *Industrial Organic Pigments*, 4th ed. Weinheim: Wiley-VCH.
Kopský, V. & Litvin, D. B. (2010). Editors. *International Tables for Crystallography* Vol. E, *Subperiodic groups*, 2nd ed. Chester: International Union of Crystallography.
Laar, B. van & Schenk, H. (2018). *Acta Cryst.* A**74**, 88–92.
Lescoeur, H. (1895). *C. R. Acad. Sci.* **121**, 691–692.
Liebig, J. (1837). *Ann. Pharm.* **23**, 12–42.
Loopstra, B. O. & Rietveld, H. M. (1969). *Acta Cryst.* B**25**, 787–791.
Macrae, C. F., Sovago, I., Cottrell, S. J., Galek, P. T. A., McCabe, P., Pidcock, E., Platings, M., Shields, G. P., Stevens, J. S., Towler, M. & Wood, P. A. (2020). *J. Appl. Cryst.* **53**, 226–235.
Mehring, M., Berkei, M. & Schürmann, M. (2002). *Z. Anorg. Allg. Chem.* **628**, 1975–1978.
Müller, U. (2004). *Z. Anorg. Allg. Chem.* **630**, 1519–1537.

Müller, U. (2006). In *Inorganic Structural Chemistry*, 2nd ed., ch. 18. Weinheim: Wiley-VCH.
Müller, U. (2012). In *Symmetriebeziehungen zwischen verwandten Kristallstrukturen. Anwendungen der Gruppentheorie in der Kristallchemie*. Wiesbaden: Vieweg+Teubner Verlag. [English translation: *Symmetry Relationships between Crystal Structures* (2013), Oxford University Press.]
Nekola, H., Olbrich, F. & Behrens, U. (2002). *Z. Anorg. Allg. Chem.* **628**, 2067–2070.
Østreng, E., Sønsteby, H. H., Øien, S., Nilsen, O. & Fjellvåg, H. (2014). *Dalton Trans.* **43**, 16666–16672.
Ridout, J. & Probert, M. R. (2014). *CrystEngComm*, **16**, 7397–7400.
Sheldrick, G. M. (2015*a*). *Acta Cryst.* A**71**, 3–8.
Sheldrick, G. M. (2015*b*). *Acta Cryst.* C**71**, 3–8.
Wanklyn, J. A. (1869). *Ann. Chem. Pharm.* **150**, 200–206.
Wei, C. H. & Hingerty, B. E. (1981). *Acta Cryst.* B**37**, 1992–1997.
Weiss, E. (1963). *Helv. Chim. Acta*, **46**, 2051–2054.
Weiss, E. (1964). *Z. Anorg. Allg. Chem.* **332**, 197–203.
Weiss, E. & Alsdorf, H. (1970). *Z. Anorg. Allg. Chem.* **372**, 206–213.
Wheatley, P. J. (1961). *J. Chem. Soc. (London)*, **1961**, 4270–4274.
Wondratschek, H. & Müller, U. (2010). *International Tables for Crystallography*, Vol. A1, *Symmetry Relations between Space Groups*, 2nd ed. Chester: International Union of Crystallography.

7.7 [LT7] First crystal structure of a Pigment Red 52 compound: DMSO solvate hydrate of the monosodium salt

Bibliographische Daten:

Titel:	First crystal structure of a Pigment Red 52 compound: DMSO solvate hydrate of the monosodium salt
Journal:	Acta Crystallographica Section E
Jahr / Ausgabe:	2021 / E77
Seiten:	402–405
DOI:	10.1107/S2056989021002577
URL:	http://scripts.iucr.org/cgi-bin/paper?S2056989021002577
Autoren:	Lukas Tapmeyer, Daniel Eisenbeil, Michael Bolte und Martin Ulrich Schmidt
eSI:	http://scripts.iucr.org/cgi-bin/paper?yk2145
OpenAccess:	Ja.

Beiträge:

Lukas Tapmeyer:
Anleitung der Synthese und Kristallisation, Schreiben des Entwurfs, Korrekturen.

Daniel Eisenbeil:
Angeleitete Synthese und Kristallisation.

Michael Bolte:
Röntgenstrukturanalyse.

Martin U. Schmidt:
Korrekturen.

research communications

Acta Cryst E CRYSTALLOGRAPHIC COMMUNICATIONS

ISSN 2056-9890

First crystal structure of a Pigment Red 52 compound: DMSO solvate hydrate of the monosodium salt

Lukas Tapmeyer, Daniel Eisenbeil, Michael Bolte and Martin U. Schmidt*

Institut für Anorganische und Analytische Chemie, Goethe-Universität Frankfurt, Max-von-Laue-Strasse 7, 60438 Frankfurt am Main, Germany. *Correspondence e-mail: m.schmidt@chemie.uni-frankfurt.de

Received 29 January 2021
Accepted 8 March 2021

Edited by A. V. Yatsenko, Moscow State University, Russia

Keywords: crystal structure determination; organic pigment; solvate; hydrate.

CCDC reference: 2068733

Supporting information: this article has supporting information at journals.iucr.org/e

Pigment Red 52, $Na_2[C_{18}H_{11}ClN_2O_6S]$, is an industrially produced hydrazone-laked pigment. It serves as an intermediate in the synthesis of the corresponding Ca^{2+} and Mn^{2+} salts, which are used commercially for printing inks and lacquers. Hitherto, no crystal structure of any salt of Pigment Red 52 is known. Now, single crystals have been obtained of a dimethyl sulfoxide solvate hydrate of the monosodium salt of Pigment Red 52, namely, monosodium 2-[2-(3-carboxy-2-oxo-1,2-dihydronaphthalen-1-ylidene)hydrazin-1-yl]-5-chloro-4-methylbenzenesulfonate dimethyl sulfoxide monosolvate monohydrate, $Na^+\cdot C_{18}H_{12}ClN_2O_6S^-\cdot H_2O\cdot C_2H_6OS$, obtained from in-house synthesized Pigment Red 52. The crystal structure was determined by single-crystal X-ray diffraction at 173 K. In this monosodium salt, the SO_3^- group is deprotonated, whereas the COOH group is protonated. The residues form chains *via* ionic interactions and hydrogen bonds. The chains are arranged in polar/non-polar double layers.

1. Chemical context

Pigment Red 52 (P.R.52, $Na_2[C_{18}H_{11}N_2ClO_6S]$), is produced industrially as an intermediate in the synthesis of Pigment Red 52:1 ($Ca[C_{18}H_{11}N_2ClO_6S]$) and Pigment Red 52:2 ($Mn[C_{18}H_{11}N_2ClO_6S]$) (Czajkowski *et al.*, 1980; Hunger & Schmidt, 2018). P.R.52:1 and P.R.52:2 are used for the colouration of printing inks and lacquers (Hunger & Schmidt, 2018). No crystal structures of P.R.52, or of its various metal salts, have previously been determined. Pigment Red 48 is an isomer of P.R.52, differing by mutual exchange of CH_3 and Cl substituents. Recently, the crystal structures of two hydrates of the monosodium salt of P.R.48 have been published (Tapmeyer *et al.*, 2020). Correspondingly, similar monosodium hydrate phases could also be expected for P.R.52. Hitherto, nothing has been known about the existence of a monosodium salt of P.R.52 or its hydrates or solvates. In attempts to crystallize P.R.52 from dimethylsulfoxide, single crystals were obtained, which turned out to be a mono-DMSO solvate monohydrate of the monosodium salt of P.R.52:1. The crystal structure was determined by X-ray analysis.

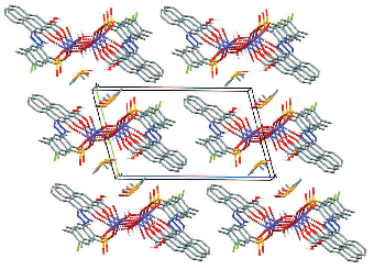

2. Structural commentary

Pigment Red 52 monosodium salt DMSO monosolvate monohydrate crystallizes in the triclinic space group $P\overline{1}$ with one pigment anion, one sodium cation, one molecule of DMSO and one water molecule in the asymmetric unit (Fig. 1).

CC BY OPEN ACCESS

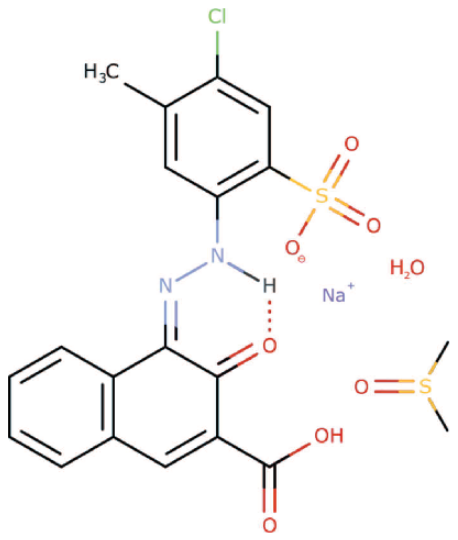

The pigment exhibits the hydrazone tautomeric form, like all industrial hydrazone pigments (formerly known as 'azo pigments') (Gilli *et al.*, 2005; Schmidt *et al.*, 2008; Hunger & Schmidt, 2018). The N—H group forms two intramolecular [$S_1^1(6)$] N—H···O hydrogen bonds (Table 1). The sulfonate group is deprotonated, whereas the carboxylic group is protonated. The protonation site is unambiguously determined by the difference electron density, from the S—O and C—O bond lengths in the SO_3^- and COOH groups, and from the hydrogen-bond pattern. Intramolecular and intermolecular bond lengths and angles are in the usual ranges. The organic anion is nearly planar, with an RMSD of 0.553 Å for all non-hydrogen atoms, except for the oxygen atoms of the sulfonate group. The dihedral angle between the naphthyl moiety and the phenyl ring is 9.84 (16)°.

The carboxylic acid group is coplanar with the naphthyl moiety [dihedral angle of 1.2 (5)°, see Fig. 1]. This coplanarity is a peculiarity, as in most other related structures, the COOH group is rotated out of the naphthyl plane (Table 2).

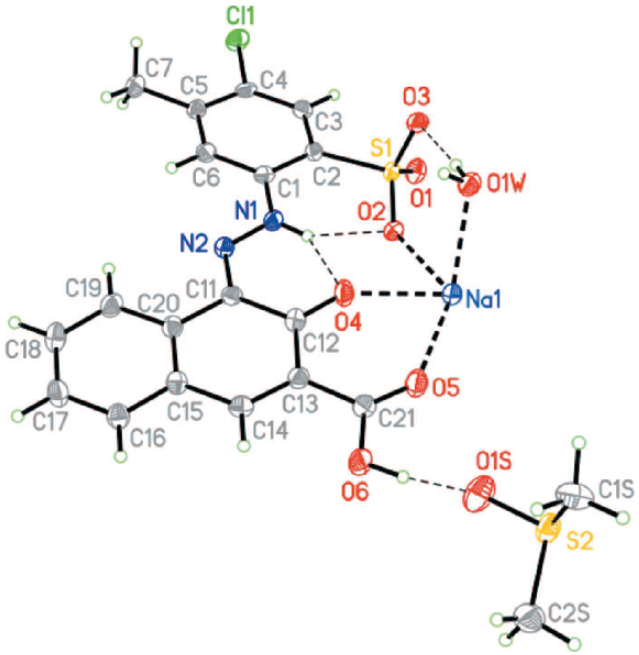

Figure 1
A perspective view of the asymmetric unit of the title compound. Displacement ellipsoids are drawn at the 50% probability level.

Table 1
Hydrogen-bond geometry (Å, °).

D—H···*A*	*D*—H	H···*A*	*D*···*A*	*D*—H···*A*
N1—H1···O2	0.82 (4)	2.14 (4)	2.747 (3)	131 (3)
N1—H1···O4	0.82 (4)	1.84 (4)	2.532 (4)	141 (4)
O6—H6···O1*S*	0.92 (5)	1.67 (5)	2.575 (4)	168 (4)
O1*W*—H1*WA*···O5^{i}	0.80 (5)	2.33 (5)	2.944 (3)	134 (4)
O1*W*—H1*WA*···O1*S*^{i}	0.80 (5)	2.48 (5)	3.138 (5)	140 (4)
O1*W*—H1*WB*···O3	0.84 (6)	2.11 (6)	2.942 (3)	176 (5)

Symmetry code: (i) $x+1, y, z$.

3. Supramolecular features

The protonated carboxyl oxygen atom of the COOH group donates a hydrogen bond to the DMSO molecule (Table 1). The other carboxyl oxygen atom accepts a hydrogen bond from the water molecule and additionally coordinates to the sodium ion. The sodium ion is sixfold coordinated to one oxygen atom of the COOH group, the carbonyl group, an oxygen atom of the sulfonate group, and two water molecules (one belonging to the same asymmetric unit, the other one transformed by $-x, 1-y, -z$). The sixth coordination site is occupied by an O atom of a sulfonate group of a neighbouring anion, generated by the symmetry operation $-1+x, y, z$. The coordination polyhedron is a distorted octahedron. The crystal packing is characterized by chains built *via* Na—O coordinations, running along the *a*-axis direction (Fig. 2). Within this chain, the phenyl ring is π-stacked above the O═C—C═N—N—H moiety of a symmetry-equivalent anion $(1+x, y, z)$ with

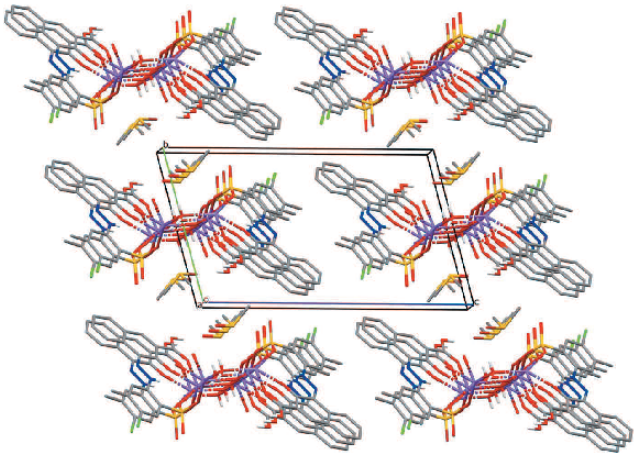

Figure 2
Packing diagram viewed approximately along [100].

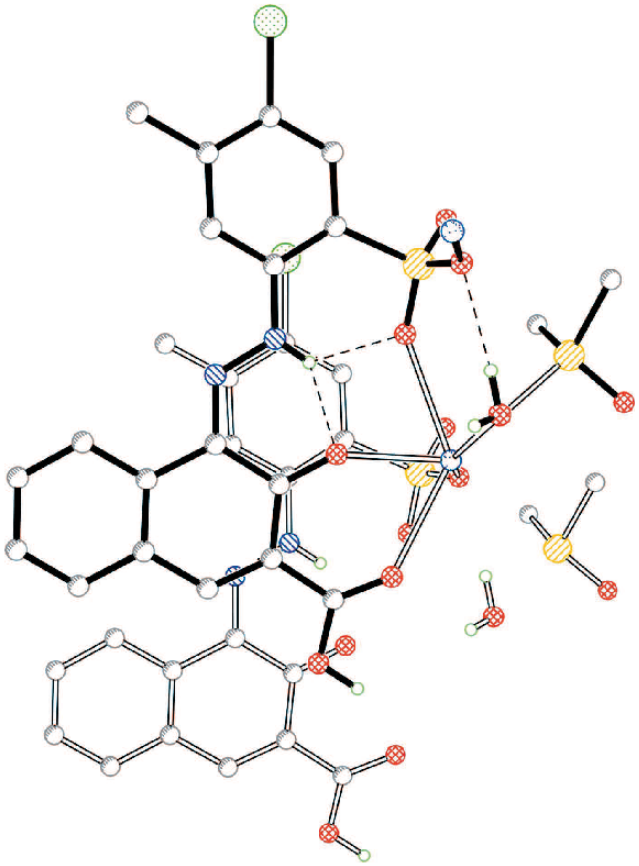

Figure 3
π-stacking of two anions, one drawn with full bonds and the other one with open bonds.

the shortest distance C6···C12 of 3.303 (5) Å. The N–NH unit is stacked above the naphthyl-COOH group with the shortest distance N1···C21 ($1 + x$, y, z) of 3.304 (4) Å (Fig. 3).

4. Database survey

For Pigment Red 52 and its derivatives, this is the first crystal structure published. Some closely related structures are compared in Table 2, *viz*. bis[6-chloro-3-(3-carboxy-2-oxoanthracenylidenehydrazono)benzenesulfonato]bis(dimethylformamide)calcium (BIHNUC; Kennedy *et al.*, 2004), [4-(4,6-dichloro-2-sulfophenyl)azo-3-hydroxy-2-naphthoato]diaquacalcium (KAQSAW; Kennedy *et al.*, 2000), {3-carboxy-1-[2-(5-chloro-4-methyl-2-sulfophenyl)diazen-2-ium-1-yl]naphthalen-2-olato}diaquasodium, {3-carboxy-1-[2-(5-chloro-4-methyl-2-sulfophenyl)diazen-2-ium-1-yl]naphthalen-2-olato}-aquasodium (GUNZAT and GUNZEX, respectively; Tapmeyer *et al.*, 2020), {3-carboxy-1-[2-(4-methyl-2-sulfophenyl)diazen-2-ium-1-yl]naphthalen-2-olato}calcium, {2-[2-(3-carboxy-2-oxy-1-naphthyl)diazeniumyl]-5-methylbenzenesulfonato}triaquacalcium, {2-[2-(3-carboxy-2-hydroxy-1-naphthyl)diazeniumyl]-5-methylbenzenesulfonato}aquacalcium (FAWQUR, FAWQIF and FAWQOL, respectively; Bekö *et al.*, 2012*a*,*b*),

Table 2
Angles (°) of the C–COO(H) plane to the mean plane of the carbon skeleton of the β-oxynaphthoic acid moiety.

Refcode	Salt	Solvate / Hydrate	|Angle|
BIHNUC[a]	$Ca[C_{17}H_{10}N_2O_6ClS]_2$	2 DMF	0.09
GUNZAT	$Na[C_{18}H_{12}ClN_2O_6S]$	2 H_2O	2.43
FAWQUR	$Ca[C_{18}H_{12}N_2O_6S]$		22.5
KAQSAW	$Ca[C_{17}H_8C_{l2}N_2O_6S]$	2 H_2O	23.3
FAWQIF	$Ca[C_{18}H_{14}N_2O_7S]$	2 H_2O	26.3
GUNZEX	$Na[C_{18}H_{12}ClN_2O_6S]$	1 H_2O	28.6
BOGDUZ[a]	$Dy[C_{13}H_7N_5O_3][BONA]$[b]	2 DMF, 2 H_2O	36.6
FAWQOL	$Ca[C_{18}H_{12}N_2O_6S]$	1 H_2O	37.7
BOGFIP[a]	$Eu[C_{13}H_7N_5O_3][BONA]$[b]	DMF, 4 H_2O	39.0
BOGFAH[a]	$Tb[C_{13}H_7N_5O_3][BONA]$[b]	DMF, 4 H_2O	39.0
BOGFEL[a]	$Sm[C_{13}H_7N_5O_3][BONA]$[b]	DMF, 4 H_2O	39.1

Notes: (*a*) This is not a pigment with a Colour Index number; (*b*) BONA = β-oxynaphthoic acid.

bis(3-oxido-4-[(1*H*-1,2,4-triazol-3-yl)diazenyl]naphthalene-2-carboxylato)bis(3-hydroxynaphthalene-2-carboxylato)tetrakis(aqua)didysprosium(III) *N*,*N*-dimethylformamide solvate, bis{3-oxido-4-[(1*H*-1,2,4-triazol-3-yl)diazenyl]naphthalene-2-carboxylato}bis(3-hydroxynaphthalene-2-carboxylato)tetrakis(aqua)dieuropium(III) *N*,*N*-dimethylformamide solvate, bis{3-oxido-4-[(1*H*-1,2,4-triazol-3-yl)diazenyl]naphthalene-2-carboxylato}bis(3-hydroxynaphthalene-2-carboxylato)tetrakis(aqua)diterbium(III) *N*,*N*-dimethylformamide solvate, bis(3-oxido-4-[(1*H*-1,2,4-triazol-3-yl)diazenyl]naphthalene-2-carboxylato)bis(3-hydroxynaphthalene-2-carboxylato)tetrakis(aqua)disamarium(III) *N*,*N*-dimethylformamide solvate (BOGDUZ, BOGFIP, BOGFAH and BOGFEL, respectively; Xie *et al.*, 2019).

5. Synthesis and crystallization

The title compound was obtained by recrystallization experiments of in-house synthesized P.R.52.

5.1. Synthesis of Pigment Red 52

2-Amino-5-chloro-*p*-toluenesulfonic acid (22.15 g, 0.1 mol) was dissolved with sodium hydroxide (6.4 g) in water (500 ml). The temperature was set at 278 K and concentrated hydrochloric acid (40 ml) as well as sodium nitrite (7.2 g) in water (100 ml) were added. The suspension was stirred for 30 min. The suspension was treated with amidosulfonic acid until all excess nitrous acid was destroyed. The suspension was then added dropwise to a solution of β-oxynaphthoic acid (18.8 g, 0.1 mol) with NaOH (20.1 g) in water (550 ml). The pH was kept at alkaline conditions, around 11 to 9, maintained by the addition of 2 *M* NaOH solution as required, and the temperature was maintained at 278 K. When the dropwise addition of the suspension was finished, the solution was allowed to accommodate to room temperature and subsequently heated to 353 K for half an hour. The red suspension was then neutralized with 2 *M* HCl, filtered off and the obtained red powder was washed with water and dried at 323 K. The yield of the crude product was about 98%, but

Table 3
Experimental details.

Crystal data	
Chemical formula	$Na^+ \cdot C_{18}H_{12}ClN_2O_6S^- \cdot C_2H_6OS \cdot H_2O$
M_r	538.94
Crystal system, space group	Triclinic, $P\overline{1}$
Temperature (K)	173
a, b, c (Å)	5.7347 (4), 10.9336 (8), 18.4692 (12)
α, β, γ (°)	104.844 (5), 97.478 (5), 95.404 (6)
V (Å^3)	1100.00 (14)
Z	2
Radiation type	Mo $K\alpha$
μ (mm^{-1})	0.44
Crystal size (mm)	0.23 × 0.09 × 0.02
Data collection	
Diffractometer	STOE IPDS II two-circle
Absorption correction	Multi-scan (*X-AREA*; Stoe & Cie, 2001)
T_{min}, T_{max}	0.445, 1.000
No. of measured, independent and observed [$I > 2\sigma(I)$] reflections	14981, 3864, 2992
R_{int}	0.049
$(\sin \theta/\lambda)_{max}$ (Å^{-1})	0.595
Refinement	
$R[F^2 > 2\sigma(F^2)]$, $wR(F^2)$, S	0.050, 0.098, 1.08
No. of reflections	3864
No. of parameters	324
H-atom treatment	H atoms treated by a mixture of independent and constrained refinement
$\Delta\rho_{max}$, $\Delta\rho_{min}$ (e Å^{-3})	0.27, −0.33

Computer programs: *X-AREA* (Stoe & Cie, 2001), *SHELXT* (Sheldrick, 2015*a*), *SHELXL* and *XP* (Sheldrick, 2015*b*), *Mercury* (Macrae *et al.*, 2020) and *publCIF* (Westrip, 2010).

X-ray powder diffraction revealed the presence of some sodium chloride as impurity.

5.2. Crystallization of the title compound

The crude in-house synthesized P.R.52 (0.59 g) was dissolved in DMSO (60 ml). The solution was transferred to a glass vessel, which in turn was placed into a further, larger vessel with water (100 ml). The outer vessel was closed with a plastic lid and stored for 20 days at room temperature, allowing the water to diffuse into the DMSO *via* the gas phase. Single crystals of the title compound were picked from the solution.

6. Refinement

Crystal data, data collection and structure refinement details are summarized in Table 3. The H atoms bonded to C were refined using a riding model with C—H = 0.95 Å and with $U_{iso}(H) = 1.2U_{eq}(C)$ or with C_{methyl}—H = 0.98 Å and with $U_{iso}(H) = 1.5U_{eq}(C)$. The methyl group attached to the phenyl ring was allowed to rotate but not to tip. The H atoms bonded to N and O were found in the difference-Fourier synthesis and freely refined.

References

Bekö, S. L., Hammer, S. M. & Schmidt, M. U. (2012*a*). *Angew. Chem. Int. Ed.* **51**, 4735–4738.
Bekö, S. L., Hammer, S. M. & Schmidt, M. U. (2012*b*). *Angew. Chem.* **124**, 4814–4818.
Czajkowski, W. (1980). *Dyes Pigments*, **1**, 17–25.
Gilli, P., Bertolasi, V., Pretto, L., Antonov, L. & Gilli, G. (2005). *J. Am. Chem. Soc.* **127**, 638–640.
Hunger, K. & Schmidt, M. U. (2018). *Industrial Organic Pigments: Production, Properties, Applications*. Weinheim: Wiley-VCH.
Kennedy, A. R., Kirkhouse, J. B. A., McCarney, K. M., Puissegur, O., Smith, W. E., Staunton, E., Teat, S. J., Cherryman, J. C. & James, R. (2004). *Chem. Eur. J.* **10**, 4606–4615.
Kennedy, A. R., McNair, C., Smith, W. E., Chisholm, G. & Teat, S. J. (2000). *Angew. Chem. Int. Ed.* **39**, 638–640.
Macrae, C. F., Sovago, I., Cottrell, S. J., Galek, P. T. A., McCabe, P., Pidcock, E., Platings, M., Shields, G. P., Stevens, J. S., Towler, M. & Wood, P. A. (2020). *J. Appl. Cryst.* **53**, 226–235.
Schmidt, M. U., Brüning, J., Wirth, D. & Bolte, M. (2008). *Acta Cryst.* C**64**, o474–o477.
Sheldrick, G. M. (2015*a*). *Acta Cryst.* A**71**, 3–8.
Sheldrick, G. M. (2015*b*). *Acta Cryst.* C**71**, 3–8.
Stoe & Cie (2001). *X-AREA*. Stoe & Cie, Darmstadt, Germany.
Tapmeyer, L., Hill, S., Bolte, M. & Hützler, W. M. (2020). *Acta Cryst.* C**76**, 716–722.
Westrip, S. P. (2010). *J. Appl. Cryst.* **43**, 920–925.
Xie, S.-F., Huang, L.-Q., Zhong, L., Lai, B.-L., Yang, M., Chen, W.-B., Zhang, Y.-Q. & Dong, W. (2019). *Inorg. Chem.* **58**, 5914–5921.

7.8 [LT8] Two monosodium salt hydrates of Colour Index Pigment Red 48

Bibliographische Daten:

Titel:	Two monosodium salt hydrates of Colour Index Pigment Red 48
Journal:	Acta Crystallographica Section C - STRUCTURAL CHEMISTRY
Jahr / Ausgabe:	2020 / C76
Seiten:	716–722
DOI:	10.1107/S2053229620008530
URL:	http://scripts.iucr.org/cgi-bin/paper?S2053229620008530
Autoren:	Lukas Tapmeyer, Steven Hill, Michael Bolte und Wilhelm Maximilian Hützler
eSI:	http://scripts.iucr.org/cgi-bin/paper?sk3752
OpenAccess:	Nein.
	Reproduced by permission of International Union of Crystallography

Beiträge:

Lukas Tapmeyer:
Synthese und Kristallisation des Monohydrates, Anleitung der Synthese und Kristallisation des Dihydrates, Koordination und Projektplanung, Schreiben des Entwurfs, Korrekturen.

Steven Hill:
Angeleitete Synthese und Kristallisation des Dihydrates.

Michael Bolte:
Röntgenstrukturanalyse des Dihydrates.

W. Maximilian Hützler:
Strukturanalyse des Monohydrates, Schreiben des Entwurfs, Korrekturen.

research papers

STRUCTURAL CHEMISTRY

ISSN 2053-2296

Two monosodium salt hydrates of Colour Index Pigment Red 48

Lukas Tapmeyer,[a] Steven Hill,[a] Michael Bolte[a] and Wilhelm Maximilian Hützler[b,c]*

[a]Institut für Anorganische und Analytische Chemie, Goethe-Universität Frankfurt, Max-von-Laue-Strasse 7, 60438 Frankfurt am Main, Germany, [b]Institut für Organische Chemie und Chemische und Chemische Biologie, Goethe-Universität Frankfurt, Max-von-Laue-Strasse 7, 60438 Frankfurt am Main, Germany, and [c]UCLouvain, Institute of Condensed Matter and Nanosciences, Place Louis Pasteur 1, Building L4.01.03, 1348 Louvain-La-Neuve, Belgium. *Correspondence e-mail: maximilian.hutzler@uclouvain.be

Received 16 June 2020
Accepted 25 June 2020

Edited by A. L. Spek, Utrecht University, The Netherlands

Keywords: pigment red 48; colour chemistry; layer structure; crystal structure; sodium salt; benzenesulfonate.

CCDC references: 2012233; 2012232

Supporting information: this article has supporting information at journals.iucr.org/c

We report herein the crystal structures of a monohydrate of Colour Index Pigment Red 48 (P.R.48) (systematic name: monosodium 2-{2-[3-carboxy-2-oxo-1,2-dihydronaphthalen-1-ylidene]hydrazin-1-yl}-4-chloro-5-methylbenzenesulfonate monohydrate), $Na^+ \cdot C_{18}H_{12}ClO_6S^- \cdot H_2O$, and a dihydrate, $Na^+ \cdot C_{18}H_{12}ClO_6S^- \cdot 2H_2O$. The two monosodium salt hydrates of P.R.48 were obtained from in-house synthesized P.R.48. Both have monoclinic ($P2_1/c$) symmetry at 173 K. The crystal packing of both crystal structures shows a layer arrangement whereby N—H···O and O—H···O hydrogen bonds are formed.

1. Introduction

P.R.48, $[C_{18}H_{11}ClO_6S]Na_2$, is the parent compound of a whole group of organic pigments (Herbst *et al.*, 2004). This group consists of salts of P.R.48 with manganese or alkaline earth metals which can be obtained by laking the disodium salt of P.R.48 with inorganic salts of the corresponding metal (Czajkowski, 1980). The pigment salts differ in solubility, stability and colour shade, and are used for various different applications in a wide range of particle sizes (Czajkowski, 1987). Thereof, the most prominent applications are the use as pigments in toner for laser printers or in the spin dyeing of synthetic fibres (Herbst *et al.*, 2004). P.R.48 is a member of the large group of pigments, within the azo colourants, consisting of a β-naphthol residue and a sulfonatophenyl moiety (Gley & Siebert, 1903). Several crystal structures of the β-naphthol pigments are known (Rafalska-Łasocha *et al.*, 2017; Bekö *et al.*, 2012; Stenger *et al.*, 2010; Christie *et al.*, 2009; Kennedy *et al.*, 2004; Gley & Siebert, 1903), of which all but one are present solely as the keto–hydrazone tautomer (instead of the azo tautomer) in the solid state (Schmidt *et al.*, 2008; Gilli *et al.*, 2005). Although even the control of crystallite sizes by synthesis conditions has been analysed (Christie *et al.*, 2009), the crystal structure of any member of the P.R.48 family is unknown so far [Cambridge Structural Database (CSD; Version 5.41 of November 2019, plus two updates of March 2020 and May 2020); Groom *et al.*, 2016]. This may be attributed to the fact that pigments in general are not known to crystallize well and also are not designed to (Kennedy *et al.*, 2000). However, knowing the crystal structure of P.R.48 would be highly desirable since the three-dimensional arrangement of the molecules, as well as the particle size of a pigment, affect the colour of the bulk material (Christie *et al.*, 2009). The aim of this study was to determine the crystal structure of P.R.48. For this, single-crystal X-ray diffraction (SC-XRD), (temper-

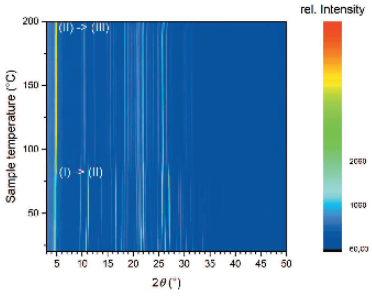

© 2020 International Union of Crystallography

Table 1
Experimental conditions and phases obtained.

The starting material is P.R.48 from in-house synthesis if not denoted otherwise.

	Solvent	Treatment	Resulting phase
A	Dibutyl phthalate and 5 *M* HCl	35 mg in 7 + 1 ml at 343 K for 60 d	(I)
B	Toluene and 5 *M* HCl	35 mg in 7 + 1 ml at 343 K for 60 d	(I)
C	Mesitylene and 5 *M* HCl	35 mg in 7 + 1 ml at 343 K for 60 d	(I)
D	Dichlorobenzene and 5 *M* HCl	35 mg in 7 + 1 ml at 343 K for 60 d	(I)
E	Glacial acetic acid	35 mg in 8 ml at 343 K for 60 d; open container	(I)
F	Dichlorobenzene	35 mg in 8 ml at 343 K for 60 d	Starting material: P.R.48
G	Dimethyl sulfoxide	35 mg in 8 ml at 343 K for 60 d	Starting material: P.R.48
H	Glacial acetic acid	90 mg in 20 ml 343/373 K in alternation for 14 d; sealed container	(II)
J		Sample **H** at ambient conditions for 10 d	(I)
K	0.4 *M* NaOH	1 g in 3,500 ml 0.4 *M* NaOH; direct precipitation with 150 ml 6 *M* HCl; washed with methanol	(I)
L	0.4 *M* NaOH	1 g in 3,500 ml 0.4 *M* NaOH; direct precipitation with 150 ml 6 *M* HCl	(I)
M		Heating of several grams of (I) to 363 K for 14 d; open container	(II) + (I)

ature-dependent) X-ray powder diffraction (PXRD), energy dispersive X-ray spectroscopy (EDX), elemental analysis (EA), and differential thermal analysis and thermogravimetry (DTA-TG) were combined.

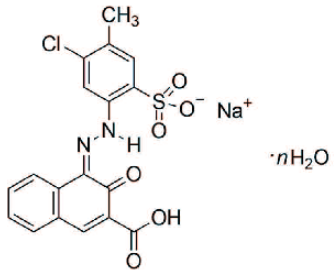

For (I): $n = 2$
For (II): $n = 1$

Scheme 1

2. Experimental

2.1. Synthesis and crystallization

2.1.1. Pigment Red 48 (*i.e.* the disodium salt). In order to synthesize P.R.48, 6-amino-4-chloro-*m*-toluenesulfonic acid (22.2 g, 0.1 mol) was dissolved in a solution of NaOH (6.62 g, 0.17 mol) in water (500 ml). Subsequently, $NaNO_2$ (7.21 g, 0.1 mol) and concentrated hydrochloric acid (40 ml, 0.48 mol) in water (100 ml) were added and the suspension was stirred for 30 min at room temperature (294 K). The remaining nitrous acid in the suspension was eliminated by the addition of a few drops of a saturated solution of sulfamic acid in water. 3-Hydroxy-2-naphthoic acid (18.8 g, 0.1 mol) and NaOH (20.1 g, 0.5 mol) dissolved in water (550 ml) were added slowly, yielding a red solid that immediately precipitated. The suspension was stirred for 2 h and then filtered. The pigment was washed with water and dried. P.R.48 was obtained in a yield of approximately 95%.

2.1.2. Pigment Red 48 monosodium salt dihydrate, (I). The dihydrate of P.R.48, $[C_{18}H_{12}ClO_6S]Na{\cdot}2H_2O$, (I), was crystallized (experiment **K** in Table 1) by dissolving P.R.48 (1.0 g) in 1 *M* NaOH (1,000 ml) and heating to reflux. After addition of water (2,500 ml), the mixture was filtered and stored at room temperature overnight. The solution was then heated to reflux again and half-concentrated (6 *M*) hydrochloric acid (150 ml) was added under stirring. A red solid precipitated and was separated by filtration from the discoloured solution. The red solid attached to the filter was suspended in methanol and therewith transferred to a glass vessel. Finally, the substance was dried at 323 K, yielding a crystalline sample from which single crystals were picked after evaporation of the solvent.

A second experiment without the final treatment of the precipitate with methanol (experiment **L** in Table 1) yielded the same solid form, as confirmed by PXRD.

A crystallization experiment by slow solvent evaporation from acetic acid under ambient conditions yielded phase (I) as well (experiment **K** in Table 1). Beyond that, several other solvents, such as toluene, dichlorobenzene or mesitylene, could be used for preparing the dihydrate (I) by either crystallization from solution or by slurry, provided that a few drops of hydrochloric acid were added to the mixture (experiments **A**–**D** in contrast to experiments **F** and **G** in Table 1).

2.1.3. Pigment Red 48 monosodium salt monohydrate, (II). The monohydrate of P.R.48, $[C_{18}H_{12}ClO_6S]Na{\cdot}H_2O$, (II), was prepared by suspending P.R.48 (90 mg) in glacial acetic acid (20 ml) at room temperature. Afterwards, the sample was stored in a 100 ml round-bottomed flask fitted with a plug at temperatures of 343 and 373 K in approximately daily alternation (experiment **H** in Table 1). After two weeks, crystals suitable for single-crystal X-ray analysis were obtained.

2.1.4. Phase transitions. Storage of any sample of (II) under ambient conditions yielded phase (I) (experiment **J**). Storage of a bulk sample of (I) at 363 K over several days yielded a mixture of (I) and (II) (experiment **M**). Keeping (I) in a stream of dry inert gas yielded phase (II). Further treatment with dry inert gas above 373 K yielded a structurally uncharacterized form (III), which was assumed to be an anhydrate form of P.R.48.

Table 2
Experimental details.

For both structures: monoclinic, $P2_1/c$, Z = 4. Experiments were carried out at 173 K. H atoms were treated by a mixture of independent and constrained refinement.

	(I)	(II)
Crystal data		
Chemical formula	$Na^+ \cdot C_{18}H_{12}ClNO_6S^- \cdot 2H_2O$	$Na^+ \cdot C_{18}H_{12}ClN_2O_6S^- \cdot H_2O$
M_r	478.83	460.81
a, b, c (Å)	18.5318 (9), 5.9396 (3), 17.4426 (10)	18.2222 (2), 5.9486 (1), 16.9361 (2)
β (°)	95.528 (4)	92.037 (1)
V (Å^3)	1911.00 (17)	1834.66 (4)
Radiation type	Mo $K\alpha$	Cu $K\alpha$
μ (mm^{-1})	0.39	3.59
Crystal size (mm)	0.19 × 0.09 × 0.02	0.33 × 0.03 × 0.02
Data collection		
Diffractometer	Stoe IPDS II two-circle	Siemens CCD three-circle
Absorption correction	Multi-scan (*X-AREA*; Stoe & Cie, 2001)	Multi-scan (*SADABS*; Sheldrick, 1996)
T_{min}, T_{max}	0.513, 1.000	0.556, 1.000
No. of measured, independent and observed $[I > 2\sigma(I)]$ reflections	13702, 3587, 3009	12502, 3314, 3049
R_{int}	0.035	0.046
$(\sin \theta/\lambda)_{max}$ (Å^{-1})	0.609	0.610
Refinement		
$R[F^2 > 2\sigma(F^2)]$, $wR(F^2)$, S	0.051, 0.123, 1.13	0.054, 0.145, 1.09
No. of reflections	3587	3314
No. of parameters	300	284
No. of restraints	6	5
$\Delta\rho_{max}$, $\Delta\rho_{min}$ (e Å^{-3})	0.44, −0.41	0.48, −0.89

Computer programs: *X-AREA* (Stoe & Cie, 2001), *APEX3* (Bruker, 2012), *SHELXS97* (Sheldrick, 2008), *SHELXT* (Sheldrick, 2015*a*), *SHELXL2016* (Sheldrick, 2015*b*), *Mercury* (Version 4.0; Macrae *et al.*, 2020), *XP* in *SHELXTL-Plus* (Sheldrick, 2008) and *publCIF* (Westrip, 2010).

Temperature-dependent powder X-ray diffractometry confirmed the phase identities of monohydrate (II), dihydrate (I) and anhydrate (III). DTA-TG were in agreement with the phase assignments also. The exact temperatures of the phase transition from (I) to (II) and finally (III) seem dependent on the enclosure of the sample. This is probably a kinetic effect of the limited diffusion of water vapour from the sample.

A list of selected experiments performed is given in Table 1.

2.2. Materials and methods

All chemicals were obtained from TCI, Acros Organics or Sigma–Aldrich and were used without further purification, if not stated otherwise. Powder X-ray diffraction data were obtained on a Stoe STADI-P diffractometer, equipped with a Ge(111)-monochromator and a line-focus X-ray tube using Cu $K\alpha_1$ radiation, and a linear position-sensitive detector. All samples were prepared in 0.7 mm glass capillaries. DTA-TG curves were collected on a Setaram TGA-92 under an inert gas flow (argon), with a heating rate of 5 K min^{-1}. EDX data were obtained using a SEM/EDX Amray 1920 EcoSEM set-up, equipped with an Oxford Instruments Si(Li) detector, controlled by an IXRF Systems controller Model 550i. Elemental analysis was performed on an Elementar vario-MICROcube.

2.3. Refinement

Crystal data, data collection and structure refinement details are summarized in Table 2. All H atoms were initially located by difference Fourier synthesis. Subsequently, all H atoms bound to C atoms were refined using a riding model, with the methyl C—H distances constrained to 0.98 Å and the aromatic C—H distances constrained to 0.95 Å. Their isotropic displacement parameters were set at U_{iso}(H) = 1.5U_{eq}(C) for methyl H atoms and at 1.2U_{eq}(C) for aromatic H atoms. For the H atoms of the methyl groups, free rotation about their local threefold axis was allowed. The coordinates of H atoms bonded to N atoms and to O atoms were refined with the N—H distances restrained to 0.88 (2) Å and the O—H distances restrained to 0.84 (2) Å. Their isotropic displacement parameters were coupled to the equivalent isotropic displacement parameters of the parent N and O atoms, with U_{iso}(H) = 1.2U_{eq}(N,O). The coordinates of the H atoms of the water molecules were refined also, with the O—H distances restrained to 0.84 (1) Å and the H···H distances restrained to 1.4 (1) Å. Their isotropic displacement parameters were coupled to the equivalent isotropic displacement parameters of the O atoms, with U_{iso}(H) = 1.2U_{eq}(O).

2.4. Validation of the composition

Samples of (I) and (II) were analysed by DTA-TG. The DTA-TG was calibrated to a sample previously identified as the dihydrate by single-crystal X-ray diffraction.

Elemental analysis was performed on samples of phase (I). Results were highly dependent on the handling of the samples (heat or moisture) but yielded no insight contradictory to the hypothesized monosodium salt. Measurements are given in Table 3.

Table 3
Elemental analysis (%) of samples from experiments listed in Table 1.

Sample	C	H	N	S
D [phase (I)]	45.45	2.96	6.35	6.70
G (P.R.48)	46.65	1.79	6.62	6.94

A sample of the monosodium dihydrate was analysed by EDX (20 keV) to confirm the sodium content. The ratio of sodium to sulfur and chlorine in the structure was 1:1:1 within the precision of the measurement. The monosodium salt was therefore accepted as confirmed. The oxygen to sodium ratio was not analysed because of the high vacuum applied to the sample for measurement (dehydration) and for sensitivity reasons.

3. Results and discussion

Our efforts to solve the structure of Pigment Red 48 (P.R.48) yielded two previously unknown derivatives. Both were synthesized by recrystallization and structurally characterized by single-crystal X-ray diffraction. In contrast to P.R.48, which is a disodium salt, both derivatives proved to be monosodium salt hydrates. Phase (I) is a dihydrate and phase (II) a monohydrate monosodium salt of P.R.48 (Figs. 1–4). Both, the dihydrate (I) and the monohydrate (II) of P.R.48 crystallize in the monoclinic space group $P2_1/c$. The lattice parameters of (I) and (II) are quite similar (Table 2). The unit-cell volume of (I) is 1911.00 (17) Å^3 compared to 1834.66 (4) Å^3 in (II) and the difference matches the spatial need of four additional water molecules per unit cell in (I) with respect to (II). The two crystal structures are characterized by a coordination chain parallel to [010] which is further extended by a hydrogen-bonded network along [001], yielding a layered structure

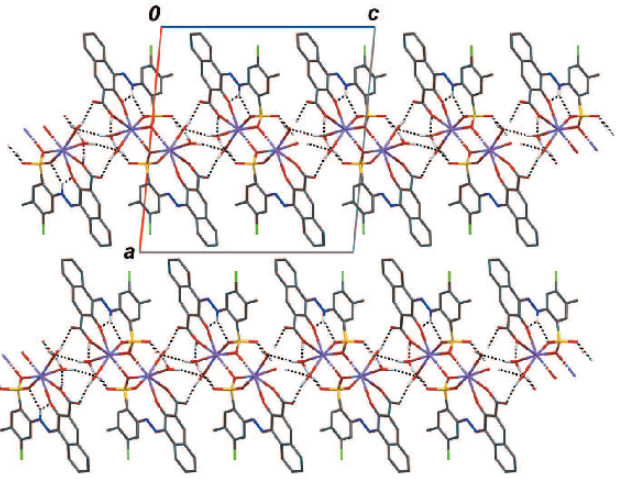

Figure 2
A partial packing diagram of (I), showing the (100) layer arrangement. Dashed lines indicate hydrogen bonds.

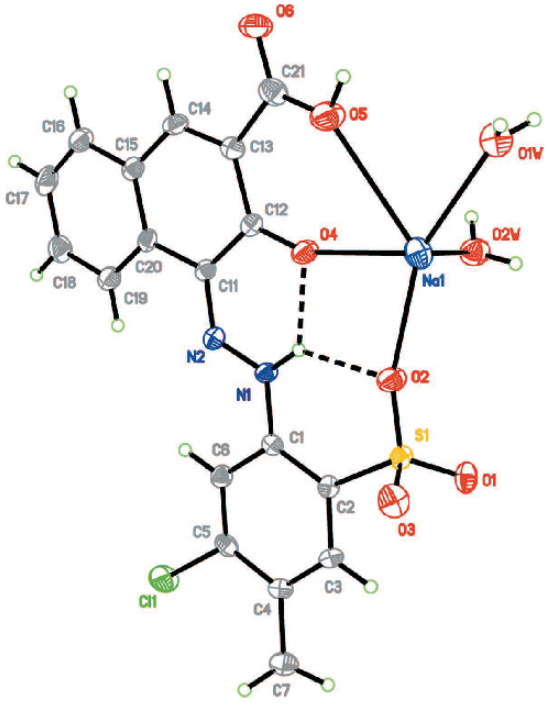

Figure 1
A perspective view of (I), showing the atom-numbering scheme. Displacement ellipsoids are drawn at the 50% probability level. Dashed lines indicate hydrogen bonds.

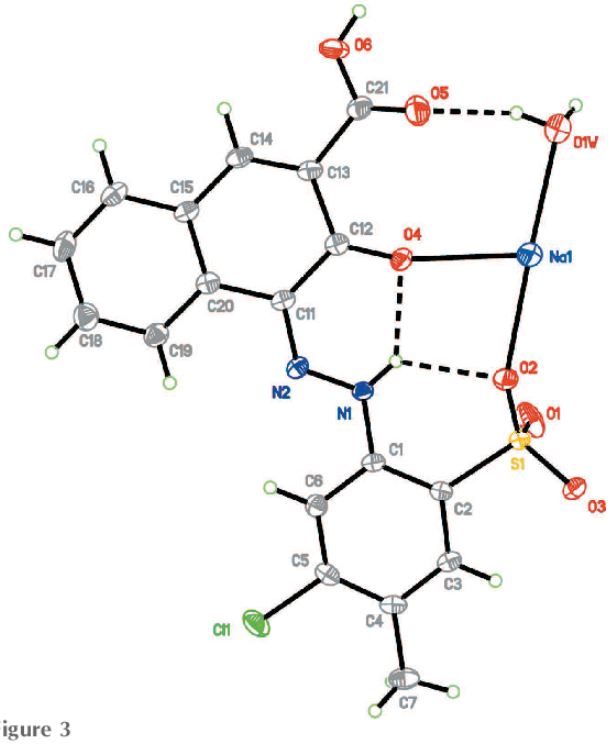

Figure 3
A perspective view of (II), showing the atom-numbering scheme. Displacement ellipsoids are drawn at the 50% probability level. Dashed lines indicate hydrogen bonds.

Table 4
Hydrogen-bond geometry (Å, °) for (I).

D—H···A	D—H	H···A	D···A	D—H···A
N1—H1···O2	0.87 (1)	2.03 (3)	2.720 (3)	135 (3)
N1—H1···O4	0.87 (1)	1.90 (3)	2.570 (3)	132 (3)
O5—H5···O2W^{i}	0.85 (1)	1.86 (1)	2.702 (3)	172 (5)
O1W—H1WA···O3^{ii}	0.84 (1)	2.01 (2)	2.808 (3)	159 (4)
O1W—H1WB···O6^{iii}	0.85 (1)	1.95 (2)	2.762 (3)	162 (4)
O2W—H2WA···O3^{iv}	0.85 (1)	1.93 (1)	2.761 (3)	167 (4)
O2W—H2WB···O1W^{iii}	0.85 (1)	2.01 (2)	2.818 (3)	159 (4)

Symmetry codes: (i) $x, y+1, z$; (ii) $-x+1, -y+2, -z+1$; (iii) $-x+1, y-\frac{1}{2}, -z+\frac{1}{2}$; (iv) $-x+1, -y+1, -z+1$.

Table 5
Hydrogen-bond geometry (Å, °) for (II).

D—H···A	D—H	H···A	D···A	D—H···A
O6—H61A···O1W^{i}	0.84 (2)	1.72 (2)	2.549 (3)	169 (4)
N1—H1···O4	0.86 (2)	1.93 (2)	2.615 (3)	136 (3)
N1—H1···O2	0.86 (2)	2.12 (3)	2.747 (3)	129 (3)
O1W—H1WB···O1^{ii}	0.84 (1)	1.96 (1)	2.761 (3)	158 (3)
O1W—H1WA···O5	0.84 (1)	1.94 (1)	2.748 (3)	159 (3)

Symmetry codes: (i) $-x+1, y-\frac{1}{2}, -z+\frac{1}{2}$; (ii) $-x+1, -y, -z+1$.

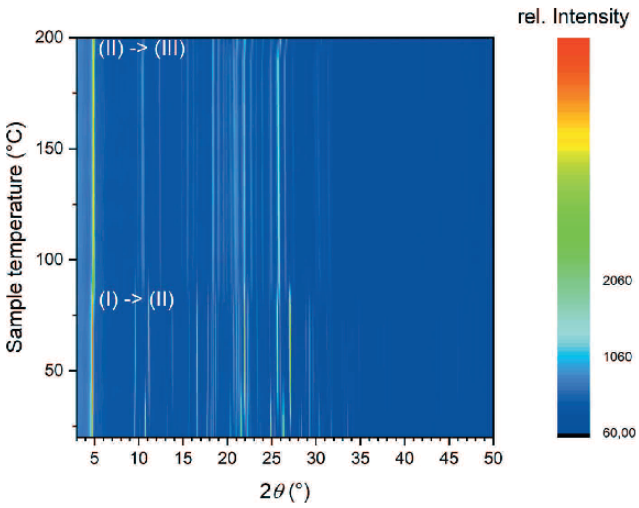

Figure 5
Temperature-dependent powder X-ray diffraction on a sample of P.R.48 monosodium dihydrate. The temperatures of the phase transitions are shifted slightly compared to the DTA-TG measurements, most probably as a result of the sample container (glass capillary).

parallel to the (100) plane in each case. In (I) and (II), atom N1 forms two intramolecular hydrogen bonds to atoms O2 and O4 (Tables 4 and 5). The water molecules are coordinated to the Na^{+} ion Na1 in both crystal structures. In (I), each water molecule forms one hydrogen bond to an atom within the same coordination network, *i.e.* O1W—H1WA···O3^{ii} and O2W—H2WA···O3^{iv}, and one hydrogen bond to the adjacent coordination network, *i.e.* O1W—H1WB···O6^{iii} and O2W—H2WB···O1W^{iii} (Table 4). In contrast in (II), the water molecule forms two hydrogen bonds to atoms within the same coordination network, *viz.* O1W—H1WB···O1^{ii} and O1W—H1WA···O5 (Table 5). In both crystal structures, the carboxylate group was found to be protonated. While in (I) atom O5 is protonated and coordinated to the Na^{+} ion Na1, in (II) atom O6 is protonated and the carboxylate group is not involved in the coordination network. Instead, atom O6 in (II)

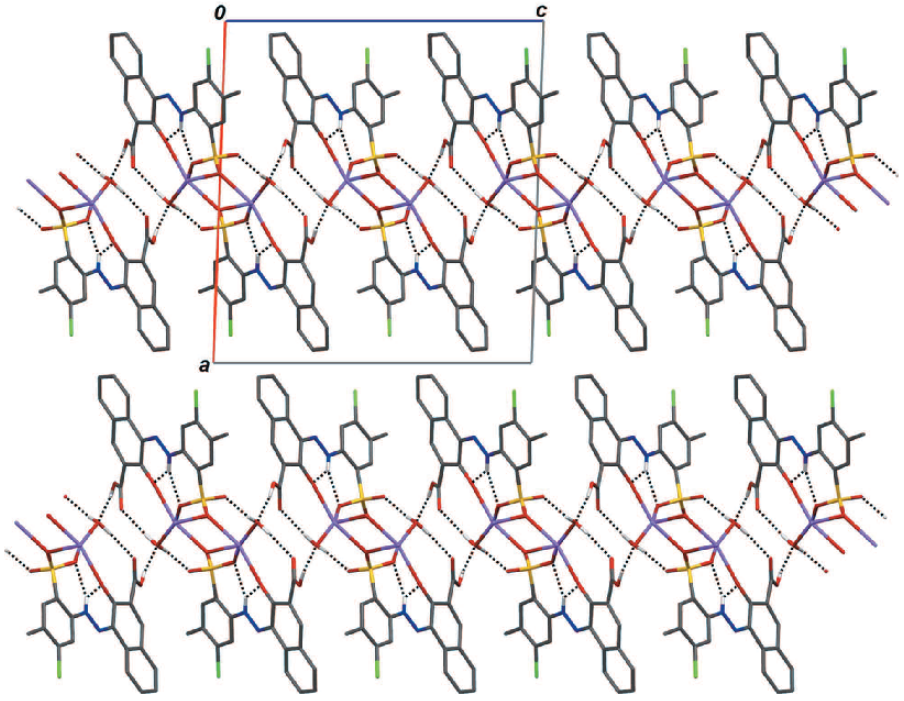

Figure 4
A partial packing diagram of (II), showing the (100) layer arrangement. Dashed lines indicate hydrogen bonds.

establishes a hydrogen-bonded connection to the adjacent coordination network *via* O6—H61*A*···O1*W*^{i} (Table 5). However, the most remarkable observation is the protonation of the carboxylate group which has not been observed in similar compounds before. This indicates a previously unknown sensitivity of the synthesis of this pigment towards pH and solvent environment.

This is reflected in the results of experiments **A**–**D** (Table 1), in which the pigment was treated with the nonpolar solvents dibutyl phthalate, toluene, mesitylene and dichlorobenzene, respectively, in the presence of aqueous hydrochloric acid. Experiments **A**–**D** yielded exclusively powders of dihydrate form (I). From water-containing acetic acid, form (I) was also obtained (experiment **E** in Table 1). In contrast, in experiments **F** and **G**, where no acid was present, neither the organic solvent nor the minor water content of the undried solvents induced the transformation of P.R.48 into one of the monosodium forms.

In order to study whether a reduced amount of water present during the crystallization has any impact on the formed phase, attempts to recrystallize P.R.48 from hot glacial acetic acid in a sealed container yielded monohydrate form (II) (experiment **H** in Table 1). In contrast, in an open container where water could be resorbed from the environment, the dihydrate was formed (experiment **E** in Table 1). This demonstrates that the phase formed indeed can be influenced by controlling the water content in the atmosphere during crystallization. We also performed experiments to study the stability of crystalline forms (I) and (II) towards the loss or uptake of water. Storage of powders of the monohydrate (II) in contact with air yielded the dihydrate (I) after 10 d. On the other hand, heating of powder samples of the dihydrate (I) to 363 K for 14 d yielded a mixture of the mono- and dihydrate (experiments **J** and **L** in Table 1). Furthermore, on heating small amounts of the dihydrate on the powder diffractometer, the transition to the monohydrate could be observed, as well as the emergence of a third uncharacterized phase (Fig. 5). Phase (I) and (II) could be identified in the temperature-dependent measurement by comparison of the powder diagrams to the simulated powder pattern from the

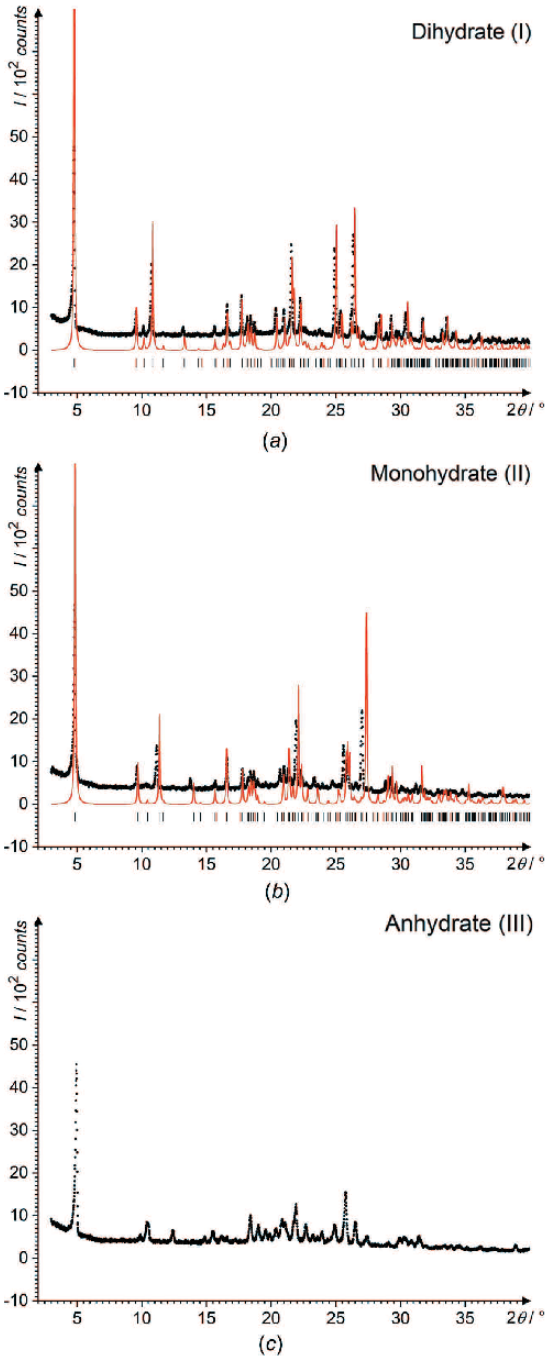

Figure 6
Excerpts from the temperature-dependent powder X-ray diffraction experiments at 20, 90 and 150 °C representing forms (I), (II) and (III), respectively. Forms (I) and (II) are compared to the simulated PXRD patterns from single-crystal structures at −100 °C. Experimental data are shown as black dots, simulated data as red lines and reflection positions as vertical bars.

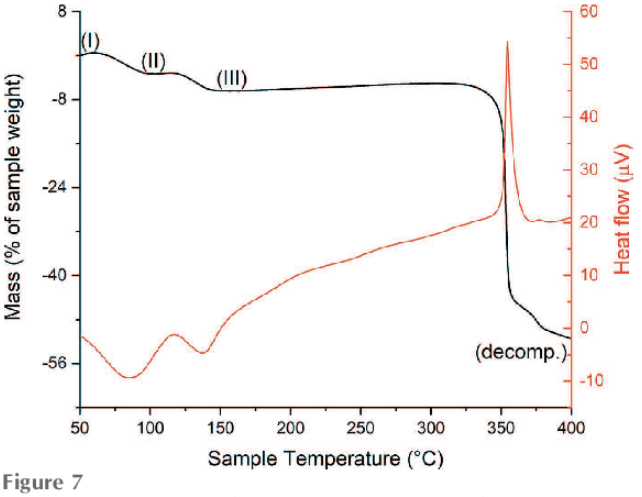

Figure 7
DTA-TG measurements (calibrated to SCXRD data) of a sample of P.R.48 monosodium dihydrate. The TG curve is depicted in black and shows two mass losses (of comparable quantity), each time corresponding to the loss of one water molecule per formula unit.

single-crystal structures (Fig. 6). These transitions were observed in the DTA-TG curves as well (Fig. 7).

Other crystal structures of P.R.48 compounds are not available yet, neither with sodium nor with other metal ions. As mentioned before, the carboxylate group is protonated (*R*-COOH), while the sulfonate group is deprotonated (*R*-SO_3^-). This is in accordance with the pK_a values which are roughly 1 for the sulfonate and approximately 5 for the carboxylate group. This situation of partial protonation has not hitherto been reported for any metal-containing hydrazone pigment.

As with most other hydrazone pigments, the molecules display the keto–hydrazone tautomer. The organic anion is planar except for the sulfonate group in both cases and for the carboxylic acid group in the monohydrate crystal structure (II). In (II), the carboxyl group is tilted with respect to the mean plane of the naphthalene moiety, forming a dihedral angle of 30.0 (2)°.

Compounds (I) and (II) have not been reported before. The protonation, as well as the type of hydrate obtained by crystallization of P.R.48, seems to be more sensitive to temperature, solvent environment, and also to the pH value, than previously known. These findings are valuable and instructive for ongoing experiments and possibly even for the manufacture of P.R.48 and its derivatives. In the broad range of applications of this pigment and its use as a precursor, the pH value and solvent environment are subject to strong variation. In order to elucidate the crystal structures of the laked forms of P.R.48, knowledge of these influences is assumed to be highly desirable.

Acknowledgements

We thank Edith Alig (Goethe-University) for measurement of the X-ray powder diagrams and DTA-TG measurements. We thank Professor Martin U. Schmidt (Goethe-University) for the opportunity to publish these results.

References

Bekö, S. L., Hammer, S. M. & Schmidt, M. U. (2012). *Angew. Chem. Int. Ed.* **51**, 4735–4738.
Bruker (2012). *APEX3*. Bruker AXS Inc., Madison, Wisconsin, USA.
Christie, R. M., Chugtai, I. & Mather, R. R. (2009). *Dyes Pigments*, **80**, 264–270.
Czajkowski, W. (1980). *Dyes Pigments*, **1**, 17–25.
Czajkowski, W. (1987). *Dyes Pigments*, **8**, 141–150.
Gilli, P., Bertolasi, V., Pretto, L., Antonov, L. & Gilli, G. (2005). *J. Am. Chem. Soc.* **127**, 4943–4953.
Gley, R. & Siebert, O. (1903). Ger. Patent DE151205.
Groom, C. R., Bruno, I. J., Lightfoot, M. P. & Ward, S. C. (2016). *Acta Cryst.* B**72**, 171–179.
Herbst, W., Hunger, K. & Wilker, G. (2004). In *Industrial organic pigments: production, properties, applications*. Weinheim: Wiley-VCH.
Kennedy, A. R., Kirkhouse, J. B. A., McCarney, K. M., Puissegur, O., Smith, W. E., Staunton, E., Teat, S. J., Cherryman, J. C. & James, R. (2004). *Chem. Eur. J.* **10**, 4606–4615.
Kennedy, A. R., McNair, C., Smith, W. E., Chisholm, G. & Teat, S. J. (2000). *Angew. Chem. Int. Ed.* **39**, 638–640.
Macrae, C. F., Sovago, I., Cottrell, S. J., Galek, P. T. A., McCabe, P., Pidcock, E., Platings, M., Shields, G. P., Stevens, J. S., Towler, M. & Wood, P. A. (2020). *J. Appl. Cryst.* **53**, 226–235.
Rafalska-Łasocha, A., Grzesiak-Nowak, M., Goszczycki, P., Ostrowska, K. & Łasocha, W. (2017). *Powder Diffr.* **32**, 187–192.
Schmidt, M. U., Brüning, J., Wirth, D. & Bolte, M. (2008). *Acta Cryst.* C**64**, o474–o477.
Sheldrick, G. M. (1996). *SADABS*. University of Göttingen, Germany.
Sheldrick, G. M. (2008). *Acta Cryst.* A**64**, 112–122.
Sheldrick, G. M. (2015). *Acta Cryst.* C**71**, 3–8.
Stenger, J., Kwan, E. E., Eremin, K., Speakman, S., Kirby, D., Stewart, H., Huang, S. G., Kennedy, A. R., Newman, R. & Khandekar, N. (2010). *e-PS*, **7**, 147–157.
Stoe & Cie (2001). *X-AREA*. Stoe & Cie, Darmstadt, Germany.
Westrip, S. P. (2010). *J. Appl. Cryst.* **43**, 920–925.

7.9 [LT9] Structure of the intermediates in the industrial separation of perinone isomers

Bibliographische Daten:

Titel:	Structure of the intermediates in the industrial separation of perinone isomers
Journal:	Dyes and Pigments
Jahr / Ausgabe:	2020 / 181
Artikelnummer:	108442
DOI:	10.1016/j.dyepig.2020.108442
URL:	https://www.sciencedirect.com/science/article/abs/pii/S0143720820303740
Autoren:	Lukas Tapmeyer, Michael Bolte, Michele Remo Chierotti und Martin Ulrich Schmidt
eSI:	https://www.sciencedirect.com/science/article/abs/pii/S0143720820303740
OpenAccess:	Nein.
	Reproduced by permission of Elsevier

Beiträge:

Lukas Tapmeyer:
Alle Synthesen und Kristallisationen, Analytik, Röntgenstrukturanalyse *cis*-Trennsalz, Schreiben des Entwurfs, Korrekturen.

Michael Bolte:
Röntgenstrukturanalyse der zwei Phasen des *trans*-Trennsalzes.

Michele R. Chierotti:
Festkörper-*NMR*-Untersuchungen.

Martin U. Schmidt:
Projektidee und Projektleitung, Schreiben des Entwurfs (insbesondere historischer Abschnitt), Überarbeiten des Manuskriptes, Korrekturen.

Dyes and Pigments 181 (2020) 108442

Contents lists available at ScienceDirect

Dyes and Pigments

journal homepage: http://www.elsevier.com/locate/dyepig

Structure of the intermediates in the industrial separation of perinone isomers

Lukas Tapmeyer [a], Michael Bolte [a], Michele R. Chierotti [b], Martin U. Schmidt [a,*]

[a] Institute of Inorganic and Analytical Chemistry, Goethe University Frankfurt am Main, Max-von-Laue-Str. 7, 60438, Frankfurt am Main, Germany
[b] Departement of Chemistry and NIS Centre, University of Torino, V. Giuria 7, 10125, Torino, Italy

ARTICLE INFO

Keywords:
Perinone
Pigment Orange 43
Intermediate
X-ray structure determination
Solid-state NMR

ABSTRACT

The industrial synthesis of perinone results in a mixed crystal containing an isomer mixture of *trans*- and *cis*-perinone. The isomers are separated by treatment with alcoholic KOH, which leads to a pale yellow precipitate and a yellow solution. The precipitate is subsequently hydrolyzed to produce pure *trans*-perinone (Pigment Orange 43). The yellow solution is treated with dilute acids to give *cis*-perinone (Pigment Red 194). The chemical structure and the stoichiometry of the intermediate pale yellow precipitate has never been determined, although this intermediate has been produced on a multi-ton scale for more than 80 years. The intermediate was assumed to be a "potassium hydroxide addition compound". X-ray single-crystal analyses reveal that this assumption is wrong. The KOH/ethanol treatment actually causes a double ring-opening of the perinone. This results in the tetra-potassium salt of 4,8-bis(benzimidazolato)-naphthalene-1,5-dicarboxylate. Two phases were isolated: The α-phase, $K_4[C_{26}H_{12}N_4O_4]\cdot 3C_2H_5OH\cdot 6H_2O$, from the industrial synthesis and the β-phase, $1.5(K_4[C_{26}H_{12}N_4O_4])\cdot 5C_2H_5OH\cdot 4H_2O$, from a recrystallization in KOH/ethanol. The molecular and crystal structures are confirmed by solid-state NMR spectroscopy through combination of ^{13}C CPMAS and MAS experiments, which revealed that the solvent layers in the crystals show a highly dynamic solvent disorder in the solid state. The intermediate of *cis*-perinone, which is formed in the isomer separation step, has been isolated as well. Also this intermediate has a ring-opened molecular structure, as revealed by single-crystal X-ray diffraction.

1. Introduction

In the chemical industry, there are astonishingly many compounds which are produced on a multi-ton scale for decades, but their molecular structure and chemical composition are still unknown. Two of these compounds are the intermediates in the industrial separation of the perinone isomers in the production of Pigment Orange 43 (*trans*-perinone, P.O.43, **1**, see Fig. 1).

Perinone has been industrially produced for at least 80 years [1]. The industrial synthesis starts from naphthalene-tetracarboxylic mono-anhydride, which is condensed with two equivalents of 1, 2-diaminobenzene, see Fig. 1 left [2,3]. The reaction yields a mixed crystal (solid solution) [2] of two isomers, *trans*-perinone (**1**) and *cis*-perinone (**2**) in a ratio of nearly one to one. The mixed crystal is registered as Vat Red 14 (see Figs. 1 and 2). The two isomers are industrially separated by treatment with hot KOH/ethanol (see Fig. 1); cooling or dilution causes the precipitation of a pale yellow intermediate (**3**), which is isolated by filtration. Astonishingly, the molecular structure and the chemical composition of this intermediate are still unknown. The yellow filtrate contains the other isomer's intermediate (**4**) whose structure is unknown as well.

The precipitated intermediate (**3**) is subsequently treated with water, to give the pure *trans*-perinone, Pigment Orange 43 (**1**). The yellow filtrate is treated with diluted acids, resulting in the formation of the red *cis*-perinone, Pigment Red 194 (P.R.194, **2**) [1]. Industrially, the intermediate (**4**) is handled only in solution. Nevertheless, this compound (**4**) can be precipitated from a hot, concentrated solution by cooling.

The molecular formulae of *cis*-perinone and *trans*-perinone are known since long [4,5]. Also the crystal structures of *cis*- and *trans*-perinone, as well as of the mixed crystal are known [2,6–11].

In contrast, the chemical composition or even the molecular structure of the intermediate **3** have apparently never been elucidated, despite of it having been synthesized on a multi-ton scale for more than 80 years [4]. Also the isolation of **4** as a solid and its chemical structure has apparently never been reported.

In the literature, the intermediate **3** is denominated as "potassium

* Corresponding author.
E-mail address: m.schmidt@chemie.uni-frankfurt.de (M.U. Schmidt).

https://doi.org/10.1016/j.dyepig.2020.108442
Received 10 February 2020; Received in revised form 9 April 2020; Accepted 10 April 2020
Available online 18 April 2020
0143-7208/© 2020 Published by Elsevier Ltd.

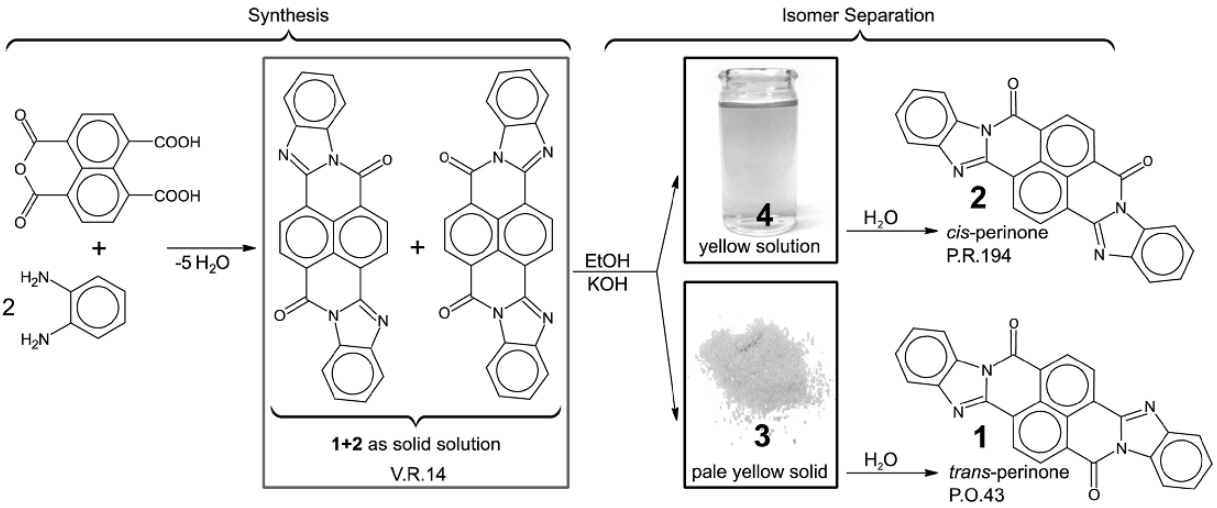

Fig. 1. Industrial synthesis and isomer separation of *trans*-perinone (Pigment Orange 43, **1**) and *cis*-perinone (Pigment Red 194, **2**). The structures of the intermediates **3** and **4** are investigated here. (For colour see online version).

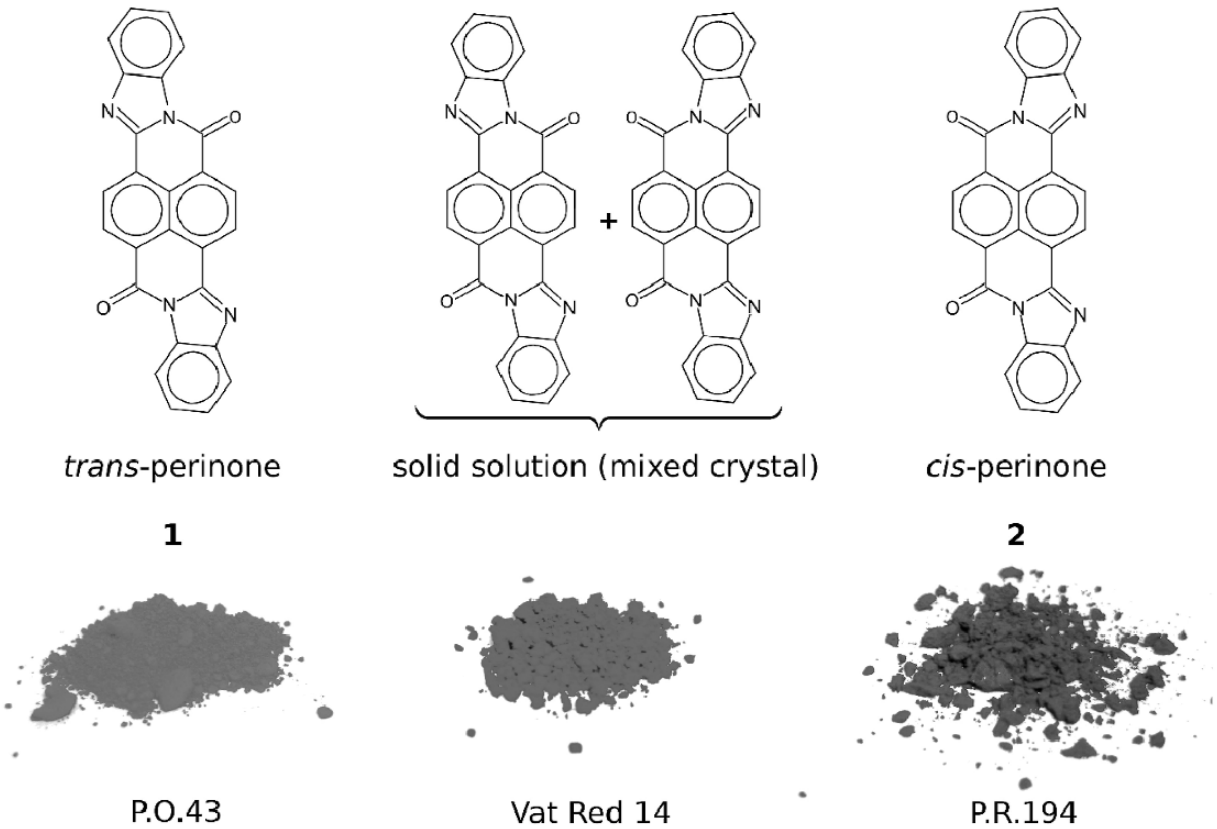

Fig. 2. Chemical structures of the perinone isomers and depiction of their colours. (For interpretation of the references to colour in this figure legend, the reader is referred to the Web version of this article.)

hydroxide addition product" [4,12]. The hitherto assumed molecular formula is shown in Fig. 4. However, it remains obscure which analytical methods were employed to establish this formula.

Here the intermediate **3** was investigated by single crystal X-ray diffraction, amended by powder X-ray diffraction (PXRD), solution and solid-state NMR and IR spectroscopy. Thereby, the molecular structure, the chemical composition and the crystal structure of **3** have finally been determined. Additionally, the intermediate **4** has been isolated. Its molecular structure and crystal structure have been determined as well.

The perinone isomers can also be separated by two other processes: (a) dissolution of the isomer mixture in concentrated sulfuric acid and fractionated crystallization of the *trans*-sulfate (**5**), whereas the corresponding *cis*-compound (**6**) remains in solution; (b) reduction of the isomers to their *leuco* forms (**7** and **8**), with subsequent oxidation, see

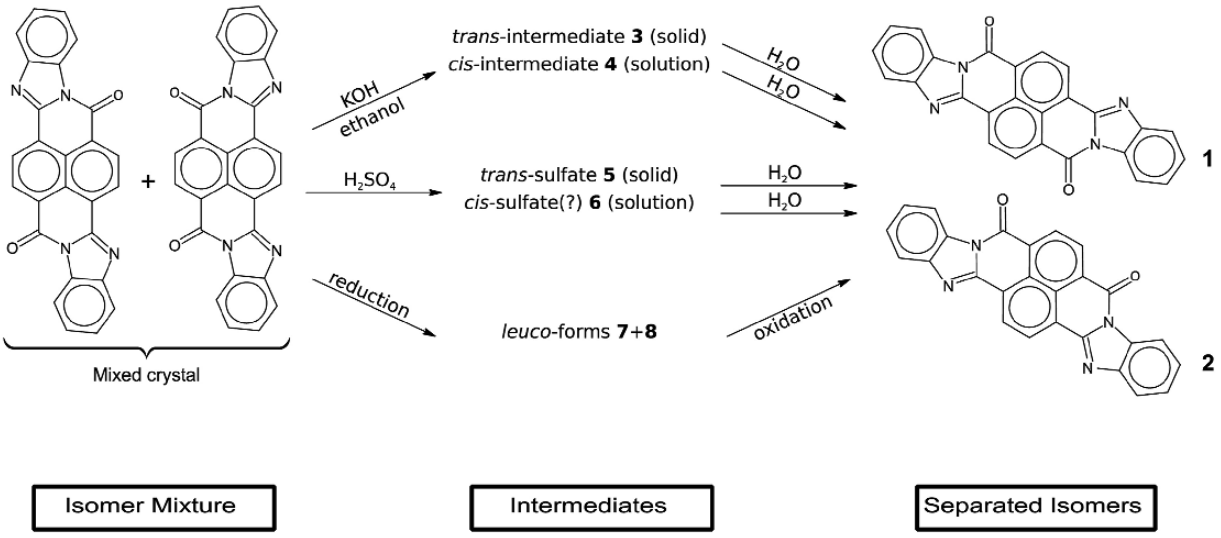

Fig. 3. Different approaches for the isomer separation of *trans*- and *cis*-perinone. Hitherto, the molecular structure of all intermediates **3**–**8** were not known. Now, the structures of **3** and **4** were determined.

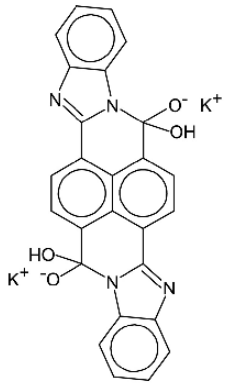

Fig. 4. Previously assumed structure of the intermediate **3** as "potassium hydroxide addition product" (**3**) [13].

Fig. 3. We tried to elucidate the structures of the intermediates **5**–**8**, but could only obtain very limited results.

1.1. Historical

Perinone was first synthesized almost 100 years ago in the laboratories of I.G. Farben (formerly Hoechst AG) in Frankfurt-Höchst, Germany. The corresponding patent was filed in 1924 [3]. The inventors, Wilhelm Eckert and Heinrich Greune noticed, that the reaction of 1,4,5,8-naphthalenedicarboxylic acid with 1,2-diaminobenzene (cf. Fig. 1) leads to a lucent red powder ("leuchtendrotes Pulver"). The authors were surprised that the product was so deeply coloured, although the starting materials, as well as the imides of 1,4,5,8-naphthalenedicarboxylic acid are colourless. The product could be dissolved in concentrated sulfuric acid, giving a yellow-brown colour. Upon reduction, the product turns green [3].

In the original patent, no statement was made about the constitution of the product. Actually, it was a mixture of *cis*- and *trans*-perinone in a ratio of about 1:1. The industrial production of this mixture started in 1926 [14], i.e. only 2 years after the first patent application. (Apparently, in 1926 the official approval for starting the production of a new chemical compound could be obtained much faster than today). The product was at first sold under the name "Indanthrenscharlach 2G" (Indanthrene Scarlet 2G) [14] and from 1929 as "Indanthrenscharlach GG" [15].[1] It was used as a vat dye for the colouration of cotton and rayon, and for printing on cotton.

In 1926, Eckert and Greune described alternative procedures for the synthesis of the perinone mixture [16,17]. Again, no structural formula was given.

The orange *trans*-isomer was apparently isolated first in 1928. Heinrich Neresheimer from Ludwigshafen and Willy Eichholz from Mannheim described the treatment of the perinone mixture with 320 parts of 60% H_2SO_4 and 20 parts of chromic acid at 120–125 °C for 3 h [18].

The first method for the separation of the two perinone isomers was invented in 1929 [1]. The approach used a fractionated crystallisation from sulfuric acid. The isomer mixture is dissolved in concentrated acid; subsequently, ice is added stepwise, which causes the orange isomer to precipitate as an orange sulfate. The red isomer remains in solution. Alternatively, a hot solution of the isomer mixture in H_2SO_4 can be cooled to room temperature, whereby the orange sulfate precipitates. Hydrolysis in water leads to the final orange product. This patent contains, for the first time, the structural formulae of the two isomers. The molecular formula and the chemical constitution of the "orange sulfate" is not known until today; see section 3.8.

In 1930, the separation of the isomers by fractionated crystallization from KOH/ethanol was invented [1]. The isomer mixture is treated with KOH/ethanol (1:7) at 70–80 °C, and subsequently cooled to room temperature. The resulting precipitate (which is the intermediate **3**) is then hydrolyzed to give the orange isomer.

None of these patents state which isomer is the red one, and which is the orange one. This was described by Fierz-David and Rossi in 1938 [14].

The orange *trans*-isomer was sold as Indanthrenbrillantorange GR, whereas the *cis*-isomer was described as "bluish-red, quite dull vat dye, which did not gain technical importance" [14].

The perinone isomers were industrially produced at the Hoechst site in Frankfurt am Main. From the spying activities of the US and British secret services in Germany after 1945, it is known that the perinone-isomers were separated using the KOH/ethanol process: "400 kg of potassium hydroxide are dissolved in 2000 kg of 90% alcohol, and then

[1] The brand name "Indanthrene" was used for many polycyclic pigments, not only for indanthrene derivatives.

200 kg of Indanthrene Scarlet GG base P [i.e. of the isomer mixture] are added. This is helt for 1 h at 75° and then cooled to 20°, and the separated potash[2] addition product is filtered off […]. The nutsch cake is then added into 420 kg of 83% alcohol and 200 kg of potassium hydroxide solution are added and again warmed to 75° for 1 h and cooled to 20°, and again filtered off on the nutsch." The resulting intermediate was subsequently hydrolyzed with water at 60 °C to give the orange *trans*-perinone [4]. Later, the *cis*-isomer was sold as Indanthrenbordo 2R (1948) [19] and Indanthrenbordo RR (1953) [20].

For many years, both isomers, as well as the mixture, have been used only as vat dyes for cotton. After 1950, the perinones found recognition as pigments. Today, both isomers are produced by Clariant (formerly Hoechst AG) in Frankfurt-Höchst. The *trans*-isomer is sold as Hostaperm Orange GR, and the *cis*-isomer as Novoperm Red TG02.

Despite being such an old product, the synthesis of the perinones is still subject to research. This includes attempts to enhance the yield of the economically interesting *trans*-isomer from 50% to about 60% [21], or to perform the synthesis in a "green", hydrothermal way [22].

The molecular structure and the chemical composition of the intermediate **3**, which precipitates from the KOH/ethanol solution, has never been determined, hitherto. In 1929, the inventors described the intermediate as "KOH compound of the orange isomer", but the authors explicitly state: "Whether this alkali treatment leads to salt-like compounds, or to addition products, or to molecular compounds, cannot be said".[3] This statement remained true for 87 years. The description "KOH addition product" is in use until today [12]. A corresponding molecular formula of a KOH addition product is also used in internal documents of the producer Clariant, see Fig. 4 [13]. However, a search in the archives of Clariant and its predecessor Hoechst AG, did not reveal any analytical investigations supporting this formula. Internally, at Clariant the product is called "Trennsalz" (separation salt), "potassium salt" or "potassium addition product".

In the following, we show that the intermediate **3** is not the assumed "KOH addition product", but a salt-like compound of a different molecular formula. A similar structure is also found for the *cis*-intermediate **4**.

1.2. Application

P.O.43 offers a bright orange shade and excellent fastness to heat, light and weathering. *Trans*-perinone thus is a high-price pigment, which is especially used for outdoor applications in plastics, such as tents and awnings. It is also used in paints [2]. P.O.43 is approved in the EU [23] for cosmetic applications except for applications on mucous membranes. It is used as colourant, for example, in soap [24] and nail polish [25]. Its off-label use in inks for tattoos and permanent makeup is also reported [26].

P.R.194 and V.R.14 have a duller shade and a good, but not excellent light fastness. Consequently, they are of less commercial interest. They can be used, for example, in paints or as vat dyes.

2. Materials and methods

2.1. Materials

Samples of P.O.43 (**1**), P.R.194 (**2**), V.R.14 (**1**+**2**) and of the intermediate **3** from the industrial production were provided by Clariant. Solvents and other reactants were obtained from Carl Roth, Fisher Chemical and Sigma-Aldrich and used without further purification.

[2] The expression "potash" is apparently an error in the FIAT report. The process does not contain potash (K_2CO_3).

[3] "Ob bei dieser Einwirkung von Alkalien salzartige Verbindungen oder Anlagerungsprodukte oder auch Molekülverbindungen gebildet werden, kann nicht angegeben werden".

2.2. Recrystallization and sample preparation of the intermediates 3 and 4

Five different samples of the *trans*-intermediate **3** and two samples of the *cis*-intermediate **4** were prepared and investigated. The samples of **3** are denoted as ***A*** to ***E***, the samples of **4** as ***F*** and ***G***.

2.2.1. Trans-intermediate (3)

Sample ***A*** is the industrial product **3**, obtained from Clariant. Samples ***B*** to ***E*** were synthesized in-house.

Sample ***B*** was prepared by heating **1** (0.7 g) in a solution of KOH (2 g), ethanol (5 g) and water (0.5 g). The mixture was stirred at 78 °C for 2 h. The resulting yellow precipitate was isolated by filtration and dried in vacuum at room temperature.

Samples ***C***, ***D*** and ***E*** were obtained by recrystallization of ***A*** from a solution containing KOH, water and ethanol in a ratio of 1:2:9 (in the following referred to as "1:2:9-solution"). This solution was used by the German industry before 1945 for the isomer separation of 1 part of perinone [4].

Sample ***C*** was obtained by recrystallization of sample ***A*** (2 g) in "1:2:9-solution" (5 mL). The suspension was heated to reflux for 3 h, wherein after one and after 2 h additional "1:2:9-solution" (30 mL each) were added. This resulted in a yellow solution from which a predominantly fine, pale yellow powder precipitated on cooling. The inhomogeneous crystalline powder was filtered off at room temperature and analyzed by means of powder diffraction. A single-crystal suitable for structure determination could also be picked from the sample.

The filtrate was kept at 4 °C for several months but yielded neither crystals suitable for single-crystal diffraction nor a sufficiently crystalline powder for powder diffraction. Only some thin and very fine deposit on the wall of the vessel could be observed.

Sample ***D*** was prepared for NMR experiments in solution. A deuterated and more dilute analogue of the "1:2:9-solution" was prepared. KOD was synthesized *in situ* by mixing potassium dioxide (KO_2, 80 mg) and D_2O (0.25 mL) under stirring for 10 min. Subsequently, ethanol-d_6 (0.75 mL) was added. The solution was stored overnight to allow all side-reactions to subside (e.g. formation of deuterium peroxide, which in turn decomposes in alkaline solution to D_2O and oxygen [27]). About 0.5 mL of this solution were used to dissolve a few grains of sample ***A*** and used for solution NMR experiments.

Sample ***E*** was prepared from the already fairly good crystalline sample ***A*** in order to obtain good single-crystals. ***A*** was cured for several hours as suspension in a saturated solution in the "1:2:9-solution" at room temperature, giving single crystals suitable for X-ray analysis.

2.2.2. Cis-intermediate (4)

Sample ***F*** was prepared by reaction of pure **2** (1 g) with KOH (4 g) in water (2 g) and ethanol (36 g) under reflux. On cooling to room temperature, a yellow powder precipitated.

Sample ***G*** was prepared by storing a part of sample ***F*** (yellow suspension) in a sealed vessel at 50 °C for 30 h. The solution turned reddish. Upon cooling to room temperature, fine needles of **4** precipitated, which were suitable for single-crystal X-ray diffraction.

2.3. Determination of solubility and stability

Solubility experiments were carried out with the sample ***A*** in several solvents at room temperature and under heating to reflux.

2.4. NMR in solution

Perinone is insoluble or almost insoluble in all common solvents, such as $CDCl_3$, benzene or DMSO. The intermediate **3** is either insoluble, or decomposes in solvents. Hence, D_2SO_4 and KOH/ethanol were used to record NMR spectra in solution.

For ^1H and ^{13}C NMR measurements of the intermediate **3** in solution,

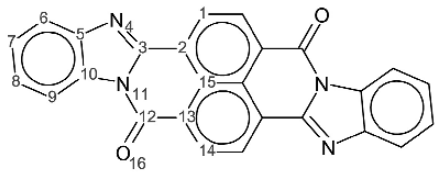

1

Fig. 5. Atom numbering for NMR assignment of **1**. Symmetry copies not labelled. For the assignment of the signals, see also [28].

the sample ***A*** was dissolved in a solution of deuterated ethanol/KOD as described earlier (sample ***D***, section 2.2). Measurements were carried out at room temperature on a Bruker AV500 spectrometer operating at 500 MHz for the ^{1}H nucleus.

Additionally, sample ***A*** was decomposed with deuterated sulfuric acid and measured directly.

Spectra of solutions of **1** in deuterated sulfuric acid were collected as well. For this measurement, a sample of **1** was synthesized from sample ***A*** by hydrolysis with water, washing and drying.

Measurements in D_2SO_4 were carried out on a Bruker AV500 or on a Bruker DRX600, the latter with a ^{1}H frequency of 600 MHz.

NMR-Signals of **1** in D_2SO_4 (for atom numbering see Fig. 5):

^{1}H NMR (D_2SO_4, 500 MHz): 9.85 (d, J = 7.8 Hz, 2H, H1/H14), 9.69 (d, J = 7.8 Hz, 2H, H1/H14), 9.34 (d, J = 8.2 Hz, 2H, H9), 8.60 (d, J = 8.1 Hz, 2H, H6), 8.53–8.46 (m, 4H, H7/H8) ppm.

^{13}C NMR (D_2SO_4, 126 MHz): 154.3, 141.1, 131.7, 127.8, 127.6, 127.4, 126.5, 125.3, 122.8, 122.5, 116.8, 113.6, 111.5 ppm.

NMR-data of **3** directly reacted with D_2SO_4 are given in the ESI.

NMR-Signals of **3** in KOD/EtOD (sample ***D***)

^{1}H NMR (500 MHz, KOD/EtOD): 8,73 (m, 4H, naphthalene), 7.66 (m, 4H, H atoms corresponding to H6/H9), 7.07 (m, 4H, H atoms corresponding to H7/H8) ppm.

^{13}C NMR (126 MHz, KOD/EtOD): 176.64, 163.67, 145.61, 140.07, 135,73, 131.00, 128.47, 126.33, 118.75, 115.78 ppm.

2.5. Infrared spectra

Infrared spectra of **1** and **3** (sample ***A***) were measured to confirm the NMR results. A Shimadzu IRAffinity-1S spectrometer with a Specac diamond ATR-setup was used. Details and spectra are given in the electronic supporting information (ESI).

2.6. Elemental analysis

Elemental analysis of sample ***A*** gave a composition of

41% C, 3.7% H and 6.6% N.

Calculated for the "KOH addition product" shown in Fig. 4: $C_{26}H_{12}N_4O_2{\cdot}4KOH$: 49% C, 2.5% H and 8.8% N. Calculated for the chemical composition of α-**3** (sample ***E***) as determined by single-crystal X-ray analysis (see 3.5.3): $K_4[C_{26}H_{12}N_4O_4]{\cdot}3C_2H_5OH{\cdot}6H_2O$: 45% C, 5.0% H and 6.6% N. Calculated for the chemical composition of β-**3** (sample ***C***) as determined by single-crystal X-ray analysis (see 3.5.5): 1.5 $(K_4[C_{26}H_{12}N_4O_4]){\cdot}5C_2H_5OH{\cdot}4\ H_2O$: 49% C, 4.7% H and 7.0% N. Calculated for **1**: 76% C, 2.9% H and 14% N. The differences between calculated and experimental values may be caused by the reaction of the hygroscopic intermediate **3** to **1** during the elemental analysis.

Additionally, the chemical composition of **3** was assessed gravimetrically: Sample ***A*** was hydrolyzed by water. The resulting orange powder of **1** was filtrated off, washed with water and dried. A weight loss of 52% could be observed. The expected weight loss on hydrolysis of α-**3** was 51%. The difference is attributed to impurities in sample ***A*** (K_2CO_3, ethanol) and incomplete recovery of **1** in the filtration step.

2.7. Powder X-ray diffraction

Powder diffraction data were collected on a Stoe Stadi-P diffractometer equipped with a focusing Ge(111) monochromator and a linear position-sensitive detector. Cu-$K_{\alpha1}$ radiation was employed for all powder measurements. Samples were prepared in glass capillaries with a diameter of 0.7 mm and measured under rotation at room temperature in transmission unless remarked otherwise. The measurement covered a 2θ range from 2 to 80° in steps of 0.2° with 150 s per step. Indexing was performed using DICVOL09 as implemented in the program DASH [29].

2.8. Single-crystal X-ray diffraction

Single crystal X-ray diffraction data of **3** (samples ***C*** and ***E***) were collected on a Stoe IPDS II diffractometer equipped with a Genix microfocus source and mirror optics at 173 K. Mo-$K_{\alpha1}$-radiation was employed. The data were scaled by the frame-scaling routine in the X-area package [30]. The structure was solved by direct methods using SHELXS and refined by the full-matrix least-squares method using SHELXL [31]. All CH protons of the main molecule were found by difference Fourier synthesis. The hydrogen atoms at the ethanol and water molecules were set to chemical sensible, idealized positions. In α-**3** and β-**3**, all non-H atoms were refined anisotropically. In the case of **4**, data were collected on a Siemens Bruker three circle diffractometer equipped with an Incoatec microfocus source. Cu-K_{α}-radiation was employed. The data were scaled by use of SADABS [32]. The structure was solved by direct methods using SHELXS and refined by the full-matrix least-square method using SHELXL [31]. All CH protons of the main molecule were found by difference Fourier synthesis but due to limited data, all H-positions were set to chemical sensible, idealized positions. The crystal quality was quite poor. All non-H atoms were refined isotropically with only one displacement parameter for each ethanol molecule. The atoms linking the main residue with the substituents were constrained to the same displacement as well.

2.9. Solid-state NMR

Preliminary solid-state ^{1}H MAS, ^{13}C and ^{15}N CPMAS NMR spectra of sample ***A*** were recorded on a Bruker (wide-bore) Advance III spectrometer operating at 850, 214 and 86 MHz for the ^{1}H, ^{13}C and ^{15}N nuclei, respectively. Samples were packed in 4 mm diameter cylindrical PTFE rotors and spun in a H/C/N-sensitive probe. Different magic angle spinning frequencies were utilized to identify rotational side bands.

Conclusive solid-state NMR spectra of sample ***A*** were acquired on a Jeol ECZR 600 instrument, operating at 600.17 and 150.91 MHz for the ^{1}H and ^{13}C nuclei, respectively. The powder samples were packed in 3.2 mm diameter cylindrical zirconia rotors with a volume of 60 μL and spun at 20 kHz. ^{13}C CPMAS spectra were acquired using a ramp cross-polarization sequence (contact time of 3.5 ms; ^{1}H 90° pulse of 2.1 μs; optimized recycle time of 2.54 s; 4500 scans). ^{13}C MAS (direct excitation magic angle spinning) spectra were acquired with a ^{13}C 90° pulse of 2.15 μs, recycle times of 2 s for 10000 scans. In all spectra, the two pulse phase modulation (TPPM) decoupling scheme with a 119.0 kHz radio-frequency field was used. ^{13}C chemical shifts were referenced to glycine (^{13}C methylene signal at 38.48 ppm) used as external standard.

2.10. Theoretical approaches

Density functional theory has been used with the aim to investigate possible ordered structures and tautomeric states with the program package CASTEP [33]. DFT-D calculations were executed employing the Perdew-Burke-Ernzerhof generalized gradient approximation exchange-correlation density functional and ultra-soft pseudopotentials (cut-off 520 eV; the Brillouin zone is sampled by 1 x 2 x 2 k-points) [34, 35]. Dispersion correction was done by the Grimme06 model [36].

The Dreiding force-field [37] was used for model generation for

structure determination from powder data and for fast preliminary geometry optimization to locate protons.

Infrared spectra were calculated with Gaussian 09 on B3LYP/6-31G* level [38].

3. Results and discussion

The industrial intermediate **3** has been investigated for its solubility and stability. X-ray powder diffraction revealed the existence of two different crystal phases of **3**, the industrial α-phase (α-**3**) and the β-phase (β-**3**) having a slightly different chemical composition. Single-crystals of both phases could be grown. The crystal structures of both phases were determined by X-ray structure analysis. NMR in solution as well as solid-state NMR provided further information on the intermediate **3**.

The crystal structure of **4** could be elucidated by single-crystal structure analysis as well, resulting in a structure similar to that of **3**.

3.1. Solubility and stability

Samples of **3** and **4** are relatively stable as crystalline powder in dry air.[4] Suspensions of **3** and **4** in ethanolic KOH are stable as well.[5] In contact with moisture or CO_2, the pale yellow intermediate **3** is converted to the orange *trans*-perinone **1**. Analogously, the nearly colourless powder of **4** is converted to the red *cis*-perinone **2** in contact with water.

Keeping a suspension of the *trans*-perinone **1** in KOH/ethanol at room temperature leads to slow conversion of **1** to **3** within several days.

Samples of **3** tend to be inhomogeneously coloured with shades from pale yellow to almost colourless. The yellow colour presumably arises from minute contamination, e.g., with traces of **1**.

According to literature, the intermediate **3** should have a modest solubility in ethanol [12]. Apparently, this is only valid if the solution contains a significant amount of KOH. In most solvents, **3** easily reacts to **1** in the absence of potassium hydroxide. Even pure ethanol[6] or methanol seems sufficient as reaction partner, as a bright orange to red colour develops in mixtures of these alcohols with **3**. The observed reaction in "pure" alcohols could also be attributed to traces of water in the solvent or admission of moisture from air.

In a mixture of ethanol and KOH (5:1 by weight), **3** has a solubility of 6–10 g/L at room temperature.

The measured solubility of **3** in KOH/ethanol is adulterated by impurities from the crystallization process (e.g. excess potassium hydroxide or solvent). Adsorbed ethanol on the crystals increases the apparent solubility. The solubility is reduced by the presence of CO_2 which reacts with KOH and results in K_2CO_3. The potassium carbonate sometimes even forms fairly large crystals, especially in aged samples or samples that were not handled with all of the appropriate care.[7]

At higher temperatures, the solubility in KOH/ethanol increases slightly. No attempt was made to quantify this temperature dependency.

Both isomers of perinone (**1** and **2**) can be dissolved in concentrated sulfuric acid under protonation. Both isomers give reddish brown solutions [7]. The structures of the protonated species are not known (see section 3.8).

3.2. NMR in solution

The ^{13}C NMR spectrum of **1** in D_2SO_4 shows 13 peaks. This number is in agreement with the inversion symmetry of the molecule containing 26 carbon atoms. The ^1H NMR spectrum agrees with the centrosymmetry, too. The NMR spectra of *cis*-perinone in D_2SO_4 confirm the mirror symmetry (C_{2v}) of the *cis*-isomer.

The NMR spectra were also used to establish the isomer purity of **1**. Signals of the *cis*-isomer were not present, confirming that our sample of **1** contained the *trans*-isomer only.

The intermediate **3** (sample ***A***) was reacted with D_2SO_4. The resulting solution had the same reddish-brown colour as a solution of **1** in D_2SO_4. Both solutions contained similar peaks in the ^1H NMR spectrum, but the peaks were shifted. In the D_2SO_4 solution of **3**, additional signals were observed, which were attributed to ethanol molecules and traces of diethyl ether (which results from the reaction of ethanol with D_2SO_4). Other impurities in the sample were not investigated in further detail. The overall shift of the peaks results from dilution of the D_2SO_4 by water [39]. These observations indicated that the intermediate **3** contains ethanol and water molecules in the crystal lattice.

^1H, ^{13}C (^1H gated decoupling) as well as $^1H/^{13}C$ NMR spectra of **3** were recorded in KOD/ethanol-d_6 (sample ***D***). The unusual solvent rendered comparisons with literature data difficult. The ^{13}C spectra in KOD/ethanol contained only 10 signals (in contrast to 13 signals in D_2SO_4), which is in clear disagreement with the assumed formula of **3** depicted in Fig. 4. These findings are interpreted in sections 3.5.1 and 3.5.2.

3.3. Crystal phases

3.3.1. Crystal phases of the trans-intermediate (3)

The X-ray powder patterns of different samples of the intermediate **3** show, that there are actually two different phases, which we call α and β. The α phase is obtained in the industrial production (sample ***A***).

Sample ***B***, which was obtained by heating P.O.43 in suspension in KOH/ethanol at 78 °C (see section 2.2), consisted of poorly crystalline α-**3** and some impurities.

β-**3** is formed by recrystallization of sample ***A*** in a boiling mixture of KOH, water and ethanol (1:2:9) (sample ***C***).

In contrast to the phase transition on recrystallization from "1:2:9-solution", keeping powder samples of α-**3** or crystals of α-**3** suspended in the "1:2:9-solution" at room temperature retains the α-phase (sample ***E***).

3.3.2. Crystal phases of the cis-intermediate (4)

Sample ***F***, which was obtained by dissolving P.R.194 in KOH/ethanol at reflux, followed by cooling to room temperature (see section 2.2), consisted of **4** and some impurities, as shown by PXRD. Most probably, there are more phases of **4**. The powder pattern of sample ***F*** shows peaks not attributable to the single-crystal structure of **4** (which was determined from crystal needles from sample ***G***). Furthermore, amorphization of the sample ***F*** could be observed in dry air. This holds true for crystals from sample ***G*** as well[8], indicating a desolvatation and the existence of a solvate-free form or another solvate with lower solvent content.

3.4. Attempted structure determination of 3 from powder data

The industrial sample ***A*** of the *trans*-intermediate **3** is a well-crystalline powder, but did not contain single-crystals suitable for X-ray structure analysis. Therefore, attempts were made to determine the crystal structure from powder data.

The X-ray powder diffractogram of sample ***A*** (α-**3**) was of good quality. The diffractogram was successfully indexed with a monoclinic

[4] Powder samples of **3** in a closed container in dry air exhibit a reddish orange surface layer after about a year. Crystals of **3**, stored in a sealed vessel under argon, remain unchanged.

[5] The suspensions remained unchanged over several weeks.

[6] "Ethanol, absolute" by Fisher Chemical (99.8+ %) and "Rotipuran® Ethanol, absolute" by Carl Roth (≥99.8%), both with comparable results.

[7] Also the first single-crystal, which we found in a sample of **3** and analyzed by X-ray structure analysis, turned out to be K_2CO_3 instead of **3**.

[8] The amorphization of ***G*** could be observed several times on the diffractometer, because dry nitrogen is used to cool the single crystals during the X-ray exposure. The crystals decompose, but no red colour is observable. This indicates a desolvatation, but no reaction of **4** to **2**.

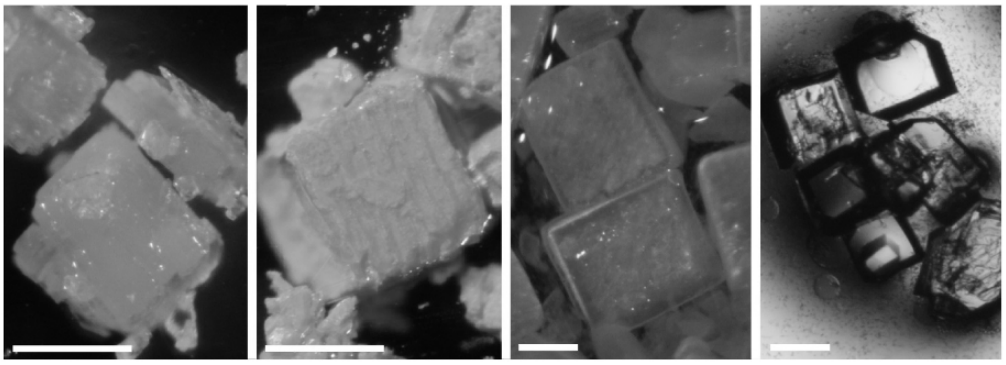

Fig. 6. Sample ***A*** from industrial production (α-**3**, left), (slowly) hydrolyzed sample ***A*** (second left), sample ***E*** (α-**3**, third left) and crystals from sample ***C*** (β-**3**, right). Upon hydrolysis, the grain shape is mostly retained (second left). The white bars in the images have a length of about 100 μm.

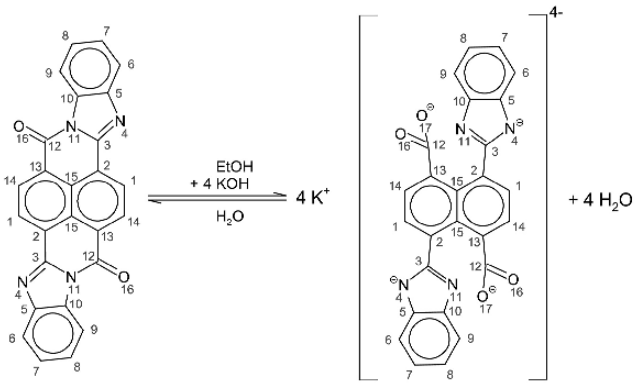

Fig. 7. Molecular structure of the intermediate **3** (right), and reaction from **1** to **3**, with atomic numbering.

unit cell with cell parameters of $a = 27.7$ Å, $b = 12.3$ Å, $c = 12.1$ Å and a monoclinic angle of $\beta = 107°$. The systematic extinctions pointed to $C\,2/c$ as most likely [40] space group. A successful Pawley refinement confirmed the cell parameters and the space group [40,41].

Structure determination was tried by the real-space method with simulated annealing [29]. Since the exact molecular structure of **3** was not known at that time, different molecular models were tested. All of them contained the molecule as "potassium hydroxide addition product", as depicted in Fig. 4, in the di-anionic or tetra-anionic state. All molecular models were optimized with the DREIDING force field [37], in order to assure a sensible molecular geometry. The structure solution trials were run with different molecular models and varying numbers of ethanol and water molecules. All attempts invariably failed. No crystal structure was found which matched the experimental powder pattern.

After the structure had been solved by single-crystal X-ray diffraction it became obvious, that the structure solution from powder data failed, because the assumed molecular model was wrong. The actual molecular geometry, described in 3.5.1, dissented too much from the model which was used in the simulated annealing trials.

3.5. *Crystal structures of the trans-intermediate (3)*

The crystallization experiments, described in section 2.2, yielded two different single-crystals, suitable for structure determination by single-crystal X-ray diffraction. Both crystallizations started from the industrial sample ***A*** (see Fig. 6 left). Single crystals of the α-phase of **3** could be obtained by curing the sample ***A*** in a mixture of KOH, water and ethanol (1:2:9) for several hours at room temperature (sample ***E***). Recrystallization of sample ***A*** from the same solvent mixture at reflux led to the formation of single crystals of the β-phase (sample ***C***, Fig. 6, right).

The α-phase (sample ***E***) corresponds to the industrial phase.

The crystal structures of both phases were determined by single-crystal X-ray diffraction (for details see ESI).

Both crystal structures contain in their lattices the organic anion ("perinone anion"), potassium cations, ethanol and water molecules. The structures of the two phases (α-**3** and β-**3**) differ in their water and ethanol contents. The main common feature is the chemical structure of the "perinone anion".

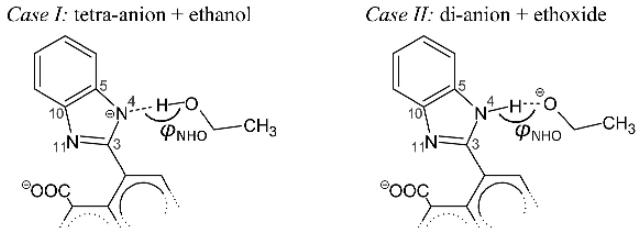

Fig. 8. Possible protonation-states of **3**.

3.5.1. *Chemical structure of the trans-intermediate (3)*

The single crystal X-ray analysis of the α- and β-phases of the *trans*-intermediate **3** revealed, that **3** is not the "potassium hydroxide addition product" depicted in Fig. 4. In contrast, the crystal structures show that, surprisingly, the conversion of **1** to **3** is accompanied by unexpected ring openings (Fig. 7). The two lactam groups (N–CO) disconnect by cleavage of the bond between C12 and N11, and carboxylate groups are formed, see Fig. 7.

Upon hydrolysis of **3** with water or dilute acid, the lactam bond is reconnected and the perinone is restored.

3.5.2. *On the protonation state of* **3**

From the single-crystal X-ray data of α-**3** and β-**3**, no distinctive conclusion on the protonation state of the organic anion (specifically of N4 or N11) could be drawn. The crystal structures of the α- and the β-phases of **3** contain four potassium cations per perinone anion. Correspondingly, there must be four negative counter-charges. There are two possible cases:

case I. The two carboxylate groups and the two benzimidazolate groups are deprotonated, leading to the tetra-anion shown in Fig. 7 and in Fig. 8, case I.

case II. The benzimidazole groups are not deprotonated, but contain a N–H group each, leading to a di-anion. To compensate for the charge of the potassium cations, two ethanol molecules per organic anion must be deprotonated (see Fig. 8, case II).

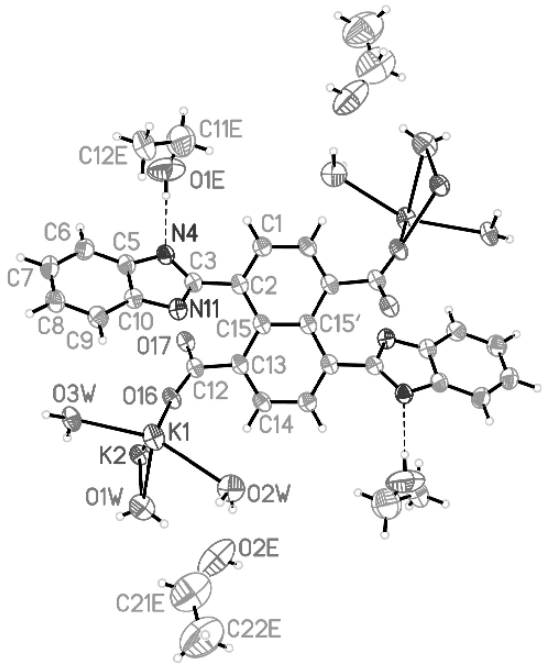

Fig. 9. Ellipsoid plot (50% probability) of α-**3**. Symmetry copies generated by the crystallographic inversion centre at the centre of the molecule are not labelled. For C11E and C12E only the major occupied positions are shown. The O–H···N bonds are shown as dashed lines.

Table 1
Bond lengths (in Å) between nitrogen and carbon in the benzimidazole system, expected for case I and case II (CSD data), in comparison to the experimental values.

	CSD mean values		experimental			
bond	case I[a]	case II[b]	α-3	β-3 frag. 1	β-3 frag. 2	β-3 frag. 3
C3–N4	1.35(4)	1.36(3)	1.354(3)	1.349(8)	1.339(7)	1.347(8)
C3–N11	1.34(4)	1.31(4)	1.341(3)	1.347(8)	1.357(7)	1.347(7)
Δ	0.01	0.05	0.013	0.002	−0.018	0.000
C5–N4	1.36(4)	1.43(5)	1.381(3)	1.389(8)	1.374(7)	1.390(8)
C10–N11	1.37(4)	1.45(5)	1.393(3)	1.391(8)	1.393(7)	1.391(8)
Δ	−0.01	−0.02	−0.008	−0.002	−0.019	−0.001

[a] CSD-search fragment: C_{cycl}-$N^{\ominus}$-C-N(H_0)-C_{cycl} (223 hits).
[b] CSD-search fragment: substituted imidazole (139 hits).

From the viewpoint of an organic chemist, both cases look chemically reasonable. In such cases, a consideration of the pK_a values should be helpful. However, the pK_a values of the perinone di-anion are unknown. The experimental determination of the pK_a values of **3** in solution is hampered by the instability and limited solubility of **3**. Theoretically, the pK_a values could be calculated; but pK_a values, calculated in the gas phase or in solution, do not necessarily reflect the situation in the solid-state environment. The same holds true for experimental pK_a values.

In the crystal structures, there is a short contact between the atom N4 of the benzimidazole and the oxygen atom of an ethanol molecule (compare Fig. 9 and Fig. 17). Obviously there is a hydrogen bond. This could either be a $N^{\ominus}\cdots$H–O bond (case I) or a N–H$\cdots^{\ominus}$O bond (case II), see Fig. 8.

From the X-ray data of α-**3** and β-**3**, the position of the hydrogen atom in question could not be localized in the difference Fourier maps because of limited crystal quality.

In case II, the bond lengths C3–N4 and C3–N11 should differ by about 0.05 Å (CSD-Search with Mogul [42]), whereas they should be about equal in length in case I. Experimentally, their two bond lengths are equal within the precision of the measurements. This holds true for α-**3** as well as for all corresponding bond lengths of the three symmetrically independent fragments in β-**3** (see Table 1). This points to case I. Similarly, the bond lengths C5–N4 and C10–N11 should differ by about 0.02 Å for case II, whereas they should be roughly equal in case I. Also here, all experimental values point to case I.

Table 2
Angles in the hydrogen bond between an N atom of the benzimidazole group and an ethanol molecule for case I and case II in α-**3** and β-**3**. Hydrogen atoms on calculated positions.

phase	angle	case I ϕ(N···H–O)/°	case II ϕ(N–H···O)/°	both cases ϕ(N···O–C)/°
α-**3**	N4–H–O1E	179.4	128.8	113.7(6)
β-**3**[a]	N4A-H-O41E	173.6	155.4	104.7(6)
	N4–H–O21E	179.9	152.0	105.6(7)
	N4B–H–O51E	179.5	97.2[bc]	109.1(8)
	N11B–H–O31E	179.7	120.3[b]	104.6(6)

[a] Three symmetrically independent fragments. In the third fragment both atoms N4 and N11 have a close contact to an ethanol molecule.
[b] H atom either at N4B or N11B.
[c] Not a reliable H bond.

The geometry of the hydrogen bond was investigated as well. The H atom in question was placed in a calculated position either at the O atom (case I) or at the N atom (case II). For case I, the $N^{\ominus}\cdots$H–O angle is roughly 180°, which is a typical value for hydrogen bonds. For case II, the N–H$\cdots^{\ominus}$O angle is between 120 and 155°, which is quite uncommon for a reliable hydrogen bond (see Table 2). Hence, these angles are a clear argument for case I.

The angle N···O–C, incorporating the CH_2 group of the ethanol molecule, should be about 111 ± 14° for case I[9], and 119 ± 14° for case II [10], which is no significant difference. The experimental values (Table 2) are closer to 111°, which is a weak favour for case I.

Another minute, yet productive argument in favour of case I is, that all hydrogen atoms of the C–H groups of the perinone anion could be located by difference Fourier synthesis, but no H atom was found at the N atoms. The hydrogen atoms of ethanol and water molecules could not be located reliably from the X-ray data, because the ethanol and water molecules are disordered, as visible from the larger thermal parameters, from the reduced occupancies of several atoms, and from the solid-state NMR experiments (see section 3.5.3.). Hence, the proton of the OH group of the ethanol molecule cannot be expected to be found in any case. Therefore, the inability to locate the proton of the N–H–O hydrogen bond is an argument for case I.

In the solid-state infrared spectra, no N–H-bands could be observed. In addition, no ethoxide could be detected. Ab initio calculations were employed to generate reference IR spectra, but the resulting gas-phase spectra were not comparable to the measured solid-state spectra. Hence, the IR spectra gave a fade hint in favour of case I.

The ^{1}H NMR spectra of **3** in ethanol-d_6/KOD did not contain signals of N–H, but also in case II these signals would not be visible due to a rapid exchange of the H atom with the deuterated solvent.

The ^{13}C NMR spectra of **3** in ethanol-d_6/KOD solution showed only ten signals. This finding proves the magnetic equality of the atom pairs C5/C10, C6/C9 and C7/C8 of the benzimidazole group. Thus, either both nitrogen atoms (N4 and N11) are not protonated or a fast exchange

[9] CSD search fragment: N···H–O–CH_x with: N having aromatic bonds to two C atoms), x = 2,3 and d(N···O) ≤ 3.27 Å. 2075 hits, CSD mean value 110.6° ± 13.8°.
[10] CSD search fragment: N–H···O–CH_x with: N having single bonds to two C atoms), x = 2,3 and d(N···O) ≤ 3.27 Å. 6230 hits, CSD mean value 119.4° ± 13.5°.

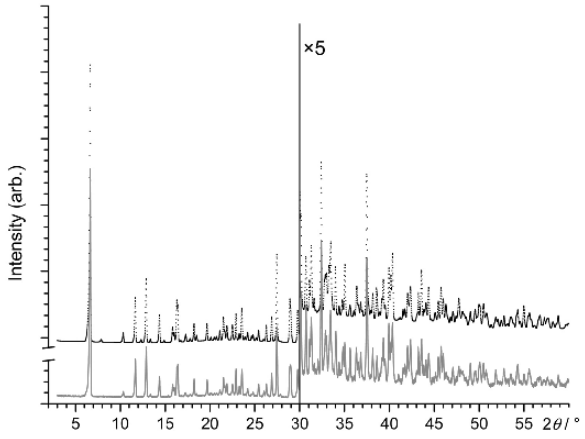

Fig. 10. Experimental powder pattern of sample ***A*** (untreated industrial sample; black, upper, dashed curve) and simulated powder pattern of α-**3** (red, lower curve). Both measurements, powder and single crystal, were performed at 173 K. (For interpretation of the references to colour in this figure legend, the reader is referred to the Web version of this article.)

takes place since the attached carbons act magnetically equivalent. Hence, the ^{13}C NMR spectra show that the intermediate **3** has a ring-opened structure not only in the solid, but also in KOH/ethanol solution. The protonation state in solution remains obscure.

Solid-state NMR (^{1}H, ^{13}C and ^{15}N) provided no clear answer on the protonation state.[11]

DFT-D calculations were set up to determine the protonation state of α-**3**. Several attempts were made: (1) optimization of the whole unit cell; (2) optimization of only the ethanol molecules; (3) optimization of only the proton position of the N···H···O hydrogen bond in the otherwise fixed structure. (4) Several approaches with different numbers of ethanol and water and (5) approaches with super cells and different numbers of ethanol and water. All approaches gave no decisive results or were far too expensive in terms of computing time. The optimizations of the whole unit cell did not converge, probably due to disorder or dynamics. Super cell calculations, set up to account for partly occupied solvent positions proved not feasible. Calculations with a moveable proton between O1E1 and N4 in an otherwise fixed structure favoured a N···H–O bridge rather than a N–H···O bridge, but the energy difference was rather small.

3.5.3. *Crystal structure of the industrial α-phase of* **3** *(α-***3***)*

Single-crystals of the industrial phase α-**3** have been obtained by curing sample ***A*** in 1:2:9-solution (sample ***E***, section 2.2). The crystal structure has successfully been determined at 173 K (Fig. 9). This crystal structure corresponds to the industrial product. This was confirmed by comparison of a simulated powder pattern of α-**3** with an experimental powder diagram of the industrial sample (sample ***A***), both measured at 173 K (see Fig. 10).

Compound α-**3** crystallizes in the monoclinic system. A unit cell with the dimensions $a = 27.6799(16)$ Å, $b = 12.3372(5)$ Å, $c = 12.0253(7)$ Å and $\beta = 106.951(4)^\circ$ (at 173 K) has been found, which corresponds to the values obtained by X-ray powder diffraction. The unit cell volume is 3928.1(4) Å^3 at 173 K. The space group was determined as *C* 2/*c*, as already found by X-ray powder diffraction. Further crystallographic details are given in Table 3.

Table 3
Crystal structural data of the intermediates α-**3**, β-**3**, and **4**.

Compound	α-**3** (*trans*, industrial phase)	β-**3** (*trans*)	**4** (*cis*)
Chemical composition	$K_4[C_{26}H_{12}N_4O_4]$ · $3C_2H_5OH$ ·$6H_2O$	1.5 ($K_4[C_{26}H_{12}N_4O_4]$) ·$5C_2H_5OH$·$4H_2O$	$K_4[C_{26}H_{12}N_4O_4]$ ·$3C_2H_5OH$·$3H_2O$
Formula	$C_{32}H_{42}K_4N_4O_{13}$	$C_{32.67}H_{37.33}K_4N_4O_{10}$	$C_{32}H_{36}K_4N_4O_{10}$
CCDC number	1983275	1983274	1989666
M_r	847.09	802.40	793.05
Crystal system	monoclinic	triclinic	monoclinic
Space group	*C* 2/*c*	$P\,\bar{1}$	$P\,2_1/n$
Z, *Z*′	4, 0.5	3, 1.5	4, 1
T/K	173	173	293(2)
a/Å	27.6799(16)	9.7342(9)	6.586(2)
b/Å	12.3372(5)	16.3726(15)	34.99(2)
c/Å	12.0253(7)	19.1558(17)	16.636(19)
α/°	90	68.834(7)	90
β/°	106.951(4)	84.851(7)	102.11(6)
γ/°	90	77.963(7)	90
V/Å^3	3928.1(4)	2784.0(5)	3748(5)
ρ_{calc} (Mg · m^{-3})	1.432	1.436	1.405
Crystal habit	block	block	thin flat needles
Crystal colour	light brown	light brown	colourless
Crystal size/mm	0.28 × 0.28 × 0.25	0.26 × 0.26 × 0.23	1 × 0.1 × 0.05
Radiation	Mo-K_α	Mo-K_α	Cu-K_α
λ/Å	0.71073	0.71073	1.54178
Θ range/°	2.379–26.901	2.058–25.566	2.526–33.289
N° of meas. refl.	18813	25658	9272
R_{int}	0.0313	0.0611	0.2212
$R[F^2>2\sigma(F^2)]$	0.0536	0.0946	0.0986
w$R(F^2)$	0.1509	0.2725	0.2589
S	1.050	1.065	1.049
N° of reflections	4224	10220	1361
N° of parameters	294	685	204
N° of restraints	84	134	16
$\Delta\rho_{max}$	0.770	1.063	0.626
$\Delta\rho_{min}$	−0.532	−0.773	−0.746

The unit cell contains four perinone anions, which are situated on crystallographic inversion centres. The asymmetric unit is composed of half a perinone tetra-anion, two potassium cations, one and a half molecules of ethanol and three water molecules. Hence the chemical composition of the industrial intermediate is: $K_4[C_{26}H_{12}N_4O_4]\cdot 3C_2H_5OH\cdot 6H_2O$.

The organic tetra-anion is composed of a central naphthalene system, which is tetra substituted in 1,4,5,8-position by two benzimidazolate and two carboxylate substituents. There is a strong intramolecular repulsion between the neighbouring substituents, caused by steric requirements and by the Coulomb repulsion between the negatively charged carboxylate and benzimidazolate groups. This leads to a distortion of the molecule in two ways: (1) a rotation of the four substituents against the naphthalene plane, (2) an out-of-plane bending of the substituents causing a deformation even on the naphthalene system

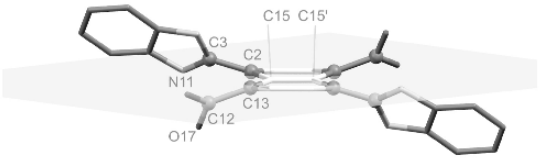

Fig. 11. Organic anion in α-**3**. Mean plane (light blue) of the six central naphthalene carbon atoms depicted in white. The naphthalene system and its substituents are nonplanar, which is well visible from the carbon atoms depicted as grey balls. (For interpretation of the references to colour in this figure legend, the reader is referred to the Web version of this article.)

[11] Solid-state ^{15}N spectra were recorded overnight. The samples turned orange, visually indicating a reaction of **3** to **1** during the measurement. Three weak peaks were observable. They might be interpreted as two signals from **1** and one signal from **3**, which is an indication for the magnetic equivalence of the two N atoms of the benzimidazole group, which could, however, also be caused by dynamical effects in case I or case II.

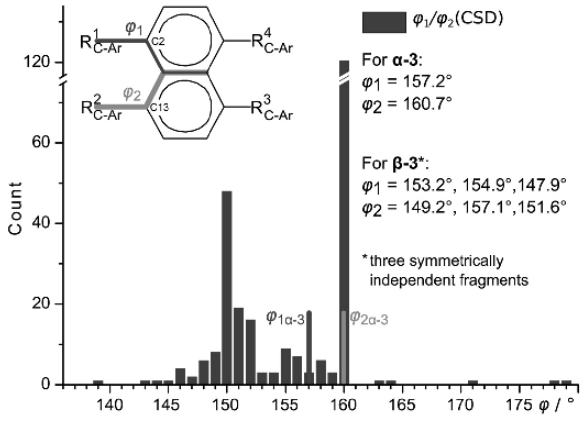

Fig. 12. Distribution of torsion angles of 1,4,5,8-tetrasubstituted molecules in the CSD. The inset shows the CSD query motif. The CSD search was restricted to only aromatic substituents R^1-R^4. In the experimental structures of α-**3** and β-**3**, R^1 and R^4 are the COO^- groups and R^2 and R^3 the benzimidazolate groups.

itself.

Ad (1): The carboxylate group is rotated against the naphthalene plane by 34.7(3)° as manifested by the torsion angle ϕ(O17–C12–C13–C15). The neighbouring benzimidazole is rotated in the same direction by 39.2(3)° (ϕ(N11–C3–C2–C15)), see Fig. 11.

Ad (2): The naphthalene system deviates by 0.035 Å RMS from its mean plane. The carbon atoms C13 and C2 are by 0.12 Å below and above the mean plane. The carbon atom of the carboxylate moiety (C12) is 0.63 Å below this plane and the bonding carbon atom of the benzimidazolate (C3) is 0.55 Å above (see Fig. 11). The corresponding torsion angles are ϕ_1(C12–C13–C15–C15′) = 157.2(2)° for the carboxylate group, and ϕ_2(C3–C2–C15–C15′) = 160.7(2)° for the benzimidazolate group (Fig. 12). A CSD search for 1,4,5,8-tetrasubstituted naphthalene compounds was performed. In case of aliphatic substituents, the naphthalene system is almost planar ($\phi_1 = \phi_2 = 180°$). For aromatic substituted naphthalenes, torsion angles between 155° and 167° are frequent (see Fig. 12). Hence, the perinone's geometry is no outlier.

The benzimidazolate mean plane forms a dihedral angle of 44.5° with the naphthalene mean plane. Similarly, the carboxylate plane forms a dihedral angle of 46.2° with the naphthalene's mean plane (Fig. 14).

Those rotations are caused by steric requirements and by the Coulomb repulsion between the negatively charged benzimidazolate and carboxylate groups.

Because of the nonplanarity, the electronic conjugation between the π-systems of the naphthalene group and the π-systems of the carboxylate and the benzimidazolate groups is strongly hampered. The interrupted conjugation explains the colour differences between the bright orange perinone **1** and the almost colourless intermediate **3**.

Also the π-stacking of neighbouring molecules, which generally contributes significantly to the colour of organic pigments, is hindered

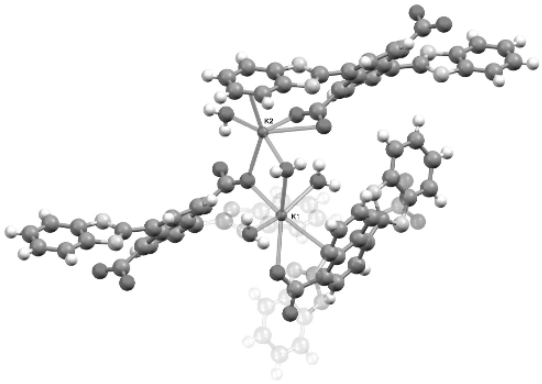

Fig. 14. Coordinative environment of K1 (lower) and K2 (upper) in α-**3**. C atoms in grey, H white, O red, N blue, K violet. Coordinative bonds depicted as transparent green cylinders. (For interpretation of the references to colour in this figure legend, the reader is referred to the Web version of this article.)

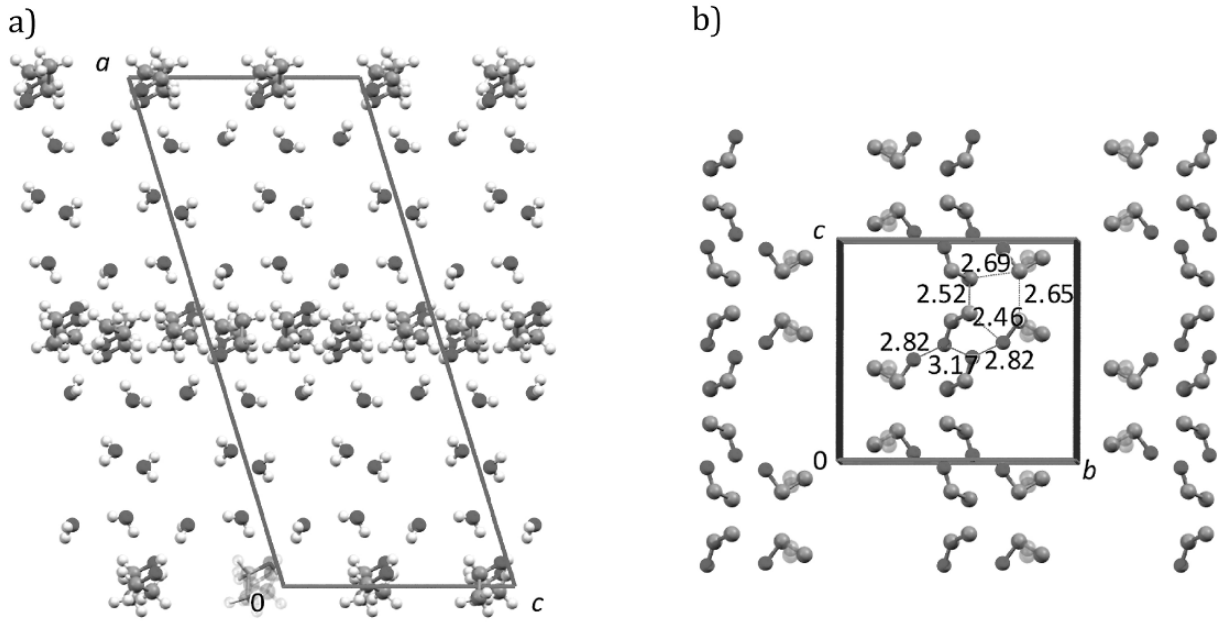

Fig.13. Arrangement of ethanol and water molecules in α-**3**. (a) View along the b-axis. Only major occupied positions of disordered positions are shown. (b) Arrangement of the ethanol molecules in the ethanol layer. View along the *a*-axis. The numbers show the short intermolecular distances between C and O atoms of the ethanol molecules. O···O distances of 2.8–3.1 Å are typical for hydrogen bonds, but O···C and C···C distances of 2.5–2.7 Å are only possible between average positions in highly dynamic or disordered systems. The minor occupied atomic positions are drawn more transparent.

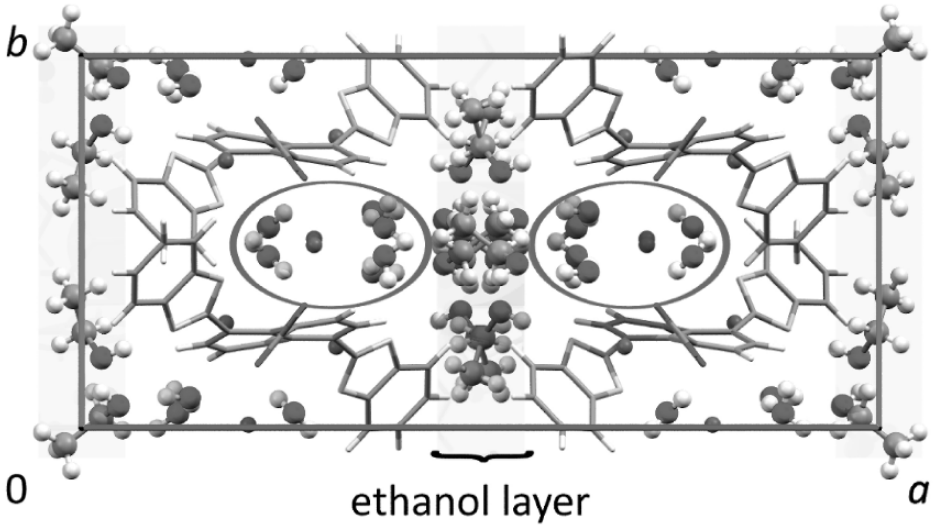

Fig. 15. Crystal structure of α-**3**. View along the *c*-axis. The K^+ ions, ethanol and water molecules are drawn as ball-and-stick model, the tetra-anions as capped sticks only. The channels of water molecules are marked by a red ellipsis. (For interpretation of the references to colour in this figure legend, the reader is referred to the Web version of this article.)

by the strong out-of-plane bending of the benzimidazolate fragments. Actually, the distance between neighbouring naphthalene centres is more than 8 Å.

The structure contains two symmetrically independent potassium cations, both on a general position. The first potassium ion (K1) is six-fold coordinated by the carboxylate groups (η^1) of two anions, by three water molecules and by the π-system of the naphthalene system of one anion (Fig. 14). The second cation (K2) is six-fold coordinated as well. It coordinates two-fold to the carboxylate (η^2) and the benzimidazoles π-system of one anion, to the carboxylate group (η^1) of another anion, and to two water molecules (Fig. 14). Astonishingly, the potassium cations do not coordinate to the negatively charged N atoms of the benzimidazolate fragments.

All water molecules in the structure are coordinated to potassium anions. The water molecules are arranged in channels parallel to the *c*-axis around the K^+ ions, see Fig. 15.

The most prominent hydrogen bond pattern in the structure is a second level $C_4^4(22)$ chain, linking the carboxylate moiety of one organic anion to the benzimidazole nitrogen (N4) of another via a water molecule [43,44].

Both ethanol molecules are disordered. The ethanol molecule which is H-bonded to the atom N4 of the benzimidazolate (O1E, C11E, C12E, Fig. 9) is disordered on two orientations with occupancies of 70 to 30%. The other ethanol molecule (containing O2E) is disordered around a twofold axis, with an occupancy of 0.5 for all atoms. Thus, only half of these molecules are present simultaneously, whereas the other position remains unoccupied. This disorder results in an overall number of 3 ethanol molecules per perinone anion.

The ethanol molecules form layers parallel to the (100) direction, i. e., in the *bc*-plane (see Figs. 13 and 15). This ethanol layer contains short intermolecular C···C contacts of 2.5–3 Å. Such small distances are chemically unreasonable. They can only occur between the average atomic positions in a highly dynamic structure or in a disordered structure. In any case, not all atomic positions are occupied simultaneously. Most probably, both effects are present in α-**3**.

3.5.4. *Dynamical aspects of the structure of α-3*

The X-ray data reveal that both ethanol molecules in the structure α-**3** are disordered. The nature of the disorder, whether static or dynamic, was investigated by solid-state NMR spectroscopy. Depending on the type of experiment, solid-state NMR can either highlight signals

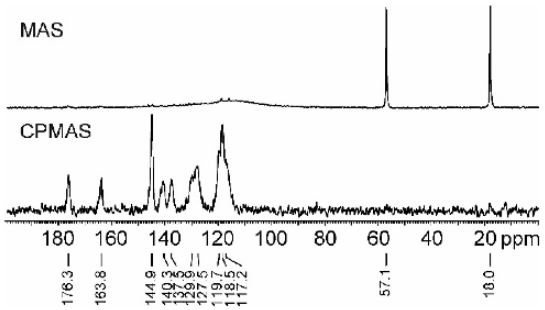

Fig. 16. Solid-state NMR spectra of α-**3**. ^{13}C (150.9 MHz) CPMAS (bottom) and MAS (top) spectra acquired at a spinning speed of 20 kHz.

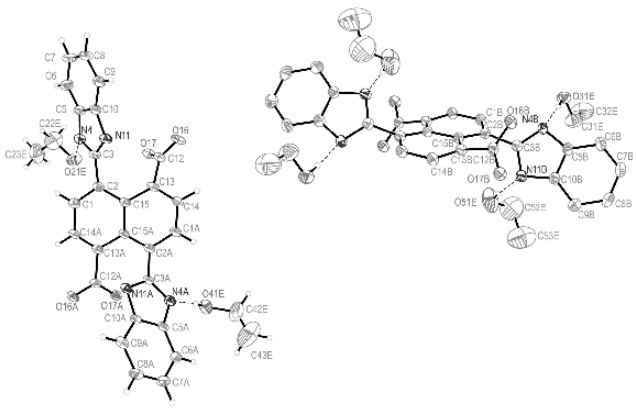

Fig. 17. Ellipsoid plot (50% probability) of β-**3**. Symmetry copies without label. One ethanol molecule and all water molecules and potassium ions omitted for clarity. Hydrogen bonds shown as dashed lines.

arising from rigid or from highly dynamic parts of a structure. For rigid structures, CPMAS (cross-polarization magic-angle spinning) experiments are employed. Dynamic, liquid-like aspects were investigated by MAS (direct excitation magic-angle spinning) experiments [45,46]. The

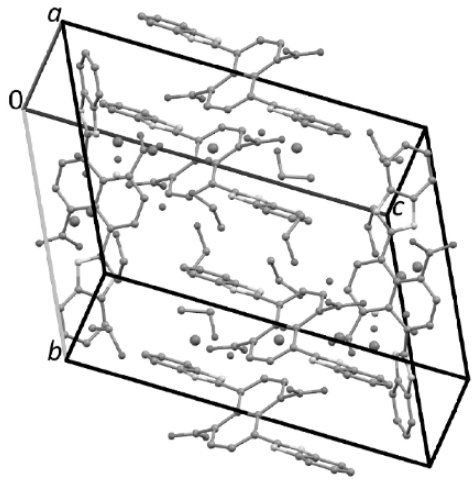

Fig. 18. Crystal structure of β-**3**. H atoms are not shown.

^{13}C CPMAS and MAS spectra of α-**3** are shown in Fig. 16.

The ^{13}C CPMAS spectrum shows aromatic and carbonyl resonances (around 110–150 and 160–180 ppm, respectively), which can be assigned to the rigid (in the NMR time scale) perinone tetra-anion. Interestingly, no aliphatic signals attributable to the ethanol molecules are present. Apparently, the ethanol is too dynamic to be seen in CPMAS spectra. On the other hand, the ^{13}C MAS spectrum is characterized by only two sharp peaks (~45 Hz width) at 18.0 and 57.1 ppm, which can be attributed to the ethanolic CH_3 and CH_2, respectively. Since the MAS experiments highlights resonances attributed to highly mobile moieties only, this clearly suggests a very fast exchange between all ethanol positions.

The crystal data show that such a fast exchange between all ethanol positions is well possible. All ethanol molecules are crystallographically disordered, leaving space at the respective momentarily unoccupied positions. There is enough space in the ethanol layer for the ethanol molecules to move from one position to another with only a small energy barrier. This fast movement explains the solution-like lines in the MAS spectrum.

3.5.5. *Crystal structure of the β-phase of* **3** *(β-**3**)*

Single-crystals of the β-phase of **3** (sample ***C***) could be obtained by recrystallization of sample ***A*** from a boiling mixture of KOH, water and ethanol (1:2:9). The crystal structure was determined from X-ray analysis.

The compound β-**3** crystallizes in the triclinic system with unit cell dimensions of $a = 9.7342(9)$ Å, $b = 16.3726(15)$ Å, $c = 19.1558(17)$ Å, $\alpha = 9.7342(9)°$, $\beta = 84.851(7)°$ and $\gamma = 77.963(7)°$, resulting in a cell volume of 2784.0(5) Å^3 at 173(2) K. The space group is $P\,\overline{1}$.

Like α-**3**, also β-**3** contains a ring-opened tetra-anion. Even the conformation of the anion is similar. The carboxylate groups as well as the benzimidazolate groups are rotated against the naphthalene plane[12], and bent out of the plane (Fig. 12).

The unit cell contains three tetra-anions, with one of them on a crystallographic inversion centre and two on a general position.

The asymmetric unit is composed of one and a half perinone anions, six potassium cations, five molecules of ethanol and four water molecules. Correspondingly, the chemical composition of β-**3** is 1.5 $(K_4[C_{26}H_{12}N_4O_4])\cdot 5C_2H_5OH\cdot 4H_2O$.

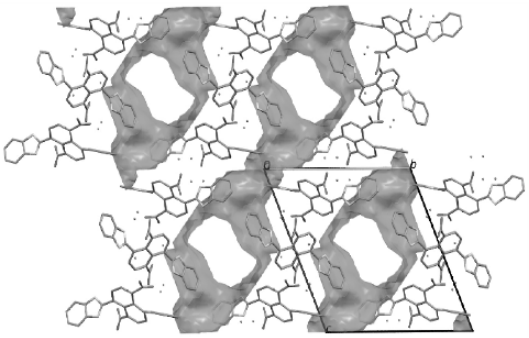

Fig. 19. Crystal structure of β-**3**. Ethanol and water molecules are situated in channels. The outer surface of the channels is drawn in red. The channels are connected to a two-dimensional layer formed by ethanol molecules. View along the a-axis. (For interpretation of the references to colour in this figure legend, the reader is referred to the Web version of this article.)

All potassium ions, water and ethanol molecules are situated on a general position (see Fig. 18 and Fig. 19). The six unique potassium ions have coordination numbers of 6–8. The phase β-**3** is another solvate form (or, as some might say a "pseudopolymorph") of α-**3**. Both phases contain the same tetra-anions, but differ in the numbers of ethanol and water molecules. In the α-phase there are 3 ethanol molecules and 6 water molecules per $K_4[C_{26}H_{12}N_4O_4]$ moiety. The β-phase contains 10/3 ethanol and 8/3 water molecules per $K_4[C_{26}H_{12}N_4O_4]$ moiety. The lower water content of the β-phase is in agreement with the higher temperatures during its crystallization, which generally hampers the inclusion of water molecules in the crystal lattice [47].

In the crystal structure of β-**3**, the potassium cations and organic tetra-anions form a coordination network parallel to (011). The water and ethanol molecules are arranged in channels parallel to the *a*-axis, see Fig. 19. The channels are connected by close contacts between ethanol molecules,[13] resulting in a layer of ethanol molecules parallel to (011), i. e. between the coordination network of K^+ cations and organic anions. Within these ethanol layers, the molecules are probably mobile and disordered, as it is evident from the large and anisotropic displacement parameters of the atoms of the ethanol molecules. However, the limited crystal quality of β-**3** does not allow detailed discussion of this disorder.

3.6. *Crystal structure of the cis-intermediate* (**4**)

Single-crystals of the cis-intermediate **4** have been obtained by reaction of pure **2** with KOH in ethanol and storage at elevated temperature (sample ***G***, see section 2.2). The crystal structure has successfully been determined at 293(2) K.

The intermediate **4** crystallizes in the monoclinic system in the space group $P\,2_1/n$. Crystallographic data are given in Table 3.

The cis-intermediate **4** has a ring-opened structure, like the *trans*-intermediate **3**, see Fig. 20.

The crystal quality was low, but better crystals could not be grown. Hence, the protonation state of the anion could not be determined from the X-ray data. In analogy to the investigations made on α-**3** and β-**3**, one should assume that the cis-intermediate, too, adopts the tetra-anionic state. Like in α-**3**, there is a hydrogen bond from the atom N4 of both benzimidazolate units to an ethanol molecule each (see Fig. 20b).

The geometry of the cis-tetra-anion in the structure of **4** resembles the geometry of the *trans*-tetra-anions in the structures of α-**3** and β-**3**. Like in **3**, the carboxylate groups as well as the benzimidazolate groups

[12] Torsion angles for the COO group: ϕ(O16–C12–C13–C15) = −150.0(6)°, ϕ(O16A–C12A–C13A–C15A) = −132.6(6)°, ϕ(O16B–C12B–C13B–C15B) = 42.6(8)°; for the benzimidazole group: ϕ(N11–C3–C2–C15) = −37.8(9)°, ϕ(N11A–C3A–C2A–C15A) = 53.7(8)°, ϕ(N11B–C3B–C2B–C15B) = 136.2(6)°.

[13] d(C12E-C22E) = 3.727 Å.

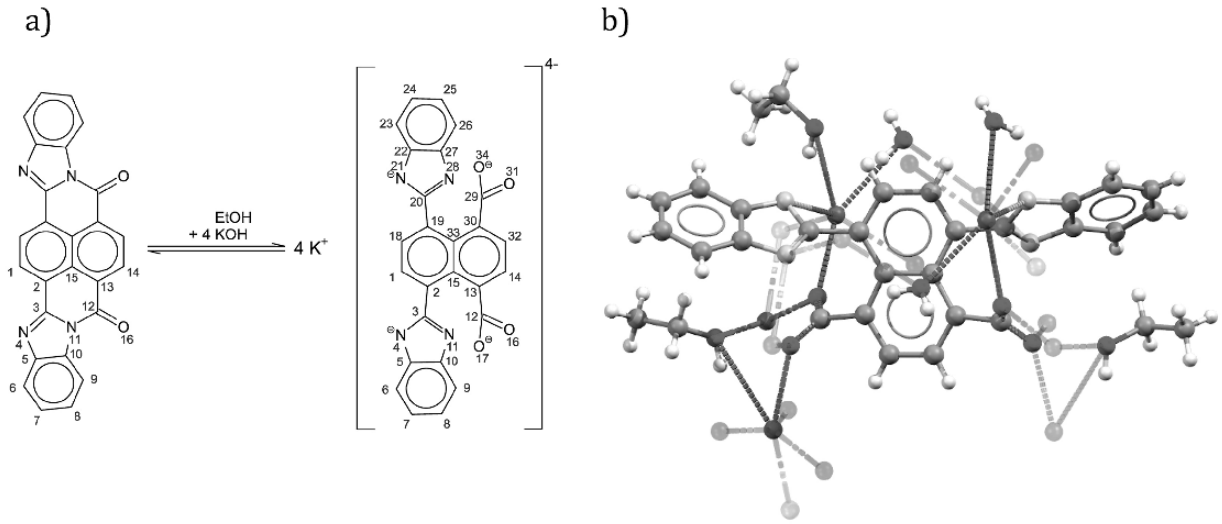

Fig. 20. Structure of the *cis*-intermediate **4**. (a) Molecular structure. (b) Section from the crystal structure (coordinating symmetry copies depicted transparent).

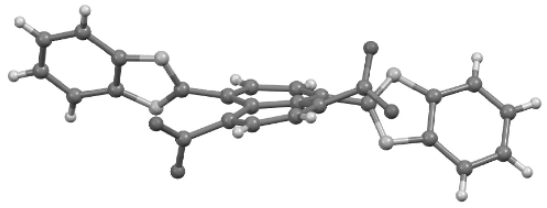

Fig. 21. Organic anion in **4**. C atoms in grey, H white, O red, N blue.

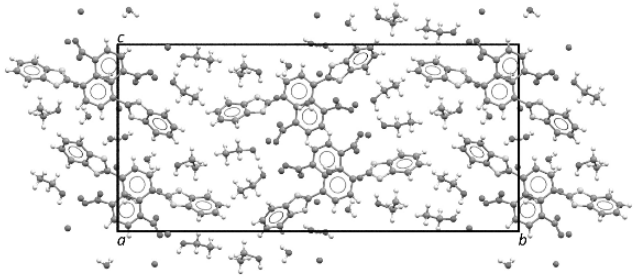

Fig. 22. Crystal structure of the cis-intermediate **4**. View along the *a*-axis. C atoms in grey, H white, O red, N blue, K violet. (For interpretation of the references to colour in this figure legend, the reader is referred to the Web version of this article.)

are rotated against the naphthalene plane,[14] and bent out of the plane. This leads to a considerable distortion of the naphthalene plane, see Fig. 21.

The asymmetric unit is composed of one perinone tetra-anion, 4 potassium cations, 3 molecules of ethanol and 3 water molecules. Hence the chemical composition of **4** is: $K_4[C_{26}H_{12}N_4O_4]\cdot 3C_2H_5OH\cdot 3H_2O$.

All four potassium cations coordinate directly to the N atoms of the benzimidazolate groups. This coordination is in contrast to α-**3**, where the benzimidazolate groups only act as π ligands to the K^+ ions. In β-**3**, both coordination modes are present.

The organic tetra-anions and potassium cations form a two-dimensional coordination network parallel to (010), i.e. parallel to the *ac*-plane, see Fig. 22.

In KOH/ethanol solution, the ^{13}C NMR spectra of **4** show in total 10 signals, like for the *trans*-intermediate **3**. This proves, that the *cis*-intermediate **4** has a ring-opened structure in solution, like in the solid state. The protonation state of **4** in solution is not known, but presumably, the intermediate **4** is a tetra-anion like in the solid state (see Fig. 20a).

3.7. On leuco-perinones (*7*, *8*)

Upon reduction, the isomer mixture of perinones turns green, as described by Eckert & Greune in 1924 and 1926 [2,3]. However, the molecular and crystal structure of resulting *leuco*-forms **7** (*trans*) and **8** (*cis*) are unknown till today. Reduction of the pure *trans*-perinone **1** with potassium dithionite leads to a suspension of green colour. In the course of our investigations, the *trans-leuco*-form **7** was isolated from this suspension by centrifugation, and analyzed. As a solid, **7** exhibits a dark green to black colour. All investigated samples of **7** were amorphous by means of powder X-ray diffraction.

No NMR-data of **7** could be obtained, because all isolated green solids (including **7**, prepared by reduction with dithionite) were insoluble in the usual solvents for NMR spectroscopy (including D_2O and ethanol-d_6).

A greenish substance of similar hue as **7** is obtained, when P.O.43 (**1**, 720 mg) is stored in ethanolic KOH (7.5 mL and 2 g KOH) for three months at room temperature (in a sealed 10 mL flask). A powder X-ray diagram of this sample only showed reflections of poorly crystalline **3** (α-phase).

Samples of **3** in KOH/ethanol, stored at 50 °C for several weeks, produced a greenish solution and a slimy brown-reddish residue, which was amorphous by means of X-ray powder diffraction.

Hence, the molecular structure of the trans-leuco-form **7** and the chemical composition of the green suspension remain obscure. The structure of the cis-leuco-form **8** was not investigated.

3.8. On the intermediates in the H_2SO_4 process

The dissolution of the perinone isomer mixture in concentrated sulfuric acid leads to a yellowish brown solution, as already observed by Eckert & Greune in 1924 [3]. From this solution, an "orange sulfate" (**5**) of the *trans*-isomer can be precipitated by cooling or by addition of a small amount of water [3]. According to our experiments, the solubility

[14] Torsion angles: ϕ(C15–C2–C3–N11) = 55° and ϕ(C33–C19–C20–N28) = 58°.

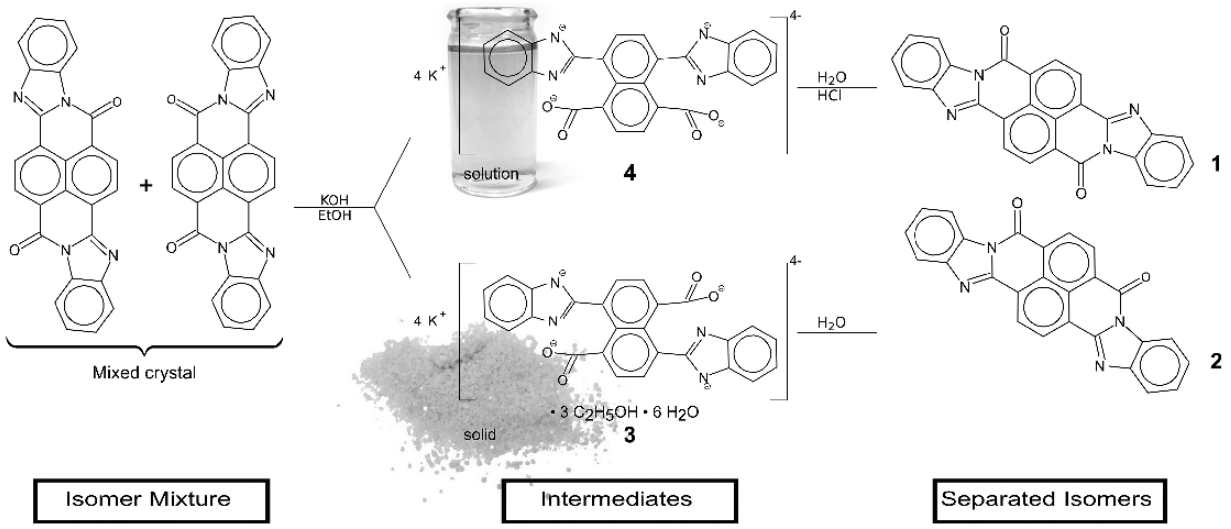

Fig. 23. Structure of the intermediates in the industrial separation of perinone isomers.

of perinone in sulfuric acid is quite high and moisture from air is sufficient to precipitate the "orange sulfate" over the course of days. Without the addition of water, a considerable amount of perinone remains in solution at room temperature. The precipitate is rather complicated to isolate from the acid.

The orange sulfate can also be obtained by reaction of **1** with a vapour of sulfuric acid at 220 °C under reduced pressure.

Reaction of the obtained orange powders with water restores **1** and releases sulfuric acid.

The "orange sulfate" is more yellowish than **1** and the powder pattern of this (microcrystalline) substance strongly deviates from that of the starting material. The powder diagram indicates more than one phase; none of them could be identified (see ESI) and it was not possible to determine the crystal structure by powder diffraction, despite various attempts.

The ^{1}H and ^{13}C NMR data of a D_2SO_4 solution of **1** indicates, that the molecule retains its centrosymmetric structure (at least in time-average), and that no ring opening takes place (section 3.2). The NMR data and the observed solubility can be explained by a protonated perinone molecule. However, the number of added protons and the protonation sites are not known.

Hence, the molecular structure of **5** and the chemical composition of the corresponding "orange sulfate" precipitate remain obscure.

The corresponding cis-intermediate **6** remains in solution in H_2SO_4, presumably as protonated species. Its ^{1}H and ^{13}C NMR spectra are similar to that of the trans-intermediate **5**, but the signals are shifted. Further structural investigations have not been made.

4. Conclusion

After more than 80 years of industrial production, the molecular formulae of the intermediates in the industrial separation of perinone isomers are finally elucidated. Hitherto, neither their molecular structure, nor their crystal structures, nor even the chemical composition of the industrial precipitate of the *trans*-intermediate were known. In contrast to earlier assumptions, the intermediates **3** and **4** are no "KOH addition products", but products of a ring-opening reaction of the perinone skeleton (Fig. 23). The distinction between the *cis*- and *trans*-isomers remains intact. The *trans*-intermediate **3** has a lower solubility in KOH/ethanol, which allows the separation of the isomers. The ring-opening is reversible: Treatment of the isolated *trans*- and *cis*-intermediates, **3** and **4**, with water leads to a ring-closure, restoring *trans*-perinone (**1**) and *cis*-perinone (**2**), respectively. Thus, the different solubilities of the intermediates **3** and **4** and the fully reversible ring openings allow the separation of the perinone isomers in the industrial process.

In both perinone isomers, the ring-opening is accompanied by a rotation of the benzimidazolate moieties against the naphthalene fragment by 43.5°–57.6° (α-**3** has a dihedral angle of 45.6°; β-3: the molecule on a general position has dihedral angles of 43.5° and 57.6°, the molecule located on a centre of inversion has a dihedral angle of 51.3°). This rotation results in an interruption of the conjugation of the π-systems, which causes the observed colour change from the bright orange *trans*-perinone (P.O.43, **1**) and the deep red *cis*-perinone (P.R.194, **2**) to the almost colourless[15] intermediates **3** and **4**.

The *trans*-intermediate phase α-**3**, which precipitates from KOH/ethanol in the industrial process, contains ethanol and water molecules in its crystal lattice, and has a composition of $K_4[C_{26}H_{12}N_4O_4]\cdot 3C_2H_5OH\cdot 6H_2O$, as determined by single-crystal X-ray diffraction. A second crystal phase (β-**3**) of slightly different composition was synthesized and its structure was determined, too. The *cis*-intermediate (**4**), which is industrially handled only in solution, was isolated as a solid; a single crystal could be grown, and its structure was determined as well.

In the crystal structure of α-**3**, the potassium cations are π-coordinated to the benzimidazolate group, whereas they form a single coordination bond to the N atom of the benzimidazolate in **4**, and a mixture of both in β-**3**. In all structures, the water molecules are coordinated to the potassium cations, whereas the ethanol molecules occupy the voids between the molecules. The ethanol molecules form layers. According to solid-state NMR investigations of α-**3** (^{13}C CPMAS and MAS) the ethanol molecules are highly dynamic, whereas the organic anions are quite rigid.

The protonation state of the perinone anions could not be determined from single-crystal data. NMR methods were used to identify the intermediate as tetra-anion and IR spectroscopy confirmed this conclusion. Besides the KOH/ethanol treatment, two other methods are known for the separation of the perinone isomers: fractionated crystallization from sulfuric acid, or reduction to the leuco forms. The corresponding intermediates – protonated species or reduced species – were investigated, too, but their structures could not be unravelled, despite of various attempts.

[15] The yellow colour of the precipitate **3** and of the solution of **4** in KOH/ethanol in the industrial process is apparently caused by impurities. The pure compounds **3** and **4** as crystalline solids are almost colourless.

Authorship contribution statement

Lukas Tapmeyer: Synthesis, crystallisation, analytics, manuscript writing. **Michael Bolte:** Single-crystal structure analysis. **Michele R. Chierotti:** Solid-state NMR. **Martin U. Schmidt:** Project leader, history, manuscript writing.

Declaration of competing interest

The authors declare that they have no known competing financial interests or personal relationships that could have appeared to influence the work reported in this paper.

Acknowledgements

The authors thank Sophie Müller (Clariant) for the industrial samples of perinone and of the intermediate **3**, Sibylle Aust (Clariant) for searches in the archives of Hoechst AG and Clariant, Christian Czech (Goethe University; now Amcapharm Pharmaceutical GmbH) for the support with CASTEP (DFT-D) calculations, Jan Klett (Johannes Gutenberg University, Mainz) for the Gaussian (ab initio) calculations, Yvonne Thiemann (Max Planck Institute of Biophysics, Frankfurt) for non-ambient X-ray experiments, Johanna Baldus and Clemens Glaubitz (both Goethe University) for preliminary solid-state NMR experiments, and Edith Alig (Goethe University) for the X-ray powder diffractograms.

Appendix A. Supplementary data

Supplementary data to this article can be found online at https://doi.org/10.1016/j.dyepig.2020.108442.

References

[1] Eckert W, Sieber H. Verfahren zum Trennen von Küpenfarbstoffen. Deutsches Patent DE567210. 1932.
[2] Hunger K, Schmidt MU. Industrial organic pigments: production, crystal structures, properties, applications. Fourth ed. Weinheim: Wiley-VCH; 2018.
[3] Eckert W, Greune H. Verfahren zur Darstellung von Küpenfarbstoffen. DE430632. 1924.
[4] FIAT. German dyestuffs and dyestuff intermediates, including manufacturing processes, plant design, and research data. Field Information Agency Technical. Volume 1. Dyestuff intermediate processes and analytical procedures. Washington, DC: Office of Military Government for Germany (U.S.); 1948.
[5] Fierz-David HE, Rossi C. Über die Darstellung von Naphthoylen-imidazolinen. Helv Chim Acta 1938;21:1466–89. https://doi.org/10.1002/hlca.193802101182.
[6] Teteruk JL, Glinnemann J, Heyse W, Johansson KE, van de Streek J, Schmidt MU. Local structure in the disordered solid solution of *cis*- and *trans*-perinones. Acta Crystallogr Sect B Struct Sci Cryst Eng Mater 2016;72:416–33. https://doi.org/10.1107/S2052520616004972.
[7] Mizuguchi J. Crystal structure and electronic characterization of trans- and cis-perinone pigments. J Phys Chem B 2004;108:8926–30. https://doi.org/10.1021/jp031351d.
[8] Paulus EF, Kunstmann W. Forschungsbericht 265 III.3. Hoechst Am Main: Hoechst AG; 1978.
[9] Mizuguchi J. Crystal structure of trans-bisbenzimidazo[2,1-*b*:1',2'-*j*]benzo[*lmn*][3,8]-phenanthroline-6,9-dione, $C_{26}H_{12}N_4O_2$. Z für Krist - New Cryst Struct 2003;218:137–8. https://doi.org/10.1524/ncrs.2003.218.1.137.
[10] Mizuguchi J. Crystal structure of bisbenzimidazo[2,1-*b*:2',1'-*i*]benzo[*lmn*][3,8]phenanthroline-8,17-dione, $C_{26}H_{12}N_4O_2$. Z für Krist - New Cryst Struct 2003;218:139–40. https://doi.org/10.1524/ncrs.2003.218.1.139.
[11] Zherebtsov DA, Schmidt MU, Niewa R, Sakthidharan CP, Podgornov FV, Matveychuk YV, et al. Two new polymorphs of cis-perinone: crystal structures, physical and electric properties. Acta Crystallogr Sect B Struct Sci Cryst Eng Mater 2019;75:384–92. https://doi.org/10.1107/S2052520619003287.
[12] Herbst W, Hunger K, Wilker G. Industrial organic pigments: production, properties, applications. Third ed. Weinheim: Wiley-VCH; 2004.
[13] Clariant. Internal document on the synthesis of P.O.43. Frankfurt am Main; 2008.
[14] Fierz-David HE, Rossi C. Über die Darstellung von Naphthoylen-imidazolinen. Helv Chim Acta 1938;21:1466–89. https://doi.org/10.1002/hlca.193802101182.
[15] Schultz G. Farbstofftabellen. Band 1: Künstliche organische Farbstoffe bekannter Konstitution oder Herstellungsweise, Vol. 1. Leipzig: Akademische Verlagsgesellschaft; 1931.
[16] Eckert W. Verfahren zur Darstellung von Küpenfarbstoffen. DRP456236. 1928.
[17] Eckert W, Greune H. Verfahren zur Darstellung von Küpenfarbstoffen. DRP457980. 1928.
[18] Neresheimer H, Eichholz W. Verfahren zur Darstellung von orange färbenden Küpenfarbstoffen. DRP507832. 1940.
[19] Schaeffer A. Die Küpenfarbstoffe. Aufbau, Eigenschaften, Anwendung. Band A: Aufbau der Küpenfarbstoffe. Hoechst Am Main: Farbwerke Hoechst; 1948.
[20] Die Küpenfarbstoffe und ihre Verwendung in der Färberei und im Zeugdruck. Vienna: Springer Vienna; 1953.
[21] Dietz E, Kapaun G, Schiessler S. Verfahren zur Herstellung von Küpenfarbstoffen und Pigmenten der Perinon-Reihe. Deutsches Patent DE3836674A1; 1990.
[22] Taublaender MJ, Glöcklhofer F, Marchetti-Deschmann M, Unterlass MM. Green and rapid hydrothermal crystallization and synthesis of fully conjugated aromatic compounds. Angew Chem Int Ed 2018;57:12270–4. https://doi.org/10.1002/anie.201801277.
[23] European Parliament. Commission regulation (EC) No 1223/2009 of the European parliament and of the council of 30 november 2009 on cosmetic products. Official Journal of the European Union; 2009.
[24] Imperial Leather UK. Product packaging "imperial leather soap classic packaging". Ingredients declaration 2018.
[25] Intoglam corp. Material safety data sheet: color gel by intoglam. 2016.
[26] Piccinini P, Contor L, Pakalin S, Senaldi C, Raemaekers T. Institute for Health and Consumer Protection. Safety of tattoos and permanent make-up: state of play and trends in tattoo practices. Luxembourg: Publications Office; 2015.
[27] Holleman AF, Wiberg N. Lehrbuch der anorganischen Chemie. 102. Auflage. Berlin New York: Walter de Gruyter; 2007.
[28] Taublaender MJ, Glöcklhofer F, Marchetti-Deschmann M, Unterlass MM. Green and rapid hydrothermal crystallization and synthesis of fully conjugated aromatic compounds. Angew Chem Int Ed 2018;57:12270–4. https://doi.org/10.1002/anie.201801277.
[29] David WIF, Shankland K, van de Streek J, Pidcock E, Motherwell WDS, Cole JC. DASH: a program for crystal structure determination from powder diffraction data. J Appl Crystallogr 2006;39:910–5. https://doi.org/10.1107/S0021889806042117.
[30] STOE & Cie GmbH. https://www.stoe.com.
[31] Sheldrick GM. A short history of SHELX. Acta Crystallogr A 2008;64:112–22. https://doi.org/10.1107/S0108767307043930.
[32] Sheldrick GM. SADABS. Karlsruhe. Germany: Bruker AXS; 1996.
[33] Clark SJ, Segall MD, Pickard CJ, Hasnip PJ, Probert MIJ, Refson K, et al. First principles methods using CASTEP. Z Krist – Cryst Mater 2005;220. https://doi.org/10.1524/zkri.220.5.567.65075.
[34] Vanderbilt D. Soft self-consistent pseudopotentials in a generalized eigenvalue formalism. Phys Rev B Condens Matter 1990;41:7892–5.
[35] Perdew JP, Burke K, Ernzerhof M. Generalized gradient approximation made simple. Phys Rev Lett 1996;77:3865–8. https://doi.org/10.1103/PhysRevLett.77.3865.
[36] Grimme S. Semiempirical GGA-type density functional constructed with a long-range dispersion correction. J Comput Chem 2006;27:1787–99. https://doi.org/10.1002/jcc.20495.
[37] Mayo SL, Olafson BD, Goddard WA III. DREIDING: a generic force field for molecular simulations. J Phys Chem 1990;94:8897–909. https://doi.org/10.1021/j100389a010.
[38] Frisch MJ, Trucks GW, Schlegel HB, Scuseria GE, Robb MA, Cheeseman JR, et al. Gaussian 09, revision B.01. Wallingford CT: Gaussian, Inc.; 2009.
[39] Batamack P, Fraissard J. Proton NMR studies on concentrated aqueous sulfuric acid solutions and Nafion-H. Catal Lett 1997;49:129–36.
[40] Markvardsen AJ, David WIF, Johnston JC, Johnson JC, Shankland K. A probabilistic approach to space-group determination from powder diffraction data. Acta Crystallogr A 2001;57:47–54.
[41] Pawley GS. Unit-cell refinement from powder diffraction scans. J Appl Crystallogr 1981;14:357–61. https://doi.org/10.1107/S0021889881009618.
[42] Bruno IJ, Cole JC, Kessler M, Luo J, Motherwell WDS, Purkis LH, et al. Retrieval of crystallographically-derived molecular geometry information. J Chem Inf Comput Sci 2004;44:2133–44. https://doi.org/10.1021/ci049780b.
[43] Etter MC, MacDonald JC, Bernstein J. Graph-set analysis of hydrogen-bond patterns in organic crystals. Acta Crystallogr B 1990;46:256–62. https://doi.org/10.1107/S0108768189012929.
[44] Grell J, Bernstein J, Tinhofer G. Graph-set analysis of hydrogen-bond patterns: some mathematical concepts. Acta Crystallogr B 1999;55:1030–43. https://doi.org/10.1107/S0108768199007120.
[45] Chierotti MR, Amin M, Hassan YS, Haikal RR, Garino C, Alkordi MH. Combined solid-state NMR and computational approach for probing the CO_2 binding sites in a porous-organic polymer. J Phys Chem C 2017;121:8850–6. https://doi.org/10.1021/acs.jpcc.7b00660.
[46] d'Agostino S, Fornasari L, Grepioni F, Braga D, Rossi F, Chierotti MR, et al. Precessional motion in crystalline solid solutions of ionic rotors. Chem Eur J 2018. https://doi.org/10.1002/chem.201803071.
[47] Hilfiker R, editor. Polymorphism: in the pharmaceutical industry. First ed. Wiley; 2006.

8 Weitere eigene Patente, Veröffentlichungen und Tagungsbeiträge

Patente:

S. D. Gumbert, L. Tapmeyer & M. U. Schmidt: *Neue Kristallphasen von Flupirtin-Maleat*, **2015**, DE102015013478.

Veröffentlichungen ohne Bezug zur Promotion:

X. Li, L. Tapmeyer, M. Bolte & J. van de Streek: *Crystallographic and Dynamic Aspects of Solid-State NMR Calibration Compounds: Towards ab Initio NMR Crystallography*, ChemPhysChem **2016**, Vol. 17, Issue 16, S. 2496-2502, DOI: 10.1002/cphc.201600398.

Poster:

L. Tapmeyer, M. U. Schmidt & M. Bolte: *Polymorph screening and crystal structure solution of 3-methylglutaric acid*, MS38-P1, 29th European Crystallographic Meeting, **2015**, Rovinj, Kroatien. (Ohne Bezug zur Promotion)

L. Tapmeyer, C. Saal & M. U. Schmidt: *A pharmaceutical co-crystal structure from powder diffraction data*, MS13-P04, 15th European Powder Diffraction Conference, **2016**, Bari, Italien.

L. Tapmeyer, W. M. Hützler & M. U. Schmidt: *Trust your pow(d)er (data)*, MS09-P162, 16th European Powder Diffraction Conference, **2018**, Edinburgh, Schottland.

9 Erklärung und Versicherung

[Die Erklärung und Versicherung ist in der elektronisch publizierten Version nicht enthalten]

10 Lebenslauf

[Der Lebenslauf ist in der elektronisch publizierten Version nicht enthalten]

Weitere Aktivitäten während des Promotionszeitraumes

10.06.2016 Teilnahme am *13th TOPAS Bruker Users' Meeting* in Bari, Italien vom 10. bis 12. Juni 2016.

12.06.2016 Teilnahme mit Posterpräsentation an der *15th European Powder Diffraction Conference* in Bari, Italien vom 12. bis 15. Juni 2016.

23.06.2016 Messzeit an der *Diamond Light Source*, Beamline I15, in Oxfordshire, England.

19.09.2016 Teilnahme an der 9. Sommerschule „Grundlagen der Einkristallstrukturbestimmung" im Kloster Hardehausen in Warburg/Westfalen vom 19. bis 23. September 2016.

2016-2021 Fachliche Betreuung von Praktika und Abschlussarbeiten im Arbeitskreis Schmidt sowie Anleitung von wissenschaftlichen Hilfskräften.
3 Wissenschaftliche Hilfskräfte
3 Schülerpraktika
6 Vertiefungspraktika im Bachelorstudium
5 Bachelorarbeiten
7 Arbeitskreispraktika im Masterstudium
2 Vertiefungspraktika im Masterstudium
2 Industriepraktika im Masterstudium (Protokollkorrektur)
2 Masterarbeiten
1 Wissenschaftliche Hausarbeit (Staatsexamen Lehramt; Beratung bei der praktischen Arbeit).

WS16-SS21 Assistenz im Praktikum
„Anorganisch Chemisches Praktikum AC I (L2/L3/L5)".

WS16-SS21 Assistenz im Praktikum
„Anorganisch Chemisches Praktikum AC II (L3)"
mit Blockpraktikum
„Präparative Anorganische Chemie".

2016-2021 Beteiligung an der Klausurerstellung, -durchführung und -korrektur:
„AC2 Festkörperchemie" (Bachelorvorlesung)
„Technische Chemie" (Mastervorlesung)
„Röntgenstrukturanalyse" (Mastervorlesung)
„Röntgenpulverdiffraktometrie" (Mastervorlesung)
„Polymerchemie" (Mastervorlesung).

2017-2021 Wartung und Pflege der nicht zentral verwalteten EDV-Systeme im Arbeitskreis Schmidt.

22.06.2018 Messzeit an der *Diamond Light Source*, Beamline I15-1 (PDF), in Oxfordshire, England.

29.06.2018 Teilnahme am *14th TOPAS Bruker Users' Meeting* in Bari, Italien vom 29. Juni bis 01. Juli 2018.

01.07.2018 Teilnahme mit Posterpräsentation an der *16th European Powder Diffraction Conference* in Bari, Italien vom 01. bis 04. Juli 2018.

2018-2020 Teilnahme am Qualifizierungsprogramm:
„Zertifikat Hochschullehre" des
Interdisziplinären Kollegs Hochschuldidaktik (IKH).

22.06.2021 Abschluss „Zertifikat Hochschullehre" des
Interdisziplinären Kollegs Hochschuldidaktik (IKH).

2019-2021 Auftragsröntgenstrukturanalysen für andere Arbeitskreise der Universität Frankfurt.

18.04.2019 Messzeit an der *Diamond Light Source*, Beamline I15-1 (PDF), in Oxfordshire, England.

18.09.2019 Teilnahme am Seminar „Tipps und Tricks für SHELX 2019" in Aachen vom 18. bis 20. September 2019.

2019-2020 Einzelne Vorlesungsstunden in der Vorlesung
„AC2 Festkörperchemie" (Bachelorvorlesung).

2019-2021 Einzelne Vorlesungsstunden in der Vorlesung
„Röntgenstrukturanalyse" (Mastervorlesung).

2019-2021 Einzelne Vorlesungsstunden in der Vorlesung
„Röntgenpulverdiffraktometrie" (Mastervorlesung).

2019-2021 Portierung der alten Webseite in das *CMS* (FIONA 7) der Universität und Pflege der Webseite des Arbeitskreises Schmidt.

29.06.2020 Teilnahme an einem (online stattfindenden) „Seminar Patent & Gebrauchsmuster: Gewerblicher Rechtsschutz" vom 29. Juni bis 1. Juli 2020.

2020 Gelegentliche Vertretung im Seminar
„Seminar zum Praktikum
Anorganisch Chemisches Praktikum AC II (L3)".

08.12.2020 Teilnahme an einer (online stattfindenden) „Schulung / Unterweisung §§ 27, 29 GGVSEB und Kapitel 1.3 ADR" zur korrekten Abfüllung bzw. Verpackung von Gefahrstoffen, insbesondere chemischen Abfällen.

2020-2021 Technische Betreuung der OLAT-Kurse „Technische Chemie" und „Festkörperchemie" im Sommersemester 2020 und im Sommersemester 2021.

2021 Technische Betreuung der OLAT-Kurse „Röntgenstrukturanalyse" und „Röntgenpulverdiffraktometrie" im Wintersemester 2020/21.